ASSESSMENT OF WATER AVAILABILITY FOR SUSTAINABLE AGRICULTURAL PRODUCTION UNDER CLIMATE CHANGE SCENARIO IN NAGALAND

THESIS SUBMITTED IN PARTIAL FULFILLMENT OF THE REQUIREMENTS FOR THE DEGREE OF DOCTOR OF PHILOSOPHY

BY

VISAKHONUO KUOTSU

Ph.D. REGN NO. AET/00442

DEPARTMENT OF AGRICULTURAL ENGINEERING & TECHNOLOGY

SCHOOL OF ENGINEERING & TECHNOLOGY,
NAGALAND UNIVERSITY, KOHIMA CAMPUS,
MERIEMA – 797004

OCTOBER, 2025

ASSESSMENT OF WATER AVAILABILITY FOR SUSTAINABLE AGRICULTURAL PRODUCTION UNDER CLIMATE CHANGE SCENARIO IN NAGALAND

BY

VISAKHONUO KUOTSU AND
DR. PRAMOD CHANDRA DIHINGIA

Submitted

In partial fulfillment of the requirements for the Degree of Doctor of Philosophy in

Agricultural Engineering and Technology

of

Nagaland University

DECLARATION

Nagaland University

October, 2025

I, **Visakhonuo Kuotsu**, hereby declare that the subject matter of this Thesis is the record of work done by me, that the contents of this Thesis did not form the basis of the award of any previous degree to me or to the best of my knowledge to anybody else, and that the Thesis had not been submitted by me for any research degree in any other University/Institute.

This thesis is being submitted to Nagaland University for the degree of Doctor of Philosophy in Agricultural Engineering and Technology.

(VISAKHONUO KUOTSU)

(PRAMOD CH. DIHINGIA)
Supervisor

(Prabhakar Sharma)
Head

(KHAN CHAND)
Co-Supervisor

NAGALAND UNIVERSITY

Kohima Campus

School of Engineering & Technology

Kohima Campus: Meriema – 797004, Nagaland

Dr. Pramod Chandra Dihingia

Assistant Professor

Department of Agricultural Engineering & Technology

School of Engineering and Technology

CERTIFICATE – 1

This is to certify that the thesis entitled **"Assessment of Water Availability for Sustainable Agricultural Production under Climate Change Scenario in Nagaland"** submitted to Nagaland University in partial fulfillment of the requirements for the award of degree of Doctor of Philosophy in Agricultural Engineering and Technology is the record of research work carried out by Ms. Visakhonuo Kuotsu, Registration No. PhD/AET/00442 under my personal supervision and guidance.

The result of the investigation reported in the thesis has not been submitted for any other degree or diploma. The assistance of all kinds received by the student has been duly acknowledged.

Date: (PRAMOD CH. DIHINGIA)

Place: Kohima Supervisor

(KHAN CHAND)

Co-Supervisor

NAGALAND UNIVERSITY
Kohima Campus
School of Engineering and Technology
Kohima Campus: Meriema – 797004, Nagaland

CERTIFICATE – II

VIVA VOCE ON THESIS OF DOCTOR OF PHILOSOPHY IN AGRICULTURAL ENGINEERING AND TECHNOLOGY

This is to certify that the thesis **"Assessment of Water Availability for Sustainable Agricultural Production under Climate Change Scenario in Nagaland"** submitted by Ms. Visakhonuo Kuotsu, Admission No. 2009, Registration No. Phd/AET/00442 to the NAGALAND UNIVERSITY in partial fulfilment of Agricultural Engineering and Technology has been examined by the Advisory Board on …….

The performance of the students has been found to be **Satisfactory/Unsatisfactory.**

Members	**Signature**
1. Dr. Pramod Chandra Dihingia (Supervisor)	……...
2. Dr. Khan Chand (Co-Supervisor)	……
3. Prof. Pradip Kumar Bora (External examiner)	……
4. Dean, SET (Ex – Officio member)	……

Members of Advisory committee

1. Dr. Rajkrishna Mondal	……
2. Dr. Rohen Heisnam	……

Head
Department of Agricultural Engineering and Technology

Dean
School of Engineering and Technology

ACKNOWLEDGMENT

In everyone's life, the day comes when one has to share sentiments in words. Sometimes, words are needed to express the feelings of the mind because the feelings of the heart are beyond the grasp of words. When I came to complete this research work, so many memories rushed through my mind, which are full of gratitude to those who encouraged and helped me at various stages of this research work and also throughout my life. It gives me immense pleasure to record my feelings at this place.

I am deeply grateful to my supervisor, **Dr. Pramod Chandra Dihingia**, Assistant Professor, Department of Agricultural Engineering and Technology, SET, Nagaland University, Kohima Campus, for his earnest supervision, guidance, and encouragement during this research work. This research could not have been completed without his continual monitoring and advice. I am incredibly grateful to him for allowing me to work as his pupil and for sharing his vast knowledge with me. I am also grateful to my co-supervisor, **Dr. Khan Chand**, Professor and Head, Department of Agricultural Engineering, School of Agricultural Sciences, Nagaland University, Medziphema Campus, for his useful ideas and support during my research work, which enabled me to complete it.

I would like to express my sincere appreciation to **Prof. Prabhakar Sharma**, HOD, Department of Agricultural Engineering and

Technology, SET, and **Prof. Sujata Dash**, Dean, SET, for sharing their valuable knowledge during my research work.

I consider it an honor to express my heartfelt gratitude to the members of the Advisory Committee, Dr. Chitrasen Lairenjam, Associate Professor, Department of Agricultural Engineering, SAS; Dr. Rajkrishna Mondal, Associate Professor, Department of Biotechnology, SET; and Dr. Rohen Heisnam, Assistant Professor, Information Technology, SET, for their valuable suggestions.

I also feel very grateful to the numerous departments in the study area. I truly appreciate the assistance and support provided by the Department of Soil and Water Conservation-Nagaland, the Department of Agriculture-Nagaland, and the District Agriculture Office-Nagaland. In particular, special thanks to Shri Hoshito Chophi, DAO- Dimapur, Shri Bode Shuya, DAO- Chumoukedima, Smti. Sentinaro, AO-Kohima.

I express my profound gratitude to NFST- National Fellowship for Scheduled Tribe, Ministry of Tribal Affairs, for the financial sponsorship that provided impetus and resources during my research.

I sincerely acknowledge from my heart and soul, thanks to all my esteemed friends, especially Miss Imyanglula, Miss Lochumi Kikon, and Mr. Narang Tassang, for their invaluable contribution and support that encouraged me throughout the venture.

Above all, it is beyond my ability to express in words my profound reverence and indebtedness to my father Lt. Ralo Kuotsu, who

was the driving force behind my pursuit of this degree, as well as my dearest mother, siblings, and relatives for their spiritual, material, and physical support that strengthened and made means possible in all ways. Prima facie, I thank the Almighty God for giving me knowledge, good health, and well-being to complete my studies.

Sincere thanks to all those who joyfully cooperated during the course and all those who are not mentioned but directly or indirectly contributed to the preparation of this manuscript.

It's always difficult to single out all the individuals who have contributed in many ways to this research. I recall with respect and affection the assistance given by one and all.

Date:

Place: Meriema (VISAKHONUO KUOTSU)

CONTENTS

LIST OF TABLES

LIST OF FIGURES

LIST OF ABBREVIATIONS

AMC	-	Antecedent Moisture Condition
I_{AWA}	-	Agricultural Water Availability Index
CN	-	Curve number
et al.	-	And other
Fig.	-	Figure
FAO	-	Food and Agriculture Organization
GIS	-	Geographic Information System
Ha	-	Hectare
Ham	-	Groundwater recharge
HSG	-	Hydrologic Soil Group
IDW	-	Inverse Distance Weighted
IPCC	-	Intergovernmental Panel on Climate Change
km^2	-	Square Kilometer
kW/ha	-	kilowatt per hectare
LST	-	Land Surface Temperature
m	-	Meter
m^3/day	-	Meter cube per day
MCM	-	Million Cubic Meters
mm	-	millimeter
MJ	-	Megajoule
MODIS	-	Moderate Resolution Imaging Spectroradiometer

NASA	-	National Aeronautics and Space Administration
NDVI	-	Normalized Difference Vegetation Index
NIR	-	Near Infrared
RCP	-	Representative Concentration Pathways
SCS	-	Soil Conservation Service
SDSM	-	Statistical DownScaling Model
USDA	-	United States Department of Agriculture
USGS	-	United States Geological Survey
WRIS	-	Water Resource Information System

ABSTRACT

In the present study, an attempt was made to develop an agricultural water availability index (I_{AWA}) for the assessment of future water availability and its impact on climate change, and estimate the agricultural mechanization index in Kohima and Dimapur districts, Nagaland, India, to recommend suitable agricultural implements under less water availability situation. The daily rainfall data for 17 years (2003 to 2020) was collected from the Department of Soil and Water Conservation, Government of Nagaland, Kohima, for the study. The MODIS (Moderate Resolution Imaging Spectroradiometer) satellite images from NASA, specifically for 2011, were used to analyze the soil moisture. To assess the groundwater depth and quality such as pH level, electrical conductivity, nitrate concentration, and fluoride levels, the data from 2004 to 2020 were used from the India WRIS (Water Resources Information System). Surface runoff was estimated using the SCS – CN method (Soil Conservation Service – Curve Number) which incorporated the rainfall data, soil map, and Land Use Land Cover (LULC). CanESM2 (second-generation Canadian Earth System Model) global climate model was used to predict future climate scenarios. For the estimation of agricultural mechanization, a survey was conducted among the 101 farmers with a view to collect data of the present status of farm mechanization and the costs of cultivation involved for the major crops in the study area. Further to analyze and interpret the data, the software programs such as ArcGIS, SDSM, and CROPWAT were used.

The study showed that the highest rainfall occurred in July (556.33 mm) and the lowest in December (3.56 mm). From the study, the soil moisture was found to be low over 50% of the study area during the winter season. In the study area, the groundwater quality in the study area was found to be good, meeting the required standards for drinking purposes regarding pH, electrical conductivity, nitrate, and fluoride. It also revealed that the groundwater depth decreases during the dry season. The surface runoff was found to be lowest in January (0.22 mm) and highest in July (385.18 mm), which was consistent with the rainfall pattern, with more runoff occurring during the rainy season. The results revealed that the present water availability was highest during the monsoon season with its peak in July (380 mm) and

lowest during the winter season, with its off-peak in January (10 mm), which showed a clear seasonal pattern of water availability.

The study predicted the rainfall in the study area with coefficient of determination i.e. R^2 values of 0.92 for Kohima and 0.85 for Dimapur. The model also predicted the maximum and minimum temperatures in Kohima with the help of R^2 values of 0.99 and 0.98; and 0.92 and 0.93 in Dimapur. Future climate projections revealed that there would be an increase in both rainfall and temperature, with significant shifts in the distribution of rainfall across months. Despite the overall increase in rainfall, it is expected that there will be water shortages during the winter season, as water availability was found to be lacking for crop needs during the winter.

Human power still being the primary source of farm power in the study area. Chili and potato farming were found to be the most profitable crops among the six major crops, i.e., rice, maize, beans, potato, soyabean, and sugarcane, suggesting that farmers should consider shifting to these crops to improve economic returns in the face of fluctuating water availability. The mechanization index was low, indicating heavy reliance on traditional farming methods. Improved implements and tools such as a garden rake, khurpi, sickle, hand fork, hand hoe, Naveen dibbler, tubular maize sheller, and improved seed drill, were recommended to reach the mechanization index of mechanized states of India like Punjab, Haryana, U.P. It is expected that these findings can serve as vital information for implementing precautionary measures in the future for developmental activities or better management of water resources, for climate change adaptation strategies to enhance crop production by utilizing agricultural inputs properly.

Keywords: Agricultural water availability index (I_{AWA}), Climate Change, Rainfall, Mechanization Index (MI), Water resource management

CHAPTER 1

INTRODUCTION

Water is an essential energy resource for the survival of all living beings on Earth. Water supports life on this planet in the growth of every organism, human needs, and economic development. Life on Earth has existed since all species have their habitats in and around water resources. Despite water encompassing around 70% of the Earth's surface, a minuscule fraction of freshwater is utilized for human consumption. For agricultural production, nearly 70% of the withdrawal volume of water is used, while the industrial sector and the domestic use only 22% and 8% volume of water, respectively (Aivazidou *et al*., 2016).

The availability and scarcity of water are not only a concern for the future, but also a reality in both the developed and developing worlds (Tidwell *et al*., 2018; Kumar *et al*., 2018). Potentially, water scarcity can impede society's desired economic and social growth. As a result of increased demand for water caused by population growth, urbanization, and industrialization, as well as climate change, water scarcity is occurring all over the world. In many advanced and developing countries, there have been reports of conflicts over future water allocations for various purposes (Tidwell *et al*., 2018).

The population of the country rose from 1.21 billion in 2011 to 1.31 billion over the 10 years, representing 17.7% of the global population (Vohra and Franklin, 2021). The per capita water availability in the country has declined from 1519 m^3/year in 2011 to a projected decline of 1486 m^3/year for 2021 (Parikh and Nair, 2019). Due to the spatial variation in rainfall, the per capita water availability also varies from basin to basin. The water demand is a global phenomenon due to overpopulation and related factors; all humans have started depleting in an unplanned and unscrupulous manner by exploiting water resources. The scarcity has been observed in arid regions and areas with torrential downpours (Krishna *et al*., 2004). Water scarcity is a serious problem that impedes any society's long-term growth (Shah and Narain, 2019).

Therefore, quantifying water availability, consumption, and management has become crucial in the current scenarios to plan for growing crops systematically. Water availability implies the provision of water over what is already allowed for consumptive use within a specific basin, indicating the quantity of water accessible for further development. Water availability and usage are heavily influenced by the hydrology of the basin, climatic conditions, land use characteristics, legal and regulatory structures, and the values of the basin's inhabitants. Water availability and the dynamics of water resource usage in an area must be characterized (Barlow *et al*., 2004). The World Business Council for Sustainable Development defines water scarcity as cases in which all needs, agricultural, industrial, or domestic, cannot be met, given the lack of water. Agriculture is a critical sector in most developing countries. It enables farmers to accomplish the developmental objectives, such as equity, self-reliance, and growth.

India has five primary climatic regions: tropical, arid, semi-arid, temperate, and alpine significantly influence its ecological landscapes and agricultural practices. The country is geographically diverse; therefore, during dry seasons, many regions experience water scarcity. During that time of the year, millions of people rely on groundwater as their main source of drinking water as well as for agricultural purposes. In India, over-extraction of groundwater has depleted crucial water tables in different regions of the country.

Anthropogenic and climatic activities persistently impact many hydro-meteorological systems. These effects manifest as trends in rainfall, temperature, evapotranspiration, stream flows, etc. Further, these trends could be geographical (a trend in place) or temporal (a trend in time) in time. Such tendencies are crucial for researching several facets of climate change. Climate change could affect water supply availability and short-term uncertainty in several places. Possible regional effects of climate change include more frequent and severe floods and droughts as well as long-term changes in mean renewable water supplies caused by changes in temperature, humidity, soil moisture, wind intensity, nature and extent of vegetation, duration of accumulated snowpack, and runoff (Solomon *et al*., 2007). Water use would be affected by climate change-related behavioral changes, such as shifts in heating and

cooling demand. Although annual global per capita runoff would likely rise in a warming climate, increases (mostly in East and Southeast Asia) are expected to happen mostly in high-flow seasons, raising the demand for water capture and storage and the possibility of flooding (Bates *et al*., 2008).

India is prone to the effects of worldwide climate change that strikes Indian agro-climatic conditions, resulting in erratic rainfall patterns, higher temperatures, and eventually influencing the replenishment of aquifers and rivers. The devastating consequences of water scarcity are leading to lower crop yields and increased food prices in India. Ultimately, reduced water availability impacts agriculture in the country. If such a situation prevails in the future, India and other developing countries whose economy is based on agriculture will be affected. In such cases, the changing climate scenarios would be of concern for a growing population, rising industrialization, and related needs for new energy and food. Given the area's great sensitivity to these changes, an increase in extreme weather events will be quite significant. The forecast indicates that warming will differ by site, with more and less rainfall. Moreover, changes in climate variability, as well as the frequency and intensity of certain extreme weather events, would result.

The climate of India's North Eastern Region (NER) ranges from subtropical to alpine, within a heavy rainfall zone. The region is defined by its diverse topography, great diversity in slopes and elevations, land tenure systems, and farming techniques. Despite receiving heavy rainfall, the North-Eastern States face increased water scarcity daily due to inadequate water management. Irrigation systems in the region are underdeveloped, and for agricultural purposes, water storage and distribution mechanisms have not been created. Consequently, most NER farmers rely on the southwest monsoon for their farming operations; meteorological data indicate many states are experiencing "drought" or drought-like conditions. The north-eastern region of India is expected to be more vulnerable to the consequences of climate change (Das *et al.*, 2009).

Considering that 70% of the population in Nagaland depends on climate-sensitive industries, including agriculture, fisheries, forestry, etc., climate change is a significant concern in Nagaland. Despite Nagaland's ample water resources, including springs, perennial rivers, sufficient rainfall, and groundwater aquifers, the state is

confronting a challenge due to freshwater scarcity. Water Resources Development and Management in Nagaland (Chorley, 1969) observes that the study of water offers a rational connection between knowledge of physical and social surroundings. Water, a limited resource, will become a major limiting factor in socio-economic development unless early action is taken.

Numerous studies have also emphasized the depletion of water resources in the state, leading to a drought-like situation (Dash *et al*., 2012; Goyal *et al.,* 2019; de Fraiture & Wichelns, 2010; Yadav, 2020; Sarkar and Maity, 2020; Salman *et al*., 2020). Amongst all North-East states, Nagaland was evident to receive less rainfall in 2014 (Dikshit and Dikshit, 2014).

Agriculture in the state is rain-fed, with 90% of the crops grown during the *kharif* season. The average productivity of food grain was 2091 kg/ha, closely aligning with the national average of 2490 kg/ha. Food grains production in the state was 570.44 Mt in 2011-2012, which increased to 755.59 Mt in the year 2020-21, registering a percentage increase of 24.50% (Ngullie and Deka, 2022). Recent trends indicated a growing focus on cash crops such as chilies, tomatoes, and ginger (Roy *et al*., 2020). However, because the present pace of food production in the state is insufficient to fulfill the population's growing demand, the state has to import food from other states. The state, unlike the rest of the northeast region, has a certain distinct factor, viz., undulating topography, hilly terrain, high rainfall, heavy landslides, demography, community, and an individual-based land tenure system, etc., that hampers the application of the modern agricultural farming system.

From the scenarios mentioned above, it is understood that there is a pressing need to formulate the water availability index, including all the water availability factors, such as quantity, quality, and accessibility, into a single index variable that can portray the complete picture of the water situation for agriculture in the study area. This primary informative indicator can assist the decision-makers in quickly quantifying, such as quantity, quality, and accessibility, which can show the whole picture of the water situation for agriculture in the study area.

Furthermore, projected rainfall, river runoff, and temperature estimates can provide a more accurate representation of future water supply. From these projections

of future water availability, planners and policymakers may establish more effective management targets to solve water shortages and surpluses. To alleviate the seriousness of the situation, the priority must be given to the management and development of water resources in Nagaland by indexing available water, advocating a proper utilization plan, and recommending a suitable mechanization strategy for the state.

Research gap and rationale

While the context above establishes the scale of water scarcity and the NER paradox of "high rainfall yet frequent scarcity," most prior work has evaluated single components (rainfall trends, groundwater status, or runoff) independently for Nagaland and the wider NER. A comprehensive agricultural water availability assessment that integrates rainfall, soil-moisture storage, surface runoff, and groundwater quantity–quality into a single decision-support metric is largely absent. This gap makes it difficult to compare spatial–temporal patterns and to prioritize interventions. The present thesis addresses this by formulating an Agricultural Water Availability Index (I_{AWA}) tailored to hilly ecosystems, enabling integrated diagnosis of "quantity–quality–accessibility" and informing location-specific strategies for conservation, storage, irrigation, and mechanization.

Hypotheses

1. A composite index, incorporating multiple hydro-climatic variables (e.g., precipitation, runoff, soil moisture, groundwater levels) and agricultural demand, can accurately represent the spatiotemporal variation of agricultural water availability in the study area.
2. The developed I_{AWA} will reveal significant spatial variability, identifying specific sub-regions within the study area that are more water-stressed than others.
3. The implementation of specific water management strategies (e.g., improved irrigation efficiency, rainwater harvesting, or reservoir management) can significantly mitigate the negative effects of climate-induced water variability.

4. The adoption of specific water-efficient agricultural implements (e.g., drip irrigation systems, conservation tillage equipment) is positively correlated with improved water-use efficiency at the farm level.

Keeping in view the facts and research gaps as stated above, the present research has been undertaken in Kohima and Dimapur districts, with the following objectives:

1. To develop an Agricultural Water Availability Index for assessing the current situation of water availability in the study area.
2. To assess the impact of climate change on the temporal and spatial variation of water availability in the study area.
3. To identify and recommend an acceptable climate change adaptation strategy to address water shortage or excess in the near future.
4. To assess mechanization index and recommend suitable agricultural implements under less water availability situation.

CHAPTER 2

REVIEW OF LITERATURE

Assessment of water availability for sustainable agricultural production under a climate change scenario in Nagaland is the main objective of this present research work. Assessment is done for two unique districts of Nagaland, viz. Kohima (hilly topography) and Dimapur (valley), where the method of cultivation and type of crop grown are different. The data collected from secondary sources of the last seventeen years (2003-2020) for rainfall, MODIS (Moderate Imaging Spectroradiometer) for 2011, groundwater depth data for sixteen years (2004-2019), groundwater quality data for 2020, were assessed and predicted for the future period of 2021-2038, 2039-2059, 2060-2080, and 2081-2100, taking 20 years interval except for 2021-2038 (18 years). Further, the mechanization index was also assessed in the study area to recommend some suitable implements and machines to cater to the need for mechanization.

In the past, researchers have made attempts to assess the Agricultural Water Availability Index, the impacts of climate change on spatial and temporal variation of water availability, studies on acceptable climate change adaptation strategies to address water shortage or excess, farm power availability, and agricultural mechanization index to enhance the degree of farm mechanization.

The relevant published literature was reviewed and highlighted on all these aspects in this Chapter.

This chapter is organized under the following headings:

2.1 Agricultural Water Availability Index for assessing the current situation of water availability.

2.2 Assessment of the impact of climate change on temporal and spatial variation of water availability.

2.3 Identify and recommend an acceptable climate change adaptation strategy to address water shortage or excess in the near future.

2.4 Assessment of mechanization index and recommend suitable agricultural implements under water shortage or excess field situation.

2.1 Agricultural Water Availability Index for assessing the current situation of water availability

The agricultural water availability index (I_{AWA}) is a method that includes insight into water availability from rainfall, soil moisture, groundwater quantity and quality, and surface runoff.

2.1.1 Rainfall interpolation

Rainfall is an essential data point for managing water resources, modeling hydrology and ecology, assessing recharge, and scheduling irrigation. Typically, well-planned networks of rainfall stations collect this data as observational information. The rainfall is characterized by significant diversity in both spatial and temporal dimensions. Estimating rainfall may be achieved using spatial interpolation algorithms.

Dirks *et al.* (1998) evaluated four different spatial interpolation techniques for rainfall data gathered from 13 rain gauges covering an area of 35 sq. km on Norfolk Island. The comparison sought to identify the most efficient way to get continuous rainfall estimates over the island for different integration times. Surprisingly, the more complicated kriging technique was outperformed by the computationally simpler techniques, such as inverse-distance weighting (IDW), Thiessen, and areal-mean. The study suggested the inverse-distance approach for spatial interpolation, especially with dense spatial networks, to better integrate the traits of spatially changing rainfall.

Yunfeii *et al*. (2007) compared the effectiveness of IDW, simple kriging, and ordinary kriging interpolation techniques for rainfall data in the Ganjiang drainage region. The most appropriate approach was found using several interpolation techniques with identical parameters and taking trend and anisotropy into account. When the mean is known, findings indicate that straightforward kriging has the greatest accuracy. Kriging effectively reflects larger-scale rainfall trends, while IDW

is better for local detail changes. Weak autocorrelation was observed in the rainfall data, and the exponential semivariogram model provided the highest precision. Ignoring trend influence and anisotropy did not affect interpolation precision.

Tao *et al*. (2009) examined the rainfall series from 30 rain gauges to improve small-scale rainfall interpolation in the Great Lyon area. Results revealed that the Kriging model and parameter should vary based on the rainfall series, and IDW and Spline methods may be more suitable for regions with a high density of rain gauges.

Chen and Liu (2012) investigated the correlation between interpolation accuracy and two important IDW components: power (α value) and search radius. With a subset of 12 from the Taichung Irrigation Association used for cross-validation, the study gathered data from 46 rainfall stations spanning 1981 to 2010. Using the root mean squared error, the perfect values for the radius of influence and control parameter (α) were estimated. The findings indicated that the best radius of influence for IDW fell between 10 and 30 km and that the ideal alpha values differed from zero to five. Moreover, the research indicated that, especially in the dry season, IDW was a suitable technique for spatial interpolation with strong correlation coefficients exceeding 0.95.

Mahalingam *et al*. (2014) studied the spatial variations of 0rainfall in Mysore district, Karnataka, India. The region where average rainfall may be anticipated in the future was determined by calculating the coefficient of variation after year-by-year spatial fluctuations in rainfall (2000–2012) were examined using the IDW technique in GIS. The results revealed that the study area has fluctuations in rainfall, with low, moderate, and high variations observed in 1,156 sq. ft. km², 5,026 Sq. Km, and 58.93 Sq. Km, respectively.

Yang *et al.* (2015) investigated various spatial interpolation techniques to generate fine daily rainfall data from regional climate simulations. Examined to both station rainfall data and simulated rainfall were four often used techniques: ANUDEM, Spline, IDW, and Kriging. Several factors were used to assess the efficacy of these approaches. The results indicated that the Inverse Distance Weighting (IDW) method was relatively straightforward to use in a Geographic Information System (GIS) and

outperformed the other methods by a small margin. The IDW method was then applied with a spatial resolution of 100 meters to produce a 40-year sequence of rainfall data for the Greater Sydney Region (GSR) at daily, monthly, and annual intervals. The obtained data were used to forecast the erosive potential of rain and, evaluate and develop community-level climate change adaptation plans.

Pandey *et al*. (2016) performed spatial interpolation using rainfall data from several raingauge stations in the Bisalpur catchment. They used various techniques in GIS, such as Theissen polygons, Natural Neighbor (NN), IDW, Trend, Spline, Kriging, and Topo to Raster. The results were evaluated using RMSE, variance, correlation, fractional bias, and FA_2 (%). Among these methods, Topo to Raster produced the most reliable interpolation results, while the worst performance was observed with NN. Therefore, Topo to Raster was chosen as the most reliable model for interpolation.

Das *et al*. (2017) evaluated the performance of Kriging, IDW, and Spline spatial interpolation techniques. For 19 standard meteorological weeks, the weekly average rainfall data from 1901 to 1985 were used. By assessing the mean absolute deviation and mean squared deviation errors, the analysis sought to identify the most effective interpolation technique. The study concluded that the IDW approach was the best spatial interpolation method since it performed better than the other two strategies.

Aher *et al*. (2019) estimated spatio-temporal variability in rainfall using 15 years of daily rainfall data (2000-2014) from 39 rain gauge stations in and around the Upper Godavari basin by statistical computations and GIS techniques. Mean annual rainfall, mean half-decadal, and other statistical parameters are used by the study to find orographic effects and spatial rainfall distribution. Rainfall is spatially estimated with inverse distance weighting interpolation. With rising monsoon intensity from 2000 to 2006 and declining intensity later, the study findings reveal significant spatio-temporal variability in rainfall during 2010-2014 and lower variability during 2005-2009. The method finds micro-level rainfall variation that can support the sustainable management of water resources.

Ryu *et al.* (2021) employed compressed sensing (CS), a novel framework for signal acquisition and smart sensor design, to propose new spatial precipitation interpolation schemes. The interpolation of precipitation maps was achieved in high resolution by obtaining sparse coefficients of radial basis functions (RBFs). Two types of CS matrix methods were designed: one derived from an m × n (n × m) weights matrix of IDW and an n × n RBF matrix, and the other consists of an m × n RBF matrix based on a few observation vectors and several unknown vectors. The proposed CS methods can be represented at high resolution due to interpolation based on many bases, preventing variance values from being smaller than actual values.

Noor *et al.* (2022) investigated the intensification of rainfall on the island of Java; the area where rain occurs is a key parameter for climate change. They use spatial classification and interpolation methods, such as Random Forest and IDW, for rainfall interpolation. Daily models achieve the best accuracy in the 5D model sub-model C, while monthly models achieve the best in the B4M sub-model. Results showed daily predictions for June 1-4, 2022, predict light rain, sunny, and cloudy days from June 5-7, and cloudy days in August and June 2022. Monthly predictions show cloudy conditions in most of Java, with light rainfall in May, July, October, and September.

Shadeed *et al.* (2022) found the optimal approach to create interpolated rainfall surfaces in the Faria catchment, Palestine. Using seasonal rainfall data from 16 sites across two rainy seasons (2016/2017 and 2017/2018), six GIS-based spatial interpolation methods—including IDW, Spline completely regularized, Spline with Tension, Ordinary Kriging (OK), Universal Kriging (UK), and Regression—were evaluated by visual observation and cross-validation. The findings indicated that the UK was the most appropriate tool for mapping rainfall distribution in the study area since it had the greatest correlation coefficient and the lowest mean relative error. The performance of the various techniques in the catchment was also affected by the spatial distribution of rain gauges across seasons.

Paradkar and Mittal (2024) conducted a study on the precipitation patterns in southern Rajasthan, specifically analyzing the quantity and temporal fluctuations. The researchers employed the Standard Meteorological Weeks (SMW) and historical

weekly rainfall data. They applied the IDW interpolation technique available on the ArcGIS platform for geographical analysis. With an average weekly rainfall varying from 2.1 to 68.4 mm, the results show a significant amount of rain between SMW-22 and SMW-42. Weekly rainfall showed notable variation as the standard deviation often surpassed the average. Apart from the peak monsoon season (SMW-30), most stations in the study area showed no significant trend in annual rainfall data. These results improve understanding of the regional rainfall patterns, which are crucial for the efficient control of water resources and agricultural activities.

Workneh *et al.* (2024) analyzed Ethiopia's six rainfall station regimes, covering 1.13 million sq. km, and used high-resolution spatiotemporal rainfall data for hydrological studies. The techniques consisted of IDW, kriging, multivariate linear interpolation, and individual linear interpolation depending on elevation, aspect, slope, and kriging. Cross-validation of rain gauge stations and ENACTS data evaluated the performance of these techniques. The findings validated the need for six rainfall regimes for interpolation research. While slope and aspect-based interpolations did well in regimes II and III, elevation-based interpolation was predominant in regimes I and IV. The study advises kriging for regions with little orographic and local climatic variation and elevation-based interpolation for mountainous areas.

2.1.2 Soil moisture storage

The water content in the soil, held in the gaps between soil particles, is soil moisture. Soil moisture affects relationships between the land surface and atmosphere, therefore affecting weather and climate. Remote sensing data can show complete information about the Earth's surface when compared to conventional soil moisture monitoring techniques.

Wan *et al.* (2004) used Terra-Moderate Resolution Imaging Spectroradiometer (MODIS), Land Surface Temperature (LST), and Normalized Difference Vegetation Index (NDVI) data to create a near-real-time drought monitoring system. Surface reflectance and thermal qualities are combined in the Vegetation Temperature Condition Index (VTCI). Using ground-measured precipitation data across a study

area spanning portions of Texas and Oklahoma in the Southern Great Plains, USA, a case study was conducted to evaluate the VTCI approach. Linear correlation analyses of VTCI and total monthly precipitation, as well as deviation from normal monthly precipitation, revealed that VTCI was closely associated with recent rainfall events and prior rainfall quantities, implying that VTCI could be a more effective and real-time drought monitoring strategy.

Hossain *et al.* (2006) investigated the mapping of regional variation in surface moisture in Southern Africa using reflective and thermal ASTER data. Their findings demonstrated that employing various techniques to measure changes in surface moisture provides valuable insights for monitoring drought conditions in Southern Africa. The triangular space method proved to be a more precise technique for estimating moisture fluctuations.

Wang *et al.* (2007) established the regression connections at a 1 ^{km} scale by combining three years of 1 km NDVI and LST records from the Moderate Resolution Imaging Spectroradiometer (MODIS) in conjunction with ground-measured soil moisture data. The findings showed a strong relationship between MODIS NDVI and LST and the ground-recorded soil moisture. The land cover and soil type influenced the regression relationships. For the study area, the regression links can generate soil moisture estimates at a low resolution.

Potithep *et al.* (2009) identified one of the most important factors in the biological process to grasp the belowground biomass or soil carbon as the soil's moisture or water content. This work attempted to correlate the data from satellite photos to evaluate the water content of the soil. It looked at how soil water content and the normalized soil index (NDSI), set using near- and shortwave infrared wavelengths, interacted with one another. Results indicated that NDSI-based channel 6 at 10 cm depth had the greatest linear relationship ($R^2 = 0.81$).

Han *et al.* (2010) studied the soil moisture using the multitemporal data products from the Moderate Resolution Imaging Spectroradiometer (MODIS) in the larger Changbai Mountains. Data products included Land Surface Temperature (LST),

Normalized Difference Vegetation Index (NDVI), and land cover categories. The data was narrowed down to four significant time points across nine distinct periods in 2007, specifically focusing on the inversion of soil moisture conditions. The temperature-vegetation dryness index (TVDI) was calculated from the wet-edge and dry-edge correlations to show changes over time in the moisture levels of the soil on the land surface in the study area. The results showed that the combination of Normalized Difference Vegetation Index (NDVI) and Land Surface Temperature (LST) can greatly enhance the ability to precisely assess soil moisture levels over a large geographical area and with regular measurements. The parameters correctly reflect the moisture level of the surface soil and strongly correlate with the relative field-collected soil moisture (R^2>0.70). Seasonal variations show that the TVDI trend is lower in the wet season in the specified area.

Pandey and Pandey (2010) studied the spatial and temporal variability of the soil moisture at C.T.A.E. Udaipur, India, and reported that the krigged values were more representative and a genuine representation of soil moisture values. Historical soil moisture values allow one to predict the krigged soil moisture values at a given time and location. The statistical characteristics indicate a considerable reduction in soil moisture variability following kriging. These projected values, coupled with the essential knowledge about the crops to be cultivated and their anticipated yield, aid in optimal irrigation scheduling.

Yang *et al.* (2013) proposed a modified triangle approach, known as the Ts/VI space, for the calculation of the temperature vegetation dryness index (TVDI). The space was constructed with the Normalized Difference Vegetation Index (NDVI) and the Enhanced Vegetation Index (EVI). Using 20 MODIS images (land surface temperature and vegetation index products), this approach calculated the TVDI to evaluate the soil moisture situation in the Northern China Plain. In situ moisture data gathered from 133 agricultural sites were used to validate the TVDI. Eventually, the relationship between TVDI and precipitation was looked at. The research found that while the TVDI calculated using EVI is often more sensitive to soil moisture conditions, the TVDI computed using NDVI is quite responsive to soil moisture at a

depth of 20 cm. There was a strong correlation between TVDI and rainfall. Rain would increase the moisture level of the soil, therefore allowing the computation of the TVDI.

Feng *et al.* (2014) evaluated soil moisture levels by observing the temperature vegetation dryness index (TVDI). The LST-VI space was constructed utilizing nine pairs of MODIS products (MOD09A1 and MOD11A2) with moderate resolution, covering five provinces in Southwest China. NDVI, EVI, and MSAVI were utilized consecutively to generate three LST-VI spaces. We analyzed the correlations among the three TVDIs derived from LST-NDVI, LST-EVI, and LST-MSAVI, and the soil moisture measurements from 98 sites. The results illustrated the efficacy of TVDI in assessing soil surface moisture levels. The TVDI obtained from the LST-EVI space (TVDIE) exhibited a more robust correlation with soil moisture as compared to TVDI computations based on the LST-NDVI and LST-MSAVI spaces. The usefulness of the TVDIE approach for monitoring soil moisture conditions was established by analysis of multiple TVDIE space stages.

Bhambure *et al.* (2017) investigated to assess the soil moisture variation and vegetation indices for the Savitri basin. The moisture variation in the area was estimated by the NDWI and VI-LST methods using the satellite data Landsat 7 and Landsat 8. The NDWI (Normalized Difference Water Index) was calculated using Near-infrared (NIR) and Short-wave infrared (SWIR). Moreover, the Landsat imagery for 1999, 2000, 2002, and 2003 was classified into three moisture classes, i.e., very low, low, and moderate. In addition, the moisture percentage was demarcated by threshold DN values. LST was calculated using thermal (band 6) of the Landsat. The MSAVI and LST images were stacked to create a feature space image. The image was the unsupervised classification method into the three classes. In 1999, the moisture variation occurred between 21.95 to 23.54 percent at a DN value of 80000; in 2000, the moisture variation was 21.75 to 23.49 percent at a DN value of 80000. In 2002 and 2003, moisture variation was 24.71 to 32.40 and 7.92 to 24.07 percent at DN values 40000 and 30000. Moisture available is moderate in the land portion, and the hilly section is low.

Bai *et al.* (2020) estimated the soil moisture profiles using satellite NDVI and LST products at the regional scale. Conducted in the Qilian Mountain Ranges, China, the study was split into 31 zones according to altitude, vegetation, and soil type. At every zone, long-term in situ soil moisture observation stations were set up; five layers' worth of moisture was gathered using soil moisture probes. Estimating soil moisture (0-70 cm) on a regional scale, several linear regression equations were created for each soil layer at the 31 zones. With a soil moisture content of 14.5%, the findings revealed that the eastern area had more soil moisture than the western one. The findings and methods provide fresh uses of remote sensing to assist hydrological studies in mountainous regions and soil moisture data collection.

Hassim *et al.* (2020) compared rainfall interpolation in the Langat River Basin using the IDW, OK, Simple Kriging (SK), and Kernel Smoothing (KS) techniques. Reference data came from rainfall records from 2008 to 2017. The study sought to contrast these techniques with a geostatistical wizard in ArcGIS. Mean error, Root The efficacy of the methods was assessed using the mean error, RMSE (Root Mean Squared Error), RMSSE (Root Mean Square Standardized Error), and ASE (Average Standard Error). The SK approach outperformed the Langat River Basin's IDW, OK, and KS methods by showing better statistical evaluation. The work highlights the significance of complete rainfall data in hydrology models.

Koley and Jeganathan (2020) used Landsat 8 Optical Land Imager (OLI) and Sentinel 2A Multispectral Instrument (MSI) to project the surface soil moisture at high spatial resolution. Soil moisture at 30 m and 20 m, respectively, was estimated using the thermal and short-wave infrared bands of Landsat and Sentinel images. Dryness was estimated using the red and near-infrared bands. By combining multi-sensor and multi-resolution feature space, the study closes the gap. Using Soil Moisture Active Passive (SMAP) and Climate Change Initiative (CCI), the downscaled soil moisture data were validated; a notable correlation was found for thermal band-derived soil moisture, short-wave band-derived soil moisture, and red and NIR band-derived dryness. The study also revealed temporal continuity and spatial spread errors in the projected soil moisture.

Peng *et al.* (2020) studied the temperature vegetation dryness index (TVDI), which combines LST and NDVI. They calculated the TVDI using LANDSAT 8 operational land imager/thermal infrared sensor images and 96 in situ soil moisture measurement observation points. Results revealed a significant negative relationship between the TVDI and soil moisture, indicating that the TVDI can indicate soil moisture conditions in the Longmen Mountains (TZ). Emphasizing the spatial patterns of soil moisture content in the TZ, western China, the paper offers a method for optimizing soil parameterization in agricultural water management using remotely sensed soil moisture.

Sabah and Afsar (2020) investigated the soil moisture changes using different perspectives, including soil moisture index (SMI), NDVI, LST, and SMI with LST and NDVI. Satellite images from Landsat 8 OLI/TIRS and Landsat 4-5 TM were used. The study found that SMI with LST decreased due to increased LST, while SMI with NDVI and LST and NDVI increased. High values of no-change classes graphically revealed all changes.

Felegari *et al.* (2022) conducted a study on the Normalized Difference Vegetation Index (NDVI) in the forested region of Gilan. They utilized data from Landsat sensors and SMAP sensor photos spanning a period of three years, from 2016 to 2018. The findings indicated that Gilan province saw the highest levels of rainfall and soil surface moisture in 2016, but the lowest levels were seen in the same province in 2017. The NDVI value reached its peak in 2017, measuring 0.441, and hit its lowest point in 2016, measuring 0.392. The study also discovered a negative correlation between the soil surface moisture diagram and NDVI. Specifically, there is a negative correlation when the moisture diagram is decreasing and increasing, and vice versa when it is increasing.

Sharma *et al.* (2022) investigated the trends in the MODIS/TERRA-derived NDVI over Gautam Buddh Nagar, India, from 2005 to 2018. The region is sub-humid and has urbanization zones, forests, and arable land. NDVI-derived vegetation growth patterns revealed notable seasonal cycles and the interannual fluctuations. The NDVI seems to be more sensitive to LST than the soil moisture and precipitation because its

correlation with the LST is stronger. Winter had the highest NDVI values, followed by monsoon, post-monsoon, and pre-monsoon.

Naga *et al.* (2023) investigated the enduring correlations between the satellite-derived Normalized Difference Vegetation Index (NDVI) and many parameters during India's Kharif season from 2000 to 2018. The study determined that NDVI effectively represents the various stages of crop phenology and experiences year-to-year fluctuations that are driven by the El Niño Southern Oscillation. The Normalized Difference Vegetation Index (NDVI) exhibited a substantial dependence on surface soil moisture (SSM) and groundwater storage (GWS), displaying a large negative correlation coefficient with Land Surface Temperature (LST). The wavelet coherence spectrum showed a synchronized association with rainfall, SSM (soil moisture), GWS (groundwater storage), and an opposite phase connection with LST (land surface temperature), with less strong connections between 2004 and 2008.

Carlson (2024) examined the issue of remote sensing of soil water content based on a right triangle method. The fractional vegetation cover (NDVI) space and the pixel distribution in temperature revealed a resemblance to a right triangle. The model emphasizes overcoming the difficulties caused by sparse or low-resolution data and simplifies the analysis and interpretation of remote sensing data by adopting the form. The results showed that the right triangle model might be a useful tool for thermal and optical remote sensing.

2.1.3 Groundwater quantity and quality

Groundwater is a vital resource, but it is being overused and polluted. Focusing on the interrelationship between quantity and quality, the groundwater amount and quality show the best present knowledge on controlling groundwater resources.

Dash *et al*. (2010) investigated the pollution concentration levels and groundwater depth of the Delhi area. Groundwater depth and quality characteristics—including chloride, electrical conductivity, fluoride, magnesium, and nitrate—were attempted to be mapped in terms of their spatial variability. While ordinary kriging

was used to examine the geographical variation of groundwater depth and quality data, indicator kriging was used to evaluate groundwater quality parameters equal to or above the pollution threshold values. The semi-variogram parameters fit the spherical model for water quality parameters and the exponential model for water depth well. Groundwater depth was within 20 meters in 43% of the study area, as indicated by the created spatial variability maps. Of the examined area, 69% had salinity more than 2.5 dS m^{-1}; 36% had nitrate levels more than 45 mgl^{-1}. While 24% had the greatest probability (0.8-1.0) of surpassing the threshold value for electrical conductivity, the probability maps showed that 2% of the area had the highest likelihood of exceeding the threshold value for nitrate concentration in groundwater. The spatial variability and probability maps generated will enable water resource managers and legislators to develop guidelines for the sensible use of groundwater resources for drinking and agricultural use in the research area.

Srinivas *et al.* (2011) examined the groundwater samples for various physicochemical characteristics using the water quality index (WQI) to determine their acceptability for drinking. It was discovered that seven places had WQI values inside the parameters. High WQI scores were primarily caused by fluoride content. Appropriate corrective actions and groundwater augmentation structures are suggested in the research area to enhance groundwater quality.

Thakor *et al.* (2011) conducted an assessment of the Water Quality Index (WQI) and examined the impact of industry, agriculture, and human activity on its water quality of Pariyej Lake. To determine the Water Quality Index (WQI) for the summer, winter, and rainy seasons, measurements were taken of various physico-chemical parameters. All the metrics, including pH, Total Hardness, Calcium, TDS, Chloride, DO, Nitrate, BOD5, and Sulphate, were within the acceptable limits. Nevertheless, the amounts of both total alkalinity and magnesium are above the permissible limits set by the Indian Standards. Nevertheless, the WQI values obtained in the present study were found to be below 75 for different seasons, suggesting that the quality of water was below standard and unsuitable for human consumption.

Yadav *et al.* (2012) examined the hydrological characteristics of the groundwater in Agra. A total of 12 sites were utilized to gather water samples over the period spanning from February to May. The physicochemical parameters, including TDS (1020-4950 mgl-1), EC (1580-5200 m mhos), pH (7.2-7.7), Total Alkalinity (330-525 mgl-1), Turbidity (1.1-31.4 NTU), Total Hardness (240-1425 mgl-1), Calcium (72-436 mgl-1), Chloride (295-1140 mgl-1), Sodium (126.5-1254.9 mgl-1), Magnesium (14.6-151.2 mgl-1), and Potassium (1.9-60.6 mgl-1), were observed to exceed the natural background level of groundwater.

Singh *et al.* (2013) examined the artificial groundwater recharge zones using the geographical information system (GIS) and remote sensing for augmenting groundwater resources in the Bist Doab basin of Indian Punjab. The results indicate that 15, 18, 37, and 30% of the study sites, respectively, fall under "poor," "moderate," "good," and "very good" groundwater recharge categories. The western and middle parts of the region have the most possible recharge since high infiltration rates caused by the distribution of flood plains, alluvial plains, and agricultural land. The eastern and middle parts of the study area have the least effective recharging potential because of a low infiltration rate. The findings of the study could be used to create a good groundwater management strategy for the long-term, sustainable use of constrained groundwater resources.

Puzari *et al.* (2015) evaluated the drinking water quality from the Dimapur district of Nagaland and the Karbi Anglong district of Assam. Various quality parameters, such as hardness, arsenic, alkalinity, fluoride, pH, etc, were determined. The findings indicated that the research locations' water quality needs to be improved. Additionally, they discovered areas with excessive fluoride concentrations.

Ebrahimi *et al.* (2016) investigated the groundwater situation of the Damghan basin in Iran by examining various indicators of water quality for drinking as well as irrigation purposes and over time quantity depletion. The quantity analysis revealed a 30.92 million m^3 average annual withdrawal rate from this basin, which caused a total water level drop of 7.4 million m^3 between 1966 and 2010. The roughly 35-fold rise in total discharge rates during this time frame indicates that this basin has been

overexploited. This overexploitation has therefore caused groundwater quality to suffer. Piper and Chadha's diagram analysis of the hydrochemical facies of water gathered from sampling wells revealed Na-Cl as the general dominating type of water in the study area. During the quality assessment suitability of groundwater was assessed for irrigation and consumption. All regions were discovered to contain groundwater unfit for drinking as per the standard of the World Health Organization (WHO) recommendations. Research on key quality indicators also revealed that groundwater's high salinity rendered it unsuitable for agricultural applications. Ionic ratio analyses were used to analyze the saltwater intrusion, which was found to be the primary cause of the Damghan basin's excessive salinity and declining groundwater quality.

Adhikary and Dash (2017) compared the performance of four interpolation techniques. These techniques consisted of two stochastic methods—ordinary kriging (OK) and universal kriging (UK)—and two deterministic ones—inverse distance weighting (IDW) and radial basis function (RBF). The work aimed to forecast the spatiotemporal variation of groundwater depth in the National Capital Territory (NCT) of Delhi, India. Groundwater table data from 110 different Delhi sites for the year 2006, both before and after the monsoon season, were used to conduct an analysis. The study revealed that the IDW approach lagged behind the OK, UK, and RBF ones. The RMSE (root mean square error) values were observed to be 27.52%, 27.66%, and 51.11% lower for the OK, RBF, and UK methods, respectively, compared to the IDW technique. Additionally, the R^2 values were discovered to be 16.12%, 14.21%, and 21.36% higher for the RBF, OK, and UK methods, respectively, compared to the IDW method.

Njaben (2018) compared different spatial interpolation methods, viz., Kriging, Inverse distance weighting (IDW), and Radial basis functions (RBF), for the best spatial representation of the level of groundwater in the Salman district, Southwest Iraq. Based on a statistical comparison of the interpolation models, it was determined that the universal Kriging (UK) method had the lowest root mean square error (RMSE) value of 10.65, the lowest mean error (ME) value of 5.365, and the

groundwater level shows the highest coefficient of determination (R^2) value of 0.981in the study area.

Rao *et al.* (2018) analyzed the physical and chemical properties of groundwater at 30 different well sites throughout the Guntur region, Andhra Pradesh, India. The geographical information systems (GIS) and remote sensing techniques were used to accurately map the spatial distribution of groundwater quality. Utilizing ArcGIS 10.4, the interpolation technique known as inverse distance weighted (IDW) was employed. The IDW interpolation method estimated the spatial distribution of groundwater parameters, including chlorides, magnesium, carbonates, sodium, bicarbonates, sulfates, specific conductivity, hardness, potassium, and pH. This analysis facilitates the comparison of many metrics over different years.

Anand *et al.* (2020) conducted a spatio-temporal trend analysis using 32 years (1984-2015) of data on the depth of the groundwater table in the Bhavani River basin, Tamil Nadu, India. A study was conducted on the seasonal fluctuation of groundwater levels in 57 tube wells throughout different periods: pre-monsoon (March-May), post-monsoon (January-February), southwest monsoon (June-September), and northeast monsoon (October-December). The trend of the groundwater table was examined using Sen's slope estimator and the Mann-Kendall test. The investigation revealed a significant decrease in the groundwater table, with an average decline of more than 15 meters below the ground level. This finding emphasizes the excessive use of groundwater. During the southwest monsoon, it was revealed that over 50% of the basin had a decrease in the water table, which corresponds to the summer season. The study, which conducted a spatio-temporal analysis, suggests the installation of rainwater collecting structures in the study region to enhance the replenishment of groundwater.

Bagoria *et al.* (2020) studied soil parameters in the Sabour block of Bhagalpur district. They collected 80 composite surface soil samples from 14 panchayats and analyzed their data using the interpolation technique. The results showed that 52.5% of soil samples were neutral, while 41.25% were slightly alkaline. The study suggests

that normal EC is safe for crops, but low organic carbon levels suggest proper management practices.

Naleo *et al.* (2020) studied groundwater quality for drinking purposes at Patkai Campus, Dimapur, Nagaland. Eleven samples (Well 1 to Well 10) were taken to calculate the Water Quality Index (WQI), considering 11 parameters, i.e., pH, calcium, total hardness, calcium, nitrite, chloride, magnesium, sulfate, iron, total dissolved solids, fluoride, and Manganese. Data comparison with the second edition of the Bureau of Indian Standards (IS: 10500 (2012) Drinking Water Specification) was used. The outcome reveals an iron concentration over the permitted range. 0.3, meaning that a total of 8 out of 10 wells exceed the limit. The greatest values fall between 1.5 and 1.9. Four out of ten wells also have considerable turbidity in some samples. The pH reading that does not meet the BIS standard is from well No. 10, which shows a pH reading lower than the permitted range, ranging from 5.9 to 6.5 to 8.5. The magnesium concentration at well No. 10 is higher than the permitted limit of 200, i.e.,307.77. According to the study, the area's groundwater requires some sort of treatment before consumption and needs to be shielded from contamination risks.

Chaudhari *et al.* (2021) examined groundwater quality in the South-West zone of Surat City, Gujarat. The Water Quality Index (WQI) was calculated using groundwater data gathered from 2006 to 2015 for the Sultanabad water measuring station from the website (India-WRIS website). It also makes an approximation of the quality of the groundwater for the following ten years. According to the observed WQI results, the groundwater was determined to have a respectably high concentration of electrical conductivity, Total Dissolved Solids, Chlorine, Sulphate, Nitrate, and other contaminants that degrade its quality for drinking and other domestic uses. The findings of this study point to the necessity of a concrete improvement in groundwater quality achieved by a suitable technique like managed aquifer recharging (MAR). According to the findings of this investigation, groundwater quality falls into the low category per BIS (Bureau of Indian Standards).

Joshi *et al*. (2021) undertook a patio-temporal analysis of groundwater table depths in North Western India. Consistent water table depth data of 4417 wells from 1974 to 2010 were analyzed, and changes in groundwater levels were mapped using a geostatistical interpolation technique for both pre- and post-monsoon seasons. A trend filtering approach was applied to the data sets for determining the linear trend and rate of water-level change. Study indicated a rapid depletion of ground water storage by − 32.30 ± 0.34 cubic km and − 24.42 ± 0.34 cubic km for the pre- and the post-monsoon period during 2002 to 2010. Spatial heterogeneity in groundwater levels and storage was observed, and domain-specific groundwater management strategies were suggested

Krishnan and Sankararajan (2021) conducted a study on water suitability for irrigation and household determinations in Padmanabhapuram, district of Kanyakumari. For the study, 18 sampling locations were chosen, taking 10 parameters into consideration to determine the Water Quality Index (WQI). Twelve sampling sites were found to be appropriate for drinking, according to the findings. According to the integrated map, 883,417 m^2 (46.03%) and 950,704 m^2 (49.54%) of the area have poor water quality, respectively. 2725 m^2 (0.14%) and 7659 m2 (0.4%) were covered in excellent and good water quality for drinking purposes. The research area's 3.87 percent, or 74,336 m^2, cannot be used for food or drink. The results showed that electrical conductivity and total dissolved solids were more than the permissible limit at sampling stations (S14, S15, and S16), whereas there were more residual sodium carbonate values at S8.

Ghoderao *et al.* (2022) analyzed the quality of the groundwater of Jabalpur district, Madhya Pradesh, considering the following parameters: pH, Copper (Cu), Electrical Conductivity (EC), Chromium (Cr), Sulphate (SO_4), Nitrate (NO_3), Iron (Fe), Chloride (Cl), Total Hardness (TH), Sodium (Na), and Total Alkalinity (TA). The Water Quality Index (WQI) varies from 17.90 to 176.88 in the study area. The WQI rating indicates that sites 1, 3, and 4 are unsuitable for drinking water or have low water quality, whereas sites 2 and 5 have excellent drinking

conditions. They also suggested that the groundwater in the area with deteriorating water quality must be treated before consumption.

Wang *et al.* (2023) examined the impact of agricultural activities on groundwater dynamics and interaction with surface water in arid regions. It compares hydrogeochemical characteristics between irrigated and desert areas, focusing on the impact of rapid irrigation agriculture development. Results showed that cultivated land area increased by 121.8% between 2000 and 2020, mainly from grassland and bare land. Groundwater EC ranges from 786 to 49,400 μS/cm, with weakly alkaline properties. Shallow groundwater has a higher EC than other water components. Non-irrigation areas have greater stable isotopic and EC values, while desert areas have more depleted middle groundwater isotopic values. Streamflow and confined water are suitable for agricultural irrigation, while phreatic water in the oasis is unsuitable for irrigation. The long-term development of irrigation agriculture has led to groundwater level decline and salinization, with a strong interaction between phreatic and surface water.

Zavarah *et al.* (2023) developed a Groundwater Quantity-Quality-based Drought Index (GQQI) using multivariate Copula analysis of groundwater quantity and quality indicators. The index was applied to evaluate the quantity and quality of groundwater in the Lake Urmia basin, with 1084 monitoring wells. The GQQI was correlated with SSI, SGI, and SWI drought indices by 88%, 86%, and 61%, respectively. The index indicates more severe droughts than other indices, indicating the combined effects of groundwater quantity and quality. The multivariate GQQI can better represent drought severity and identify severe and extreme conditions than other univariate drought indices.

Gautam and Rai (2024) investigated the issue of groundwater resources in the Bist-Doab region of Punjab, India. The Multi-Criteria Decision Analysis (MCDA) was applied to analyze and create a detailed map (zoning) to identify the areas where the groundwater was abundant and of good quality for drinking and farming purposes. The study revealed that the groundwater quality in urban regions was poor and unsuitable for drinking purposes. It also revealed that many agricultural areas had groundwater

that was moderately good for irrigation purposes. It also highlighted that due to increased urbanization, the natural water infiltration had been affected. The study recommended sustainable practices in land use and more careful planning to ensure clean and adequate groundwater availability for the future.

2.1.4 Surface runoff

Surface runoff is a percentage of rainfall that prevents excess water from flowing into the surface due to saturated or impervious pores. It is crucial in water resources management and planning and is influenced by rainfall duration, intensity, and distribution.

Dube *et al.* (1991) developed curve numbers for different land uses in a Himalayan watershed by trial and error. From the developed curve numbers, runoff volume was estimated and compared with the measured data, and the results were well within the error limit of 25%, which is acceptable.

Yu (1998) gave a theoretical justification for the SCS method for runoff estimation. The most important presumption of the SCS curve number approach is that the actual retention to potential retention ratio and the real runoff to potential runoff ratio are equal. However, no theoretical or empirical support has been found for this assumption. This work demonstrates that the precise connection between rainfall and runoff in the SCS technique can be mathematically calculated with two straightforward but reasonable assumptions.

Mishra *et al.* (2004) assessed a substantial collection of rainfall-runoff data from 234 watersheds of varying sizes in the USA. Reviewed the revised model that utilizes the Soil Conservation Service Curve Number (SCS-CN) approach and includes the antecedent moisture in the calculation of direct surface runoff. The t-test findings and ranking-based grading comparison indicate that the improved MS model significantly outperforms the current SCS-CN technique.

Pandey *et al*. (2008) offered a technique for calculating direct surface runoff from long-duration rainfall that is dependent on the length of the rain and is based on

the well-known Soil Conservation Service Curve Number (SCS-CN) approach. Analysis of data from five Indian (large, in terms of area) watersheds reveals the calculated curve numbers to decrease with the considered duration, showing a characteristic value of minimum CN or maximum initial abstraction to occur in a watershed for a pre-selected AMC. Testing the proposed procedure on the separate (measured) rainfall-runoff event data sets from the same watersheds suggests the satisfactory workability of the method.

Sharkh (2009) analyzed an un-gauged watershed, using the empirical method (Q=CIA) for the estimation of runoff at its outlet, The watershed modeling system (WMS) is a comprehensive hydrologic modeling environment that provides a tool for all phases of watershed modeling including automated watershed and sub-basin delineation, geometric parameter computation, hydrologic parameter computation, and result visualization.

Pandey *et al*. (2009) evaluated the runoff using SCS-CN and GIS for agricultural watersheds. They claimed that a flexible and commonly used technique for runoff estimation is the curve number method, sometimes called the hydrologic soil cover complex method. This approach considers several significant watershed characteristics: soil permeability, land use, and antecedent soil moisture conditions. Runoff from the SCS-CN model altered for Palestinian circumstances has been estimated in the current work using a traditional database and GIS for the Wadi sued watershed in the Dura region of the Hebron district, West Bank.

Kumar *et al.* (2010) estimated the volume of runoff for a given rainfall event by adopting the SCS-CN method in the Mediterranean watershed. A thorough land cover and soil survey was conducted. From this study, it was said that the watershed was dominated by the soils, which were coarse in texture with higher hydraulic conductivities. The total runoff was greatly influenced by the medium-textured soils, and the linear formula underreported the runoff generated.

Muthu *et al*. (2015) utilized the GIS-based SCS-CN method to estimate the surface runoff. The soil characteristics, land use and land cover data, and the seasonal

rainfall patterns were analyzed, and the surface runoff depths for different hydrological soil groups were determined. The results indicated higher runoff depths in the inner part of the block, suggesting the need for water-harvesting structures. The research emphasizes the importance of accurate surface runoff estimation for water and land management, highlighting the role of engineering and vegetative measures in water conservation practices.

Tailor and Shrimali (2016) estimated the runoff of the Rupen-Khan watershed of Meshsana district in Gujarat from 1998 to 2014 by the SCS Curve Number method. IRS LISS III data, basin map, and drainage map are used for the generation of the land use and land cover (LULC) map and the hydrological soil group map, which is further utilized to assess the curve number and Antecedent Moisture Content. The hydrological soil group is identified from the existing LULC map, soil infiltration rate, and soil texture. Researchers prepared separate maps of the hydrological soil group and curve numbers. This method was found to be suitable for ungauged watersheds also.

Kumar *et al.* (2017) estimated the rainfall and runoff relationship using the SCS-CN method through the GIS approach in the Pappiredipatti watershed of the Vaniyar subbasin. The runoff ranged from 169-191 mm (2000-2014), and the computed normal, wet, and dry conditions curve numbers were 85.92, 72.8, and 93.46. The rainfall varied between 410 to 1650 mm.

Ara and Zakwan (2018) used the modified SCS-CN (Soil Conservation Service-Curve Number) method for estimation of runoff in the eastern canal originating on the Sone River, India, occupying an area of 70196 sq. km, and evaluated the factors like slope, area of the watershed, and vegetation cover. To calculate the antecedent moisture, the daily runoff for the year 2007 was used. The total runoff acquired in 2007 was calculated to be 17.98 mm. July, which accounted for 39.85% of the total runoff, saw the highest runoff. While the highest was in July (45.8 cm), the lowest rainfall documented in 2007 was in April (1.36 cm). The curve numbers (CN) I, II, and III were calculated to be 52.58, 72.53, and 85.86, respectively.

With the greatest contribution from the monsoon month, the total runoff for 2007 from the study area was calculated to be 17.98 mm.

Gandhi and Patel (2019) adopted the SCS-CN method for the runoff estimation for 20 years for the sub-basin of the Rajkot district. Using GIS, different thematic maps such as land use/land cover, soil map and slope map, and runoff volume were estimated. The runoff for the study area was estimated from June to September. The runoff coefficient was calculated using the rational formula and was found to be 0.06. By using the SCS-CN method, the CN for the watershed was calculated and found to be 68.06 under AMC-II, and again, the result by the SCS-CN method is compared with the rational formula and runoff coefficient method. After comparing the results of both adopted methods, it was concluded that maximum runoff was generated in July because of the higher precipitation in all three methods.

Sharma and Kanga (2020) studied the Sind River Basin, which has an area of 26207.02 sq. km and is located in the northern part of Madhya Pradesh, India. The average annual runoff from the year 2005–2014 was observed as 133.71 mm/year, whereas the maximum runoff for the river basin was estimated at 231.43 mm in the year of 2009, and the minimum runoff was 32.41 mm in the year of 2006. The average annual rainfall observed was 777.07 mm/year, whereas the maximum rainfall was 995.16 mm in 2009, and the minimum rainfall was 606.69 mm in 2006. Most of the study area was covered by group C of the hydrological soil group.

Walega *et al.* (2020) conducted a study on three places that include the coastal region of South Carolina, low low-relief watershed in Arkansas, and a high-relief watershed of North Carolina for the estimation of peak runoff and storm direct runoff using the modified SCS CN method. Empirical formulas were used for the determination of maximum retention, which was developed by Chen in 1982, which then used to estimate CN. They incorporated antecedent moisture content into the Original SCS CN method equation. This method is found to be unsuitable when the swamp and pond adjustment factor, $F_{p,}$ was taken as 0.72, which is the recommended value.

Shrestha *et al.* (2021) examined the influence of land-use change owing to urbanization on surface runoff during the era of fast urban expansion from 1980 to 2015 in Xiamen, China, using the SCS-CN method. The Landsat images from 1980, 1990, 2005, and 2015 were classified, and land-use change was analyzed. Results of analyses showed a 14.01% decrease in farmland area and a 15.7% increment in the built-up area from 1980 to 2015. Surface runoff for the rainfall return periods of 5, 10, 20, and 50 years was simulated using the GIS-based SCS–CN method. Results showed that the highest increase of 10.63% in surface runoff occurred between 1990 and 2005. With the fast growth in urban development from 1980 to 2015, the amount of runoff contributed by built-up land use type increased from 14.2% to 27.9%, which showed the effect of urbanization on runoff. The land use and surface runoff relationship stated the significant impact of land-use change on the surface runoff of the area.

Raghavan *et al.* (2022) conducted a study to assess the spatial and temporal variations in runoff potential under changing climatic scenarios using geospatial techniques in the Northern Part of Karnataka, India. Spatial runoff estimation models at the sub-district level were developed, and estimated runoff was validated using observed data, and results showed a good correlation (R^2=0.90). Results showed that the runoff potential ranged from 10 to 20 percent of the mean annual rainfall from 1951 to 2013. Khanapur subdistrict showed the most rain and runoff potential. Results revealed a growing trend in the number of subdistricts falling under the low-rainfall category (1100mm). The study also reveals how drought affects rainfall and runoff potential; the runoff produced from the maximum portion of the study area was Representative Concentration Pathway (RCP) 4.5 and RCP 2.6 scenarios, respectively. By the 2080s, the anticipated rise in runoff potential is>30.0% under RCP 8.5, 20.0% to 30.0% under RCP 4.5, and 10.0% to 20.0% under RCP 2.6 scenarios, respectively. The research indicated quite a high potential for supplemental irrigation, groundwater recharge, harvesting, and runoff use for in-situ moisture preservation, which will guarantee the long-term viability of the area.

Muneer *et al.* (2022) assessed the runoff in Ratga, an agricultural watershed in the Iraqi Western Desert, using the SCS-CN method, geographic information system, generalized regression neural network (GRNN), field observation data, and spatial data. Spectral reflectance data were used to determine the soil type of the study area, and the GRNN model performed admirably in predicting soil type, with a maximum absolute error of 8.44% for sand, 14.11% for silt, and 4.15% for clay soil. The results of the SCS method showed that CN values for normal conditions range from a low value of 70 to a high value of 85. The results of the study found that from 2018 to 2020, the maximum volume of surface runoff was 4,324,528 m^3.

Kale *et al.* (2022) estimated runoff using the SCS curve number method from the Kudavale micro watershed in the Dapoli Tehsil of Ratnagiri district of Maharashtra State. ArcGIS was used to extract the land use land cover map and hydrological soil group map; the CN was computed. The land use and land cover maps were created from Landsat 8 photos at 30 m resolution. Field-collected soil samples were analyzed using the Bouyoucous hydrometer technique to identify the soil texture; hydrologic soil group maps were then generated. The land use and land cover map indicated that the area under agricultural, forest, barren, and residential categories was 15.42 percent, 59.90 percent, 21.22 percent, and 3.4 percent, respectively. AMC I, II, and III conditions had curve number values of 58.31, 69.68, and 84.36, respectively. According to the textural study, the study area contained hydrologic soil group A, C, and D types. Runoff estimation was done on 30 years of rainfall data, from 1990 to 2019, collected and examined. Over 30 years, the average runoff of the watershed was 1532.27 mm, or 41.15% of total rainfall.

Akash *et al.* (2023) estimated the runoff in Nalgoda District, India, a semi-arid region facing water scarcity issues. The SCS-CN method was employed with data sources of DEM, soil maps, land use and land cover maps, and the daily rainfall data (10 years). The study revealed the curve number values for different soil conditions. They also stated that the approach was accurate for the calculation of runoff.

Mujeeb (2023) assessed the surface runoff in the Sanjab watershed in the Enjeal district, Afghanistan. GIS 10.4 Environment was used to generate soil, land use,

and slope maps. Surface runoff was estimated using rainfall data from 2012 to 2021by applying the SCS-CN method. In the year 2019, it was revealed that the highest surface runoff volume was recorded at 17,298,885 cubic meters, while in the year 2014, the lowest was at 9,061,754 cubic meters.

Vinutha *et al.* (2024) assessed the surface runoff in the Kurumballi sub-watershed in Shivamogga district, Karnataka, India. The surface runoff based on the SCS-CN method was evaluated using the land use and land cover (LULC), soil types, and rainfall patterns. The study revealed that the total estimated surface runoff volume was found to be 21,065,849.7 cubic meters. It also revealed that the study area was mostly classified into two hydrological soil groups: B (moderate infiltration) and D (poor infiltration).

2.2 Assessment the impact of climate change on temporal and spatial variation of water availability

Climate change significantly impacts the hydrological cycle, as changes in the precipitation and temperature play a key role in disrupting the cycle. It intensifies temporal and spatial variations in rainfall, the melting of snow, and water availability.

Fowler *et al.* (2007) reviewed the latest advances in downscaling methods for the hydrological modeling, connecting to climate change models to impact studies. Studies were carried out on the current downscaling literature, investigating new development fields, in particular for hydrological impacts. Since the 1990s, there has been a thorough assessment of the strengths and weaknesses of different downscaling methods. It concluded that many of the impacts of climate change will not be demonstrable in the near future (Wilby, 2006). There is a need for decision-making tools that are robust to future uncertainties for planning and management. It also concluded that for assessing climate change impacts, probabilistic methods seem to offer a more promising way.

Chu *et al.* (2009) studied the climate change scenarios in the Haihe River, China, by statistical downscaling of daily mean temperature, precipitation, and pan

evaporation. It found that statistical downscaling techniques successfully bridge the gap between local-scale hydrological response and large-scale climate change. Among them, SDSM is often used for its simplicity and power. SDSM can also be used to accurately simulate T Mean. The findings from H3A2 and H3B2, therefore, have exact mistakes in predicting extreme occurrences. Better simulations can be achieved by considering the pattern of seasonal change in storms and the quantity of precipitation. The total quantity of rain would mostly drop in comparison to the present climate.

Anandhi *et al*. (2009) utilized a support vector machine (SVM) to assess the role of predictors in downscaling surface temperature to river basins for IPCC SRES scenarios in India. For emission scenarios from 1978 to 2100, they ran simulations from the third-generation Canadian Coupled Global Climate Model (CGCM3) and used the National Centres for Environmental Prediction (NCEP) reanalysis dataset. The study discovered that SVM models for downscaling maximum and minimum temperatures performed better with land surface predictor variable usage.

Souvign *et al.* (2010) found that downscaling the AOGCMs (Atmosphere-Ocean General Circulation Models) is crucial for transferring climate change predictions to local levels. For the linear trends and extreme events, they accurately simulated maximum and minimum temperatures.

Hassan *et al.* (2013) predicted the future rainfall and temperature values using the statistical downscaling models in Peninsular Malaysia. It concluded that on a local scale, both the SDSM and LARS-WG models are suitable methods to evaluate the effects of climate change. Though SDSM performs better than LARS-WG, it slightly underestimates the lengths of wet and dry spells.

Al-Ghafri *et al.* (2014) analyzed the future temperature and precipitation variations in Muscat, Oman's capital city, using the MIROC general circulation model and the LARS stochastic Weather Generator. The results showed significant warming, ranging from 0.93^{O}C to 3.1^{O}C, with differences in precipitation projections being more significant than consistent warming. The lowest scenario predicted a 36.4% decrease in precipitation, while the highest scenario predicted an increase of 9.6% to 12.5%.

Further improvement is needed to address the spatial gap between the GCM grid scale and the local scale.

Hassan *et al*. (2014) examined statistical downscaling models for local meteorological variables in Peninsular Malaysia using SDSM and LARS-WG approaches. Results showed SDSM performed better than LARS-WG, and both models showed a general trend in mean daily temperature readings, despite not yielding exact findings.

Singh *et al*. (2015) projected the future precipitation and temperature by statistical downscaling in the Sutlej River Basin, India. It revealed that a rise in annual average TMax, TMin, and precipitation occurred in all scenarios under different scenarios for the 2020s, 2050s, and 2080s.

Saraf and Regulwar (2016) assessed the statistically downscaled weather data using the SDSM model in the upper Godavari River basin in India. Future precipitation, maximum temperature (Tmax), and minimum temperature (Tmin) were projected using two GCMs, CGCM3 and HadCM3. Presented for future periods—2020s, 2050s, and 2080s—were the changes in Tmax, Tmin, and precipitation under scenarios A1B and A2 of the CGCM3 model and A2 and B2 of the HadCM3 model. The scatter plots and cross-correlations helped to confirm the dependability of the simulation—maximum temperature rises in the future for nearly all the scenarios for both GCMs.

Jaiswal *et al*. (2016) described the impact of climate change on precipitation using the Statistical Downscaling Model (SDSM) in the Tighra Dam Catchment in Gwalior and Madhya Pradesh, India. Predictor variables come from the third-generation Coupled Global Climate Model (CGCM3) simulations of the National Centre for Environmental Prediction, or NCEP reanalysis dataset for 1979–2003. Cross-correlations are used to verify the dependability of the simulation.

Gulacha *et al.* (2017) used the SDSM for the Wali-Ruvu River Basin in Tanzania to assess the process of generating localized climate change scenarios for

temperature and precipitation. In this instance, ground stations and NCEP reanalysis atmospheric data from the United States National Center for Environmental Prediction were used. Had CM3 been the GCM employed, with A2 and B2 scenarios applied. Results indicated that for the Wami-Ruvu basin, the mean rainfall would change by 44–107%, 69–328%, and 68–648% during the 2020s, 2050s, and 2080s for the A2 scenario, while by 37–117%, 56–199, and 76–346% respectively for the B2 scenario. From 0.2 to 7.5 °C in the 2020s–2080s time frame, the average monthly maximum temperature showed a rising trend. During the same time, the minimum temperature fell from- -0.4 to -1.5 °C.

Jaiswal *et al.* (2018a) examined Raipur's lowest temperature, which was predicted using the Canadian Global Climatic Model (CGCM) predictors for three future periods for A1B and A_2 climatic forcing circumstances. Using the statistical downscaling model (SDSM), the k-fold validation technique has been used to produce multi-temporal series for the following periods: FP-1 (2020–2035), FP-2 (2046–2064), and FP-3 (2081–2100). The particular humidity at 850 hPa (nceps850gl), the 500 hPa geopotential height (ncepp500gl), and the surface airflow strength (ncep_fgl) were found to be the most helpful pertinent predictors to combine future scenarios.

Jaiswal *et al.* (2018b) studied the climate change assessment of precipitation in the Tandula Reservoir system of Chhattisgarh. Future rainfall data forecast under SRES of A1B and A_2 climatic forcing conditions. Multiple linear relations in calibration from 1981–1995 were tested with independent data from 1996–2003 for validation.

Abraham *et al.* (2018) evaluated the prediction of future runoff conditions under a changing climate using the multi-model outputs from CMIP5 over the Lake Ziway Catchment in the Central Rift Valley of Ethiopia. Using bias-corrected precipitation and maximum and minimum temperature data from HadGEM2-ES, CSIROMK-3-6-0, and CCSM4 models under typical concentration paths RCP 8.5 and RCP 4.5, future climates were derived. The Soil and Water Assessment Tool (SWAT) was used to model future Katar and Meki-river inflows toward Lake Ziway. Precipitation fell under the RCP 4.5 and RCP 8.5 projections, but maximum and

minimum temperatures rose. RCP 8.5's monthly average precipitation change percentage for the HadGEM2-ES model showed extremes from +23.15% in the 2080s to -51.19% in the 2050s. While the greatest drop was seen on RCP 4.5 at 17.49% for the CCSM4 model, the CSIRO MK-3-6-0 model's annual runoff depth from the Katar River dropped by up to 19.45% on RCP 8.5. On RCP 8.5 for the HadGEM2-ES model, the Mekong River had a maximum annual drop of 20.28% during the 2080s. Future water planning and management depend on ideal water use allocations at all water resource development projects, since the River flow in the area will decline in the future.

Rahmat *et al.* (2021) employed the General Circulation Model (GCM) to simulate daily weather patterns for three different concentration pathways (RCP2.6, RCP4.5, and RCP8.5) at three time intervals (Δ2030, Δ2050, and Δ2080). The researchers specifically investigated how climate change impacts rainfall variability in Johor. In addition, a forecast of the annual precipitation pattern for the initial year of 2030 was also generated. A total of eight locations in Johor, Malaysia, were chosen for this study. These sites were selected based on their ability to provide daily rainfall data for a period of thirty years, specifically from 1988 to 2017. Only sites with less than 10% missing data were included in the selection. Compared to records, it is estimated that the average annual rainfall will increase by 17.5%, 18.1%, and 18.3% under RCP 2.6, 4.5, and 8.5, respectively. Furthermore, the application of the Mann-Kendall (MK) test did not reveal any discernible trend for RCP 2.6. However, the RCP 4.5 scenario showed a significant upward trend in Muar and Kota Tinggi, while the RCP 8.5 scenario identified an increasing trend in all regions except Pontian and Kluang. The highest amount of future rainfall occurred when greenhouse gas concentrations from the RCP 8.5 scenario were utilized.

Vijayakumar *et al.* (2021) conducted a study on the investigation of trends in yearly rainfall and temperature throughout the coastal region of Odisha. They used various CMIP5 models and RCP scenarios to forecast the temporal-spatial variations. The results indicated that there was a rising but statistically insignificant trend in yearly rainfall across all districts, except for Ganjam. There was a notable rise in both the

lowest and maximum temperatures. Future climate forecasts indicate that the annual mean rainfall is expected to change within specific ranges over different periods. For the near century (2011-2039), the rainfall is projected to vary between 0.1% and 2.2% (RCP 4.5), and between -0.3% and 0.7% (RCP 8.5). In the mid-century (2040-2069), the rainfall is predicted to range from 1.5% to 3.2% (RCP 4.5), and from 3.6% to 7.9% (RCP 8.5). Finally, in the late century (2070-2099), the rainfall is expected to vary between 3.7% and 6.6% (RCP 4.5), and between 8.5% and 14% (RCP 8.5). Anticipated climate change will have a moderate effect on the total amount of rainfall, but it will have a substantial effect on how the rainfall is distributed. Predictions indicate that the annual mean maximum temperature will climb by 0.61–0.66°C, 0.68–0.72°C, and 1.35–1.55°C in the near, mid, and late centuries, respectively, under the RCP 4.5 scenario. Under the RCP 8.5 scenario, the temperature is expected to rise by 1.79–1.97°C, 1.73–2.01°C, and 3.08–3.44°C in the near, mid, and late centuries, respectively. Seasonal projections indicate increased fluctuations in temperature and precipitation during both winter and summer, as indicated by the RCP scenarios. Agriculture is anticipated to be both positively and badly impacted by future climate change. Kharif is anticipated to yield more detrimental outcomes compared to Rabi.

Asif *et al.* (2023) examined the climatic factors affecting hydrological regimes in the region, including surface runoff, groundwater storage, and forested watersheds. Extreme events like droughts, floods, wildfires, and changing precipitation patterns are causing water supply deficiencies and affecting water flows and quality. The region's climate diversity leads to spatial and seasonal variations, with winter being expected to be warmer than other seasons, causing earlier runoff and a decline in snowmelt. An integrated water resource management approach and climate-induced innovative technologies are needed to secure water resources and prepare for future challenges.

Chien *et al.* (2023) examined the impact of climate mitigation technologies and natural resource management on greenhouse gas emissions in China from 1991-2021. It finds that renewable energy output, consumption, natural resource rent, and depletion negatively correlate with GHG emissions, while industrialization and

population growth have positive associations. The research provides guidelines for regulators to formulate regulations related to climate change using these technologies and effective resource use.

Syam *et al.* (2024) examined the significant impact of climate change significantly on precipitation, temperature, and hydrological cycles, in the Krishna River Basin (KRB), India. The historical data (1961-2005) of rainfall and temperature were used to calibrate and validate statistical downscaling model (SDSM) to predict the future climate variables under three greenhouse gas concentration scenarios (RCP2.6, RCP4.5, and RCP8.5) for the future period of 2011-2100. The results revealed that the maximum and minimum temperatures are projected to rise throughout the 21st century and also indicated that the RCP8.5 (2071-2100) predicted an increase of upto 2.3°C in maximum temperature and 2°C in minimum temperature. The study also revealed that the overall rainfall was expected to increase by 32%, making the region wetter. It also revealed that monsoon rainfall may increase by 45% in high-rainfall areas and 12% in low-rainfall areas.

2.3 Identify and recommend an acceptable climate change adaptation strategy to address water shortage or excess in the near future

Adapting strategy is the only way to eliminate climate change's impact on water resources. A climate change adaptation strategy reduces the adverse effects of climate change while maximizing the benefits, which involves adjusting policies and actions.

Mukheibir and Ziervogel (2007) argued that climate-induced impacts on cities can only be directly addressed at the municipal level, so solutions that target vast numbers of people can be introduced. Therefore, municipal-scale adaptation to climate impacts must be considered and coordinated.

Chaturvedi *et al.* (2012) employed 18 General Circulation Models (GCMs) based on the Coupled Model Intercomparison Project Phase 5 (CMIP5) to forecast future temperature and precipitation in India. They included four Representative

Concentration Pathways (RCPs) scenarios, namely 2.6, 4.5, 6.0, and 8.5, spanning the time period from 1880 to 2099. The study revealed that the average climate projection from the CMIP5-based model ensemble was more accurate in representing the observed data compared to any individual models. The projected average temperature increase in India from the 1880s to the 2080s, as determined by ensemble models, ranged from 2°C to 4.8°C. These forecasts were based on the RCP 2.6 and RCP 8.5 scenarios. The forecast precipitation for India is expected to increase by 6%, 10%, 9%, and 14% by the 2080s compared to the base period of 1961-1990 under the scenarios RCP 2.6, RCP 4.5, RCP 6.0, and RCP 8.5, respectively. A study has recommended the utilization of various climate models to enhance the accuracy of climate projections for India. It was recommended to utilize the globally coordinated regional downscaling experiment (CORDEX) Regional Climate model (RCM) future climate projections for India in order to improve accuracy and provide more precise advisories.

Olmstead (2013) examined the empirical research on water supply, demand, and climate change adaptation currently available for integrated assessment modeling. It explores the economic impacts of climate change, the ability of adaptation to mitigate these impacts, and the responses of water users to water prices, conservation policies, and infrastructure investments. The paper highlights the importance of linking existing research with IAMs and the role of water management institutions in climate change adaptation.

Iglesias and Garrote (2015) analyzed European regions' risks and adaptation strategies by reviewing 168 publications over the past 15 years. They evaluate agronomic and policy measures to develop concrete plans and respond to regional challenges. The study suggests that technological change will shape adaptation choices in the coming decades. The greatest action is improving adaptive capacity and responding to water demands, but implementation requires revamping water policy, farmer training, and viable financial instruments.

Azhoni *et al* (2017) explored how a nation's ability to adapt to climate change's hydrological impacts depends on its water governance institutions. They used India as an example, analyzing inter-institutional networks and barriers to adaptation using

internet data mining and interviews. The study reveals a disconnect between climate change and water, with institutions like the Ministry of Water Resources, Earth Sciences, and Agriculture showing lesser involvement. The inter-institutional network is centralized, but complex dynamics exist between institutions. Institutional barriers, bureaucratic processes, and systemic failures hinder effective inter-institutional networks, highlighting the need for more comprehensive institutions in climate change adaptation.

Brown *et al.* (2019) found that population growth and climate change will pose significant challenges for water management in the US. They projected serious water shortages in some regions without further adaptation efforts. Current improvements in water use efficiency are likely but insufficient to avoid future shortages. Past adaptations like reservoir storage have little promise, while stream flow removals and groundwater mining can lower shortages but have external costs.

Anderson *et al.* (2020) studied climate change, which is expected to significantly impact agriculture and food security, with varying impacts across regions and crops. As the global population grows, agriculture must adapt to ensure future food security. Adaptation strategies include changing land and cropping practices, developing improved crop varieties, and modifying food consumption and waste. Advances in genomics and agronomy can mitigate climate change impacts, but significant investment is needed. Long-term food security depends on the political will to reduce fossil fuel burning.

He *et al.* (2021) predicted a significant increase in global urban water scarcity from 933 million in 2016 to 1.693-2.373 billion by 2050, with India being the most severely affected. The number of large cities exposed to water scarcity is expected to rise from 193 to 193-284, including 10-20 megacities. Infrastructure investment can help alleviate water scarcity in over two-thirds of water-scarce cities, but significant environmental trade-offs must be considered.

Khaniya *et al.* (2021) discussed the benefits of implementing Eco-based Buildings (EbAs) in Sri Lanka, focusing on water management issues. They highlight

the benefits of EBAs in water supply regulation, water quality regulation, and extreme event moderation. The study recommends EBAs over grey infrastructure-based solutions for climate change adaptation in Sri Lanka due to cost-effectiveness, eco-friendliness, and long-term benefits. The findings will help fill knowledge gaps and inform decision-makers and water resources planning agencies for future climate change adaptation actions in Sri Lanka.

Mishra *et al.* (2021) studied a comprehensive overview of water security, its evolution with environmental changes like urbanization and socioeconomic factors, and its implications. It presents sustainable solutions to achieve water security, ensuring reliable access to safe water for everyone at affordable prices. Despite progress in water resource management, implementation remains limited. A comprehensive sustainable approach requires connecting social, economic, and environmental systems at multiple scales. The paper captures the changing dimensions and new paradigms of water security.

Kılkış *et al.* (2022) reported that the urgency of mitigating climate change presents opportunities for a 43% reduction in greenhouse gas emissions by 2030. These editorial reviews 28 research articles on renewable energy systems, energy security, transport transformation, system restructuring, biomass upgrading, green hydrogen innovations, heat transfer, and sustainable combustion. The special issue discusses new catalysts, hybrid reactions, hydrogen fuel cell electrocatalysts, and waste heat recovery from granules in concentrating solar power or slags. The widespread upscaling of solutions requires an effective approach that involves integrated, coordinated, and synergistic action to protect the planet's life-support systems.

Elgendy *et al.* (2023) reviewed 131 climate change adaptation (CC) studies in water resources management, identified gaps, and highlighted the importance of systems reoperation in updating reservoir operation curves using optimization algorithms. Low-impact development measures were preferred in storm drainage and flood mitigation systems. Future research should integrate environmental, social, and

economic aspects and incorporate land use and cover changes. This comprehensive review is crucial for improving CC adaptation strategies in water management.

Bartlett and Howes (2023) reviewed systematically the literature on adaptation options and their implementation. They found that there is a cautious approach to addressing the growing concern for water quality, with most strategies using coping or incremental approaches. However, strategies with low resilience may not be suitable for future climate change challenges.

Jatav (2024) examined the farmers in Bundelkhand and Central Uttar Pradesh, using the Livelihood Vulnerability Index (LVI) to compare the levels of vulnerability across different districts and assess how socioeconomic factors influence adaptation strategies. The data was collected using multistage random sampling from 480 farmers across 16 villages, 8 development blocks, and 4 districts. The results revealed that over 95 of the farmers in Jhansi and 82.5% in Barabanki reported declining rainfall over the past decade, and 95% of the farmers in Jhansi reported hotter summers. The LVI revealed that the farmers in Jhansi were the most vulnerable, while those in Barabanki were the least vulnerable. The study suggested the urgent need for climate adaptation measures such as promoting climate-smart agriculture, improving irrigation infrastructure, and enhancing access to education and agricultural training to help farmers make informed decisions.

2.4 Assessment of mechanization index and recommend suitable agricultural implements under water shortage or excess field situation

Farm mechanization is a key component of agricultural development. Farm productivity is linked to available power, efficient implements, and proper utilization. Agricultural mechanization optimizes the use of inputs like seeds, fertilizers, plant protection agents, and water for irrigation and promotes poverty reduction by making farming a more appealing enterprise. A higher mechanization index (MI) can lead to more efficient water usage through advanced farming equipment and practices.

Singh (2006) analyzed the impact of factors like fertilizer, irrigation, and farm power on yield through multiple linear regressions. It was found that irrigation and

farm power significantly contributed to increased yield using mechanical and electrical energy. The mechanization index (MI) was calculated by comparing the cost of machinery used to the total animation and machinery costs. The study found that human labor cost remains the largest component in the wheat crop's cultivation cost, with an MI of 145%. States with higher mechanization indices had lower cultivation costs due to increased yield.

Rasooli and Ranjbar (2008) analyzed the agricultural mechanization in the Sarab Region, Eastern Azarbayjan Province, focusing on the number of tractors, machine types, and mechanization capacity. The study found an average mechanization level of 0.83 hp/ha, with partial energy expenditure per hectare of 1.24%, 2.23%, and 96.35%. The study highlighted the importance of machines in production but found that most farming operations had low mechanization levels. To achieve 1.5 hp/ha, 775 tractors were needed. The study also provided guidelines for improving mechanization and increasing farm production.

Olaoye and Rotimi (2010) assessed the agricultural mechanization levels on farms in two Southwest Nigerian states and analyzed their productivity. Factors influencing profitability were identified through a structured questionnaire and inventory of farm machinery. The Agricultural Mechanization Index was used to evaluate mechanization levels and productivity. The average level of mechanization was 31.3% in the Ogun and Osun States and 30.6% in the two states. The average physical productivity for maize and cassava was 1.2 to 1.7 tons/ha, while for cassava, it was about 11.5 tons/ha. The sustainability analysis revealed that the low production scale contributed to inconsistent agricultural mechanization policy, a lack of favorable conditions for full integration, a lack of essential infrastructure, and financial credits.

Thebe and Koza (2012) evaluated the current farm power systems in Zimbabwean smallholder irrigation schemes and explored agricultural mechanization interventions to increase productivity. The study assessed three smallholder irrigation schemes across eight administrative provinces, focusing on land preparation and harvesting. Conventional tillage and harvesting machinery were found to be commercially unsuitable due to the 100m lengths of run in the furrow and border-strip

irrigation schemes. Unconventional tillage, such as conservation tillage, offered affordable solutions. Modernization of irrigation systems was also recommended to limit labor input and farm power requirements. The study's findings are valuable for addressing mechanization challenges in the smallholder irrigation sector.

Chinsango *et al.* (2013) analyzed the agricultural mechanization levels at two wards of Bindura North district in Zimbabwe. The average mechanization was 0.42 hp per ha, lower than the standard of 1.5 to 2 hp/ha for optimal productivity. The mechanization capacity was 6.8% for the A_1 model and 60% for commercial and A_2 farming systems. The level of mechanization was lower than expected at national levels, and the lack of a comprehensive national irrigation policy was noted. The average production levels of maize and tobacco under the A_1 resettlement models were significantly lower than elsewhere in the region.

Jalalzadeh *et al.* (2016) estimated the effects of the mechanization level index using a system dynamics methodology on the mean yield of farm crop products in Iran. The methodology involved a 70-year period from 1981 to 2051, with constant parameters, logical relations, and statistically estimated functions. The model was tested using simulation software, identifying three economic production regions: the first from 1.342 kW/ha to 2.013 kW/ha, the second from 2.013 kW/ha to 2.386 kW/ha, and the third from 2.386 kW/ha. The maximum profitable point for farm crop production was 2.218 kW/ha.

Pradhan *et al.* (2016) examined the status and potential of agricultural mechanization in Sunsari district, Nepal, focusing on using traditional farm equipment and human labor. The research found that agricultural mechanization is at a rudimentary stage, with tractors being the primary power source. Tractors reduce labor utilization but do not significantly impact crop yield or intensity. Tractor-owned farms have higher family incomes due to off-farm activities. Geographic information system mapping identified that 96.8% of the total cultivated area can be covered using a tractor, and 1.5% can be served with power tillers. However, 1.7% of the area lacks efficient operation of tractors and power tillers.

Abbas *et al.* (2017) assessed the mechanization index (MI) and its impact on corn productivity in Pakistani farmers. Results showed that large farmers had higher MI and corn yields than small and medium farmers. Factors such as education level, ownership status of machines, and external support for agriculture machinery also influenced MI. The study suggests that improving farmers' educational levels through literacy campaigns and long-term investments in support services infrastructure is necessary to increase MI at Pakistani corn farms.

Bawatharani and Karunarachchi (2017) determined the Mechanization Index (MI) of different vegetable crop cultivation in the Bandarawela Divisional Secretariat (DS) division. A sample of 100 farmers from five major vegetable cultivation DS divisions was collected using a stratified random sampling technique. Primary data was collected through questionnaires, personal interviews, and discussions with key informants. Secondary data was obtained from relevant articles, government centers, and organizations. The study found that cabbage cultivation had the highest MI at 2.29%, followed by tomato cultivation at 0.5%. The highest power per unit area was found in cabbage cultivation.

Singh and Kumar (2017) assessed the mechanization feasible for the Indian condition. A study of 280 farmers in seven districts of Madhya Pradesh found that average power availability was 1.80 kW/ha, with mechanical power contributing 80 to 88%. Farmers received better net returns from wheat production (₹19,591/ha) and gram production (₹18,695/ha), with a benefit-cost ratio (BCR) of 1.71 and 1.86, respectively. The production function fitted well with a coefficient of multiple determinations (R^2) of 0.80 to 0.97 across the crops. Human labor was significant for soybean and gram production, while machinery and miscellaneous factors contributed significantly to wheat and gram productivity. The mechanization index was higher in crops like wheat (57.61%) and gram (44%), while it was lower in paddy (40%), soybean (40.4%), and maize (43.5%).

Kalita (2018) studied the extent of agricultural mechanization in Assam. Agricultural production is positively correlated with energy input, leading developed countries like India to use machines in agricultural activities. However, traditional

methods and instruments were used in labor-surplus countries like India, leading to labor displacement due to machine use. In Assam, a state in India, farmers, particularly educated ones, have developed a tendency to use machines in agricultural activities. A field study in five agricultural zones found that small holding sizes and tenancy prevalence have not remained constraints for agricultural mechanization. Farmers increasingly use machines in plowing and other activities, considering cost factors.

Barman and Deka (2019) examined the factors affecting farm mechanization adoption in the Central Brahmaputra Valley and Upper Brahmaputra Valley Zone of Assam, India. Data from 240 sample farms was collected from 2014-15. Factors affecting mechanization adoption included age, education level, land holding size, access to irrigation, extension agents, high-yielding varieties, and institutional credit. Younger farmers preferred mechanization more than older ones. The study found that the linkage of extension functionaries at the grassroots level was crucial for promoting farm mechanization.

Haong *et al.* (2020) evaluated the level of mechanization in lime cultivation among 555 lime farmer households in the Mekong River Delta. The results indicated that there were just a few machines and equipment use, with the majority being utilized for land preparation and tree care. From 2016 to 2019, there was no change in the rate of growth and investment in mechanization. The study also suggested possible technical remedies for lime cultivation, such as the implementation of mechanization for small and medium-sized farms and the inclusion of plant care considerations. It was suggested that the quality of lime fruit may be improved by using semi-mechanized harvesting systems, enhancing storage facilities, and optimizing packing methods.

Raina *et al.* (2021) studied farm mechanization in the Kangra district of Himachal Pradesh. The study showed a net savings of Rs. 4454, 2330, and 658/ha for land preparation operations and Rs. 3910, 2347, and 2551/ha for sowing operations. Mechanization practices saved 56–67-man days of human labor and 23-35 bullock days/ha in major crops. Total added expenses ranged from Rs 10652/ha in maize to

13665/ha in paddy. Per hectare, net savings were Rs 8531, 15152, and 5685/ha for maize paddy and wheat.

Singh *et al.* (2023) assessed a training program on farm mechanization in 2021 for 120 farmers in Kamrup district, Assam, organized by the ICAR-Central Plantation Crops Research Institute in Kahikuchi. The study found that most respondents' knowledge levels increased after participating, but there was a significant financial problem in purchasing farm machinery among respondents. There was a need for more awareness and training programs for rapid farm mechanization in the region. Educational qualifications and previous training experience were positively and significantly correlated with the respondents' knowledge level.

Aruna *et al.* (2024) assessed the mechanization index of sugarcane cultivation in Mandya District, Karnataka, India, focusing on the efficiency of farm machinery usage in different operations. The data which included land holdings, machinery use, farm operations, and energy requirements, were collected from 50 farmers on a random selection and the mechanization index was evaluated. The results revealed that the study area comprised of 30% marginal farmers, 40% small farmers, 26% semi-medium farmers, and 4% medium farmers. It also revealed that the total mechanization index in sugarcane cultivation was found to be 50.5%, with semi-medium farmers having the highest index at 51.85%. The mechanization index was highest for seedbed preparation (98.46%) and irrigation (97.37%) while it was zero for planting and harvesting due to manual operations and lack of equipment.

CHAPTER 3

MATERIALS AND METHODS

This chapter deals with the description of the research and techniques employed in the study undertaken in two stages. In the first stage, the Agricultural Water Availability Index (I_{AWA}) was developed and the impact of climate change on temporal and spatial variation of water availability was assessed. Based on the outcome of the first stage of the study, the second stage was designed to recommend suitable agricultural implements under less water availability situations after assessing the mechanization index. A detailed methodological framework to achieve the outcome of the aforementioned objectives of the present study is presented in **Fig 3.1**.

The materials and methods employed in the research are presented under the following main headings:

3.1 To develop an agricultural water availability index for assessing the current situation of water availability in the study area.

3.2 To assess the impact of climate change on temporal and spatial variation of water availability in the study area.

3.3 To identify and recommend an acceptable climate change adaptation strategy to address water shortage or excess in the near future.

3.4 To assess mechanization index and recommend suitable agricultural implements under less water availability.

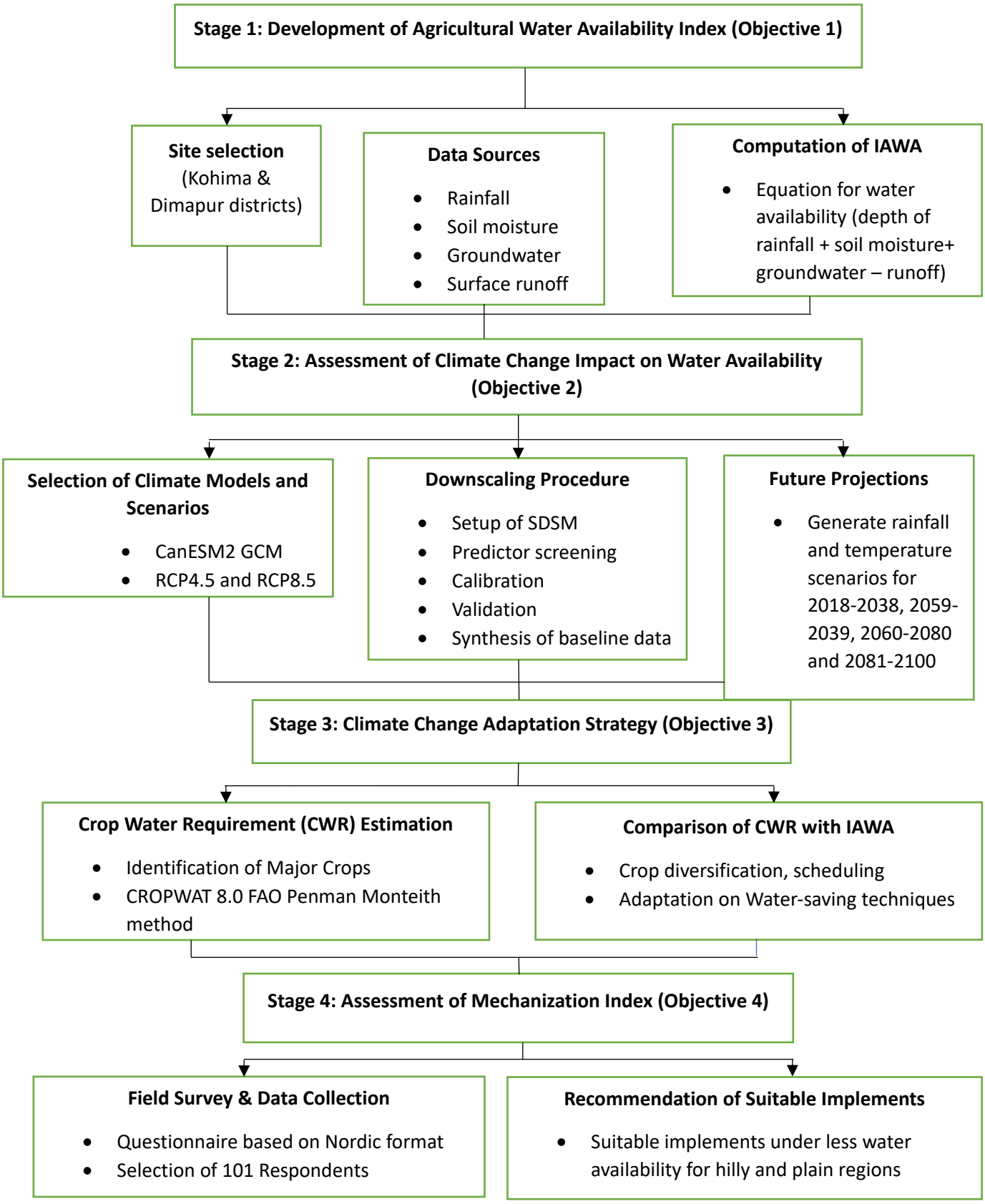

Fig 3.1 A methodological framework of the present study

3.1 Site selection

The present study was conducted in two districts, viz. Kohima and Dimapur districts, Nagaland (**Fig 3.2**).

Kohima covers a geographical area of 1,595 sq. km, with approximately 490.5 sq. km covered by forests, 7 sq. km classified as barren and uncultivable land, and a net sown area of 138.88 sq. km. The primary agricultural practices in the district include wet rice cultivation and jhum cultivation (Anon1, 2016). Dimapur, on the other hand, covers 927 sq. km, with 379 sq. km consisting of plain area. The district has a net cultivable area of 503.25 sq. km, while 281 sq. km is categorized as non-cultivable land. Falling within the humid subtropical agro-climatic zone (ACZ), and primarily follows a mono-cropping system (Anon1., 2016).

Given that Dimapur is largely composed of plains, whereas Kohima is characterized by hilly terrain, the study area has been selected to capture the contrasting agricultural and geographical features of these districts.

3.1.1 Geographical identity of the study area

Geographically and climatologically, Kohima district is located at 25°31′21″N and 25°54′30.06″N latitudes and 93°54′17″E to 94°16′4″E longitudes and has a high-altitude of 1261 m above the mean sea level (msl) (Belho and Rawat., 2023). It is the state capital and one of the oldest districts of Nagaland. The population of Kohima district, as recorded in the 2011 census, is 267,988, which comprises 138,966 males and 129,022 females. Kohima has a literacy rate of 85.23%, higher than the national average of 74.04%. It is on a lofty slope, with the town meandering around the crests of the adjacent mountain ranges (Anon2., 2023). Topographically, based on the agro-ecological situation, the district has three distinct regions, viz. AES-I (Below 1000 m), AES-II (between 1000-1500 m), and AES-III (Above 1500 m) (Anon1., 2016).

The Dimapur district lies between 25°48′N and 26°00′N latitudes and 93°30′E and 93°53′E longitudes and has an average altitude of 260 m above the mean sea level (msl) (Neog, 2025). Most of the Dimapur district is situated in low-lying areas

(Anon2., 2023). The city is renowned as a "mini-India" due to its diverse population of individuals from many regions. According to the 2011 census report, the population of Dimapur district is 379,769.

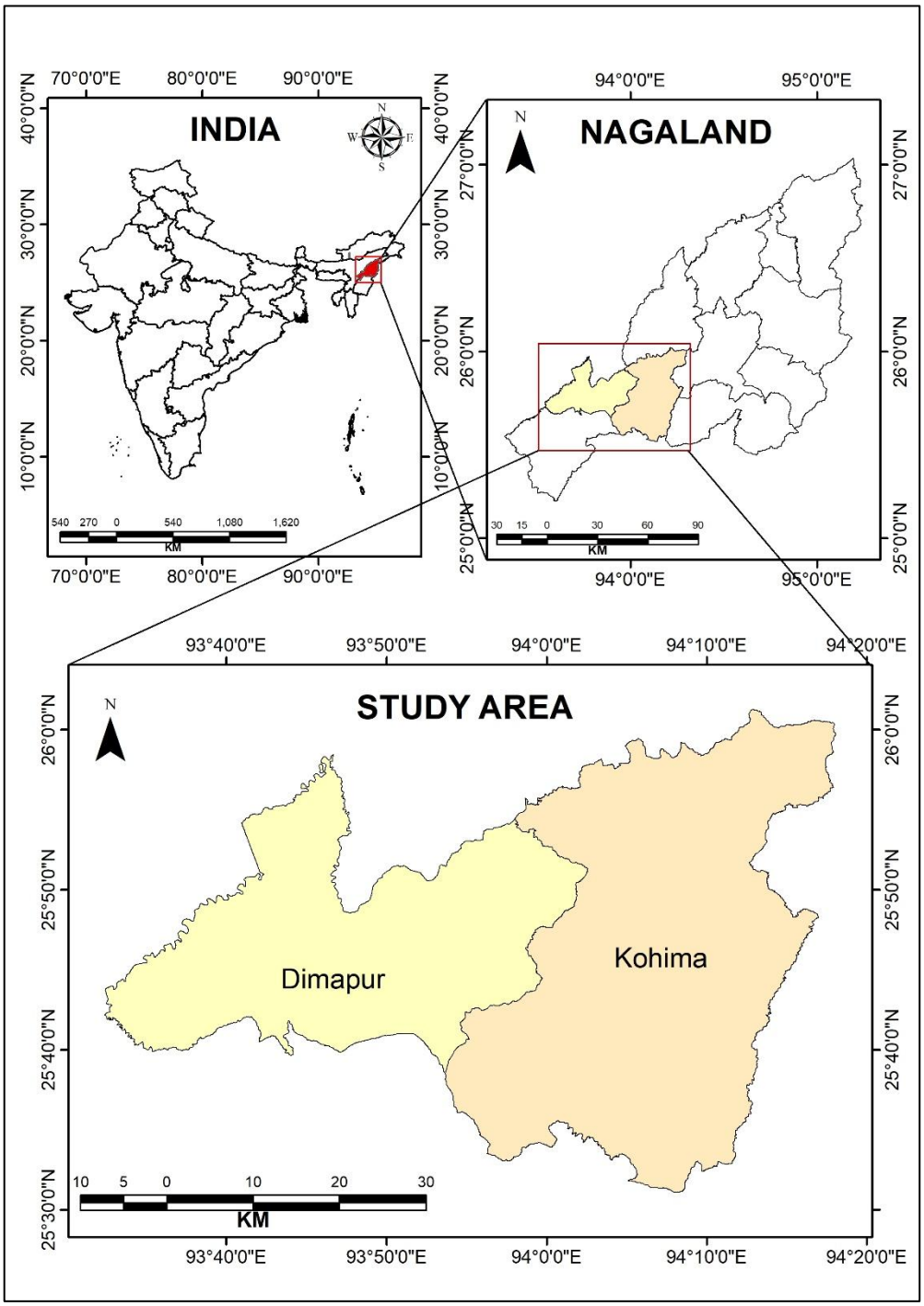

Fig 3.2 Location of the study area (Kohima and Dimapur)

3.1.2 Soil and climate

The soils of the Kohima district have been classified into different groups based on fertility status. Due to a high degree of weathering of acidic parent material under a humid climate with strong and heavy rainfall, a major portion of the district has strongly acidic soils (42.6%), followed by moderately (30.7%) and very strongly acidic soils (20.9%) (Anon1., 2016). The soils have been derived from the tertiary group of rocks, and red clay soil is the most predominant type of soil found in the district (Anon3., 2013). Kohima district has a milder variation of a humid subtropical climate. It has a nice, temperate climate, mild winters, and pleasant summers. December and January are the coldest months, with frost and sometimes snowfall at higher elevations. The temperature rises to 32ºC during the peak summer and reaches 2ºC in winter. It experiences heavy rainfall during monsoon, and its average annual rainfall is 2500 mm (Jongkor *et al*., 2022).

The soils of the Dimapur district are derived from the tertiary group of parent rocks, sandstones, mudstone, shale, and siltstone. The soils are generally acidic, very rich in organic carbon, and poor in available phosphate and potash content. The soils are fertile and can be categorized into alluvial and residual Soils (Anon4., 2019). The climate in Dimapur district is hot and humid during the summer (reaching a maximum of 40°C, minimum of 10°C, and humidity up to 93%) while the winter months are cool and pleasant. The average annual precipitation in the district is around 1504.7 mm (Jongkor *et al*., 2022).

3.1.3 Land use land pattern

Land use encompasses a range of human activities and diverse land applications for domestic and economic objectives. Land cover encompasses natural flora, water bodies, rocks, and soil. Since land use and land cover are closely linked, both the term can be used interchangeably. However, land cover frequently affects land use.

Since Kohima district is located in a hilly area, land for building infrastructure or farming is limited. The land area is experiencing strain due to ongoing upgrades and construction projects, as well as the relocation of the people to the capital. Conversely, Dimapur district has less geographical area and a high population density. The plain tract in this hilly state is unique since it contains railways, an airport, and a thriving

commercial industry. As a result, it is more prone to unregulated land use despite its limited size.

Water resources

The Dimapur district comprises two major rivers: Dhansiri and Diphu. The district is blessed with numerous perennial sources consisting of the tributary system of Chathe River, Zubza River, Dhansiri River, and Diphu (Anon1., 2016).

The Kohima district is primarily served by four main rivers: Dhansiri, Dikhu, Doyang, and Zungki. Additionally, the Doyang River has significant tributaries, including the Chubi River and the Nzhu River, which originates from the Nerhema area of Kohima district (Anon3., 2013).

3.1.4 Status of agriculture

Agriculture in the Kohima district mainly revolves around wet rice terrace cultivation and jhum (shifting cultivation). The primary crops grown include rice, maize, potatoes, and various vegetables such as chilies. Fruits like papaya, passion fruit, guava, and other tropical fruits are also cultivated. Most of the farmers rely on traditional methods, especially jhum, for growing rice and other cereals. Modern agricultural techniques, such as using high-yield seeds, fertilizers, and advanced plant protection methods, are either minimally used or completely absent. As a result, there is very little use of chemical fertilizers and pesticides, making the region well-suited for organic farming. As per the Department of Agriculture, the Government of Nagaland, the district's climate is ideal for growing a variety of crops, including strawberries, passion fruit, cabbage, squash, and a wide range of flowers, making it a promising area for organic agriculture.

Rice is the main crop grown in the Dimapur district, cultivated through rain-fed farming, terrace farming, and irrigation systems. Jhum (shifting cultivation) is also practiced in higher elevations. Maize is the second most important crop in the region. Among pulses, the major ones grown in the Dimapur district include peas, pigeon peas (arahar), black gram, and lentils. These are cultivated during both the *kharif* (monsoon) and *rabi* (winter) seasons. Mustard is the primary oilseed crop, while other oilseeds

like soybeans, sunflowers, and linseeds are also grown. Additionally, sugarcane and tea are important commercial crops in the Dimapur district.

Farm mechanization lags in the study area due to fragmented land, low capital investment capacity, a lack of technical knowledge, undulating topography, etc. The agricultural sector uses a limited number of tractors and power tillers. However, manual plows and sprayers are common in the area.

3.1.5 Tools and data used in the study

After data collection, the data were transferred to a computer and compiled. Further, processed in ArcGIS 10.5, SDSM 4.2.9, CROPWAT 8.0, and MS Office 365 software packages were used for analysis of raw data. The daily rainfall data for 18 years (2003 to 2020) for six rain gauge stations, i.e., Kohima, Dimapur, Jalukie, Wokha, and Phek, were collected from the Department of Soil and Water Conservation, Government of Nagaland, Kohima. The MODIS (Moderate Resolution Imaging Spectroradiometer) data products of LST (Land Surface Temperature) and NDVI (Normalized Difference Vegetation Index) were obtained from the NASA website (earthdata.nasa.gov). The secondary data on groundwater depth (2004-2019) and quality data (2020) were collected from the India WRIS (Water Resource Information System). Specifically, ArcGIS 10.5 was used for the spatial interpolation, visualization and analysis, and mapping of rainfall, soil moisture, groundwater, and surface runoff data. The statistical downscaling model (SDSM) software was used to assess the impacts of local climate change using a robust statistical downscaling technique. CROPWAT software was used to analyze the crop water requirement of the six major crops (rice, potato, sugarcane, soyabean, maize, and chilli) and help determine the optimal amount of water needed for crops, which can improve crop productivity. The MS Office suite was utilized for statistical analysis, documentation, and presentation purposes.

3.2 To develop an agricultural water availability index for assessing the current situation of water availability in the study area

Agricultural water availability is a function of surface and groundwater quantity and quality. The proposed agricultural water availability index can be denoted as I_{AWA} and is supposed to incorporate available information on water availability from sources, viz., rainfall, soil moisture, and groundwater, with their quality consideration. The analysis can be performed monthly on a spatially distributed grid of 30 x 30 m for the study area in a GIS environment. In general, the expression for this index is represented in terms of available water depth from the above-mentioned sources. Therefore, to achieve the goal of objective one, the Agricultural Water Availability Index (I_{AWA}) is estimated using the following equations given below, as suggested by Ahmad (2011).

$$V_{ij} = V_{Sij} \tag{3.1}$$

Where,

V_{ij} is the total depth of water from all available sources in i^{th} pixel during j^{th} month.

Further, V_{Sij} is given as:

$$V_{Sij} = P_{ij} + SM_{ij} + G_{ij} - R_{ij} \tag{3.2}$$

Where,

V_{Sij} is the algebraic sum of weighted water depths of rainfall, soil moisture, groundwater, and runoff in i^{th} pixel during j^{th} month.

P is the depth of water available from rainfall, mm.

SM is the available soil moisture, mm.

R is the depth of surface runoff, mm.

G is the groundwater depth, mm.

After solving the equation and determining the depth of available water in each pixel, the next step was determining the maximum and minimum water depth in the grid cells. The relative water depth value in each pixel can be calculated using the normalization technique in **Equation 3.3**.

$$I_{AWA,ij} = \frac{V_{ij} - V_{min}}{V_{max} - V_{min}} \quad (3.3)$$

Where,

V_{ij} is the total depth of water for the i^{th} pixel in j^{th} month.

V_{max} is the maximum water depth.

V_{min} is the minimum water depth.

The normalization value ranges between 0 and 1, where the maximum water depth can be represented as 1 and the minimum water depth as 0. The advantage of this method is its simplicity for comparative purposes because it transforms all the values to a range from 0 to 1, and hence, the comparison among different time windows and spatial extents of the area under consideration can be made.

The resulting value of I_{AWA} was assessed for long-term changes using the non-parametric Mann-Kendall (M–K) trend test. The M–K test evaluates whether a time series has a statistically significant monotonic increase or decrease without assuming normality. It computes a rank-based statistic (Kendall's S and standardized Z) under the null hypothesis of no trend. This test is widely used in climatology and hydrology because it is distribution-free and robust to outliers or skewed data (National Center for Atmospheric Research Staff, 2014). A significant positive Z ($p < 0.05$) indicates an increasing I_{AWA} trend (more water availability over time), and a significant negative Z indicates a decreasing trend (growing water deficit). By using M–K (instead of, e.g., linear regression), we avoid biases due to non-normality or serial correlation. This approach is standard in climate studies and has been applied to rainfall and drought

indices in India to infer water-resource trends. Mann-Kendall test statistic S is calculated using the given equation (Mann, 1975; Kendall, 1975; Yue and Pilon, 2004)

For a time series $x_1, x_2, \ldots\ldots, x_n$, the MK test statistic S is defined as:

$$S = \sum_{i=1}^{n-1} \sum_{j=i+1}^{n} sgn(x_j - x_i) \tag{3.4}$$

Where the sign function is:

$$sgn(x_j - x_i) = \begin{cases} +1 \; if \; (x_j - x_i) > 0 \\ 0 \;\; if \; (x_j - x_i) = 0 \\ -1 \; if \; (x_j - x_i) < 0 \end{cases} \tag{3.5}$$

A positive value of S indicates an increasing trend, while a negative value indicates a decreasing trend.

The variance of S is calculated to account for tied values (equal observations) in the series:

$$Var\ (S) = \frac{n(n-1)(2n+5) - \sum_{t=1}^{m} t_p(t_p-1)(2t_p+5)}{18} \tag{3.6}$$

Where,

n is the number of observations.

$x_j \; and \; x_i$ are the observations value in the time series i and j (j>i), respectively.

m is the number of tied groups.

t_p is the number of data points in the p-th tied group.

The standardized form of the statistic is:

$$Z = \begin{cases} \frac{S-1}{\sqrt{Var(S)}} \; if \; S > 0 \\ 0 \; if \; S = 0 \\ \frac{S+1}{\sqrt{Var(S)}} \; if \; S < 0 \end{cases} \quad (3.7)$$

The standardized statistic Z follows a normal condition:

Z > 0: upward trend,

Z < 0: downward trend,

If |Z| > $Z_{\alpha/2}$: trend is statistically significant at the chosen confidence level.

At a 95% confidence level, the critical value is 1.96; at 99%, it is 2.58.

Finally, we classified each year as dry, normal, or wet based on a percentile threshold method using **Equation 3.8 and 3.9** (Subash and Mohan, 2011; IMD, 2017).

If X is the set of ordered annual values (n years total):

25th percentile: $P_{25} = X_{[0.25(n+1)]}$ (3.8)

75th percentile: $P_{75} = X_{[0.75(n+1)]}$ (3.9)

Classification rule:

Dry year: X < P_{25}

Normal year: $P_{25} \leq X \leq P_{75}$

Wet year: X > P_{75}

3.2.1 Estimation of water availability

Rainfall, soil moisture, groundwater, and surface runoff are the major sources of water in a catchment area. Therefore, water from these sources is estimated to get accurate data.

3.2.1.1 Rainfall

The distribution of rainfall is crucial for comprehending hydrological processes. The global shift in climate is causing significant alterations in rainfall patterns, making it imperative to research hydrological processes for effective water resource management. Understanding rainfall distribution is crucial, and spatial interpolation is a key parameter in hydrological modelling.

For the determination of the agricultural water availability index (I_{AWA}), six rain gauge stations were selected from the state. The rain gauge stations are located in Kohima, Sechu, Dimapur, Jalukie, Wokha, and Phek. The secondary data on daily rainfall for 17 years (2003 to 2020) were collected from the Department of Soil and Water Conservation, Government of Nagaland, Kohima. Then, the daily rainfall data were computed into year-wise monthly averages using Microsoft Excel 2010. After the computation, the rainfall data of the selected rain gauge stations were analyzed using the Inverse Distance Weighting (IDW) interpolation technique. The IDW was developed by the U.S. National Weather Service in 1972 and is classified as a deterministic method (Feng Wen *et al*., 2012). The IDW is based on the concept of Tobler's first law (the first law of geography) from 1970. It is based on the assumption that objects are more similar when close to one another and is explicitly implemented through IDW interpolation. The IDW relies on the measured values close to the forecast location when predicting a value for any unmeasured location. The measured values nearest to the projected location will influence the predicted value more than those measured values farther away. Therefore, the IDW assumes that each measured point has a local influence that decreases with distance. The points closest to the prediction location are given more weight than those farther away. To estimate the location of s_o, the following **Equations 3.10 and 3.11** are used:

$$Z^*(s_0) = \sum_{i=1}^{N} \lambda_i Z(s_i) \quad (3.10)$$

Where,

$Z^*(s_0)$ is the value to estimate for the location of (s_0).

N is the number of sample points measured and will be considered in the prediction.

λ_i is the weight assigned to each measured point we will use. These weights will decrease with distance.

$Z(s_i)$ is the observed value at the location.

The weight is determined by using the following empirical relation:

$$\lambda_i = d_{i0}^{-p} / \sum_{i=1}^{N} d_{i0}^{-p} \sum_{i=1}^{N} \lambda_i = 1 \quad (3.11)$$

In order to regulate the impact of known points on the interpolated values depending on their distance from the output point, the IDW function in GIS was utilized for IDW interpolation with a modest weighting value (4). The purpose of interpolation in this research was to analyze the study area's spatial distributions and evaluate the rainfall measurement in the uncovered area.

3.2.1.2 Soil moisture

Soil moisture is crucial in the water cycle since it regulates the rainfall that seeps into the ground, runoff the land, or evaporates. The measurement or estimation of soil moisture from remotely sensed data has significantly advanced due to its distinct capacity to monitor extensive regions with recurrent coverage over a lengthy period.

The MODIS (Moderate Resolution Imagery Spectroradiometer) data products of LST (Land Surface Temperature) and NDVI (Normalized Difference Vegetation Index) have been used to estimate the spatial and temporal changes in soil moisture status in the study area. The tiles of MODIS products were acquired through the NASA website (earthdata.nasa.gov). The two types of MODIS data products included the 16-

day composite daily surface reflectance (MOD09A1) to derive NDVI and the daily surface temperature (MOD11A2) of 2011 at 1km resolution.

NDVI provides information about the growing states and conditions of vegetation on the ground, and LST reflects a particular state of soil moisture. Combining the two can establish a potential relationship to reveal land surface moisture. A schematic description of the relationship referred to as the 'Universal Triangle' is shown in **Fig 3.3**. The upper envelope of the trapezoid, A–C, representing the dry condition, was called the "warm edge"—the upper limit of surface temperature for a given vegetation cover. The "cold edge" was the lower limit of the trapezoid, B-D, matching the well-watered state. The LST and NDVI data were merged to create an index for spotting soil moisture following the idea shown in Figure 3.3. Defined in a scatter plot, a soil moisture index (SMI) was based on the pixel location in the LST-NDVI space. Moreover, the SMI values of 0 at the "warm edge" and 1 at the "cold edge" were set. The SMI for a given pixel E (Ts, NDVI) in the LST-NDVI space was calculated as the ratio between line M–E and M–N (Zhan *et al.,* 2004).

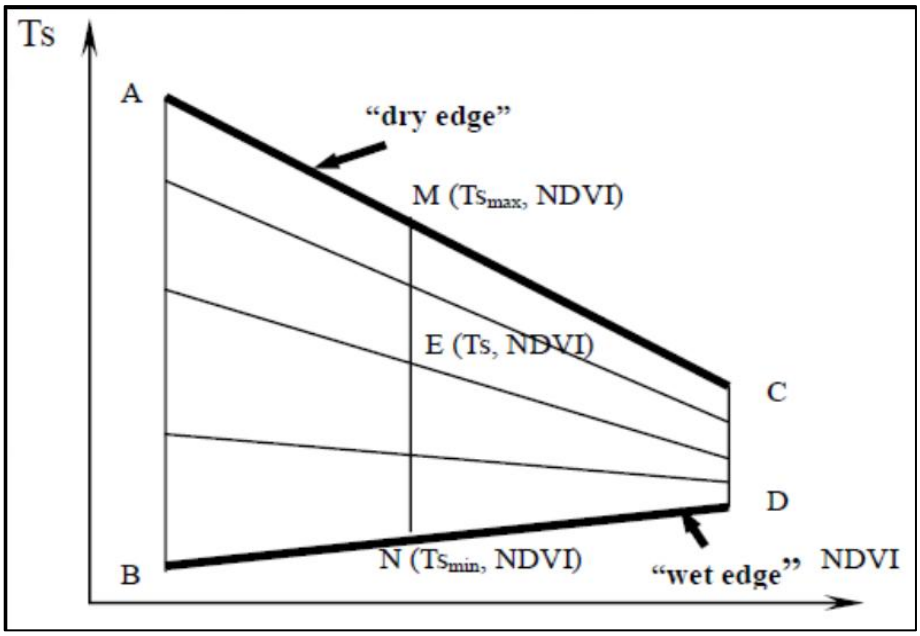

Source: Chauhan 2003

Fig 3.3 The scatterplot in LST-NDVI space and the definition of SMI

Based on an empirical parameterization of the link between LST and NDVI, the soil moisture index is calculated using **Equations 3.12, 3.13, and 3.14** as follows (Mallick *et al*., 2009):

$$\mathrm{SMI} = (\mathrm{LST_{max}} - \mathrm{LST}) \Big/ (\mathrm{LST_{max}} - \mathrm{LST_{min}}) \quad (3.12)$$

Where,

$\mathrm{LST_{max}}$ and $\mathrm{LST_{min}}$ are the maximum and minimum surface temperatures for a given NDVI and LST.

$$\mathrm{LST_{max}} = a_1 * \mathrm{NDVI} + b_1 \quad (3.13)$$

$$\mathrm{LST_{min}} = a_2 * \mathrm{NDVI} + b_2 \quad (3.14)$$

Where,

a_1, a_2, b_1, and b_2 are the empirical parameters (a present slope and b present intercept) that define the warm and cold borders of the data, as determined via linear regression.

3.2.1.2.1 Normalized difference vegetation indices

The NDVI is a vegetation index that allows mapping the relative healthiness of the biomes (Wang *et al*., 2003). The NDVI is calculated by **Equation 3.15** as follows:

$$\mathrm{NDVI} = \frac{\mathrm{R_{NIR}} - \mathrm{R_{RED}}}{\mathrm{R_{NIR}} + \mathrm{R_{RED}}} \text{ or } \frac{(\mathrm{band2} - \mathrm{band1})}{(\mathrm{band2} + \mathrm{band1})} \quad (3.15)$$

Where,

$\mathrm{R_{NIR}}$ and $\mathrm{R_{RED}}$ are the surface bidirectional reflectance values for their respective bands. Here, the values of band 1 and band 2 are 645 nanometers (nm) and 858 nm, respectively.

The annual monthly NDVI and LST for 2011 are calculated using **Equations 3.12, 3.13, and 3.14** to calculate SMI. Positive values of the NDVI imply dense and excellent vegetative cover, whereas negative values reflect no vegetation or very little vegetation. NDVI values range from -1 to 1. The surface temperature, expressed in °C, is represented by LST readings. The result is available in a range of values from 0 to 1, where values around 1 represent areas with lower levels of plant cover and surface temperature. These characteristics suggest that the surface has a higher soil moisture level and poor infiltration. The regions with significant plant cover and surface temperatures have values near 0, indicating low soil moisture content and enhanced soil surface infiltration capability.

Due to the large volume of remote sensing data analysis, the soil moisture was calculated for an average wet year. The average wet year was selected from the analysis period according to the Food and Agriculture Organization (FAO) recommendations (FAO, 2010).

3.2.1.3 Groundwater

Groundwater is a vital water resource that can be tapped whenever water is needed. Assessing the quantity and quality of groundwater reserves may lead to more important future decision-making and the subsequent implementation of any requisite regulations. The secondary data of groundwater depth (2004-2019) and quality data (2020) were collected from the India WRIS (Water Resource Information System) website (https://indiawris.gov.in). The WRIS platform was established by the Ministry of Jal Shakti, Government of India, to facilitate informed decision-making and conduct studies related to water resources planning and management. WRIS is an online platform created and maintained by the Government of India. The WRIS website provides a user-friendly design and clear documentation of its data sources and gathering processes. Given the scarcity of data for the study area, the WRIS platform can potentially address this issue (Pathak *et al*., 2024).

The groundwater level (m) data was computed into mean monthly values in MS-Excel 2010. The groundwater level was interpolated using the IDW technique in

GIS to develop the groundwater level maps. The interpolated surfaces depict groundwater depths varying between 4.4 m and 5.6 m below ground level across Kohima and Dimapur districts. Because these depths are substantially greater than the effective crop-root zone (0.3 – 1.0 m), the upward capillary flux from groundwater to the root zone is negligible. Modeling studies by Gao *et al.* (2017) and Kroes *et al.* (2018) demonstrate that upward contribution from groundwater sharply decreases beyond 2 m depth, while Zhu *et al.* (2018) found that when the groundwater table lies deeper than the capillary rise limit, its direct supply to soil-moisture storage becomes insignificant. Although groundwater data were spatially analyzed to understand depth variability, the mean groundwater level (4 – 6 m bgl) is beyond the crop-root zone. Therefore, G_{ij} was assumed negligible in the I_{AWA} computation.

The evaluation of water quality for the study is explained in the sub-sections.

3.2.1.3.1 Water Quality Index (WQI)

In this study, four parameters were chosen to calculate the water quality index (WQI). The WQI is a dimensionless number whose values fall between zero and one hundred. It is a highly sophisticated scoring system that conveys the overall state of water quality, ranging from outstanding to good to poor. The recommendations for drinking water quality criteria set by the World Health Organization (WHO) were used to determine the water quality index (**Table 3.1**). The water quality index was estimated by adding together each sub-index value of each groundwater sample as follows from **Equations 3.16 to 3.19** (Ramakrishnaiah *et al.* 2009; Sadat Noori *et al*. 2014).

$$WQI = \sum SI_i \tag{3.16}$$

Where,

WQI is the water quality index.

SI_i is the sub-index of i^{th} parameter.

Further,

$$SI_i = q_i \times RW_i \quad (3.17)$$

Where,

SI_i is the sub-index of i^{th} parameter.

q_i is the sub-rating based on the concentration of i^{th} parameter.

RW_i is the relativ6e weight of i^{th} parameter.

n is the number of parameters.

Further, the quality rating is calculated by **Equation 3.18**.

$$q_i = \frac{c_i}{s_i} \times 100 \quad (3.18)$$

Where,

q_i is the quality rating for the i^{th} parameter.

c_i is the concentration of the i^{th} parameter of the groundwater sample.

s_i is the permissible standard for the i^{th} parameter set by the WHO.

Further, the relative weight (RW_i) is calculated by **Equation 3.19**.

$$\mathrm{R}W_i = {w_i}/{\sum_{i=1}^{n} w_i} \quad (3.19)$$

Where,

RW_i is the relative weight.

w_i is the assigned weight of each parameter.

n is the number of parameters.

The assigned weight for each parameter is mentioned in **Table 3.2**.

Table 3.1 Classification of groundwater quality by WQI (based on WHO, 2011 guidelines)

WQI	Type of Water
0-50	Good
55-65	Moderate
65-70	Poor

70-75	Very Poor
>75	Unfit for drinking

Source: Ramakrishnaiah et al. 2009; Sadat Noori et al. 2014

Table 3.2 Relative weight of each parameter with its units and BIS standards

Parameter	Units	BIS	Relative Weight (Wi)
pH		6.5-8.5	0.145
Electrical Conductivity (EC)	Micro	2500	0.004
Nitrate (NO_3)	mg^{-1}	45	0.003
Fluoride (F)	mg^{-1}	1-1.5	0.823
			$\sum Wi = 1$

Source: BIS 10500:2012

3.2.1.4 Surface runoff

To estimate the surface runoff from each grid cell, the SCS curve number method (U.S. Soil Conservation Service, 1986) has been used in this study. The runoff depth was calculated by using **Equation 3.20**.

$$Q = \frac{(P-0.2)^2}{(P+0.8S)} \quad (3.20)$$

Where,

Q is the runoff depth (mm).

P is the rainfall (mm).

S is the initial abstraction and is given by **Equation 3.21**:

$$S = \frac{25400}{CN} - 254 \quad (3.21)$$

Where,

CN (Curve Number) represents the curve number.

Curve Number (CN) is a dimensionless parameter, and its value ranges from 1 (minimum runoff) to 100 (maximum runoff). The method analyses observed CN (or runoff) variation between events based on basin factors, initially explained as "AMCs" or Antecedent Moisture Conditions (Heggen, 2010). AMCs are defined in **Table 3.3**.

Table 3.3 Classification of Antecedent Soil Moisture Condition (AMC)

AMC Group	Soil characteristics	Total 5-day antecedent rainfall(mm)	
		Dormant season	**Growing season**
I	Dry condition	Less than 13	Less than 36
II	Normal condition	13-28	36-53
III	Wet condition	> 28	> 53

Source: Handbook of hydrology. Soil Conservation Department, Ministry of Agriculture, New Delhi; 1972

Soils may be classified into four Hydrologic Groups (A, B, C, and D) in **Table 3.4** as defined by SCS soil scientists, depending on infiltration, soil classification, and other criteria.

Table 3.4 USDA-SCS soil classification

Hydrological Soil	Type of Soil	Runoff Potential	Final Infiltration Rate (mm/hr)	Remarks
Group A	Deep, Well-drained sands and gravels	Low	>7.5	High rate of water transmission

Group B	Moderately deep, well-drained with moderately fine to coarse textures	Moderate	3.8-7.5	Moderate rate of water transmission
Group C	Clay loams, shallow sandy loam, soils with moderately fine to fine textures	Moderately high	1.3-3.8	Moderate rate of water transmission
Group D	Clay soils that swell significantly when wet, heavy plastic, and soils with a permanent high water table	High	<1.3	Low rate of water transmission

Source: Handbook of hydrology. Soil Conservation Department, Ministry of Agriculture, New Delhi; 1972.

The study area soils belong to Hydrologic Soil Group C (HSG-C), and the dominant LULC categories are forest, agriculture, built-up, wasteland, and waterbodies. CN values corresponding to AMC-II were taken directly from the handbook; AMC-I and AMC-III were derived using the standard SCS conversion equations given in Appendix IV. Composite CN values for Kohima and Dimapur districts were obtained by weighting the class CNs by their respective areal proportions. A merged CN for the combined study area was further derived by weighting the district composites by their total areas. The values used in this study are presented in **Table 3.5**.

Table 3.5 Class-wise Curve Number (CN) values for Hydrologic Soil Group (HSG) - C soils under different Antecedent Soil Moisture Conditions (AMCs)

LULC	HSG-C	CN (AMC-I)	CN (AMC-II)	CN (AMC-III)
Forest (woodland)	Good condition (dense canopy + litter)	59.48	77.00	89.89
Agriculture (cultivated, straight-row)	Good condition (normal tillage, >20% cover)	66.64	82.00	92.56
Built-up (mixed residential)	Lawns + impervious streets	81.59	91.00	96.68
Wasteland (barren/sparse cover)	Poor vegetation cover	81.59	91.00	96.68
Waterbodies (open water)	—	100.00	100.00	100.00

Source: Handbook of hydrology. Soil Conservation Department, Ministry of Agriculture, New Delhi; 1972.

3.3 To assess the impact of climate change on temporal and spatial variation of water availability in the study area

To fulfil the goal of the second objective, water availability from rainfall was determined under climate change scenarios, as rainfall is the main contributor to water availability. The effect of climate change on water availability is greatly influenced by two parameters, i.e., rainfall and temperature. Many researchers have revealed that rainfall and temperature are crucial physical elements that govern the environmental conditions of a region and also have a significant impact on agricultural productivity (Singh *et al*., 2013; Pathak *et al*., 2014; Sharma *et al*., 2021). Therefore, modeling the relationship between rainfall and temperature is a crucial aspect of understanding climate change scenarios.

The daily rainfall and temperature (maximum and minimum) data of Kohima and Dimapur rain gauge stations for a period of 17 years (2003-2020) have been used as the baseline period to predict the future rainfall at a span of 20-year periods, i.e., 2018-2038, 2039-2059, 2060-2080, and 2081-2100. The process of simulated rainfall for future projections is explained in the following subsections.

3.3.1 General Circulation Model (GCM)

The present study utilized the output of the General Circulation Model (GCM) of CanESM2 (second-generation Canadian Earth System Model), developed by the CCCMA (Canadian Centre for Climate Modeling and Analysis) (Mahdaoui *et al*., 2023). The CanESM2 model has been downloaded from the Canadian Climate Data and Scenarios website (https://climate-scenarios.canada.ca/). The CanESM2 model has been widely used and proven in the projection of precipitation and temperature trends in various regional climate studies (Gebrechorkos *et al*., 2019; Seng *et al*., 2021; Javaherian *et al.*, 2021; Chim *et al*., 2021; Sami *et al*., 2024).

3.3.2 Representative Concentration Pathways (RCPs) scenarios

The Representative Concentration Pathways (RCPs) are concentration pathways used in the Fifth Assessment Report of the Intergovernmental Panel on Climate Change (IPCC AR5). These pathways represent the recommended levels of greenhouse gas and aerosol concentrations, as well as land use change, that align with the general outcomes commonly utilized by the climate modeling community. The IPCC has defined four distinct RCP scenarios based on the level of radiative forcing. These scenarios outline alternative paths for carbon dioxide emissions and the resulting atmospheric concentration throughout the 21st century (Vurren *et al*., 2011). The four scenarios consist of a low-emission scenario (RCP2.6), two intermediate scenarios (RCP4.5 and RCP6.0), and one scenario with very high emissions (RCP8.5).

The present study utilized the climate change scenarios RCP4.5 and RCP8.5, which were obtained from the Canadian Climate Data and Scenarios website (https://climate-scenarios.canada.ca/). The RCP4.5 depicts a scenario in which

rigorous measures are taken to stabilize the energy absorbed by the Earth's atmosphere by the year 2100. This results in a moderate rise in mean global temperatures. In contrast, RCP8.5 represents a high-emission scenario devoid of climate mitigation measures, leading to a substantial increase in temperatures and an escalation in the frequency and intensity of extreme climate events (Moss *et al*., 2010).

3.3.3 Statistical Downscaling Model (SDSM)

The SDSM is a decision support tool developed by R.L. Wilby and C.W. Dawson. It is a weather generator commonly used to simulate climatic data for a specific station, taking into account both present and projected scenarios influenced by climate change. The SDSM utilizes the multiple linear regression approach. The purpose of this model is to forecast long-term climate characteristics, such as rainfall, for specified locations using daily data for calibration (Liu *et al*., 2017). The step-by-step procedure using the SDSM is summarized further.

The National Center for Environmental Prediction (NCEP) predictors relate the strength of each predictor-predictand relationship, and the calibration and validation step involves the establishment of statistical relationships between the selected predictors and the surface predictand (Gagnon *et al*., 2005). The NCEP reanalyzed dataset is a daily time series from 1961 to 2000, including 26 large-scale weather factors. The variable number, abbreviation, and description of the 26 GCM or NCEP weather factors are presented in **Appendix-I**. In this process, simulation of observed data was done with predictors from the NCEP re-analysis data, while for the future periods, i.e., 2018-2038, 2039-2059, 2060-2080, and 2081-2100, GCM CanESM2 with RCP4.5 and RCP8.5 scenarios have been used.

The observed daily rainfall (mm) and temperature (maximum and minimum in ˚C) data for the time period of 17 years (2003-2020) were put in separate text files and saved in the prescribed (*.dat) format for input in the SDSM model. Before downscaling, a check was made to ensure the correct date ranges, type, and integrity of all input data. The CanESM2 model has model years consisting of 365 days,

therefore, the default year length was set to 365 days. The “Standard Start Date” for the present study is taken as 01/01/2003, and the “Standard End Date” as 31/12/2020.

The advantage of SDSM is that it reduces the task of statistically downscaling daily weather series into five discrete processes: (i) screening of predictor variables; (ii) model calibration; (iii) synthesis of observed data; (iv) generation of climate change scenarios; (v) diagnostic testing and statistical analyses.

3.3.3.1 Screening of predictor variables

The screening function has been used to filter predictors. It is the most important step in the whole process of statistical downscaling. Screening variable operation is applied to select efficient large-scale predictors from the set of NCEP reanalysis data based on scatter plots, correlation matrix, partial correlation, and p-value (Mahmood and Babel, 2012; Saraf and Regular, 2016). The main purpose of the ‘Screen Variables’ operation is to assist the user in the choice of appropriate downscaling predictor variables.

After the selection of the large-scale predictor, the selected predictors from the reanalysis data NCEP and observed rainfall data (predictand) are used to establish the statistical relationships for the study area.

3.3.3.2 Model Calibration and Validation

The primary goal of the model calibration process is to determine a study area parameter set that best matches the simulated and observed rainfall during the calibration period and to compute multiple linear regression equations (forced entry method). The model structure was specified as monthly, and the process as conditional. The regression model parameters are written to a standard format file (*.PAR) and derived using Narula and Wellington's efficient dual simplex algorithm (1977). The SDSM stochastically reproduces the distribution of model residuals using the standard errors. A pseudo-random number generator produces values from a normal distribution with a standard deviation equal to the calibration standard error, following the approach of Sirois *et al.* (1981). Every day, this stochastic residual is added to the

deterministic component to increase the downscaled series's variance to fit more closely with daily observations. At last, the calibration algorithm shows the proportion of explained variance and standard error for the monthly regression model to suggest the strength of deterministic forcing. Model calibration is done using the observed rainfall data from 2003-2020; validation uses data from 2010-2020.

3.3.3.3 Synthesis of observed data

The 'Synthesize' operation is used to generate ensembles of synthetic daily weather series given by the daily observed atmospheric predictor variables. The procedure allows for the synthesis of artificial time series for later impact modeling as well as the verification of calibrated models—ideally using independent data. A .PAR file is chosen that includes related regression model weights and references to all required .dat files—both predictand and predictors. The period of record to be synthesized is also stated, together with the preferred number of ensemble members. Synthetic time series are finally written to a designated output file (*.OUT) for later analysis.

3.3.3.4 Statistical analysis for model performance

The coefficient of determination (R^2) for both the Kohima and Dimapur stations during the calibration was used to evaluate the performance of the SDSM following Mahmood and Babel (2013). The general equation of the coefficient of determination (R^2) is given below.

1. **Coefficient of determination (R^2)**

The Coefficient of determination is used to show the accuracy of the model in predicting data. The coefficient of determination (R^2) is presented in **Equation 3.22.**

$$R^2 = \frac{\sum(X_i - X')*(Y_i - Y')}{\sum(X - X')2*(Y - Y')2} \quad (3.22)$$

The value of R^2 explains the correlation between observed and downscaled values and lies between 0 and 1, where 0 indicates poor and 1 for the best.

3.3.3.5 Generation of climate change scenarios

The ‘Generate’ scenario operation creates ensembles of synthetic daily weather series given by the observed daily atmospheric predictor variables provided by a GCM (either for current or future climate experiments). Except for the model dates, the process is the same as the 'Synthesize' operation in all respects. The climate change data is generated by selecting the RCP4.5 and RCP8.5 scenarios and saved into specified (.OUT) output files. Here, the selection of the analysis future period, i.e., 2018-2038, 2039-2059, 2060-2080, and 2081-2100, taking 20-year intervals, depends on the observed data.

3.4 To identify and recommend an acceptable climate change adaptation strategy to address water shortage or excess in the near future

To fulfill the third objective, the potential major crops were identified in the study area. Then, the crop water requirement for the major crops was evaluated using the CROWAT 8.0 software. The CROPWAT is a decision support tool designed by the Land and Water Development Division of the Food and Agriculture Organization (FAO). It is a software application designed to compute the water needed for crops and irrigation. It uses data on soil, climate, and crop characteristics to calculate the crop water requirements.

The climate data, such as the maximum and minimum temperature, rainfall, relative humidity, wind speed, and sunshine hours, were obtained from the Department of Soil and Water Conservation, Government of Nagaland, Kohima. The soil and crop data were collected from the guidelines for estimating irrigation water requirements (IWRs), the Ministry of Irrigation, Government of India (1984), and the FAO. Further, the crop water requirement was converted to the same index as I_{AWA} for a better and easier comparison. The relative climate change adaptation options were proposed based on the findings of this study.

3.4.1 Computation of crop water requirement

In the present study, the CROPWAT 8.0 model has been used to compute crop water requirements. The water requirement may be defined as the quantity of water,

regardless of its source, needed by a crop or diversified pattern of crops in a certain period for its normal development under field conditions at a place.

The CROPWAT model determines the crop water requirement using the crop coefficient and reference evapotranspiration. The crop evapotranspiration (Etc) is given in **Equation 3.23** (Sinha *et al*., 2024).

$$ET_c = K_C \times ET_O \quad (3.23)$$

Where,

ET_c is the crop evapotranspiration.

K_C is the crop coefficient.

ET_O is the reference evapotranspiration.

3.4.1.1 Reference Evapotranspiration

The CROPWAT 8.0 model uses the FAO Penman-Monteith formula for the computation of evapotranspiration of reference crops. Several methods exist to determine reference evapotranspiration (ETo), and the Penman-Monteith (P-M) method has been recommended as the appropriate combination method to determine ETo from climatic data (Pawar *et al*., 2021).

The reference evapotranspiration (ETo) was calculated by the FAO Penman-Monteith method, using decision support software –CROPWAT 8.0 developed by FAO, based on FAO Irrigation and Drainage Paper 56 (FAO56). FAO56 adopted the P-M method as a global standard to estimate ETo from meteorological data (Allen *et al*., 1998; Allen *et al*., 2007). Climatic parameters used for the calculation of ETo were latitude, longitude, and altitude of the station, maximum and minimum temperature (˚C), maximum and minimum relative humidity (%), wind speed (km/day), and sunshine hours.

The Penman-Monteith equation integrated into the CROPWAT program is expressed by **Equation 3.24 (**Pawar *et al*., 2021).

$$ET_O = \frac{0.408\,\Delta(R_n - G) + \gamma \frac{900}{T+273} U_2 (e_a - e_d)}{\Delta + \gamma(1 + 0.34)} \quad (3.24)$$

Where,

ET_O is reference crop evapotranspiration, mm day^{-1}.

R_n is net radiation at the crop surface, MJ m^{-2} day^{-1}.

G is soil heat flux, MJ m^{-2} day^{-1}.

γ is psychrometric constant, kPa $^{\circ}C^{-1}$.

T is the average air temperature, $^{\circ}C$.

U_2 is windspeed measured at 2 m height, m s^{-1}.

$e_{a-}e_d$ is vapor pressure deficit, kPa.

Δ is the slope of the vapor pressure, kPa $^{\circ}C^{-1}$.

3.5 To assess mechanization index and recommend suitable agricultural implements under less water availability

Farm mechanization is essential for the efficient use of inputs, which enhances production and productivity by reducing labor-intensive tasks associated with agricultural operations. In India, farm mechanization has advanced significantly, but for various reasons, its implementation has not been uniform across all states. The degree of mechanization is very low, particularly in the northeastern states, and there are several reasons behind this. The growth of the farm equipment sector in these states has been limited by factors such as steep topography, high transportation costs, lack of state financing, financial restraints owing to socio-economic conditions, and a shortage of agricultural machinery. The farm power available in Nagaland is 0.73 kW/ha, which is way below the National average of 2.02 kW/ha.

Therefore, considering the facts, it is advocated to assess the mechanization index in the study area, which would help the researchers to recommend some agricultural implements and machines for the mechanization of the agricultural sector in the state under less water availability situation. The assessment procedure of the mechanization index is explained under the following sub-sections.

3.5.1. Preparation of questionnaire

A questionnaire was prepared in order to collect data about the demographic information of farmers, types of crops grown, production, and machinery used in the study area. The questionnaire is given in **Appendix-II.** The questionnaire was developed with the help of a standardized Nordic questionnaire (Kuorinka *et al.,* 1987).

The questionnaire is prepared in two parts. In the first part of the questionnaire, demographic information such as nature of the appointment, the present age of the respondent, gender, working habit (right-handed or left-handed), educational

qualification, ethnic group, stature, weight, work experience, hours of work per day and per week, was included.

The second part of the questionnaire comprised the number and type of crop grown, hand tools/implements used, animal-drawn implements used, power-operated implements used, price and availability of modern tools and implements, after-service facility of the agricultural implements/machines, and benefits of the agricultural implements.

The questionnaire was examined through test-retest analysis for reliability, and the correlation of items was made with physical examinations for validity.

3.5.2 Selection of subjects

Before the selection of the subjects, a meeting was conducted with progressive farmers, Gram Pradhan (*Gaon Buras*), officials from the Department of Agriculture, Government of Nagaland under Dimapur and Kohima districts, and Krishi Vigyan Kendra, and explained the aim and objectives of the study.

For the selection of the subject, a survey was carried out among the farmers/users of implements based on the number of crops grown and the land held by the farmer. In total, 101 farmers, including males and females in the age group of 18–60 years, with a minimum of 3 years of experience, were selected randomly for the study. The farmers who volunteered to make themselves available were accepted as subjects.

3.5.3 Method of data collection

The survey procedure was explained in detail to the farmers. Meetings with the farmers were conducted in the community hall to explain the purpose of the study. The farmers who were convinced about the purpose of the study and gave consent to cooperate with the study were considered for the collection of data.

Before starting the interview, the content of the questionnaire was discussed with the subjects/respondents. Each subject was interviewed individually in a face-to-face interview in a homely atmosphere. First, demographic information was collected. The questionnaire was translated into the Nagamese dialect. To prevent

comprehension difficulties, the interviewer read the question to the subject, and the answer was filled in one by one.

3.5.4 Mechanization Index assessment

Recognizing the economic impact on farming, the mechanization index approach has been calculated as suggested by Singh (2006). The empirical relation for assessment of MI is given in **Equation 3.25**:

$$MI_{ij} = \frac{CM_{ij}}{(CH_{ij}+CA_{ij}+CM_{ij})} \tag{3.25}$$

Where,

MI_{ij} is the mechanization index of i^{th} crop in j^{th} district.

CM_{ij} is the cost of use of the machine in i^{th} crop in j^{th} district.

CH_{ij} is the cost of human labor in i^{th} crop in j^{th} state.

CA_{ij} is the cost of use of animal labor in i^{th} crop in j^{th} district.

CHAPTER 4

RESULTS AND DISCUSSION

The study's empirical findings have been given in this chapter and divided into four categories based on the study's objectives. The first section analyzes water availability from different components to develop an Agricultural Water Availability Index (I_{AWA}) for the present scenario. The second segment focuses on analyzing the impact of climate change on temporal and spatial variation of water availability for future scenarios. The third section is to identify and propose a viable climate change adaptation strategy to effectively manage water scarcity or surplus in the near future. The fourth objective is to evaluate the mechanization index and provide appropriate agricultural equipment for situations with limited water supply.

4.1 Development of an Agricultural Water Availability Index (I_{AWA}) for the present scenario

Agriculture is Nagaland's primary source of employment and revenue, accounting for 25% of the state's gross domestic product (GDP) as per the Nagaland Economic Survey 2023-2024. However, the State utilizes only a minor portion of its potential cultivable land and harnesses only a fraction of its available renewable water resources. In addition, there has been a lack of research on the potential of land and water resources in the State, particularly in rural areas, especially Kohima and Dimapur districts, despite their significant importance. Therefore, an index has been developed that evaluates the agricultural potential by considering water availability from various sources such as rainfall, soil moisture, surface runoff, and groundwater. The index is a significant instrument for promoting sustainable water management in agriculture by facilitating the equilibrium between water supply and agricultural requirements.

4.1.1 Rainfall

Rainfall is the main form of precipitation in the study area. Rainfall data on a daily time scale were acquired for the stations of interest located in the study area. The

average annual or seasonal rainfall at a place needs to give sufficient information regarding its capacity to support any decision-making process, so keeping that in mind, six rain gauge stations have been selected. The daily scaled data was summed up, and a monthly depth of rainfall was calculated for each rain gauge station from 2003 to 2020, as shown in **Table 4.1**.

Table 4.1 shows the monthly average rainfall (mm) of the selected rain gauge stations. The monthly average rainfall varies across the stations; the maximum rainfall was observed in the monsoon season, i.e., from May to September, where Wokha station recorded the highest monthly rainfall in July (458.75 mm), while the minimum rainfall was observed in the winter season, i.e., from November to February where Dimapur station recorded the lowest monthly rainfall in December (3.56 mm).

Table 4.1 The monthly average rainfall (mm) of the selected rain gauge stations (2003-2020)

Month	Rain gauge stations					
	Kohima	**Dimapur**	**Sechu**	**Wokha**	**Jalukie**	**Phek**
Jan	15.57	4.49	15.08	15.95	6.74	10.48
Feb	20.41	9.95	27.97	24.81	12.78	16.64
Mar	49.49	21.68	53.36	46.81	37.05	45.60
Apr	94.23	70.36	132.75	136.78	106.15	115.46
May	279.30	105.53	202.75	215.22	141.40	177.25
Jun	270.95	172.44	269.19	380.99	252.73	248.41
Jul	353.79	166.56	305.45	458.75	258.16	302.71
Aug	322.16	164.79	293.02	377.52	277.16	245.02
Sep	254.90	128.78	228.12	360.54	193.46	192.62
Oct	142.41	103.97	130.66	153.76	126.52	150.64
Nov	17.53	12.29	21.73	22.58	17.59	21.71
Dec	11.74	3.56	12.86	11.44	9.44	10.25

For the spatial distribution of monthly rainfall, the Inverse Distance Weighting (IDW) technique was applied across the study area. The IDW function in GIS was utilized for the interpolation with a modest weighting value (4) to regulate the impact of known points on the interpolated values, depending on their distance from the output point. The purpose of interpolation in this study was to analyze the study area's spatial distributions and evaluate the measurement in the uncovered area. The spatial analysis interpretation shown in **Table 4.2** revealed that minimum rainfall was received in January, February, and December, while maximum rainfall was observed in June, July, and August. The month of July received the highest rainfall (556.33 mm), and the month of December received the lowest rainfall (3.56 mm). A similar finding was reported by Kusre and Singh (2012a), noting that Nagaland experienced higher levels of rainfall in July (528.6 mm) and lower levels in December (27.8 mm).

Table 4.2 The maximum and minimum rainfall (mm) received during each month (2003-2020)

Month	Max rainfall	Min rainfall
Jan	16.52	4.49
Feb	14.43	9.94
Mar	42.03	21.68
Apr	106.11	70.36
May	188.79	105.53
Jun	379.45	172.44
Jul	556.33	166.55
Aug	456.85	164.82
Sep	376.28	128.77
Oct	135.18	103.97
Nov	23.19	13.42
Dec	10.18	3.56

A spatial distribution map of monthly mean rainfall (mm) from 2003 to 2020 in the study area from January to June is shown in **Fig 4.1**. During January and February, the study area had comparatively low rainfall, with most of the area receiving less than 50 mm of rainfall. In January, most of the region encounters rainfall below 10 mm; however, in February, rainfall ranges from 10 to 50 mm. Starting in March, there is a discernible escalation in rainfall ranging from 50-100 mm. The eastern part of the study area has a greater level of rainfall intensity in comparison to the western part. During April, rainfall levels continue to rise, resulting in a wider distribution of locations receiving 50-150 mm of rainfall. The middle and eastern parts of the area have elevated rainfall levels, suggesting a transition towards the more humid season. In May, rainfall distribution becomes more concentrated, receiving 100-250 mm of rainfall. The central part of the study area exhibits the greatest rainfall, receiving up to 300 mm. During June, the study area has the highest amount of rainfall, known as the pre-monsoon or early monsoon season. The majority of the region receives a rainfall range of 150-350 mm, with the highest rainfall occurring in the central and northeastern parts, occasionally surpassing 350 mm of rainfall.

During the month of July, there is a substantial amount of rainfall seen throughout the study area, with a considerable chunk getting between 200-450 mm of rainfall. In August, there is a continuation of the pattern of intense rainfall, with large regions experiencing rainfall amounts ranging from 250 to 500 mm. During September, the rainfall diminishes significantly, although the area still encounters substantial rainfall, with quantities varying from 150-450 mm. During the month of October, there is a significant decrease in rainfall, with the majority of regions obtaining a range of 50-150 mm. The western and central portions of the study area receive a considerable amount of rainfall, whilst the remaining areas of the region have lower levels of rainfall. In November, the amount of rainfall reduces even more, with most of the region receiving less than 50 mm of rainfall. During the month of December, there is very little precipitation over the entire study area, receiving less than 10 mm of rainfall. This reveals that the dry season will persist, with minimal rainfall as the area transitions into the winter season.

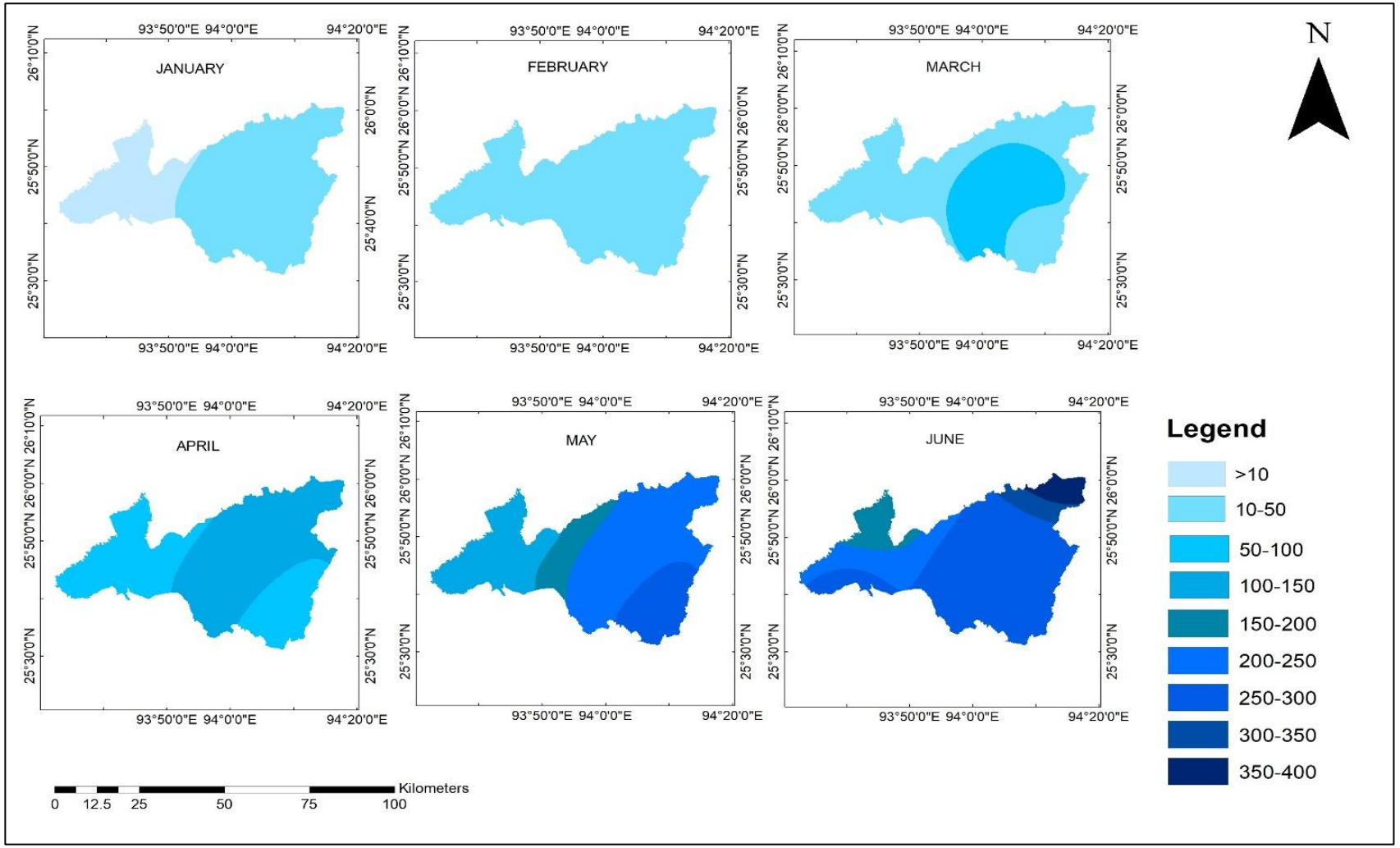

Fig 4.1 Spatial distribution map of monthly mean rainfall (mm) from 2003-2020 in the study area (Jan-Jun)

From **Fig 4.1** and **4.2**, the rainfall regime in the study area shows marked spatial variability due to differences in topography and elevation between the two districts. Dimapur, situated in the western plains at ~260 m elevation, records comparatively lower annual rainfall (≈ 1,500–1,800 mm) with strong concentration during the southwest monsoon months (June–September). The district often experiences intense short-duration rainfall events that can trigger localized flooding, followed by prolonged dry periods during winter (Nagaland PSC Notes, 2022). In contrast, Kohima, located in the central to northeastern highlands at ~1,261 m, receives significantly higher rainfall, averaging ≈ 2,500 mm annually, due to orographic uplift effects. Rainfall here is more evenly distributed across the monsoon period, with monthly totals frequently exceeding 300 mm in July and August. While this reduces flood risk compared to Dimapur, the steep slopes of Kohima intensify soil erosion hazards (Lalmalsawmzauva *et. al*., 2020).

It has been revealed that the central and northeastern parts of the study area encompass the hilly terrain of Kohima district, resulting in increased rainfall due to the ascent and cooling of moist air masses over the mountains. The southwestern part of the map encompasses the Dimapur district, which is located at a lower altitude and has relatively lower levels of rainfall. A similar study was conducted by Sema *et al.* (2017); they reported that the hilly terrain of Kohima enhances rainfall due to orographic lifting, unlike the flatter Dimapur region. The variation in rainfall patterns in Nagaland between July and December was influenced by several interrelated factors, such as the topography of the region, which plays a crucial role. The hilly terrain significantly affects rainfall distribution, due to which the northern areas receive more rainfall during the monsoon season (July) compared to the eastern and western parts, which experience a shift in rainfall patterns by December, receiving less precipitation (Kusre and Singh, 2012b).

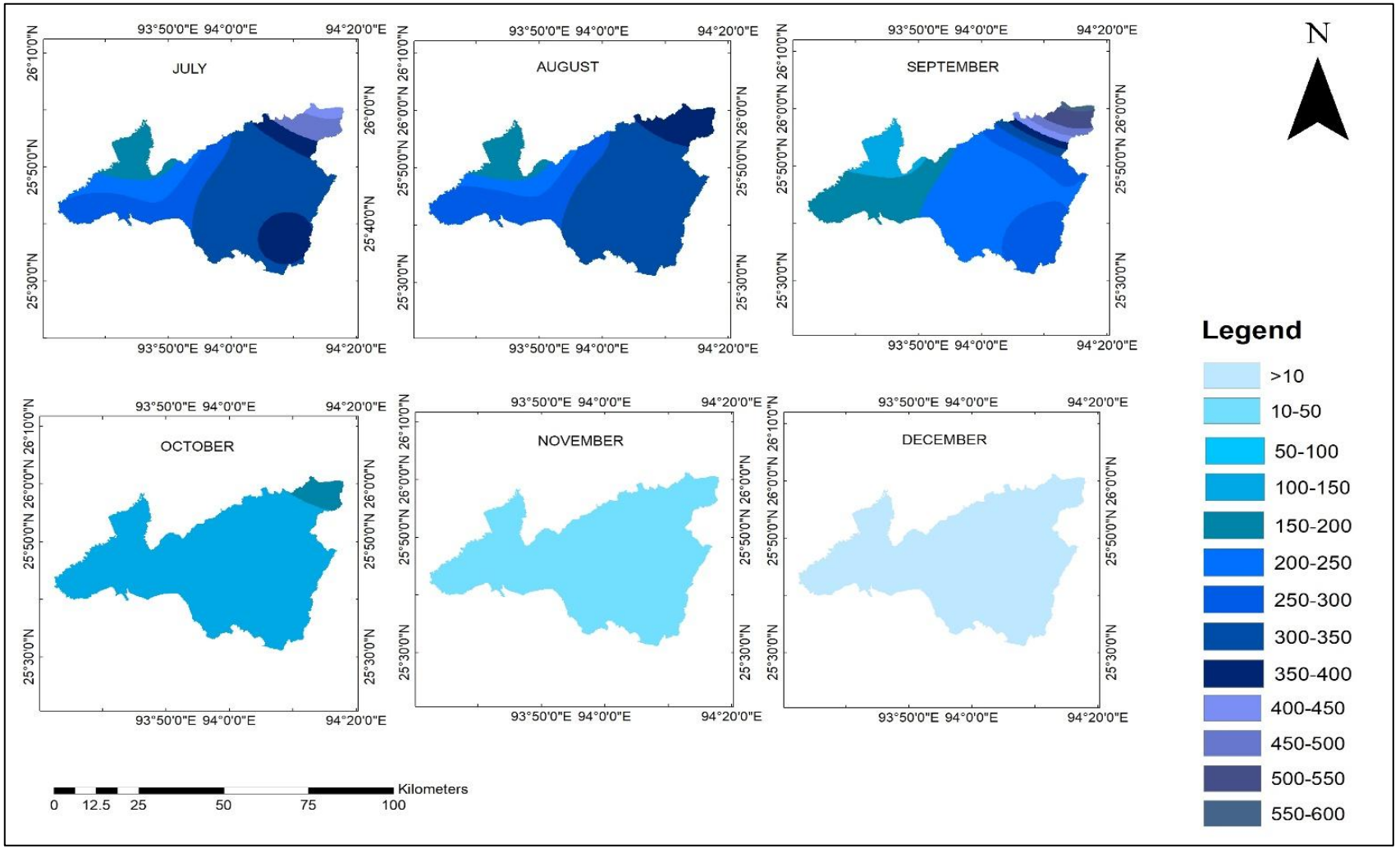

Fig 4.2 Spatial distribution maps of monthly mean rainfall (mm) from 2003-2020 in the study area (Jul-Dec)

4.1.2 Available soil moisture storage

The available soil moisture of the study area was determined according to the procedure outlined in section 3.2.2. The monthly satellite images of the Normalized Difference Vegetation Index (NDVI) and Land Surface Temperature (LST) of the study area were acquired from the National Aeronautics and Space Administration (NASA) website for 2011, as this year was observed as an average wet year for the analysis period (FAO, 2010). The mean annual rainfall in the study area that occurred during 2011 was noted as 824.48 mm. This amount of rainfall occurred at a 50 percent probability of exceedance, and according to the FAO recommendations, any year that receives rainfall at a 50 percent probability of exceedance is an average wet year; the details of this analysis can be found in **Appendix-III**. The results of the monthly soil moisture index map of 2011 indicate that the soil moisture index was in the range of 0 to 1 and was classified in four color gradients. As per the index, "1" represents a higher presence of water or moisture, and "0" indicates minimum moisture content, such as in dry areas.

During the months of January to March, the predominant colors in the area are blue and violet, which signify a low level of soil moisture as shown in **Fig 4.3**. This presumably refers to the dry season, during which there is less precipitation, leading to reduced water availability and, thus, low soil moisture. Particularly, the central and southeastern parts of the map have high levels of soil moisture, indicated by the yellow to red color. In April, there is a significant rise in soil moisture levels in some parts of the areas, indicated by a change in color from yellow to red. This increase is particularly noticeable in the southeastern half of the region. This phenomenon may be attributed to the commencement of the pre-monsoon period, during which early rainfall or increased humidity leads to an augmentation in soil moisture. The central and southern parts of May exhibit a notable abundance of high soil moisture levels. This could correspond to the zenith of the pre-monsoon season or the initial monsoon precipitation, which thoroughly saturates the soil in these regions. In June, there is a significant expansion of high soil moisture levels (shown by yellow to red color) across a large portion of the map, indicating extensive accumulation of moisture resulting

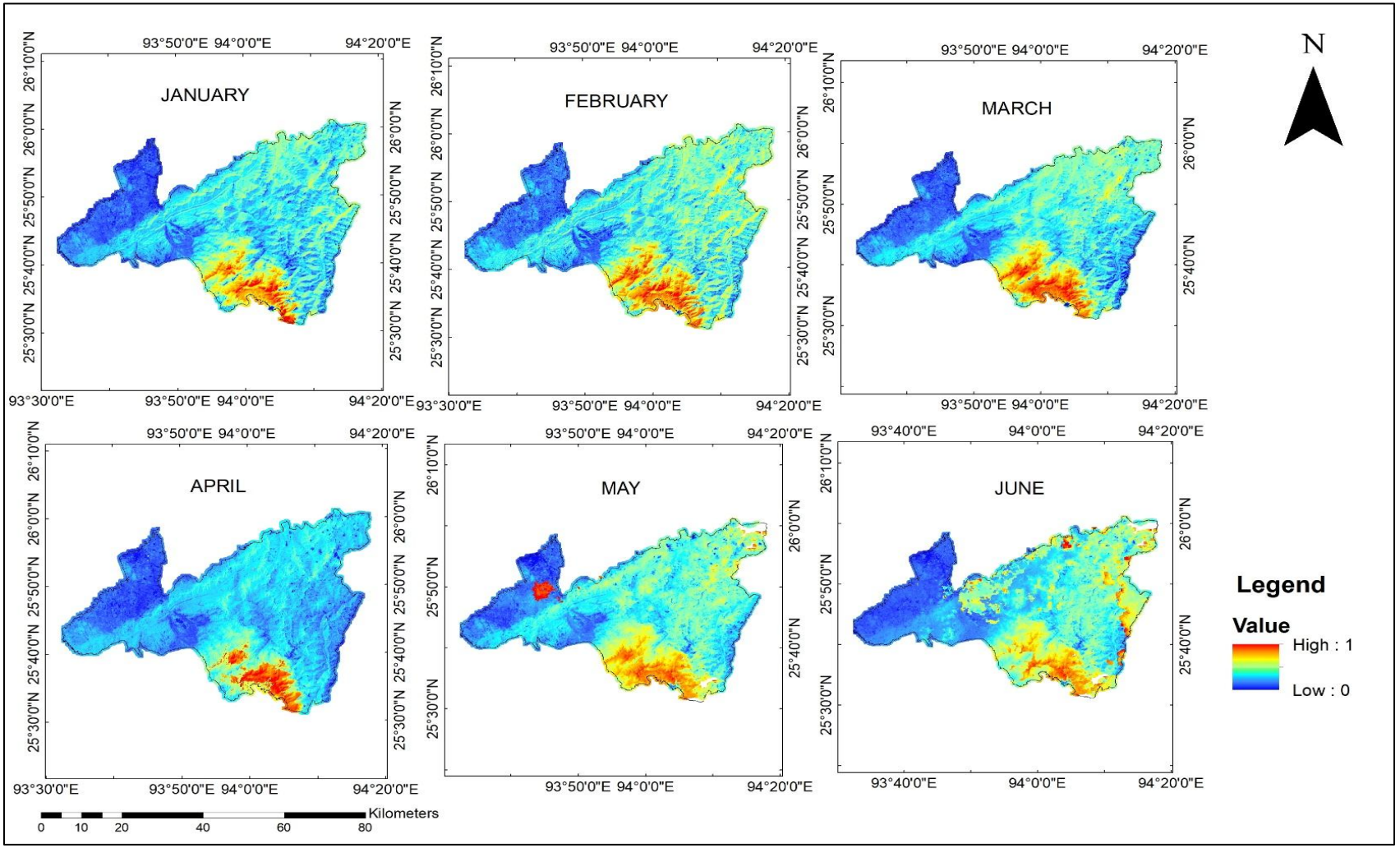

Fig 4.3 Spatial distribution map of monthly soil moisture of average wet year (2011) in the study area (Jan-Jun)

from higher rainfall during the monsoon season. This signifies the onset of the wet season, during which the soil moisture reaches its highest level.

In July, there is a notable abundance of elevated soil moisture in the southern regions, as shown by the yellow to red coloration in **Fig 4.4**. This indicates that the area is experiencing significant precipitation during the peak monsoon season, resulting in soil saturation. In August, there has been a notable expansion of areas with higher soil moisture levels, particularly in the central and northeastern part of the study area. This phenomenon is most likely caused by the influence of the monsoon, which enhances the availability of water over a wider expanse. In September, there is a comparable trend to August, where there is a large region with high levels of soil moisture. However, certain places, particularly in the northwest, begin to exhibit lower soil moisture levels (shown by the blue color), signaling the start of the post-monsoon drying phase. In October, there is a discernible decline in soil moisture throughout the region, particularly in areas indicated by blue and violet colors. This signifies the withdrawal of the monsoon and the commencement of the dry season. Nevertheless, several areas, especially in the southern part of the study area, continue to maintain significant levels of moisture, either as a result of lingering water from the monsoon season or localized precipitation. In November, the drying trend persists, with a majority of the region exhibiting reduced moisture levels. This is in line with the dry season, during which there is a drop in availability, resulting in lower soil moisture that reflects the normal conditions of the dry season.

The analysis indicated that over 50 percent of the region experienced a moisture deficit during the winter season, as seen by the majority of the area having values near 0. This observation aligns with the pattern of rainfall in the study area. Additionally, the data indicated that the southern part had greater soil moisture levels compared to the western part, which can be attributed to the higher elevation of the southern part in the study area. The reason for this is that the southern part encompasses the Kohima region, which is characterized by a mountainous and undulating terrain (Belho and Rawat, 2023). While the western part encompasses the Dimapur region, which contrasts with the rough terrain by consisting largely of flat land with warmer and humid soil (Nienu, 2024).

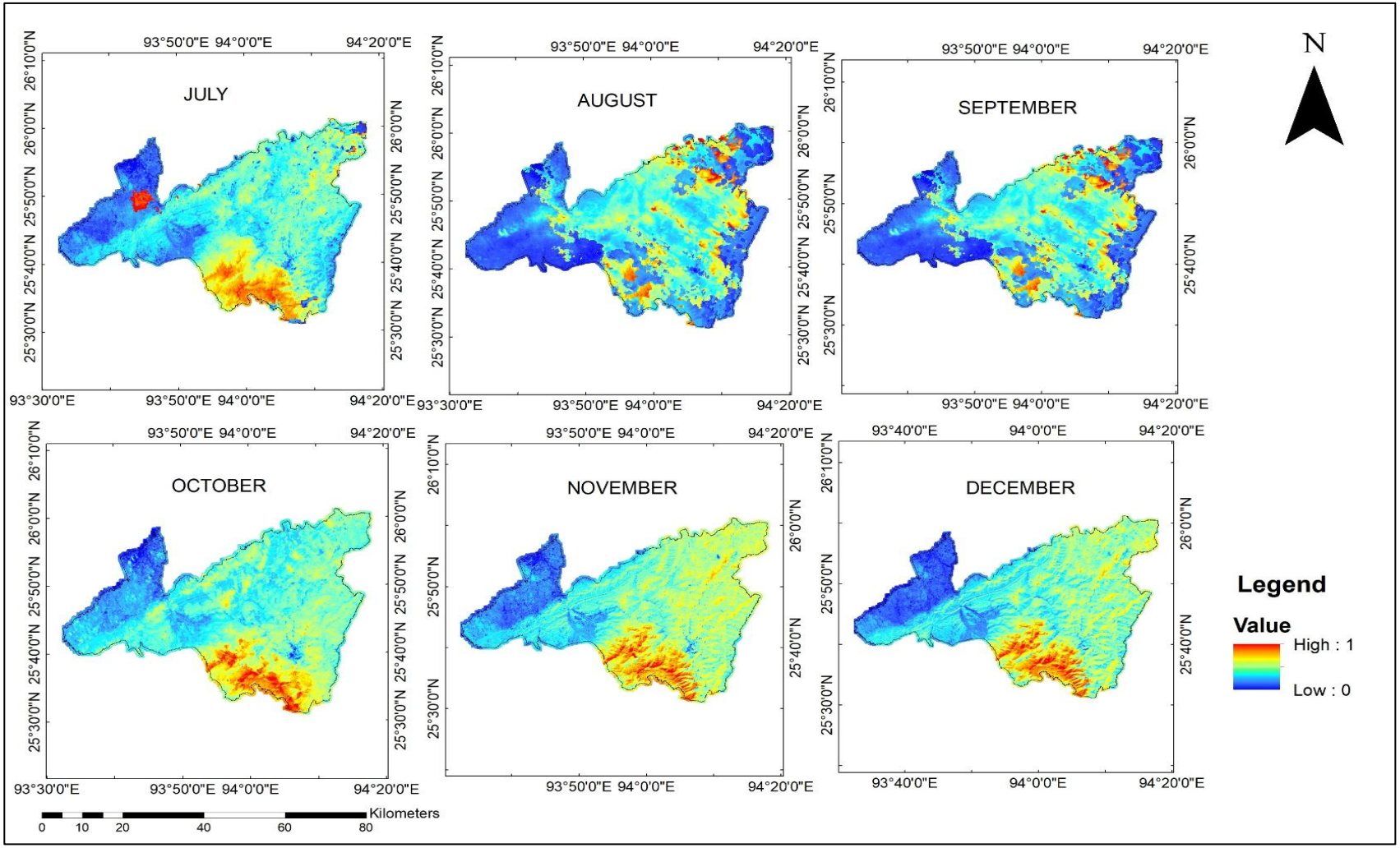

Fig 4.4 Spatial distribution map of monthly soil moisture of average wet year (2011) in the study area (Jul-Dec)

4.1.3 Groundwater

Groundwater is a vital water resource that can be tapped whenever water is needed. For spatial analysis, the groundwater depth and water quality index were interpolated using the IDW technique in GIS for the study area.

A spatial distribution map of monthly groundwater depth (m) from 2014 to 2020 in the study area from January to June is shown in **Fig 4.5**. It revealed that in January, the groundwater depth showed variability across the study area. Most regions have a depth ranging between 4.4-5.2 m. The central and eastern parts have shallower groundwater depths (closer to 4.4 m), while some parts, particularly in the west, exhibit slightly deeper levels (up to 5.6 m). In February, there was a noticeable decrease in groundwater depth in the central part of the study area, where the depth reached between 4.8-5.2 m. The eastern part shows shallower groundwater (closer to 4.4 m), indicating a slight replenishment or reduced groundwater extraction compared to the central part. By March, groundwater depths across most of the study area are deeper, generally ranging from 4.8-5.6 m. The map indicates that the groundwater levels are consistently deeper in the western and central regions, suggesting either increased usage or reduced recharge during this period. In April, the groundwater depth remains relatively deep across the study area, with most areas showing depths of 4.8-5.6 m. The uniformity in depth suggests that groundwater depths continue to decrease as the dry season progresses, possibly due to continued extraction and minimal recharge. May follows a similar pattern to April, with deep groundwater depths (5.2-5.6 m) observed throughout the study area. This indicates that the dry season continues to affect groundwater depths, with little to no recharge occurring during this month. In June, the groundwater depth remains deep across the study area, still within the range of 4.8-5.6 m. The depth does not show significant variation, which could be due to the beginning of the monsoon season, where rainfall might not yet be sufficient to cause a noticeable recharge in groundwater depths.

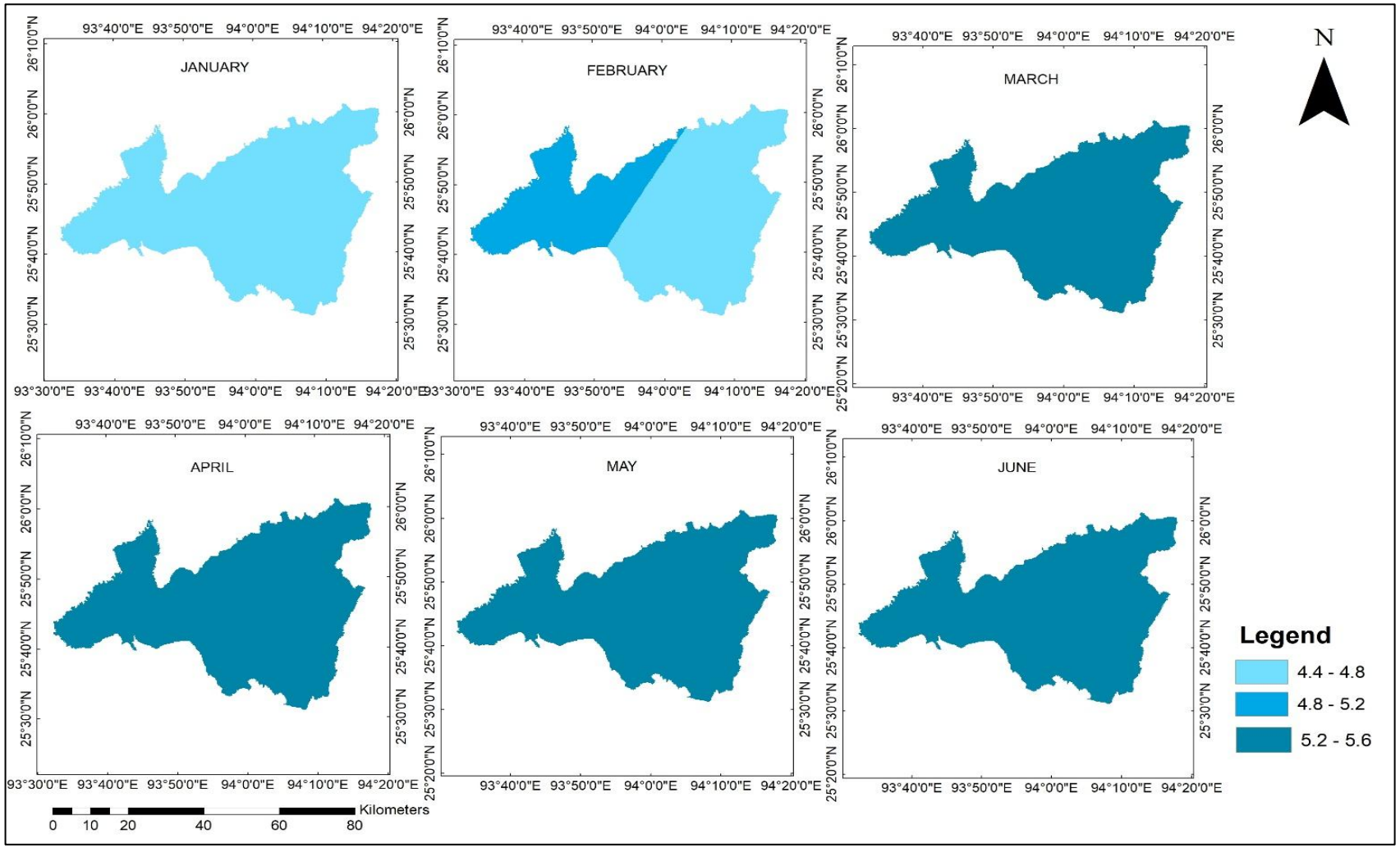

Fig 4.5 Spatial distribution map of monthly groundwater depth (m) from 2014-2020 in the study area (Jan-Jun)

A spatial distribution map of monthly groundwater depth (m) from 2014 to 2020 in the study area from July to December is shown in **Fig 4.6**. It has been observed that in July, the groundwater depth varies between 4.4 -5.6 m. The map shows a darker shade indicating deeper groundwater depths (4.4-4.8 m). The study area shows relatively uniform groundwater depth during the latter months (August to December), with minimal variation (5.2-5.6 m) across the study area. This pattern could imply that the groundwater depths are influenced by seasonal factors, possibly related to rainfall and water usage patterns in the study area. The decrease in groundwater depth from July onwards might indicate the effect of the rainy season, leading to recharge and an increase in groundwater depths, followed by gradual depletion as the dry season progresses.

Spatial groundwater-depth maps confirm that the water table lies mostly between 4.4 m and 5.6 m bgl. The consistently deep groundwater levels justify the assumption used in Equation 3.2 that G_{ij} is negligible for current agricultural conditions. The inclusion of these maps ensures visual and quantitative support for the water-balance assumption. In a similar study conducted by Bora *et al.* (2022) found that rainfall played a crucial role in determining groundwater depths in Northeast India. The study revealed significant upward trends in groundwater depths during the peak monsoon months. In Kamrup, Assam, another study was conducted by Goswami and Rabha (2020) reported the impacts of declining monthly rainfall during the monsoon (Jun-Sep) and post-monsoon (Oct-Nov) seasons. Their outcome is also reflected in the increasing trend of monthly average groundwater levels mbgl (meter below ground level) in the post-monsoon (Oct-Nov) and winter seasons (Dec-Feb). Furthermore, it was shown that the decrease in groundwater availability during winter could be attributed to the decrease in rainfall during the monsoon season.

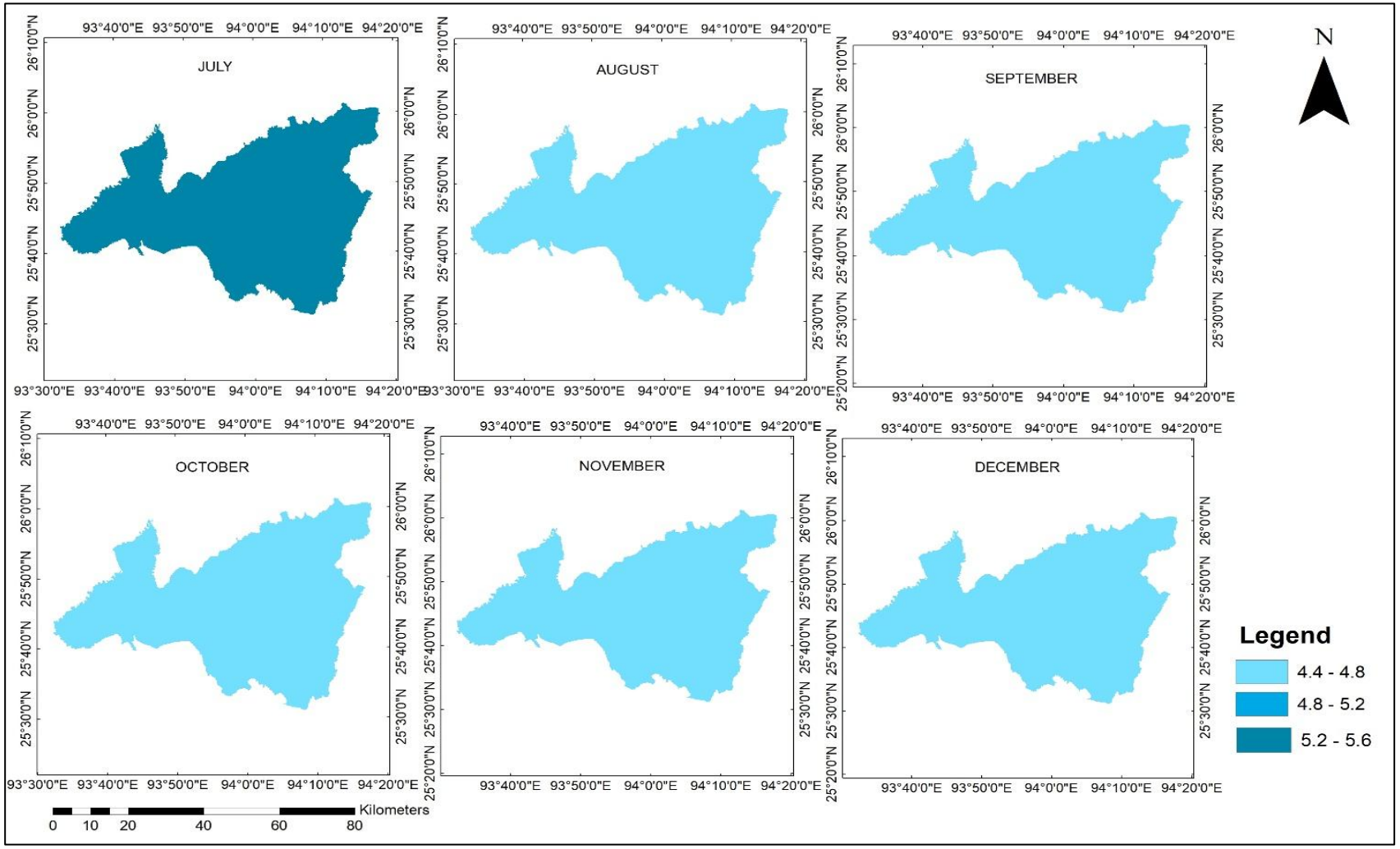

Fig 4.6 Spatial distribution map of monthly groundwater depth (m) from 2014-2020 in the study area (Jul-Dec)

4.1.3.1 Water Quality Index (WQI)

The water quality was assessed by analyzing the four parameters, as described in section 3.1.1.3.1. Further, the groundwater quality parameters, i.e., potential of hydrogen (pH), electrical conductivity (EC), nitrate (NO_3), and fluoride (F) analysis results were compared with BIS 10500 (2012) standards to examine the suitability for drinking purposes (**Fig 4.7 to 4.11**). The spatial distribution of the water quality is illustrated in **Fig 4.12**. Although WQI is traditionally applied for potable-water evaluation, the physico-chemical parameters involved—such as pH, EC- are also key indicators of soil salinity, sodicity, and irrigation water quality. Therefore, the WQI values, while developed under drinking-water standards, can also serve as supportive evidence of general water suitability for agriculture.

Recent literature corroborates that WQI-based analyses can meaningfully inform both drinking and irrigation perspectives when interpreted with proper context. For example, Ramakrishnaiah *et al.* (2009) and Vasanthavigar *et al.* (2010) applied WQI to groundwater in Indian watersheds to discuss implications for domestic as well as irrigation use. Similarly, Mammeri *et al.* (2023) demonstrated that drinking-water WQI results could be extended to irrigation assessment by comparing EC and major-ion data with the Indian irrigation standard IS 11624 (1986). A global review by Yang *et al.* (2023) further confirms that WQI frameworks can be adapted for multipurpose evaluation by adjusting weighting factors for irrigation relevance. Therefore, the WQI primarily reflects the suitability of available water resources for human consumption, its spatial pattern, and constituent hydro-chemical parameters also complement the Agricultural Water Availability Index (I_{AWA}), as both collectively depict the integrated status of water quantity and quality influencing sustainable agricultural potential across the study area. The following discussion presents the findings of the analysis.

Potential of hydrogen (pH)

Water in a pure state has a neutral pH, which shows a concentration of hydrogen ions in water. The pH in the study area was found between 2-8.4 (**Fig 4.7**). As per the Bureau of Indian Standards (BIS) Act 2012, the pH has to be in the range of 6.5-8.5 for drinking purposes. This implies that the pH value is within the

permissible limit. The pH analysis indicates that the groundwater in the study area exhibits a neutral to slightly acidic nature. Previous researchers also found that the pH level of the Dimapur area lies within the acceptable range of 7.03-7.93 (Puzari *et al.*,2015). A similar study was conducted by Peseyie and Rao (2017) and found that the pH level of groundwater in the Patkai campus, Dimapur, was within the acceptable range for determining its quality.

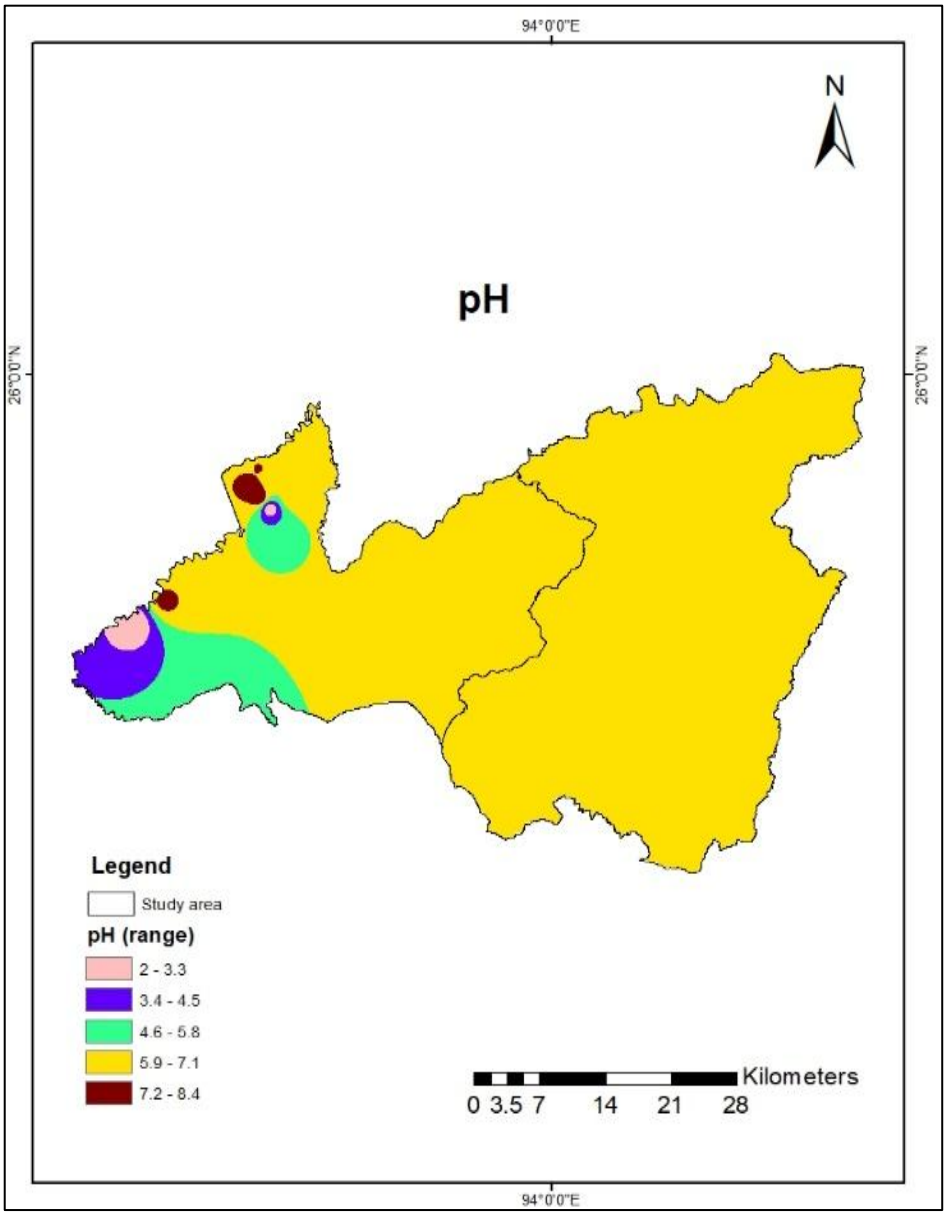

Fig. 4.7 Spatial distribution map of potential of hydrogen (pH) in the study area

Electrical Conductivity (EC)

The electrical conductivity (EC) is a measure of the dissolved substances in an aqueous solution; the higher the dissolved material in a water sample, the higher the EC will be in that substance. Electrical conductivity can serve as an approximate indicator of the overall concentration of dissolved substances in water (Sarath *et al*., 2012). As per BIS, the permissible limit for EC is 2500µS/cm. In the study, the EC is found in the range of 158-841µS/cm, which is within the permissible limit (**Fig 4.8**). A similar study was conducted by Puzari *et al.* (2015) and found that the EC was within the permissible limit (774.7µS/cm) in assessing the quality of drinking water in Dimapur. However, Keditsu *et al.* (2022) found the EC in the range of 98.7-600µS/cm in assessing the groundwater quality in Chiephobozou town, Kohima. The presence of high EC shows a higher concentration of salts in the groundwater.

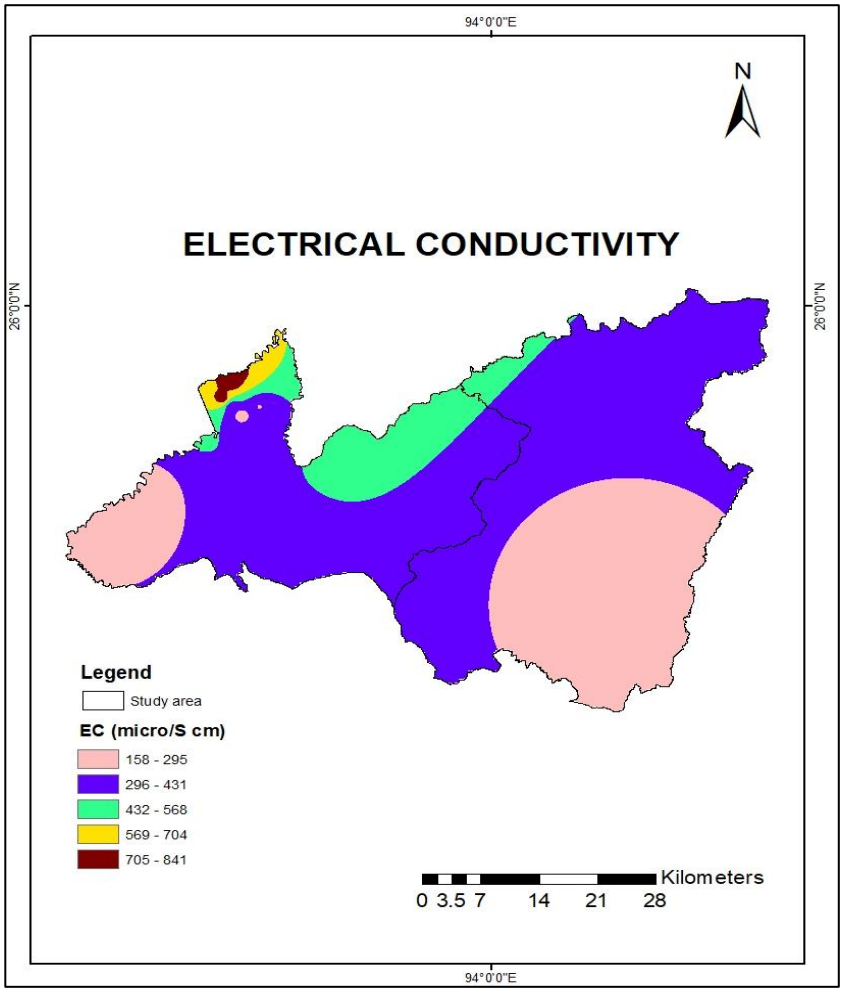

Fig. 4.8 Spatial distribution map of electrical conductivity (EC) in the study area

Nitrate (NO_3)

The nitrate (NO_3) concentration causes blue baby syndrome, thyroid disease, gastric cancer, and diabetes beyond the permissible limit (45 mg^{-1}) as per the BIS standard (2012). The nitrate concentration in the study area ranges between 1-14 mg^{-1}, which is under the desirable limit (**Fig 4.9**).

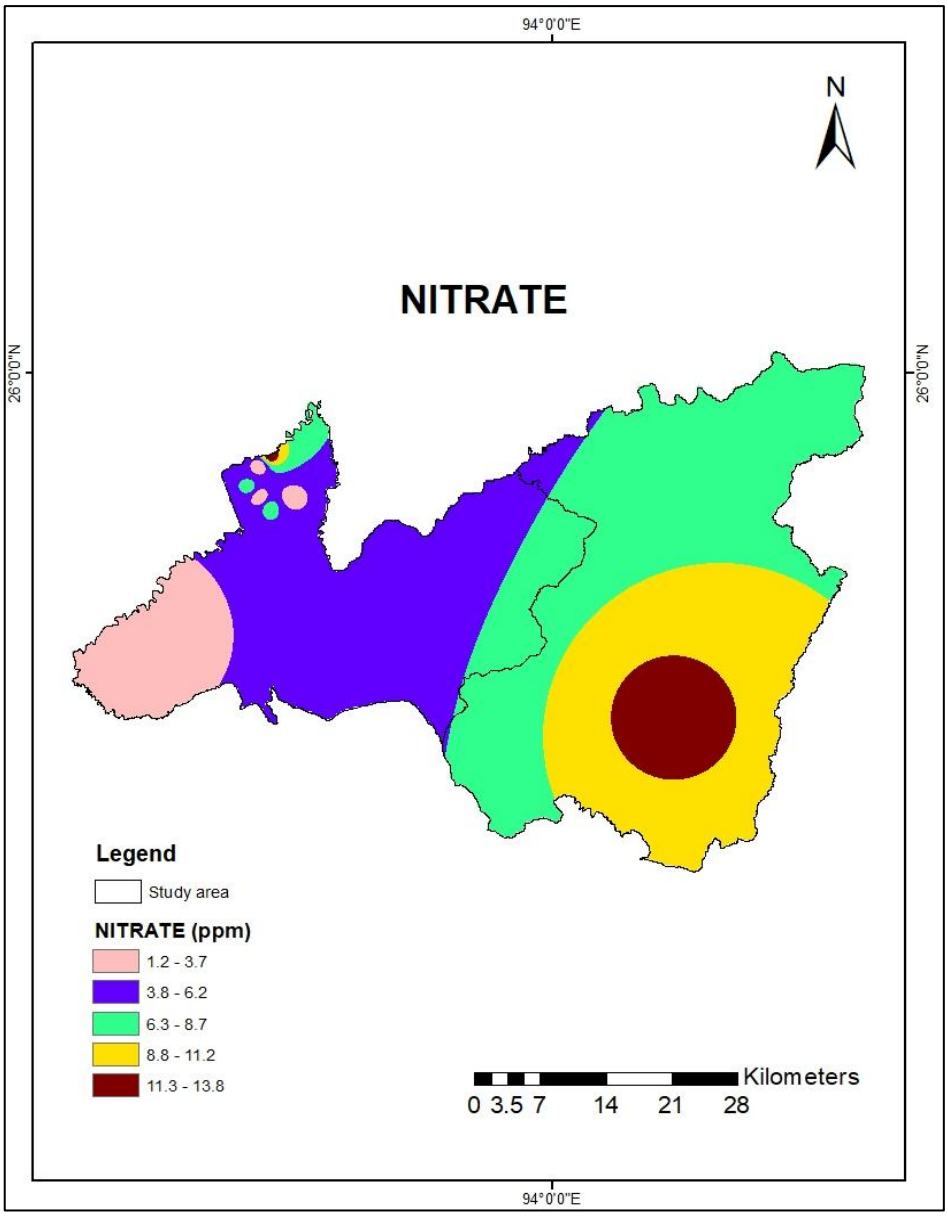

Fig. 4.9 Spatial distribution map of nitrate (NO_3) in the study area

Fluoride (F)

The primary source of fluoride in water is geogenic. Fluoride in very low doses (<0.6 mg^{-1}) in water promotes tooth decay. However, when consumed in higher doses (>1.5 mg^{-1}), it causes dental fluorosis or mottled enamel, and very high concentrations (>3.0 mg^{-1}) of fluoride may lead to skeletal fluorosis. In the present study, the fluoride concentration ranges less than 0.4 (**Fig 4.10**). A similar finding by Pamei *et al.* (2022) found that the nitrate (NO_3) level was within the permissible limit as per the BIS standards in assessing the water quality in Dimapur.

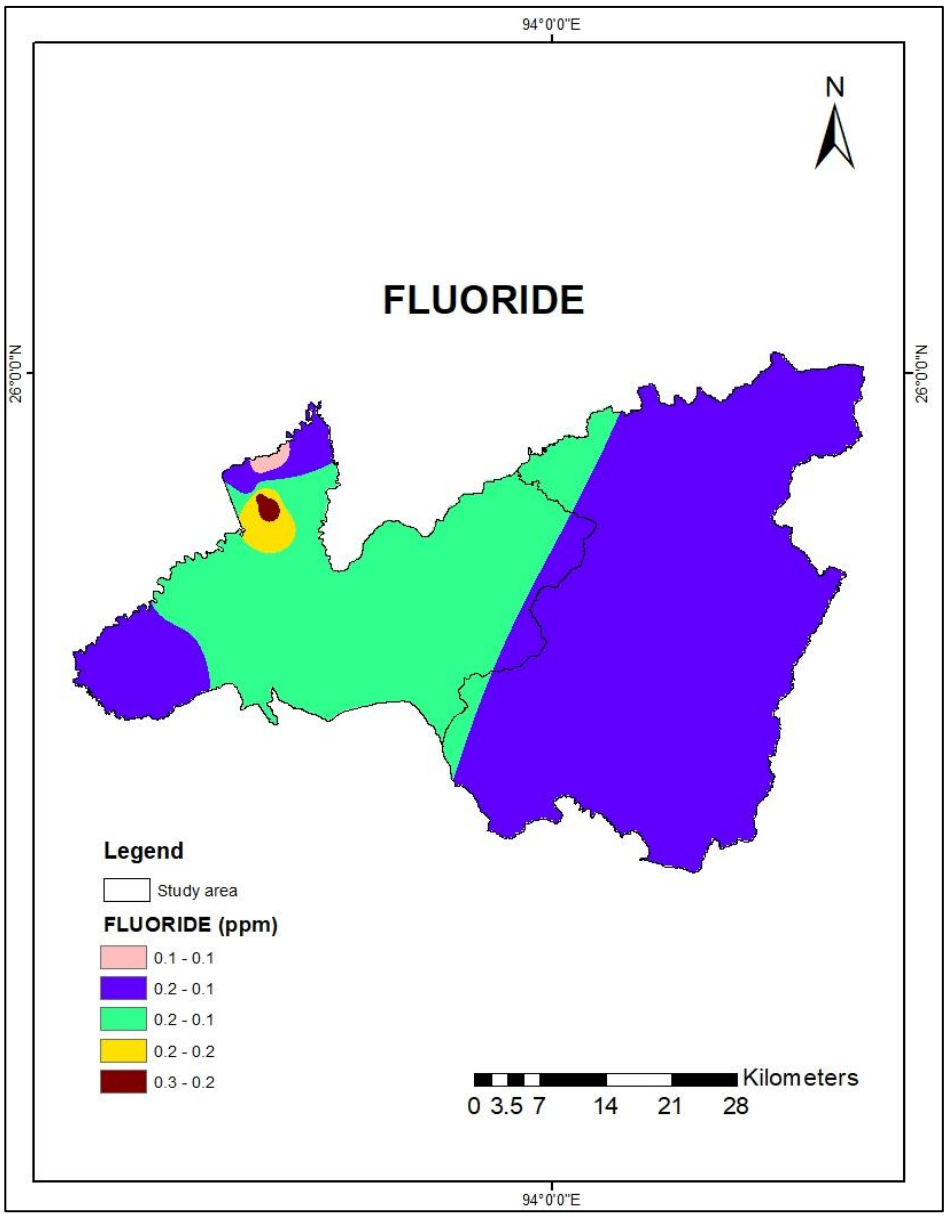

Fig. 4.10 Spatial distribution map of fluoride in the study area

Fig 4.11 shows the spatial distribution map of the water quality index (WQI) in the study area. The World Health Organization (WHO) standard has classified the water quality index (WQI) into 'Good,' 'Moderate, 'Poor,' 'Very Poor,' and 'Not fit for drinking'. It revealed that the groundwater quality in the study area was suitable for drinking purposes. The study also revealed that the four parameters, i.e., pH, fluoride, electrical conductivity, and nitrate, were within the permissible limit.

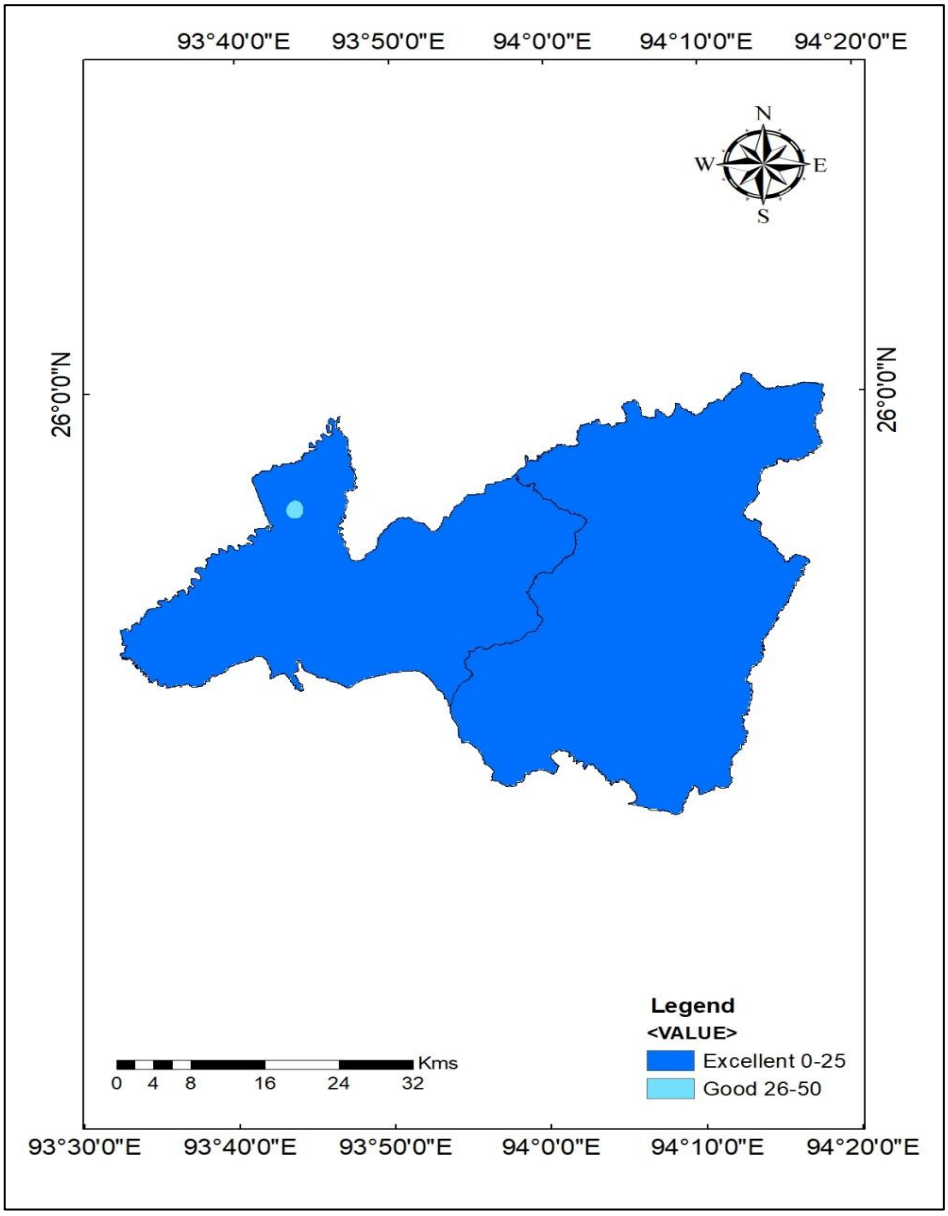

Fig. 4.11 Spatial distribution map of water quality index (WQI) in the study area

4.1.4 Surface runoff

Surface runoff from rainfall and the values of the Curve Number (CN) for the soil type in the study area were determined as per the USDA-SCS CN method (U.S. Soil Conservation Service, 1986). The composite Curve Numbers (CNs) for Kohima, Dimapur, and the merged study area were computed for AMC-I (dry), AMC-II (normal), and AMC-III (wet) using the class-wise CNs and district-specific LULC proportions. The results (**Table 4.3**) show consistently lower CNs for Kohima relative to Dimapur, reflecting its higher forest cover and greater infiltration potential. CN values increase by ~13–15 points from AMC-I to AMC-III across both districts, indicating the strong influence of antecedent moisture on runoff potential. The merged CNs were used for catchment-scale simulations to represent the combined hydrological response of the study area.

Table 4.3 Composite Curve Numbers (CN) for Kohima, Dimapur, and the merged study area under different Antecedent Moisture Conditions (AMCs)

Area/District	CN (AMC-I)	CN (AMC-II)	CN (AMC-III)
Kohima	60.81	77.87	90.33
Dimapur	64.78	80.46	91.62
Merged (Kohima + Dimapur)	62.35	78.88	90.83

The result of the surface runoff amount is shown in **Table 4.4**. The result revealed that the minimum runoff was observed in January, February, November, and December, with a value below 1. The maximum runoff was observed in the rainy months of July and August, which correlates with the rainfall pattern.

Table 4.4 Monthly maximum and minimum surface runoff (mm) in the study area (2003-2020)

Month	**Max surface runoff**	**Min surface runoff**
Jan	1.22	0.22
Feb	0.13	0.05

Mar	9.27	1.11
Apr	55.61	27.44
May	129.42	55.12
Jun	310.35	114.31
Jul	385.18	108.9
Aug	302.45	107.32
Sep	251.94	75.03
Oct	80.66	53.82
Nov	1.49	0.01
Dec	1.54	0.1

The observed increase in runoff across the study area can be explained by the interaction of soil type and land use/land cover (LULC). The soils of both Kohima and Dimapur districts predominantly belong to Hydrologic Soil Group C, which is characterised by moderately fine textures, moderate to slow infiltration rates (1.3–3.8 mm/hr), and moderately high runoff potential. Under conditions of increasing rainfall or soil saturation, infiltration is quickly exceeded, thereby enhancing surface runoff generation.

LULC patterns further amplify this response. In Kohima, with over 90% of the land area under forest, runoff generation remains relatively lower because the dense canopy, litter cover, and root systems promote interception and infiltration. By contrast, Dimapur has a larger share of agricultural land (22.32%) and built-up areas (15.72%). Cultivated land, even under good management, has a lower infiltration capacity than forest, while built-up areas introduce impervious surfaces that prevent infiltration altogether. As a result, Dimapur consistently produced higher CN values and higher runoff compared to Kohima.

The seasonal trend of increasing runoff from AMC-I to AMC-III further supports this linkage. During dry conditions (AMC-I), infiltration can still occur in most soils; however, under wet conditions (AMC-III), the soil profile becomes saturated, particularly in Group C soils, sharply reducing infiltration capacity and

elevating runoff. This explains the rapid rise in runoff observed during the pre-monsoon to monsoon transition months.

A similar finding by Qazi *et al.* (2017) observed that forest degradation in the Garhwal Himalaya increased streamflow by reducing infiltration and interception. Similarly, Sinha *et al.* (2020) showed that shifts from forest to agriculture or built-up land significantly elevated runoff and sediment yield in Indian catchments. In the Hyrcania basin, Ahmadi-Sani *et al.* (2022) demonstrated that barren and residential land uses generated the highest runoff, while dense forests had the lowest. Indian evidence from Meena *et al.* (2023) confirmed that land use systems directly affect soil compaction and runoff generation in subtropical regions. Globally, Ma *et al.* (2024) highlighted that deforestation and land cover change accelerate runoff by altering both infiltration and forest-climate feedbacks.

The spatial distribution map of monthly surface runoff (mm) from 2003-2020 in the study area from January to June is shown in **Fig 4.12**. The results revealed that in January and February, the surface runoff was minimal across the entire study area, as indicated by the lightest blue shade. This suggests that there is very little precipitation or that the land has a high infiltration capacity during these months (Cerda, 1997), resulting in surface runoff values of less than 10 mm. In March, a slight increase in surface runoff was observed in some parts, particularly in the northern parts of the study area.

However, the overall runoff remains low, with most of the area still experiencing values below 50 mm. This could indicate the beginning of a transition period where early rains start, but not enough to generate significant runoff. In April, the surface runoff begins to increase significantly, particularly in the southwestern part of the study area, where runoff values start to exceed 100 mm, as indicated by the darker shades of blue. This could be attributed to the onset of the pre-monsoon showers, which begin to saturate the soil, reducing infiltration and increasing surface runoff. In May, the map shows a more pronounced increase in surface runoff, especially in the western and southern parts of the study area. Some parts exhibited runoff values between 150 mm and 200 mm. This trend suggests that the pre-monsoon

rains are intensifying, leading to higher surface runoff due to saturated soils and possibly reduced vegetation cover. In June, the surface runoff reaches its peak during this month, particularly in the central and southern parts of the study area. The darkest shades of blue indicate areas with runoff values exceeding 300 mm. This substantial increase is likely due to the arrival of the monsoon, which brings heavy rainfall.

The spatial distribution map of monthly surface runoff (mm) from 2003 to 2020 in the study area from July to December is shown in **Fig 4.13**. The results revealed that in July, the surface runoff reached its highest level, particularly in the northern and northeastern parts of the study area, where runoff values exceeded 300 mm, and in some parts even 400 mm. The darker shades of blue indicate heavy rainfall and significant runoff due to the full onset of the monsoon season. The southern and western parts also experience substantial runoff, but to a slightly lesser degree, with values ranging between 150 mm and 300 mm. This intense runoff was likely due to the saturation of soil from persistent rainfall, leading to limited infiltration and higher surface flow. In August, there was a slight reduction in surface runoff across most of the study area compared to July. In September, the surface runoff continues to moderate, with the majority of the study area exhibiting values between 100 mm and 200 mm. The northern and northeastern parts still show higher runoff, but overall, the map reflects a continued decline in runoff intensity. This trend could be associated with the tail end of the monsoon season, where rainfall intensity begins to decrease, resulting in less surface runoff. In October, the runoff further declined, especially in the central and southern parts of the study area, where most parts showed runoff values between 50 mm and 100 mm. This reduction was consistent with the transition from the monsoon to the post-monsoon season, where rainfall becomes less frequent, and the land begins to dry out. In November, the surface runoff drastically decreases across

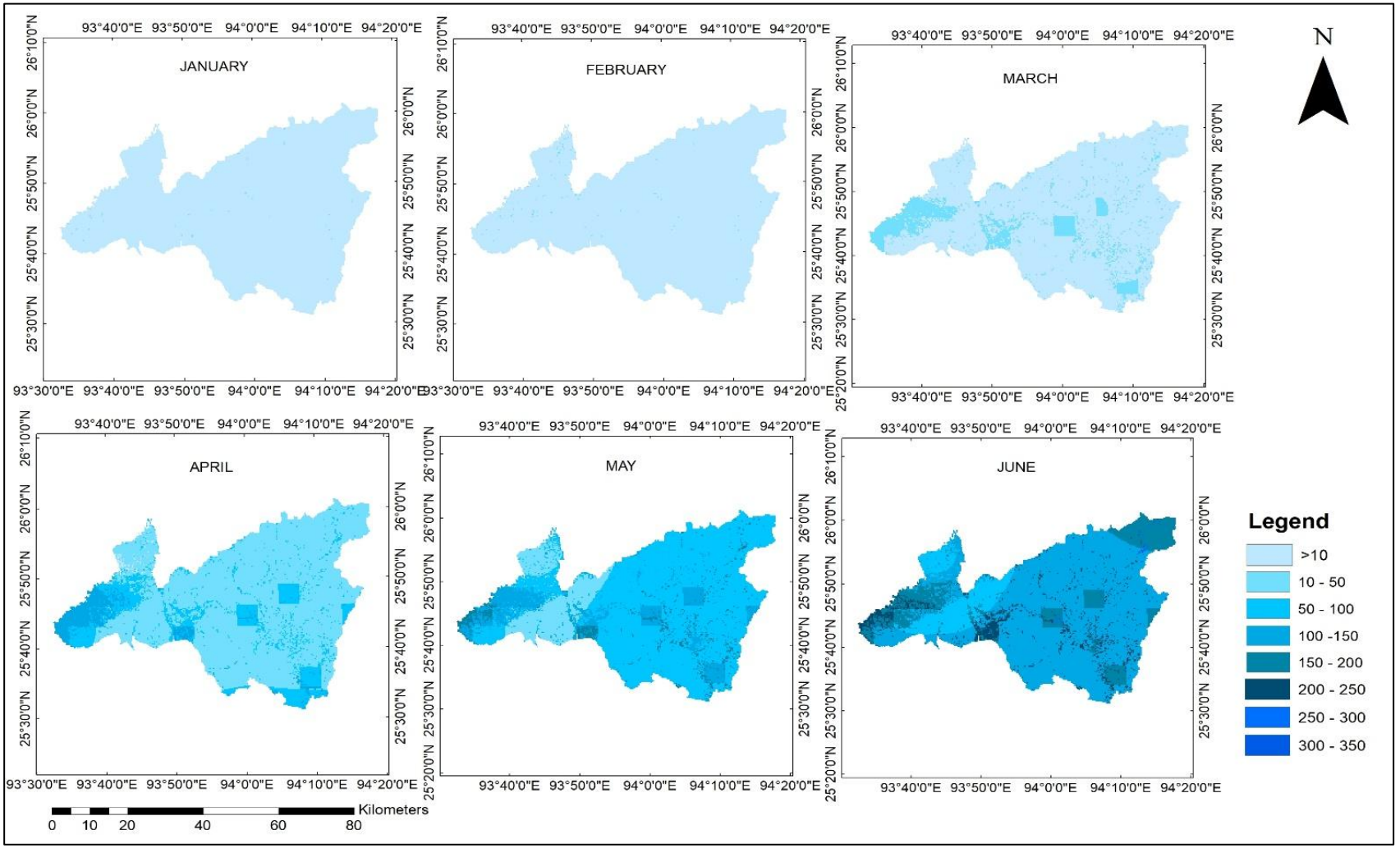

Fig 4.12 Spatial distribution map of monthly surface runoff (mm) from 2003-2020 in the study area (Jan-Jun)

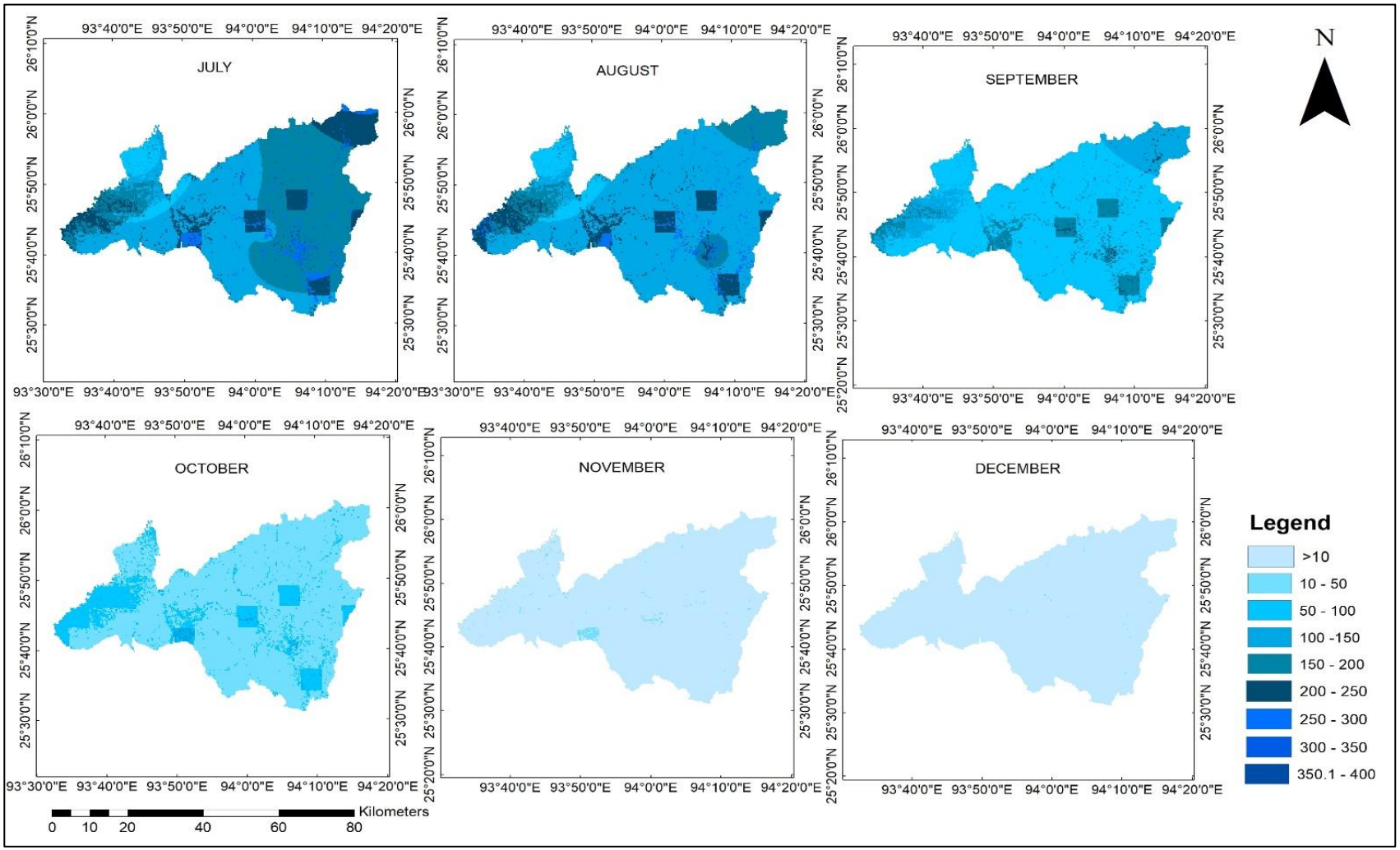

Fig 4.13 Spatial distribution map of monthly surface runoff (mm) from 2003-2020 in the study area (Jul-Dec)

the entire study area, with most regions exhibiting values of less than 50 mm. This indicated that the monsoon season had ended, and the study area was experiencing much drier conditions. The minimal runoff is likely due to the lack of significant rainfall, and the soil moisture content has reduced, allowing for greater infiltration and less surface flow. In December, the study area exhibited very low surface runoff, with most parts showing values of less than 10 mm.

A similar study conducted by Laishram and Alam (2024) found that the highest average monthly surface runoff in the Loktake lake watershed, Manipur, was observed during June, and the lowest in January. Another finding by Shinde *et al.* (2024) used the SCS-CN method and found that higher runoff was observed from June to September as rainfall was more prominent.

Agricultural water availability index (I_{AWA})

The Agricultural Water Availability Index (I_{AWA}) was calculated according to the methodology explained in section 3.3. The total depth of available water from the component sources, i.e., rainfall, soil moisture, groundwater, and surface runoff, was added, and Equations 3.1 to 3.3 were solved. The total water depth values were normalized. The normalization was done objectively to bring each water depth between 0 and 1, where 0 represents the minimum (18.5 mm) and 1 represents the maximum (354.4 mm).

The resulting water availability index for the present scenario is shown in **Table 4.5,** where the minimum index value was found to be 0.01 in December, and the maximum index value was 0.87 in July. The rainfall distribution, stored soil moisture, groundwater, and runoff collectively support computing the index value.

Table 4.5 Monthly minimum and maximum I_{AWA} for the present scenario (2003-2020) in the study area

Month	Max I_{AWA}	Min I_{AWA}
Jan	0.09	0.03
Feb	0.10	0.08
Mar	0.34	0.28

Apr	0.63	0.58
May	0.75	0.71
Jun	0.85	0.77
Jul	0.87	0.80
Aug	0.86	0.77
Sep	0.80	0.74
Oct	0.74	0.63
Nov	0.18	0.16
Dec	0.05	0.01

To complement the monthly analysis, the I_{AWA} was aggregated into annual means for each year (2003–2020). The Mann–Kendall trend test was applied to the annual series to detect long-term changes. The results indicated no statistically significant monotonic trend ($p > 0.05$), meaning that although interannual variability exists, there is no consistent increase or decrease in water availability over the study period. This aligns with regional studies noting high rainfall variability in Northeast India without a clear long-term directional change (Parida and Oinam, 2015; Patle *et al*., 2025). To improve interpretability, the annual I_{AWA} values were classified into dry, normal, and wet years using percentile thresholds shown in **Table 4.6** and a graphical representation is shown in **Fig 4.14.** Years below the 25th percentile were classified as dry, those above the 75th percentile as wet, and the remainder as normal.

Table 4.6 Annual I_{AWA} and classification of wet, normal, and dry years for 2003–2020 in the study area

Year	Annual I_{AWA}	Category
2003	0.79	Wet
2004	1.00	Wet
2005	0.68	Normal
2006	0.30	Dry
2007	0.87	Wet
2008	0.93	Wet

2009	0.36	Normal
2010	0.66	Normal
2011	0.45	Normal
2012	0.10	Dry
2013	0.15	Dry
2014	0.31	Normal
2015	0.62	Normal
2016	0.44	Normal
2017	0.75	Normal
2018	0.78	Normal
2019	0.54	Normal
2020	0.29	Dry

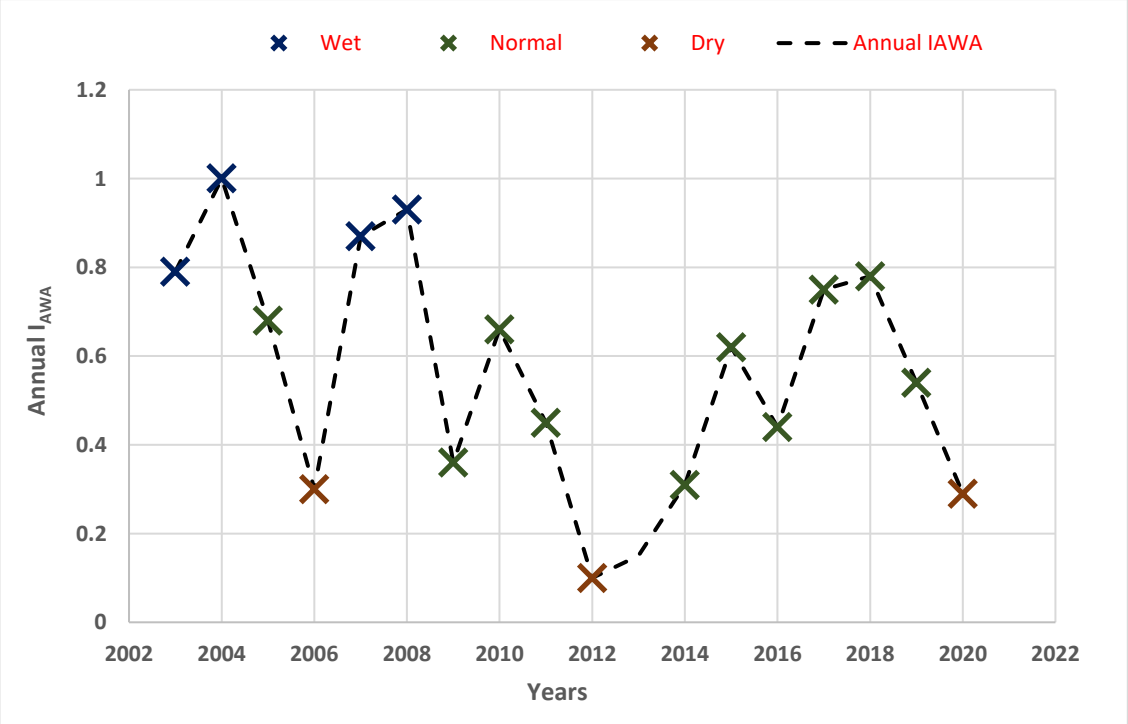

Fig 4.14 A graphical representation of the annual Agricultural Water Availability Index (I_{AWA}) with wet, normal, and dry years

The annual classification reveals alternating wet and dry years with no long-term trend. For example, 2012 and 2020 were dry years consistent with reported

monsoon deficits in Nagaland, which coincides with the article's statements “Drought-like situation” faced in the state (Press Trust of India, 2013, and Down to Earth, 2021), while 2003–2004 and 2007–2008 were wet years corresponding to high rainfall periods. This variability is typical of Northeast India, where the monsoon is highly erratic despite high mean annual rainfall (Das *et al*., 2009; Parida and Oinam, 2015). Similar findings in Mizoram (Patle *et al*., 2025) also found frequent oscillations between dry and wet years without a significant long-term decline, confirming that short-term extremes rather than gradual decline dominate agricultural water availability in the region. From an agricultural perspective, dry years coincide with water stress for crops and potential yield loss, while wet years increase risks of flooding and waterlogging. As 70% of Nagaland’s population depends on climate-sensitive sectors (Das *et al*., 2009), classifying years into wet, normal, and dry is vital for planning contingency irrigation, drought management, and flood control.

A graphical representation of monthly water availability (mm) for the present scenario in the study area (2003–2020) is shown in **Fig 4.15**. The analysis indicates a clear seasonal cycle in the availability of water resources. During January and February, water availability was close to 10 mm, reflecting the extremely dry winter months typical of Nagaland, when precipitation is at its lowest (IMD, 2020; CGWB, 2013). Moving into March and April, the values rise gradually, reaching nearly 50 mm in March and about 110 mm in April. This rise corresponds to the pre-monsoon showers, which provide modest contributions before the full onset of the southwest monsoon (Medeo and Jamir, 2023; NSDMA, 2019).

By May, water availability further increases to around 160 mm. This growth coincides with the early arrival of the monsoon, which marks the beginning of the main rainy season in the region (IASc, 2024; NSDMA, 2019). The most significant rise is seen during June, July, and August, when water availability peaks, with July reaching nearly 380 mm. This peak aligns with climatological records showing that more than 70% of Nagaland’s annual rainfall is concentrated in these three months, fueling streams, aquifers, and surface reservoirs (IMD, 2020; Statistical Handbook of Nagaland, 2021).

Following this peak, water availability begins to decline in September, with values of about 220 mm. In October, the figure drops further to around 100 mm, reflecting the retreating monsoon and transition towards the dry season (Medeo and Jamir, 2023). By November and December, water availability falls to very low levels, confirming the extended dry winter that characterizes Nagaland's hydrological regime (CGWB, 2013; Statistical Handbook of Nagaland, 2021).

Overall, the graph highlights a distinct monsoon-driven hydrological cycle: very low water availability during winter, gradual increases in spring, a sharp peak during the summer monsoon, and a steady decline through autumn. This pattern is consistent with long-term meteorological and hydrological observations across Kohima and Dimapur districts.

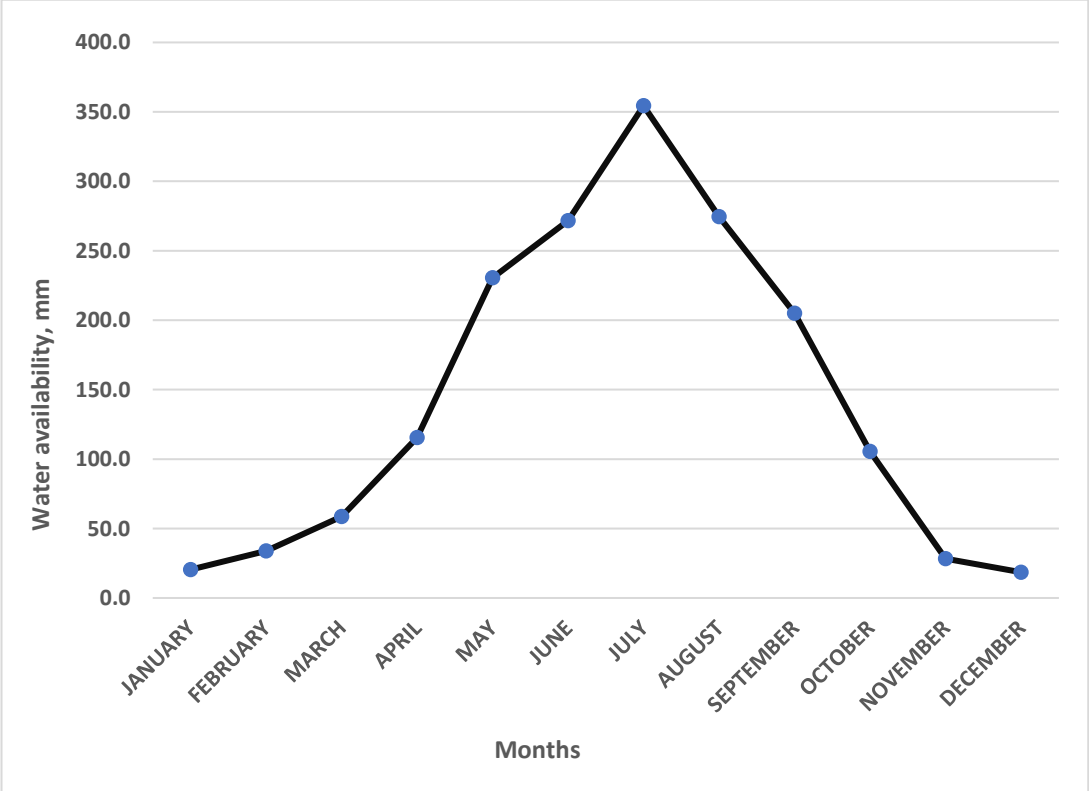

Fig 4.15 A graphical representation of monthly water availability for the present scenario in the study area (2003-2020)

4.2 The impact of climate change on temporal and spatial variation of water availability in the study area

Rainfall and temperature were determined for future scenarios to assess the impact of climate change on temporal and spatial variation in the study area. In this section, the result of the statistical downscaling model (SDSM) for downscaling rainfall and temperature data using the baseline period 2003-2020 for the study area for generating the future periods, i.e., 2021-2038, 2039-2059, 2060-2080, and 2081-2100, taking 20 years except for 2021-2038 (18 years) intervals has been discussed.

4.2.1 Statistical downscaling of regional climate

Downscaling has been performed for the two stations, i.e., Kohima and Dimapur districts of the study area. The daily rainfall and temperature (maximum and minimum) data (2003-2020) have been assessed using the widely used Statistical Downscaling Model (SDSM) software version 4.2.9 (Wilby and Dawson, 2013). The results of the methodology presented in section 3.4 for statistical downscaling have been discussed in the sub-sections.

4.2.1.1 Selection of predictors

The screening of predictor variables is an important step in the downscaling process. The approach is iterative and involves a preliminary screening of potential variables and predictors. This process is continued until an objective function is optimized (Wilby and Harris, 2006). The variables exhibiting the strongest correlation were chosen utilizing the screen variable function in the SDSM.

Initially, all predictors from historical records were compared to the observed data. The predictors that exhibited the strongest connection were selected based on their minimum or zero p-value and maximum partial r-value. The correlation statistics and p-values were utilized to quantify the strength of the association between the predictor-predictand and to assess the presence of multicollinearity among the selected predictors. To improve the accuracy of the predictions, only the correlations with a p-value less than or equal to zero were chosen. The predictors, along with the partial r value selected for rainfall and temperature, presented in **Tables 4.7** and **4.8**, compared

with the results obtained by Wilby *et al.* (2002), are considered suitable for the process of downscaling.

Table 4.7 Selected predictors with partial r values for rainfall in the study area

Sl. No.	Predictors	Rain gauge stations with partial r values			
		Kohima		Dimapur	
1	s500gl	✓	0.039	✓	0.101
2	p8_zgl			✓	0.038
3	shumgl	✓	0.078	✓	0.122
4	p1_fgl	✓	0.335		

Note: ✓ indicates the selected large-scale predictor for rainfall in the study area.

The highest correlation values represent a higher degree of association and smaller p-values describe a better chance for an association between variables. The selection of predictors was done as discussed in section 3.3.3.1. Considering all 26 predictors, only 4 predictors (s500gl, p8_zgl, shumgl, and p1_fgl) for rainfall were selected from the study area as they were strongly correlated with the observed data in the analysis (**Table 4.7**). The super predictors for Kohima and Dimapur stations were p1_fgl (Wind speed at 1000hPa) and shumgl (Specific humidity at 1000hPa), respectively.

No research has been done in the study area, contrary to the region similar study by Mahmood and Babel (2013) found that the super predictor was shumgl in the downscaling of rainfall for 14 stations in the Jhelum basin. Also, Gulacha *et al.* (2017) examined partial r values for precipitation in the range of 0.038 to 0.335. Similar results of partial r values for precipitation were also observed by Tatsumi *et al.* (2014) and Mahmood and Babel (2013). On the other hand, Bulti *et al.* (2021) also found the same super predictor (shumgl) of CanESM2 in analyzing future extreme precipitation in Adama, Ethiopia. The results show the effective implementation of the SDSM for the process of downscaling daily rainfall at a local scale using estimates of large-scale atmospheric information specific to the study area.

Table 4.8 Selected predictors with partial r values for temperature in the study area

	Predictors	Kohima		Dimapur	
T_{max} (Maximum temperature)	p500gl			✓	0.129
	p1_vgl			✓	0.041
	s500gl	✓	0.200	✓	0.054
	Shumgl	✓	0.593		
	Tempgl	✓	0.367		
T_{min} (Minimum temperature)	p8_ugl	✓	0.089		
	Shumgl	✓	0.216		
	Tempgl	✓	0.454	✓	0.039
	p1_zgl			✓	0.031
	p1_zhgl			✓	0.018

Note: ✓ indicates the selected large-scale predictor for temperature in the study area.

The selected predictors for maximum temperature (T_{max}) and minimum temperature (T_{min}) with partial r values is shown in **Table 4.8**. It is observed that the super predictors for T_{max} and T_{min} are shumgl (Specific humidity at 1000 hPa) and tempgl (Screen air temperature at 2m), respectively for Kohima station. For the Dimapur station, the super predictors for T_{max} and T_{min} are s500gl (Specific humidity at 500 hPa) and tempgl (Screen air temperature at 2m), respectively. The tempgl is super predictor for T_{min} in both the station.

A similar finding was reported by Mahmood and Babel (2013), where the super predictor was tempgl for temperature in the downscaling of rainfall for 14 stations in the Jhelum basin. Shrestha *et al.* (2021) found a comparable finding of selected predictors for maximum and minimum temperature in downscaling the three stations within the Gandaki River Basin in Central Nepal. Rana and Adhikary (2023) also found that the predictors shumgl, tempgl, and p500gl were significant in examining

the effects of climate change on future precipitation and temperature changes in the northwest region of Bangladesh. They also used the CanESM2 model for their study. While it is sufficient to utilize a maximum of two predictors for the statistical downscaling of GCM for climate variables in the SDSM platform, employing additional predictor variables can enhance the accuracy and stability of the downscaling results (Gulacha and Mulungu, 2017; Jahangir *et al.*, 2020).

4.2.1.2 Calibration and Validation of Model

In the process of model calibration, a multiple linear regression-based model has been generated using station data and the NCEP predictors. The model calibration was carried out to validate the developed empirical relationship between the predictors and the predictands. The validation process enables the production of synthetic data for the duration that the observed data is available. This model has been validated using the station-observed data and the NCEP predictors for the duration of 2010 to 2020. The observed and simulated average monthly rainfall (mm) and temperature (maximum and minimum in ˚C) in the baseline period (2003-2020) in Kohima and Dimapur stations are shown in Fig 4.16 to 4.21.

Fig 4.16 demonstrates a strong match between the observed rainfall data and the simulated model at Kohima station, except August, where the model exhibits a slightly larger peak compared to the actual data. **Fig 4.17** demonstrates a strong correlation between the observed rainfall data and the simulated model for most months at Dimapur station. However, in September, the simulated model displayed a lower value compared to the observed data. **Fig 4.18** and **4.19** demonstrate that the maximum and minimum temperatures for the Kohima station indicate a close correspondence between the observed data and the simulated model. The simulated model produced demonstrates high accuracy and can be effectively utilized for long-term temperature forecasting. **Fig 4.20** and **4.21** demonstrate that the maximum temperature recorded in Dimapur station is higher in the observed data compared to the simulated model. Given the modest discrepancy between the observed data and the simulated model, the model is deemed acceptable for predicting purposes. The minimum temperature exhibits a stronger correlation between the observed data and

the generated model. The data presented in **Fig 4.15** to **4.20** demonstrate a close correspondence between the observational data and the simulated model. This alignment supports the model's capability to accurately estimate future rainfall and temperature (Wilby *et al.*, 2002; Chu *et al*., 2010). A similar study in contrary to the region was conducted by Javaherian *et al.* (2021) and found that the CanESM2 model accurately predicted changes in climatic parameters (rainfall and temperature) in the Lar Dam Basin. The observed data and model forecast showed a strong match.

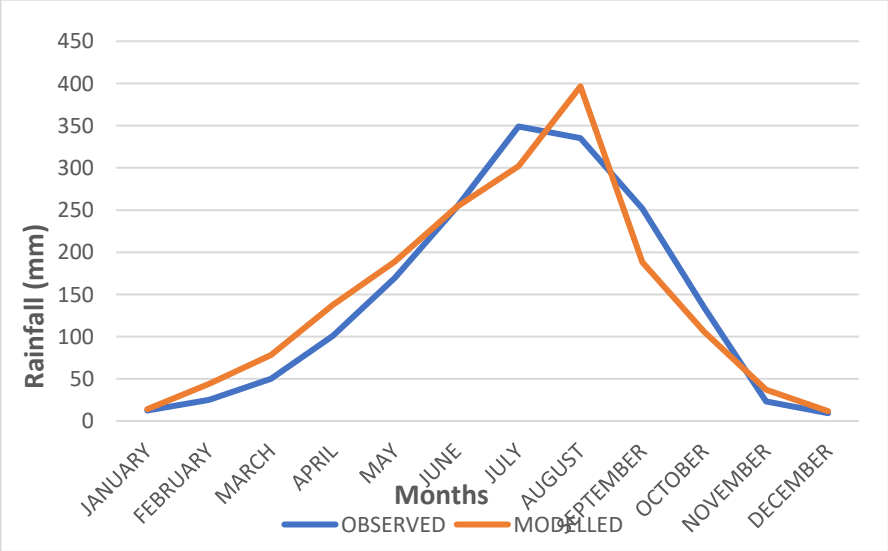

Fig 4.16 Observed and simulated average monthly rainfall (mm) in the baseline period (2003-2020) in Kohima station

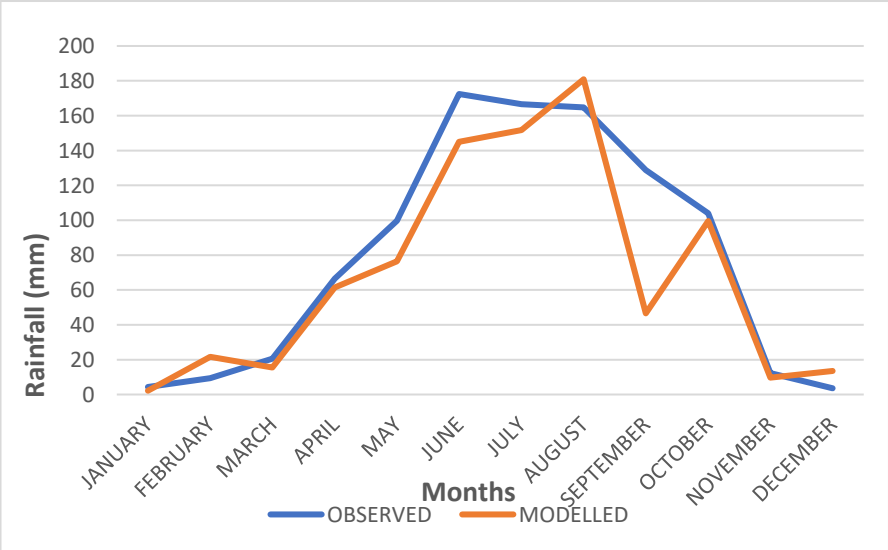

Fig 4.17 Observed and simulated average monthly rainfall (mm) in the baseline period (2003-2020) in Dimapur station

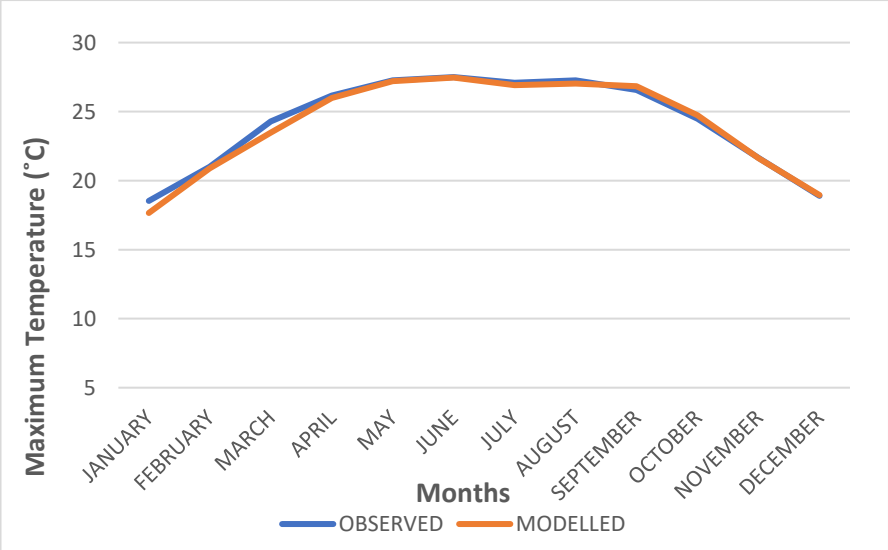

Fig 4.18 Observed and simulated average monthly maximum temperature (˚C) in the baseline period (2003-2020) in Kohima station

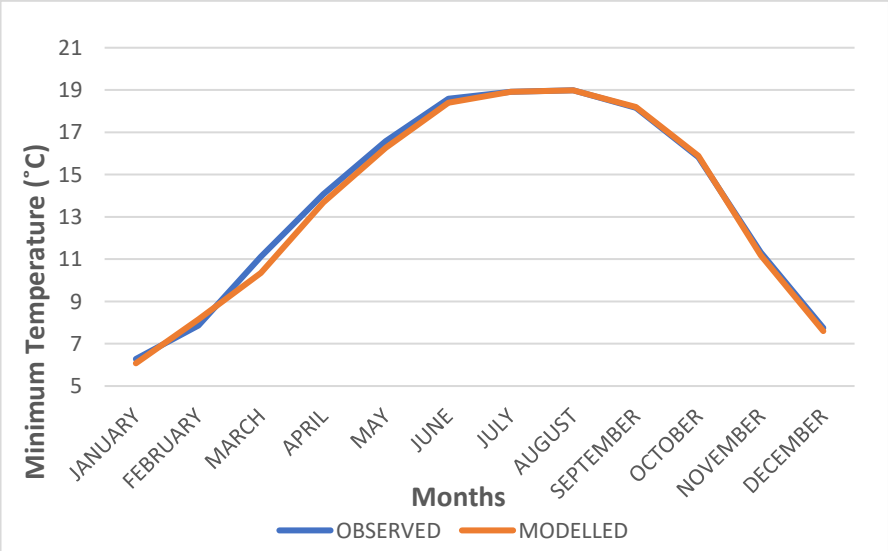

Fig 4.19 Observed and simulated average monthly minimum temperature (˚C) in the baseline period (2003-2020) in Kohima station

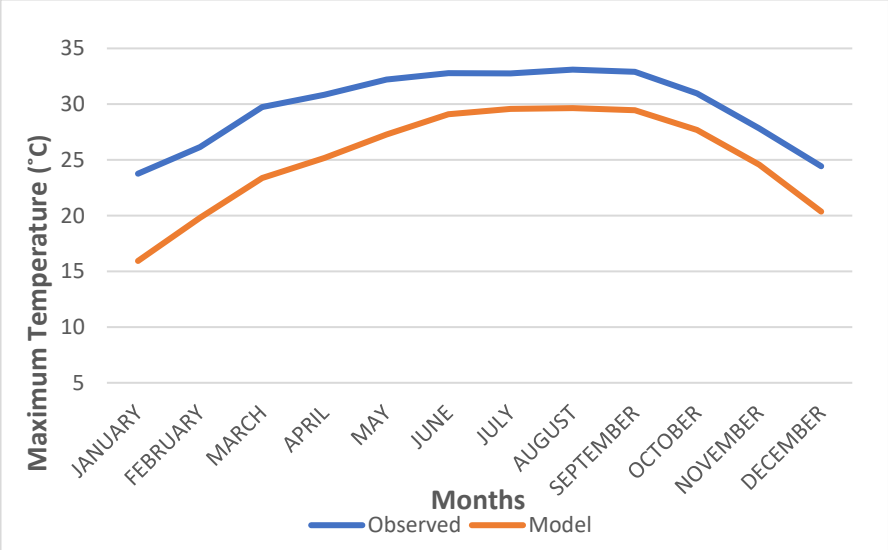

Fig 4.20 Observed and simulated average monthly maximum temperature (˚C) in the baseline period (2003-2020) in Dimapur station

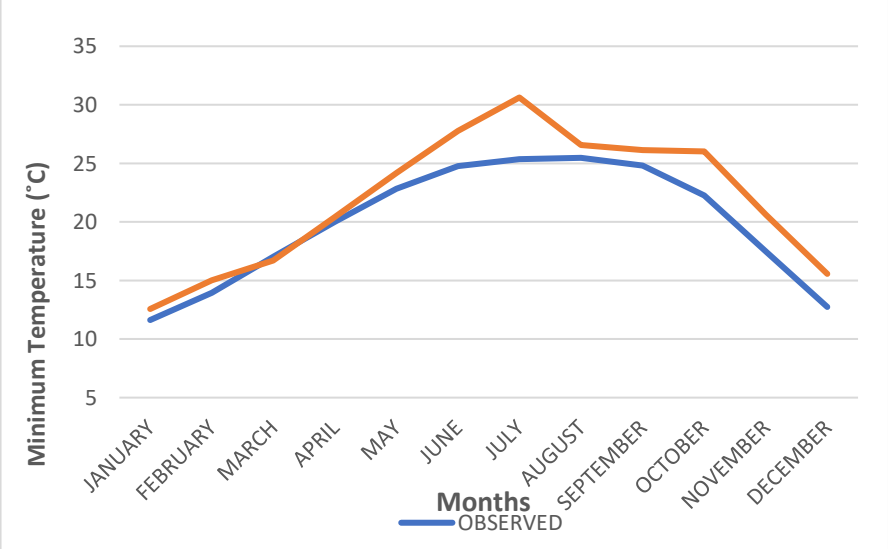

Fig 4.21 Observed and simulated average monthly minimum temperature (˚C) in the baseline period (2003-2020) in Dimapur station

4.2.1.3 Performance criteria of SDSM

The statistical analysis was done to ascertain the results of the graphical comparison, as epitomized in **Table 4.9**. The coefficient of determination (R^2) for rainfall was determined to be 0.92 and 0.85 for Kohima and Dimapur, respectively. The R^2 values for maximum and minimum temperature in Kohima station were determined to be 0.99 and 0.98, respectively. The R^2 for the maximum temperature at Dimapur was 0.92, while for the minimum temperature it was 0.93. The result of R^2 reveals that the SDSM has a good simulation effect on rainfall for both stations. It is noted that the closer R^2 to a value 1, the better the regression equation fitting data and the stronger the linear relationship.

The result is supported by Singh *et al.* (2015), who found the R^2 value in the range between 0.83 to 0.92 for rainfall and 0.80 to 0.90 for temperature during the downscaling of the observed and modelled precipitation and temperature in the Sutlej River basin, India. Also, a similar study conducted by Shrestha *et al*. (2021) also observed that the value of R^2 showed a good correlation (0.99) between observed and downscaled in the three stations for temperature and precipitation data in the Gandaki basin, Nepal. Similar values of R^2 were also observed by Shahriar *et al.* (2021) in the Chittagong division, Bangladesh. Another study conducted by Suo *et al.* (2019) also found that the determination coefficients (R^2) of observed and simulated values for maximum temperature, minimum temperature, average temperature, and precipitation were 0.94, 0.95, 0.93, and 0.64, respectively.

Table 4.9 Statistics values of R^2 between observed and simulated values of rainfall and temperature in the study area

Parameters	Kohima	Dimapur
Rainfall	0.92	0.85
T_{max}	0.99	0.92
T_{min}	0.98	0.93

4.2.2 Projected changes in rainfall and temperature (maximum and minimum) for future climate scenarios

The validated regression models have been applied to generate future climate scenarios of rainfall and temperature (maximum and minimum) using the GCM CanESM2 model for RCP4.5 and RCP8.5. The downscaled process has been carried out for the future periods 2021-2038, 2039-2059, 2060-2080, and 2081-2100. The changes in mean monthly rainfall and temperature (maximum and minimum) in the two stations under the RCP4.5 and RCP8.5 scenarios would present noticeable differences in different months.

4.2.2.1 Future projections of rainfall and temperature (maximum and minimum) in the study area

The changes in rainfall and temperature (maximum and minimum) for the future periods 2021-2038, 2039-2059, 2060-2080, and 2081-2100 relative to the baseline period or historical observations (2003-2020) under the RCP4.5 and RCP8.5 scenarios for Kohima and Dimapur stations is presented in Figure 4.21 to 4.22. The figures represent the general monthly changes in rainfall and temperature (maximum and minimum) for the observed period and climate scenarios RCP4.5 and RCP8.5. Concerning the distribution of rainfall in different seasons, it is known that the study area receives much of its rainfall in monsoon (June to September), which is supposed to be the main rainy season, followed by the retreating or post-monsoon season (October and November) (Schröder *et al.*, 2024).

From **Fig 4.22**, it was seen that in Kohima station, the RCP4.5 scenario projected higher rainfall than the RCP8.5 scenario in the period 2021-2038, except in May, September, and October, and the projected rainfall values in that period (2021-2038) seemed to be higher than the other future periods. The projected rainfall values under both scenarios in all future periods revealed that more rainfall would occur in all months except July, which showed a decreasing trend compared to the historical observations. A similar finding by Shrestha *et al.* (2021) observed that the projected precipitation would increase for the RCP4.5 and RCP8.5 in the Gandaki basin. The study by Javaherian *et al.* (2021) reported that the number of changes in the parameter of total rainfall in the prediction period is increased than the basic (observational data)

period under the three RCP scenarios, i.e., RCP2.6, RCP4.5, and RCP8.5 and the amount of least change of rainfall belongs to RCP8.5 scenario. Similarly, another study utilizing SDSM in Khyber Pakhtunkhwa found that while RCP4.5 showed an increase in precipitation, RCP8.5 exhibited a more complex pattern, with some regions experiencing a decrease in rainfall (Rahman *et al.*, 2022).

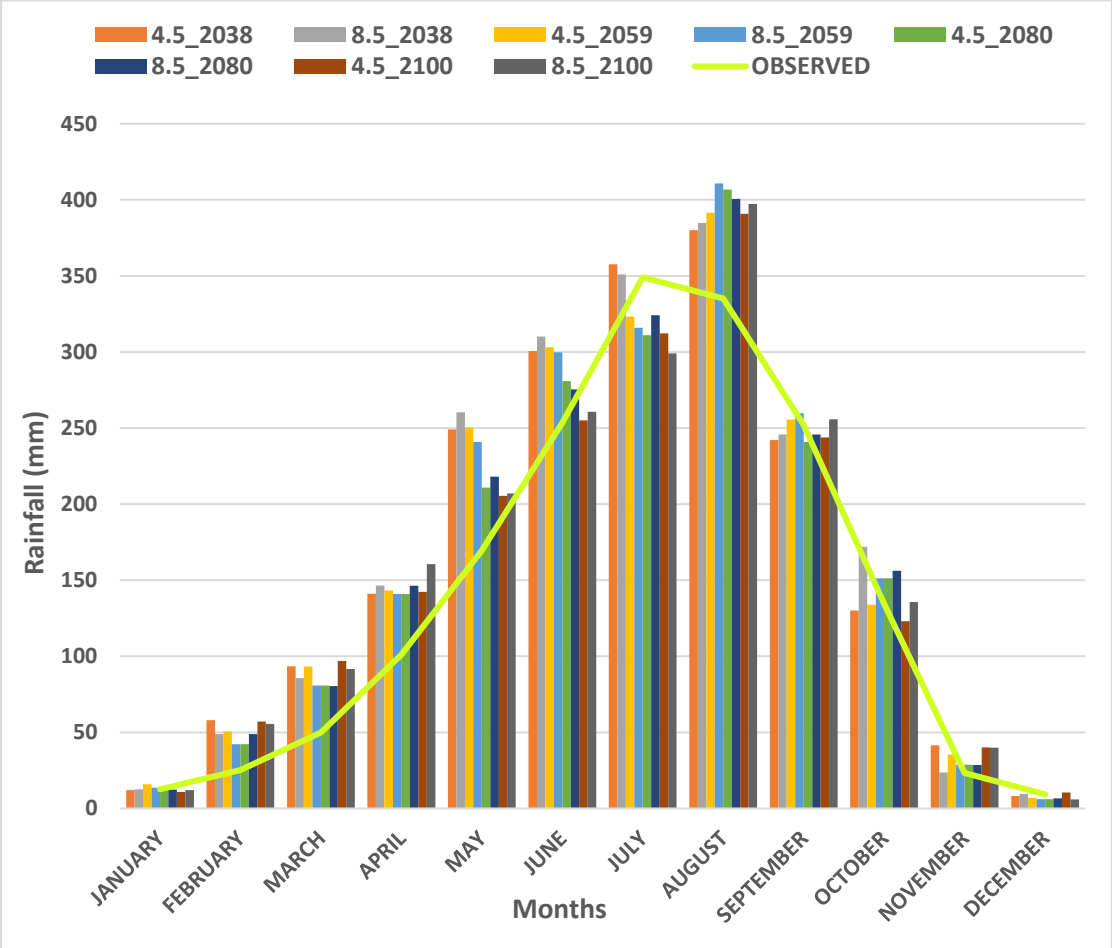

Fig 4.22 Projected monthly rainfall in the future periods 2021-2038, 2039-2059, 2060-2080, and 2081-2100 compared to the observed monthly rainfall in the baseline period (2003-2020) at Kohima station

Fig 4.23 revealed that in the Dimapur station, the RCP8.5 scenario projected higher rainfall than the RCP4.5 scenario in all future periods except in March, September, and May. The projected rainfall for both scenarios in May and June was seen to be lower than the historical observations. It also revealed that during the month of November, similar rainfall conditions were observed between the projected rainfall

under the RCP4.5 and RCP8.5 scenarios and the historical observations. A fluctuation in projected rainfall was shown in most of the months compared to the Kohima station. A similar finding by Thakor and Parekh (2022) found that the RCP8.5 projected a significant increase in rainfall using the CanESM2 model in the Vadora district. Another study in Kelantan projected a major increase in annual rainfall under RCP8.5 for the 2080s (Armain *et al*., 2021). These findings suggest that while RCP8.5 generally indicates higher rainfall forecasts, regional variations and specific modeling approaches can lead to differing outcomes, highlighting the need for localized assessments in climate predictions (Verma *et al*., 2022).

The projected modeled rainfall for the future periods 2021-2038, 2039-2059, 2060-2080, and 2081-2100 in both stations under the RCP4.5 and RCP8.5 scenarios revealed that increased rainfall is highly anticipated. Many researchers have found similar findings; however, the number of models used and the length of historical rainfall may differ considerably. In support of our findings, Dahal *et al.* (2020) and Rajbhandari *et al.* (2018) found that there was an increase in projected rainfall in the Koshi, Karnali, and Koshi river basins, respectively. This increase in rainfall may be attributed to an increase in the surface temperature, which in turn may raise the rate of evaporation, leading to increased precipitation (Anandhi *et al*., 2008). Contrary to this finding, a report by Medeo and Jamir (2022) observed that July was the wettest month in Nagaland based on the period from 2004 to 2021. As multiple factors linked to climate change contribute to the projected decline in July rainfall in Northeast India. The warming of the Indian Ocean, particularly the Bay of Bengal, and a weakening of the monsoon circulation system are the primary drivers. This leads to a shift in moisture transport, favoring other parts of India and decreasing the formation of rain-producing weather systems over the Bay of Bengal. In a study, Prabhu *et al*. (2024) revealed a similar outcome that district-level monsoon trends reported widespread declines in northeastern monsoon rainfall: approximately 68% of tehsils in NE India experienced lower June–September rainfall, with 87% of those tehsils experiencing declines in June–July. The India Meteorological Department (IMD) and government analysts note that "*July, once the peak rainfall month, is now showing a decline in rainfall, while September is becoming wetter*". In other words, the seasonal

rain peak is moving later. This trend is borne out in high-resolution data: the Council on Energy, Environment and Water (CEEW) analysis found that many parts of north and east India (including Nagaland) actually saw reduced rainfall in July–August even as overall monsoon totals rose.

The projected changes in rainfall are critical for agriculture, especially for crops reliant on monsoon rains, such as rice/paddy, which is sensitive to water availability during its growing season (Adib *et al*., 2022). Even though increased rainfall can benefit crop yields, it may lead to adverse effects such as flooding and waterlogging, particularly during the kharif season, which could negatively impact agricultural productivity (Vijayakumar *et al*., 2021). Thus, understanding these dynamics for effective agricultural management and planning in the face of climate.

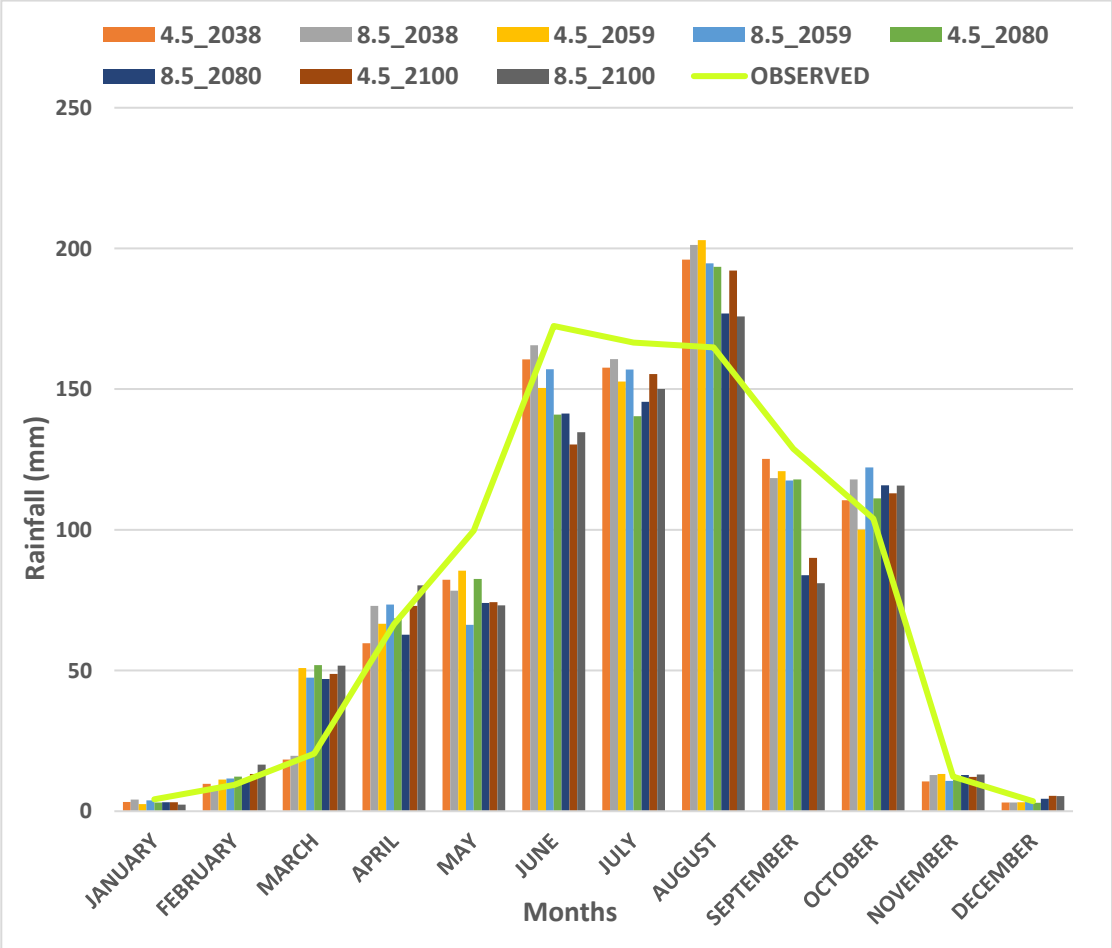

Fig 4.23 Projected monthly rainfall in the future periods 2021-2038, 2039-2059, 2060-2080, and 2081-2100 compared to the observed monthly rainfall in the baseline period (2003-2020) at Dimapur station

Fig 4.24 shows a comparison of the projected monthly maximum temperature by downscaled CanESM2 GCM under RCP4.5 and RCP8.5 scenarios with the observed monthly maximum temperature data at Kohima station. The data from the observed period or baseline period (2003-2020) indicates that the temperature reaches its highest point in June and July and then steadily decreases until December. The projected maximum temperature in January under both scenarios were lower than the baseline period. The projected maximum temperature in RCP4.5 and RCP8.5 (2021-2038, 2039-2059, 2060-2080) exceeds that of the baseline period in February, March and April. In May, June, July and August, the projected maximum temperature was more or less equal to the baseline period. In September and November, the RCP8.5 shows a higher temperature than the RCP4.5. The maximum temperature is projected to rise by around 2 to 3˚C in future periods. The RCP8.5 scenarios often exhibit higher temperatures in comparison to the RCP4.5 scenarios, which follow a more intense emission trajectory. A similar study contrary to our study region was conducted by Chen *et al.* (2021) and found that under RCP8.5, the maximum temperature was projected to increase double times more than under RCP4.5 in analyzing the changes in the temporal and spatiotemporal variation of temperature extremes in the Kaidu-Kongqi River basin, Northwest China.

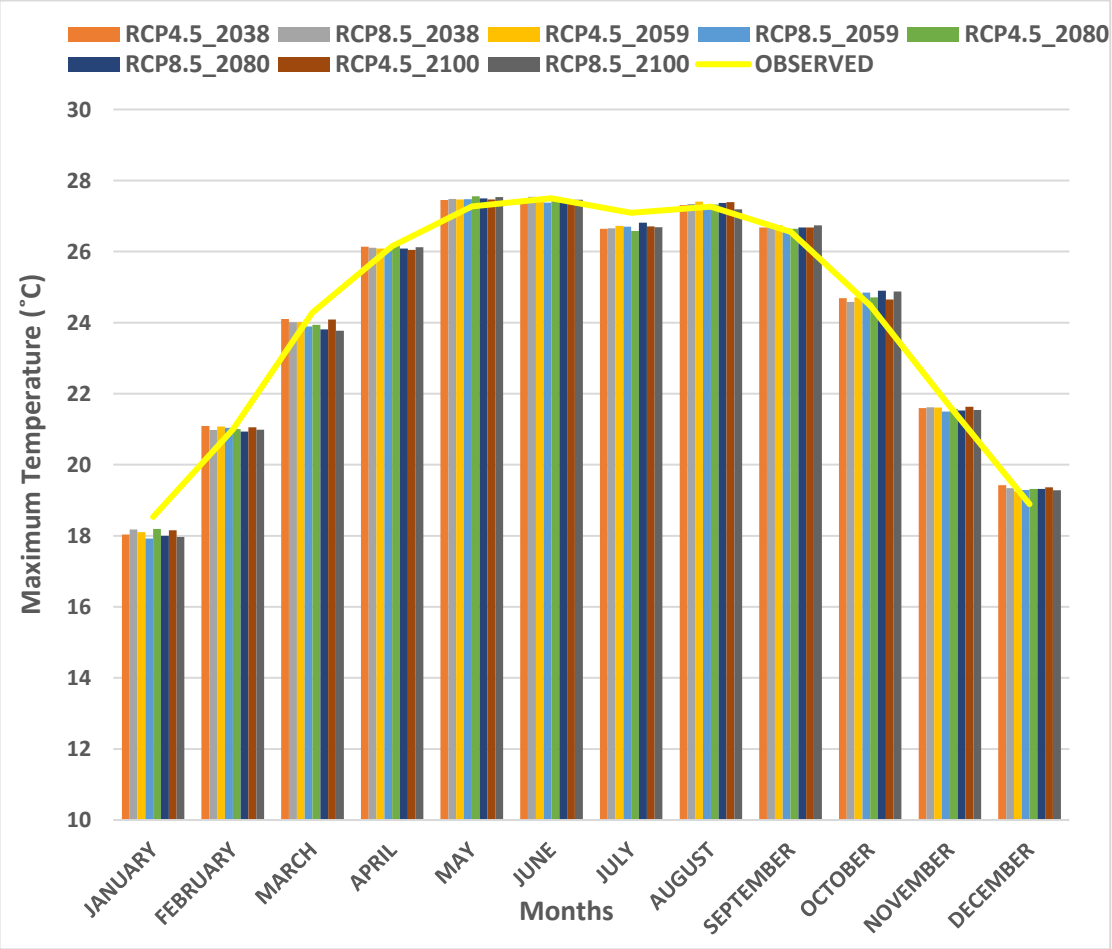

Fig 4.24 Projected monthly maximum temperature in the future periods 2021-2038, 2039-2059, 2060-2080, and 2081-2100 compared to the observed monthly maximum temperature in the baseline period (2003-2020) at Kohima station

Fig 4.25 shows a comparison of the projected monthly minimum temperature from downscaled CanESM2 GCM under RCP4.5 and RCP8.5 scenarios with the observed monthly rainfall data at Kohima station. The observed data or baseline period (2003-2020) indicates that the temperature is generally low during the winter months of January, February, and December. Conversely, the minimum temperature tends to be greater in June and July, which are part of the summer season. In January, the baseline period shows a higher temperature than the projected minimum temperature under both scenarios. The RCP4.5 and RCP8.5 (2021-2038, 2039-2059) exceeds the baseline period in February, March and April. In rest of the months, under both scenarios shows more less equal to the baseline period. A rise of around 3 to 4˚C is anticipated by the end of the 21st century. The RCP8.5 scenario typically has higher

minimum temperatures in comparison to the RCP4.5 scenario, indicating a more pronounced warming trend associated with higher emission trajectories. A study with a similar methodology but conducted in a different region was carried out by Chengcheng *et al.* (2024), who reported that RCP8.5 projects higher future temperature increases compared to RCP4.5.

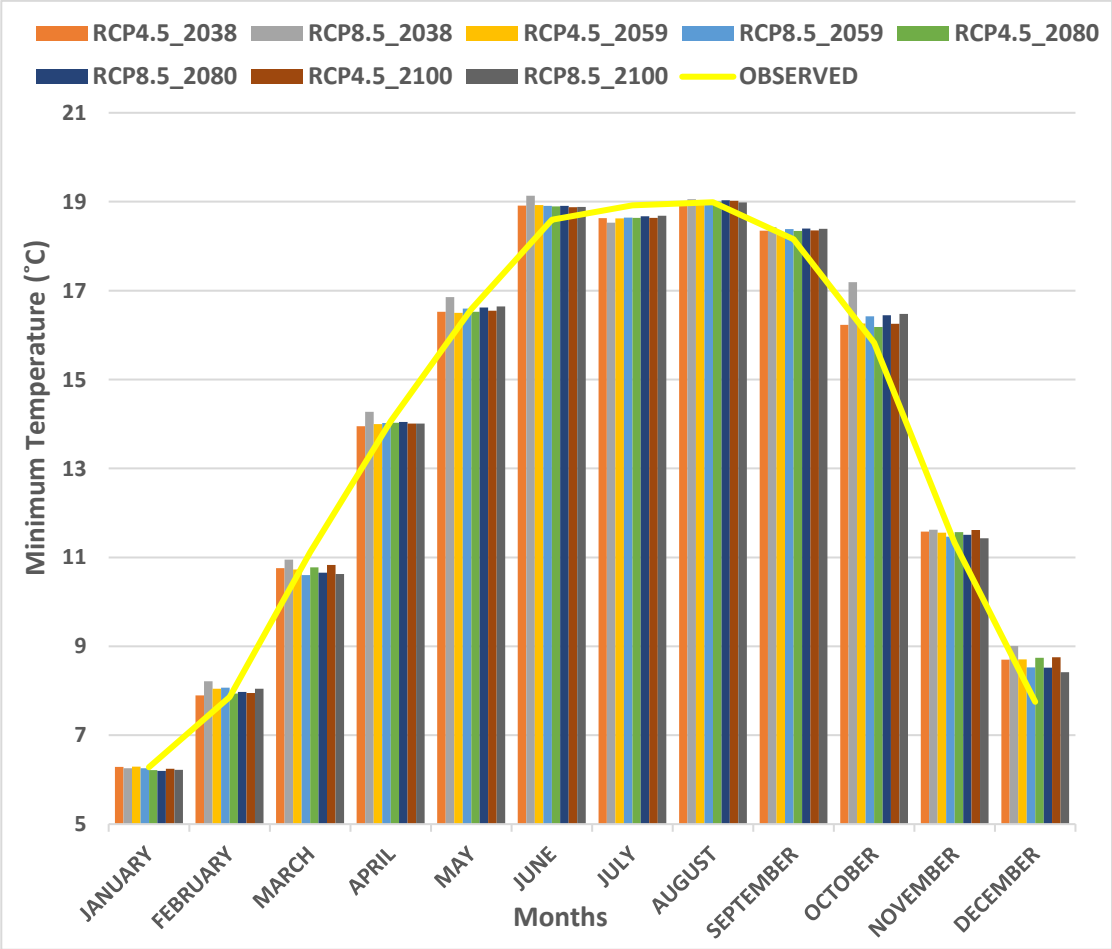

Fig 4.25 Projected monthly minimum temperature in the future periods 2021-2038, 2039-2059, 2060-2080, and 2081-2100 compared to the observed monthly minimum temperature in the baseline period (2003-2020) at Kohima station

Fig 4.26 shows a comparison between the projected monthly maximum temperature from downscaled CanESM2 GCM under RCP4.5 and RCP8.5 scenarios and the observed monthly maximum temperature data at Dimapur station. The projected maximum temperature in all future periods (2021-2038, 2039-2059, 2060-2080, and 2081-2100) under RCP4.5 and RCP8.5 scenarios is lower than that of the

baseline period (2003-2020), except from July to September. While there may be some variation across different RCP scenarios, the general trend indicates a lower temperature over time.

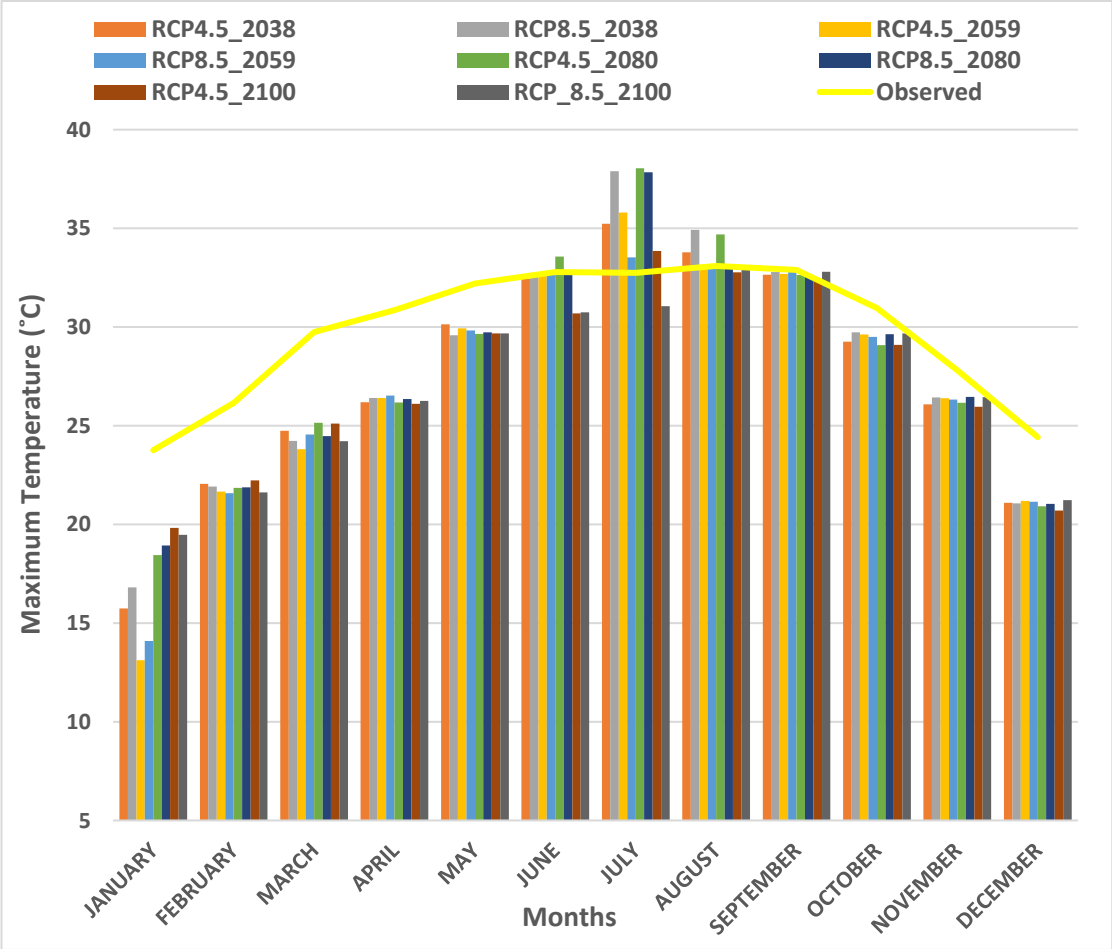

Fig. 4.26 Projected monthly maximum temperature in the future periods 2021-2038, 2039-2059, 2060-2080, and 2081-2100 compared to the observed monthly maximum temperature in the baseline period (2003-2020) at Dimapur station

Fig 4.27 shows a comparison between the projected monthly minimum temperature from downscaled CanESM2 GCM under RCP4.5 and RCP8.5 scenarios and the observed monthly minimum temperature data at Dimapur station. The projected minimum temperature under both scenarios exceeds the baseline period. The RCP8.5 scenario, which represents higher greenhouse gas concentration, demonstrates higher projections for minimum temperature compared to the baseline period. The

timeline forecasts from 2038 to 2100 show a significant rise in temperature, showing a substantial increase in minimum temperature as a result of climate change.

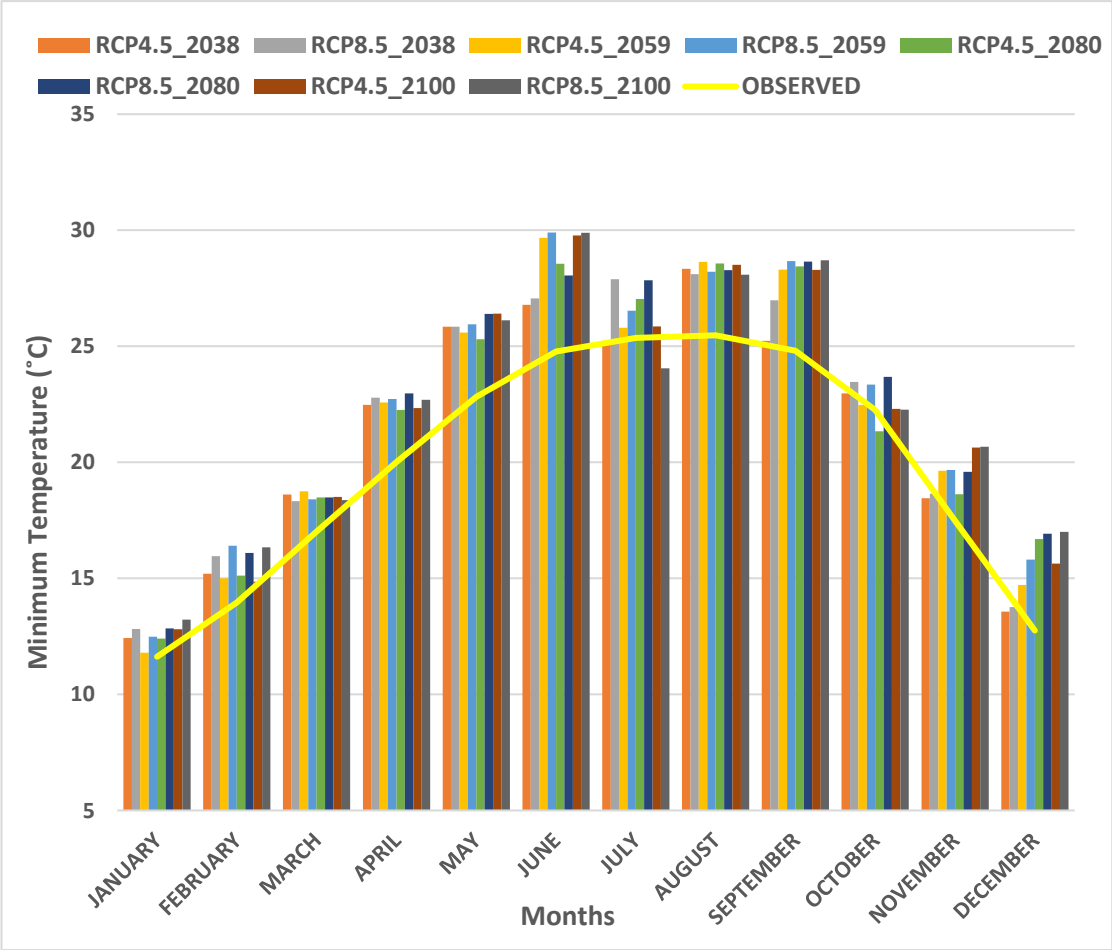

Fig 4.27 Projected monthly minimum temperature in the future periods 2021-2038, 2039-2059, 2060-2080, and 2081-2100 compared to the observed monthly minimum temperature in the baseline period (2003-2020) at Dimapur station

Several studies support these findings, including a report by Javaherian *et al.* (2021), which reveals that the CanESM2 model predicts greater increases in both maximum and minimum temperatures in the future period under the RCP4.5 and RCP8.5 scenarios. Specifically, the RCP8.5 scenario shows a higher temperature rise compared to RCP4.5 in the Lar Dam basin, Iran. Another study by Gupta *et al*. (2022) found that under RCP4.5 and RCP8.5 scenarios of the CanESM2, the future maximum temperature was projected to increase by 0.4 to 3.4°C, with RCP8.5 showing higher increases compared to RCP4.5 in the Ganges Basin, India. Similarly, a finding by

Mukherjee *et al.* (2023) also reported that under the RCP 8.5 scenario, maximum temperature was projected to increase by 5.3°C and minimum temperature by 5.9°C by the end of the century in eastern India.

4.2.3 Water Availability in the future scenarios

The projected rainfall for the future periods (2021-2038, 2039-2059, 2060-2080, and 2081-2100) under RCP4.5 and RCP8.5 scenarios has been used to generate the forthcoming water availability in the study area. The parameters, such as the groundwater and soil moisture data, are considered the same in future periods. The surface runoff was computed using the same equation explained in section 3.3.1.4 by incorporating the projected rainfall data instead of the observed rainfall. After determining all the parameters, the future water availability was calculated for each scenario using the same formula that was used to find the present water availability given in Equations 3.1 to 3.4. This was purposedly done to compare the present and future water availability.

Fig 4.28 presents a comparison of present and projected water availability under the RCP4.5 and RCP8.5 scenarios. The present water availability in May, June, and July exhibits a greater abundance of water compared to future periods in both scenarios. The anticipated water availability throughout the winter months (December to February) exhibits a notable upward trend, which is substantial when compared to the current conditions witnessed during the dry season. The anticipated increases in the dry season are a positive development, indicating enhanced water security in the study region. A similar finding was reported by Anushiya and Ramachandran (2015), where the future water availability was projected to increase during winter months, as indicated by the study's findings on seasonal water balance components in the Chennai Basin. The winter water availability may increase due to the increasing temperature, such as shifting peak river runoff to winter and spring, impacting water supply in the region (Barnett *et al*., 2005). In January and April, the future water availability is projected to increase more between 2060-2080 under the RCP8.5 scenario. For February and October, the increase is expected to occur between 2021-2038 under the RCP4.5 and RCP8.5 scenario. In March, the increase is projected to happen between 2039-2059 under the RCP4.5 scenario. In August, the increase is projected to happen

between 2081- 2100 under the RCP8.5 scenario. In the time frame of May and June 2018-2038 under the RCP4.5 scenario, the water availability was closely comparable to its present value. The projected monthly water availability in the future was greater under the RCP8.5 scenario compared to the RCP4.5 scenario. This could be attributed to the narrative of RCP8.5 (a scenario with extremely high emissions), as supported by a study conducted by Serur and Sarma (2017). In their study, they reported that the variation of rainfall and temperatures (maximum and minimum) was higher for the very high emission scenario (RCP8.5) than the intermediate emission scenario (RCP4.5), and the future trend line for both the scenarios has indicated a slight increase of both temperatures as well as rainfall for the 12 stations until the year 2100 in Weyib river basin, Ethiopia. In both RCP4.5 and RCP8.5 scenarios, the future water availability in July exhibited a notable decline compared to the current water availability. The result also revealed that from May to July, which is the main rainy season, less water availability would be experienced in the future periods under both scenarios. This changing pattern would affect agricultural production in the study area, where 70% of the population in the region depends on agriculture for livelihood. A similar finding published in the Eastern Mirror (2024) reported that insufficient monsoons are expected in the future, which would drastically affect crop production in the Northeastern region due to the impact of climate change. The increasing temperatures and shifting rainfall patterns would frequently lead to reduced crop production as a consequence of water scarcity caused by droughts, heat waves, and floods. The effect of climate change resulting in increasing temperature poses a significant threat to agricultural production and farmers' financial stability, leading to a decrease in their motivation to engage in agriculture (Javansalehi and Shourian, 2024).

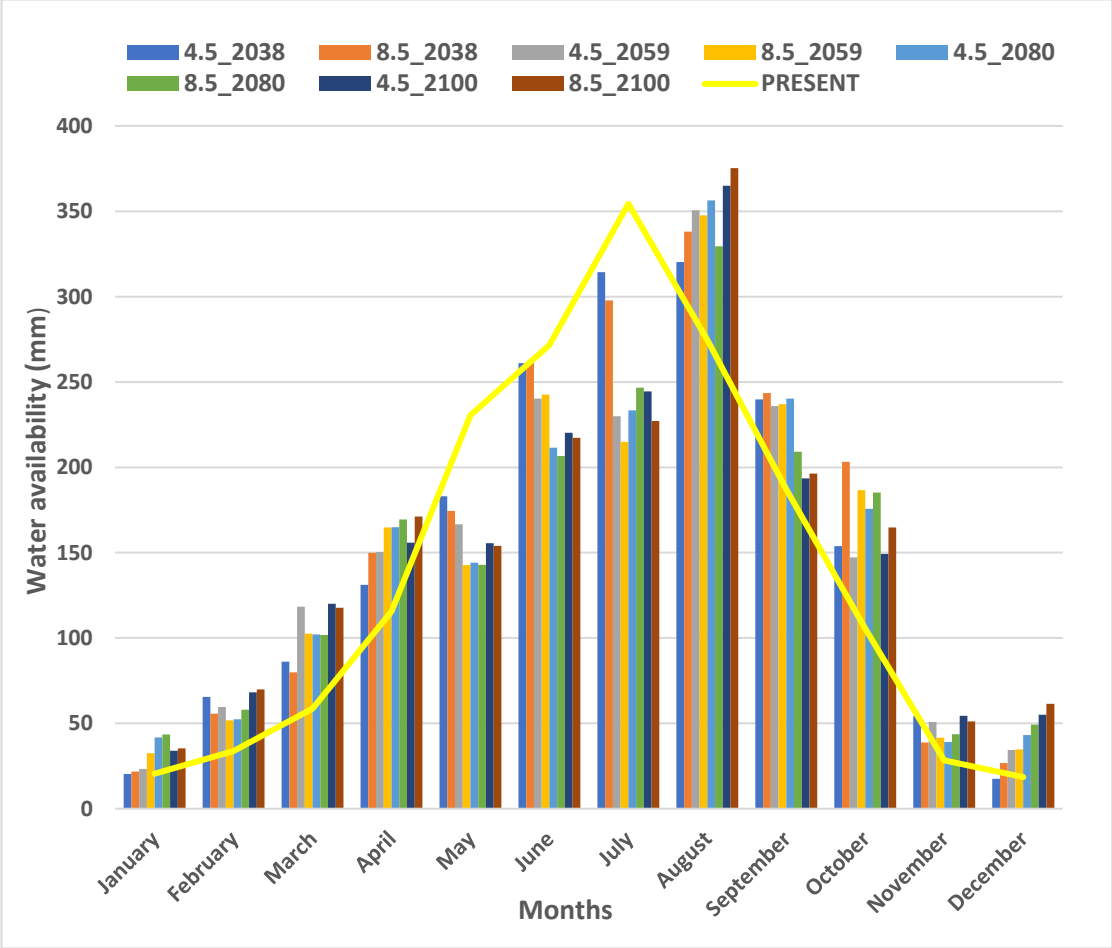

Fig 4.28 Water availability (2003-2020) and future prediction from 2021-2038, 2039-2059, 2060-2080, and 2081-2100 under RCP4.5 and RCP8.5 scenarios in the study area

4.3 Identification and recommendation of an acceptable climate change adaptation strategy to address water shortage or excess in the near future

Agriculture is the primary means of livelihood in the study area; therefore, the farmers may face challenges if there is insufficient water supply at the appropriate period for crop cultivation. Under the prevailing agricultural practices, the cropping intensities are 113.6 and 112.35 percent in the Dimapur and Kohima districts, respectively (ICAR, CRIDA). In the previous sections, it has been highlighted that the presence of water fluctuates in both spatial and temporal dimensions across different future scenarios. Consequently, cropping intensity can be enhanced by effectively utilizing surplus water during periods of peak water availability. This fluctuation could also impact water availability during crucial periods for specific crops. Therefore, to accomplish the third objective, the cropped area was analyzed to determine the major crops grown in the study area.

For this purpose, cropped areas were analyzed to identify the major crops in the study area. The details of all the major crops and their cultivated areas in the study region for the year 2022-2023 are shown in **Table 4.10**. It shows that rice and maize are the major crops in the study area. Water availability for the major crops at critical times is essential; therefore, to identify water shortages or excess, it was necessary to determine the actual crop water requirements in the study area and then compare the water availability with the actual requirement.

Table 4.10 Area (ha) under different major crops in the study area (2022-23)

CROP	DIMAPUR	KOHIMA
Rice	6136	12135
Maize	622	1833
Beans	135	332
Potato	156	805
Sugarcane	100	35
Soyabean	228	264

Source: Department of Agriculture, Govt. of Nagaland

Table 4.11 shows the cropping calendar of the major crops covering the study area. The crop calendar assists growers and agriculture extension specialists worldwide in making appropriate recommendations on crop varieties and sowing dates based on agroecological zones. It also provides a solid foundation for alternative or contingency planning of the reintegration of agricultural systems after disasters (Banerjee *et al.*, 2021). The cropping calendar illustrates that sowing occurs mostly from January to July, with March and April being the most productive months for various crops. The harvesting season is more spread out, lasting from May to December, with no harvesting between January and April.

Table 4.11 Cropping calendar of the major crops showing the sowing and harvesting period in the study area

MAJOR CROPS	JAN	FEB	MAR	APR	MAY	JUN	JUL	AUG	SEP	OCT	NOV	DEC
RICE												
MAIZE												
BEANS												
POTATO												
SUGARCANE												
SOYABEAN												

Sowing Harvest

Soil Characteristics of Kohima and Dimapur districts

According to the SLUSI (2020), about 78% of the land in Kohima district is deep to very deep. They are mostly loamy to clayey in texture, formed on the steep hill slopes in wet conditions, and have a moderate to high amount of organic matter. The ICAR-CRIDA (2021) contingency plan also talks about the loamy (≈57%) and clayey (≈43%) soils, which are often called the sandy-loam deep soils and come from weathered sandstone and shale. These fine-textured profiles help hold water, but they are more likely to wash away and erode on sloping land, which affects how the catchments respond to water.

On the other hand, Dimapur district is in the alluvial plains and has soils that are moderately shallow (60–75 cm), moderately deep (75–100 cm), and deep (> 100 cm) with coarse-loamy to fine-loamy particle size classes (ICAR-CRIDA, 2021). The SLUSI (2020) inventory shows that about 54.6% of the district is made up of very deep soils and about 38% is made up of deep soils. This means that there are a lot of depositional plains with a lot of water that can soak in. Field and laboratory analyses further indicate that loamy sand, sandy clay, and acidic red clay soils are the predominant textures (Pamei *et al*., 2022; CGWB, 2019). These deep, fine-textured soils help water move through them and recharge groundwater, but they may become waterlogged in low-lying areas during the months with the most rain.

The pedological characteristics of the two districts are very different. For example, Kohima has fine-textured, deep hill soils, while Dimapur has deep alluvial soils. These differences have a direct effect on how water moves through the study area, how much water it can hold, and how much it can hold.

4.3.1 Analysis of Reference Evapotranspiration (Eto)

The prediction of the crop water requirement is of vital importance in water resources management. The evapotranspiration rate (ET) in mm day-1 or m period-1 normally expresses crop water requirements. The level of ET is related to the evaporative demand of the air. The evaporative demand can be expressed as the reference evapotranspiration (ETo), which, when calculated, predicts the climate's effect on the crop evapotranspiration level. The effect of the weather variable on the water demand of the crop can be analyzed by the Cropwat model output. Agrometeorological variables are one of the key inputs required for the functioning of the crop simulation models. These include the maximum and minimum temperature, air humidity, wind speed sunshine hours, solar radiation, and total rainfall. Out of these temperature and rainfall have a direct impact on crop production (Bayatvarkeshi *et al.*, 2020; Zhao *et al*., 2020). In **Table 4.12**, the reference crop evapotranspiration in Kohima shows the highest (3.4 mm/day) and lowest value (1.5 mm/day) in the month of June and December, respectively, whereas in Dimapur the ETo was the highest (3.9 mm/day) in May and lowest value (1.5 mm/day) in December. The rising temperature

in that particular period can explain the increase in ETo from April to September in the study area. A similar study by Drema *et al.* (2024) found that the Eto showed a significant decrease in the winter season in the districts of Arunachal Pradesh, India. They also found that a significantly decreasing seasonal Eto trend was found mainly in monsoon and pre-monsoon seasons in all districts. Consistent with our findings, a study by Jhajharia *et al*. (2012) indicated that the ETo attains its peak in summer and then declines progressively across the sites of North East India. Liu *et al.* (2010) observed ETo rises in the upper, middle, and entire Yellow River basin, China. Bandyopadhyay *et al.* (2009) found declining trends in ETo throughout India, which was primarily caused by a major increase in relative humidity and a constant significant decrease in wind speed across the country.

Table 4.12 Average ETo for the period 2003-2020

STATIONS	**ETo in mm/day**											
	Jan	**Feb**	**Mar**	**Apr**	**May**	**Jun**	**Jul**	**Aug**	**Sep**	**Oct**	**Nov**	**Dec**
Kohima	1.6	2.0	2.8	2.9	3.3	3.4	3.3	3.1	2.9	2.5	2.0	1.5
Dimapur	2.0	2.5	3.4	3.4	3.9	3.8	3.7	3.2	3.2	3.0	2.6	1.8

4.3.2 Crop water requirement for the major crops

The crop water requirement of the major crops such as rice, maize, potato, soyabean, sugarcane, and dry beans for the period 2003-2020 has been analysed. The results are discussed below.

The daily crop water requirement of rice in Kohima and Dimapur is shown in **Fig 4.29**. The crop water requirement for rice varies during the crop growing season due to variations in reference evapotranspiration. The crop water requirement for rice was initially low due to the low crop coefficient. Still, it increased sharply till the 2nd week of May in Kohima and the 3rd week of May in Dimapur. Then it decreased after the 3rd week of June, due to the low crop coefficient. The maximum daily water requirement of rice was nearly 3.8 mm/day and 4.3 mm/day for Kohima and Dimapur respectively. The total crop water requirement for rice was 510.8 mm and 659.6 mm

for Kohima and Dimapur, respectively. A similar study conducted by Patle and Panggeng (2024) found that the total water requirement for rice was 537.1 mm in Kohima district, Nagaland. Another study conducted by Kumar *et al.* (2024) found that the crop water requirement of rice varied from 482.5 mm to 592.4 mm in different agroclimatic zones of Jharkhand, India. Also, a study by Aryal (2013) reported that the total crop water requirement of rice was 711.45 mm from June to September conducted in Kathmandu, Nepal. Similarly, Chandra and Kumari (2021) found that the crop water requirement of rice in Kharif was 616.4 mm for the Pusa region of Samastipur district, Bihar.

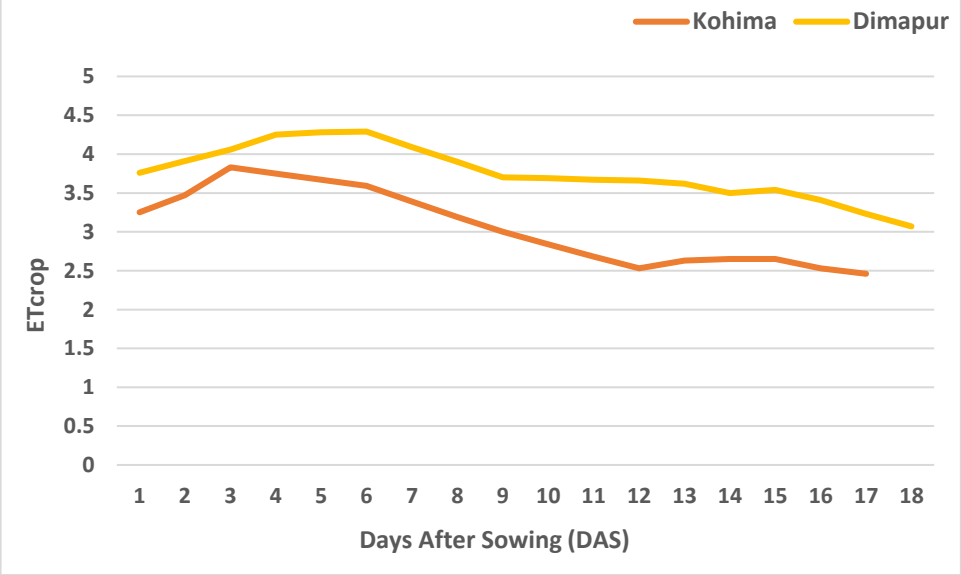

Fig 4.29 Trend of crop water requirement of rice

The daily crop water requirement of maize in Kohima and Dimapur is shown in **Fig 4.30**. The crop water requirement for maize varies during the crop growing season due to variations in reference evapotranspiration. Initially, the crop water requirement for maize was low due to the low crop coefficient. Still, it increased sharply till the 3rd week of May. Then it decreased after the 2nd week of July due to low crop coefficient. The maximum daily water requirement of maize was nearly 3.3 mm/day and 3.8 mm/day for Kohima and Dimapur respectively. The total crop water requirement for maize was 270.5 mm and 335.1 mm for Kohima and Dimapur, respectively. A similar finding by Shankar *et al.* (2012) reported that the average daily crop water requirement was 2.5 mm/day and the total crop water requirement was

495.2 mm for maize in a semi-arid region of India. In their study, the crop maize was sown in May and harvested in September. Similar results were reported by Roja *et al.* (2020) in the North coastal districts of Andra Pradesh where the maximum daily water requirement was 3.2 mm/day and total crop water requirement for maize was 238.6 mm.

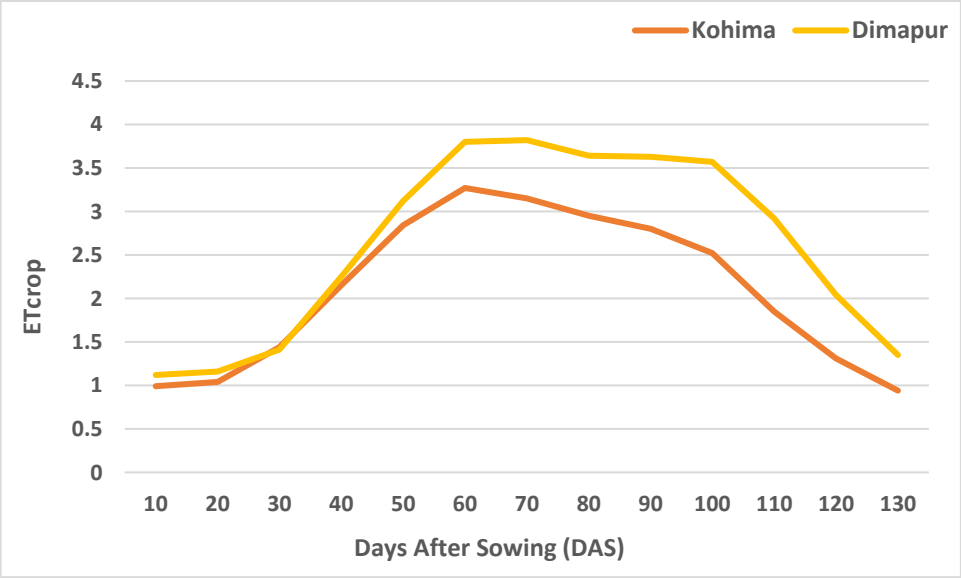

Fig. 4.30 Trend of crop water requirement of maize

The daily crop water requirement of beans in Kohima and Dimapur is shown in **Fig 4.31**. The crop water requirement for beans varies during the crop growing season due to variations in reference evapotranspiration. The crop water requirement for beans was initially low due to the low crop coefficient. Still, it increased sharply till the first week of June. Then it decreased after the first week of July due to the low crop coefficient. The maximum daily water requirement of beans was nearly 3.3 mm/day and 4.1 mm/day for Kohima and Dimapur respectively. The total crop water requirement for beans was 270.5 mm and 335.1 mm for Kohima and Dimapur, respectively. A similar finding by Patle and Panggeng (2024) found that the total crop water requirement for beans was 288.1 mm in Kohima district, Nagaland. Also, a study by Gabr (2023) found the crop water requirement for beans was 281.1 mm which was grown in July in Upper Egypt.

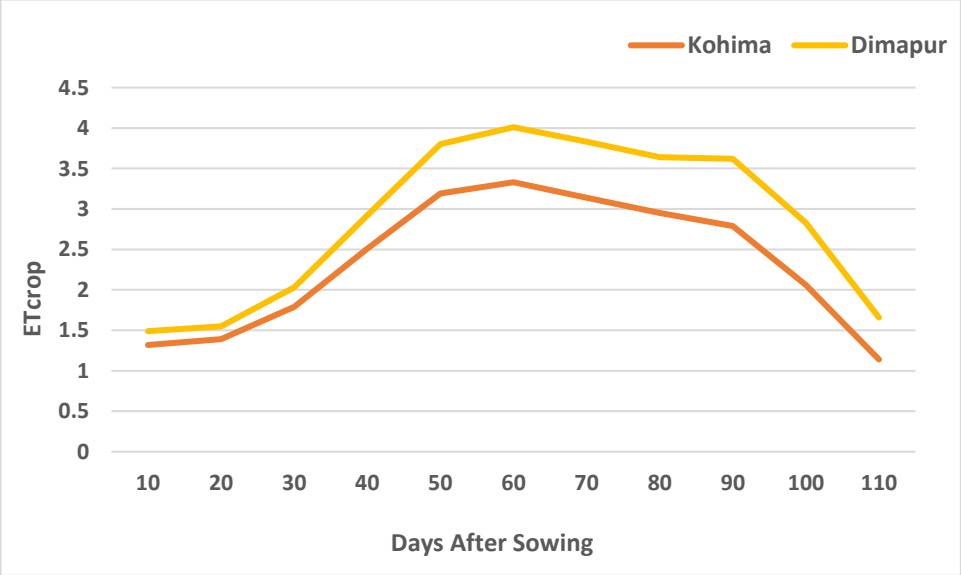

Fig. 4.31 Trend of crop water requirement of beans

The daily crop water requirement of potato in Kohima and Dimapur is shown in **Fig 4.32**. The crop water requirement for potato varies during the crop growing season due to variations in reference evapotranspiration. Initially, the crop water requirement for potato was low due to the low crop coefficient. Still, it increased sharply till the first week of June. Then it decreased after the first week of July due to the low crop coefficient. The maximum daily water requirement of potato was nearly 3.6 mm/day and 4.2 mm/day for Kohima and Dimapur respectively. The total crop water requirement for potato was 339.6 mm and 403.1 mm for Kohima and Dimapur, respectively. A similar finding by Gautam *et al.* (2019) found that the maximum crop water requirement of potato was 3.1 mm/day during the summer season in Madhya Pradesh. Also, a study by Panme *et al.* (2023) reported that the total crop water requirement for potato was 260.6 mm in the North-Eastern Region, of India.

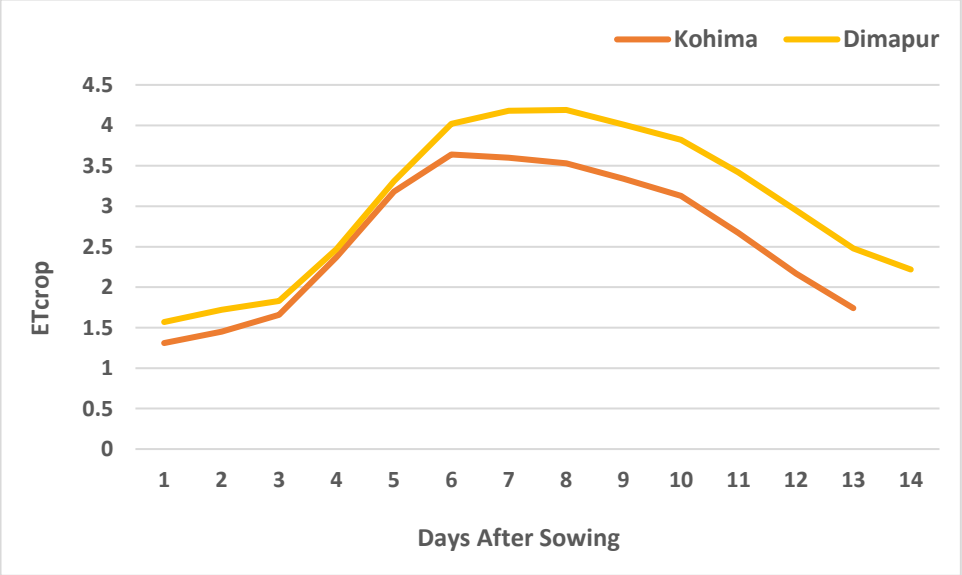

Fig. 4.32 Trend of crop water requirement of potato

The daily crop water requirement of sugarcane in Kohima and Dimapur is shown in **Fig 4.33**. The crop water requirement for sugarcane varies during the crop growing season due to variations in evapotranspiration. The crop water requirement for beans was initially low due to the low crop coefficient. Still, it increased sharply till the 3rd week of August in Kohima and the 2nd week of October in Dimapur. Then it decreased after the 3rd week of October in Kohima and the 2nd week of February in Dimapur, due to the low crop coefficient. The maximum daily water requirement of sugarcane was nearly 2.8 mm/day and 3.7 mm/day for Kohima and Dimapur respectively. The total crop water requirement for sugarcane was 534.3 mm and 1032.4 mm for Kohima and Dimapur, respectively. A similar finding by Gade and Khedkar (2023) found the crop water requirement for sugarcane was 1386.1 mm in the semi-arid region.

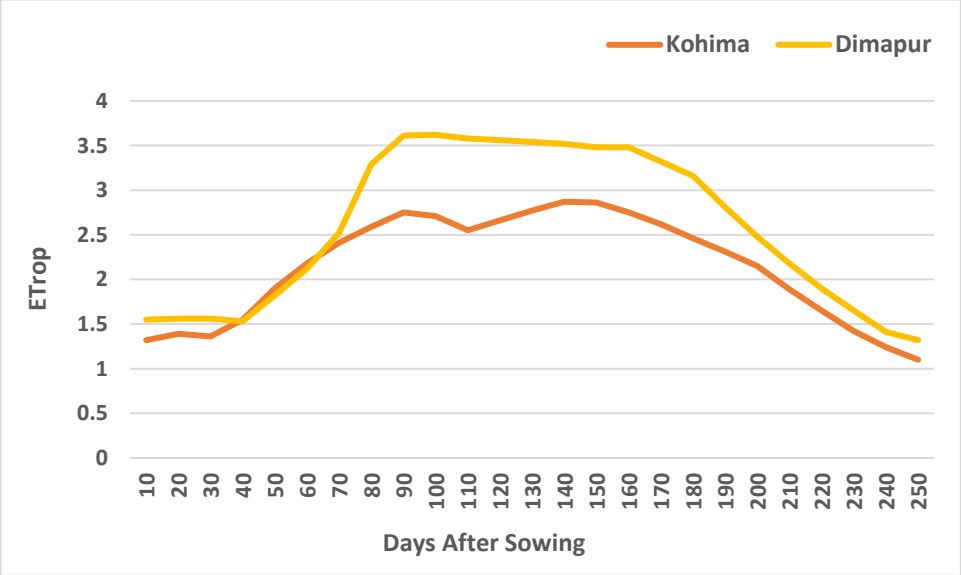

Fig. 4.33 Trend of crop water requirement of sugarcane

The daily crop water requirement of soyabean in Kohima and Dimapur is shown in **Fig 4.34**. The crop water requirement for soyabean varies during the crop growing season due to variations in reference evapotranspiration. The crop water requirement for soyabean was initially low due to the low crop coefficient. Still, it increased sharply till the first week of June. Then it decreased after the first week of July due to low crop coefficient. The maximum daily water requirement of soyabean was nearly 3.7 mm/day and 5.5 mm/day for Kohima and Dimapur respectively. The total crop water requirement for maize was 232.6 mm and 564.2 mm for Kohima and Dimapur, respectively. A similar finding by Patle and Panggeng (2024) found the crop water requirement for soyabean was 292.2 mm in Kohima district, Nagaland. Also, Phad *et al.* (2024) reported a similar result of crop water requirement for soyabean was 457.8 mm in the Marathwada region, India.

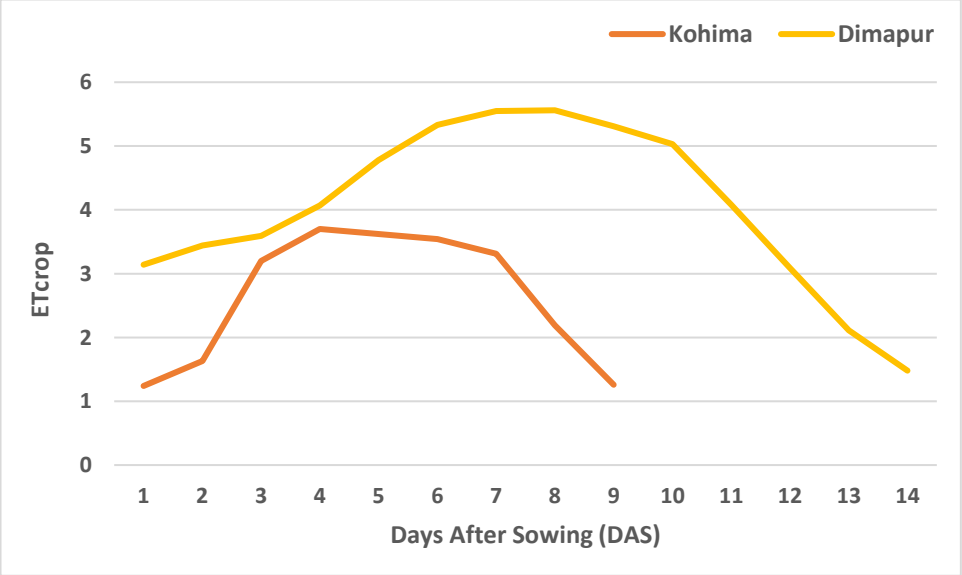

Fig. 4.34 Trend of crop water requirement of soyabean

Table 4.13 shows the comparison between the present water availability and crop water requirement of the different crops in Kohima district. The results revealed that the water availability starts at 20.43 mm in January, increasing to 33.78 mm in February and 58.59 mm in March. The crop water requirement for rice in March requires 35.8 mm, potato requires 45.9 mm, and soyabean requires 13.6 mm. The water availability in April was 115.48 mm, whereas the crop water requirement for rice was high with a value of 110.4 mm, while the other crops such as maize, beans, potato, and soyabean have moderate to high crop water requirements with a value of 34.7, 45, 91.9 and 85.3 mm respectively. In May, the water availability rises to 230.61 mm and the crop water requirements for rice, maize, beans, potato, soyabean and sugarcane have moderate to low water requirements with values of 109.9, 85.9, 93.7, 108, 108.1, and 58.5 mm respectively. In June, the water availability peaks at 271.68 mm, and the crop water requirement for rice, maize, beans, potato, sugarcane, and soyabean have moderate to low requirements with values of 90.3, 89, 88.8, 79.7, 77.5, and 25.7 mm respectively. In July, the water availability shows the highest at 354.38 mm and the crop water requirement for rice, maize, beans, potato, and sugarcane have lower to moderate water requirements with 81, 58.1, 30.9, 13.9, and 83.8 mm respectively. In August, the water availability was 274.62 mm and the crop water requirement for rice, maize, and sugarcane have low to moderate water requirements with values of 80.8,

2.8, and 87.8 mm respectively. In September, the water availability drops to 205.04 mm and the crop water requirement for maize and sugarcane have low to moderate water requirements with values of 2.5 and 60.3 mm respectively. From October to December, the water availability decreases significantly from 105.55 mm in October to 28.31 mm in November and 18.52 mm in December. The crop water requirement for sugarcane required 65.4 mm in October and 43.1 mm in November; soyabean required 1.1 mm in December. From May to August, which is usually the rainy period/season, the water availability exceeds the crop water requirements, indicating a surplus period. From April to September, where most of the crop needs are comfortably met. In January, February, October, November, and December, the availability of water may not fully meet the demands of crops like sugarcane.

Table 4.13 Present water availability and crop water requirement of the major crops in Kohima district

Month	Present water availability, mm	Rice, mm	Maize, mm	Beans, mm	Potato, mm	Sugarcane, mm	Soyabean, mm
Jan	20.43	-	-	-	-	-	-
Feb	33.78	-	-	-	-	-	-
Mar	58.59	35.8	-	-	45.9	-	13.6
Apr	115.48	110.4	34.7	45	91.9	40.7	85.3
May	230.61	109.9	85.9	93.7	108	58.5	108.1
Jun	271.68	90.3	89	88.8	79.7	77.5	25.7
Jul	354.38	81	58.1	30.9	13.9	83.8	-
Aug	274.62	80.8	2.8	-	-	87.9	-
Sep	205.04	2.5	-	-	-	60.3	-
Oct	105.55	-	-	-	-	65.4	-
Nov	28.31	-	-	-	-	43.1	-
Dec	18.519	-	-	-	-	1.1	-

Table 4.14 shows the comparison between the present water availability and crop water requirement of the different crops in the Dimapur district. The results revealed that the water availability starts at 20.43 mm in January and increases to 58.59 mm by March. The crop water requirement for maize, potato, and soyabean required 15, 48.3, and 105.2 mm, respectively in March. There was sufficient water for maize and potato but the water was not adequate to meet the high soyabean requirement. In April, the water availability was 115.48 mm and the crop water requirement for rice was 122.2 mm, nearly matching the water available. The other crops such as maize, beans, potato, and soyabean also have water requirements with values of 33.5, 50.7, 98, and 141.8 mm respectively, whereas for soyabean and rice, water was found to be insufficient. In May, the water availability rises to 230.61 mm and the crop water requirement for rice, maize, beans, and potato have moderate water requirements with values of 130.7, 95.5, 111.3, and 124.8 mm, respectively. In June, the water availability peaked at 271.68 mm, and the crop water requirement for rice, maize, beans, and potato required 112.9, 110.9, 110.9, and 101.9 mm, respectively. In June, the water availability was highest at 354.38 mm, and the crop water requirement for rice, maize, beans, and potato was 113.1,87.4,43.2, and 27 mm, respectively. In August, the water availability was 274.62 mm, and the crop water requirement for rice, maize, and beans have minimal to high water requirements with values of 108.7, 8.1, and 111.2 mm, respectively. In September, the water availability dropped to 205.04 mm, and the crop water requirement for sugarcane was 105.4 mm. In October, the water availability continues to decrease with 105.55 mm in October, 28.31 mm in November, and 18.52 mm in December. The crop water requirement for sugarcane in October and November was 95.7 and 65.6 mm, respectively. The crop water requirement for soyabean was 41.2 mm in December, showing a deficit in water availability. From May to August, the water availability comfortably meets or exceeds crop requirements. From April to September, it provides enough water for most crops, with minor deficits for high-demand crops like soybean in April. From January to March and October to December, the water availability is often insufficient to meet crop demands, especially in November and December for crops like sugarcane and soybean.

Table 4.14 Present water availability and crop water requirement of the major crops in Dimapur district

Month	Present water availability, mm	Rice, mm	Maize, mm	Beans, mm	Potato, mm	Sugarcane, mm	Soyabean, mm
Jan	20.43	-	-	-	-	-	-
Feb	33.78	-	-	-	-	-	-
Mar	58.59	15	-	-	48.3	-	105.2
Apr	115.48	122.2	33.5	50.7	98	4.7	141.8
May	230.61	130.7	95.5	111.3	127.8	48	169.5
Jun	271.68	112.9	110.9	110.9	101.9	64.6	122
Jul	354.38	113.1	87.4	43.2	27	35.9	25.5
Aug	274.62	108.7	8.1	-	-	111.2	-
Sep	205.04	56.9	-	-	-	105.4	-
Oct	105.55	-	-	-	-	95.7	-
Nov	28.31	-	-	-	-	65.6	-
Dec	18.519	-	-	-	-	41.2	-

In a similar finding by Krishnaiah and Rongsenchiba (2017) found that the wet period, characterized by sufficient water availability, varies between 151 to 181 days in districts such as Dimapur and Kohima. This aligns with the observed surplus water availability from May to August in both districts, as indicated in Tables 4.11 and 4.12. The District Irrigation Plan for Dimapur highlights the importance of aligning irrigation strategies with available water resources and crop water requirements. It emphasizes the need for efficient water management during periods of surplus and deficit, supporting the observed trends of water availability exceeding crop requirements during the monsoon season and falling short during the dry months (PMKSY, Department of Irrigation and Flood Control, Nagaland). The Central Ground Water Board North Eastern Region (2022) reports on the seasonal variation in groundwater availability and its implications for irrigation. The findings support the

observed patterns of water availability and crop water requirements, particularly the deficits during the dry months and the need for sustainable groundwater management. An article in the Morung Express (2017) reported the water requirements of key crops grown in Nagaland, such as rice, maize, and potato. It highlighted the critical stages of water demand for these crops and the importance of timely water availability to prevent yield loss. This information corroborates the crop water requirements detailed in Tables 4.13 and 4.14, emphasizing the need for adequate water supply during specific growth stages.

In water-scarce periods, a critical water supply deficit occurs for crops such as sugarcane and soybean from January to March and October to December. During March, Dimapur suffers from a serious failure in the water supply for soybean, and during November and December, for sugarcane. This indicates that these crops face stress unless supplemental irrigation systems are provided. Given the surplus water availability during the peak periods, cropping intensities could be increased by using that additional water to support more crops or expand existing cultivated areas during these months. Effective water management strategies would include scheduling and possibly storing water during surplus periods so that shortages in dry months could be offset. Several studies have highlighted the crop and water management strategies for sugarcane and soyabean in the Northeast region, India particularly in regions with challenging topographies like Nagaland (Ray *et al*., 2015; Ray *et al*., 2017; Jamir *et al*., 2023; Bhutia *et al*., 2024). The water availability in the Dimapur and Kohima districts is adequately matched with the crop requirements during the monsoon period but poses challenges during the dry periods. To ensure the sustainability of agriculture productivity and increase cropping intensities, adaptive strategies need to be undertaken that include advanced water management techniques and supplementary irrigation during critical periods. Enhancing the agricultural resilience to climate variability is likely by better-aligning crop water requirements with existing water resources, thereby assisting in fulfilling the subsistence requirements of the local farming community. The following recommendations have been given for both the districts in the study area.

Kohima District:

1. Develop new water sources:

   Explore options like building more wells to tap into groundwater and constructing reservoirs to store water, especially during rainy seasons.

2. Recycle and reuse water:

   Build new wastewater-treatment plants to recycle and reuse wastewater, which can then be used for non-potable purposes.

3. Invest in better storage:
   Improve water storage infrastructure, including tanks and other systems, to hold water for future use and manage seasonal availability.
4. Rainwater harvesting and traditional systems: Rooftop rainwater harvesting, micro-catchments, and revival of indigenous Ruza/Zabo systems, historically practiced in Nagaland, should be expanded to improve water storage and reduce erosion. Many a times research advocates the rainwater harvesting and traditional systems to tackle present water scarcity situation in Kohima (Sarkar, 2017 and Mongabay, 2023).
5. Soil and water conservation: Contour bunding, terracing, agroforestry, and vegetative hedges can mitigate runoff and conserve soil moisture, aligning with recommendations for hill agro-ecosystems in Northeast India (Sati, 2013).

6. Crop diversification and horticulture: Given its cooler climate and relatively higher water availability, diversification toward high-value horticultural crops such as vegetables, fruits, and spices under drip or sprinkler irrigation can optimize water use efficiency (Rodriguez *et al*., 2017).

7. Community-managed water sources: Watershed development and spring rejuvenation through community-led approaches can secure perennial water sources critical for hill villages (FAO, 2017).

Dimapur district:

1. Government authority may renovate and protect the traditional water bodies and tanks to improve storage capacity and recharge groundwater. Further, implement strict rules on the amount of groundwater that can be extracted to

help replenish aquifers. In the past, water was found at 30–40 feet, but now residents must dig much deeper, which indicates severe groundwater depletion. Similar recommendations were made in regard to groundwater recharge and regulation by Behera *et al*., 2024; Jain *et al*., 2024; and Monir *et al*., 2024, in their study.

2. Restore water bodies: Dimapur can renovate and protect its traditional water bodies and tanks to improve storage capacity and recharge groundwater.
3. Wastewater treatment: Establishing a wastewater treatment plant could create a new, usable water source for non-potable needs, like watering parks and gardens.
4. Dam and reservoir construction: Building reservoirs could collect and store water during the rainy season for use during dry spells.
5. Involve communities in water management: Establishing water user associations can help citizens cooperatively manage and share water resources, leading to more sustainable outcomes.
6. Implementation of traditional techniques: The indigenous "Zabo" farming system, which combines forestry and agriculture with water conservation, can be adapted to city environments. The centuries-old bamboo drip irrigation method also provides a sustainable model. Rodriguez *et al.* (2017) reported that drip and sprinkler irrigation in paddy and vegetable cultivation can save water and sustain yields under water-scarce conditions.

4.4 Assessment of mechanization index and recommendation of suitable agricultural implements under less water availability situation

Mechanization plays an essential role in agriculture as it increases crop productivity, reduces cultivation costs, and increases overall farming efficiency. As the world population grows, food demand increases, and agricultural land decreases. At this juncture, the use of appropriate agricultural machinery is the solution left to address the challenge of increasing the production of crops and the productivity of labor in limited agricultural land. These machineries are grouped based on the type of agricultural operation. Some of the implements are light in weight and can be used in dryland situations. Therefore, before the recommendation of agricultural implements,

the mechanization scenario in the study area was examined in two stages: 1) field survey and 2) analysis of primary data using the mechanization index approach.

The field survey was conducted with 101 respondents interviewed within the study area for the collection of data. General information collected from respondents in the study area can be seen in **Table 4.15**. The dataset encompasses various measurements, including the total land area, the area designated for cultivation, the area benefiting from irrigation, the area dependent on rainfall, the categorization of farmers according to their land holdings, the count of agricultural laborers, and the quantities of tube wells, tractors, electric motor pumps, diesel engines, power tillers, brush cutters, as well as the daily provision of electricity.

Table 4.15 Geographical and general information about the study area

Particulars	Kohima	Dimapur
Gross area, ha	146.3	92.7
Cultivated area, ha	58.42	61.2
Net irrigated area, ha	7.52	14.44
Rainfed area, ha	5.24	46.8
No. of cultivators		
-Below 2 ha	12	16
-2 to 4 ha	25	30
-above 4 ha	9	9
No. of Agril workers	40	51
No. of tubewells	33	48
No. of tractors		
-Below 35 hp	3	6
No. of electric motor pump	16	25
No. of diesel engine	3	5
No. of power tiller	29	40
No. of brush cutter	16	10
Electricity availability, hr/day	11	15

Source: Compiled by scholar

From the field survey, it was revealed that the average gross area evaluated was 119.5 hectares, whereas the cumulative cultivated area was noted at 59.81 hectares.

Furthermore, the personal interview showed that agricultural machinery, such as tractors, power tillers, and brush cutters, has been distributed by the State to a majority of the respondents, revealing that the majority of respondents in Kohima (60.4%) and Dimapur (71.4%) primarily used power tillers. In contrast, tractor usage was significantly lower, with only 6.3% in Kohima and 10.7% in Dimapur. Similarly, brush cutters were used by 33.3% of respondents in Kohima and 10.7% in Dimapur. Based on the information collected through the survey, the cost of cultivation of crops is assessed and outlined under the following sub-headings.

4.4.1 Cost of cultivation of crops

For the analysis of the mechanization index in the study area, six major crops were selected. The cost of cultivation of the major crops is shown in **Table 4.16**. The results show that the production values of jhum paddy, maize, chili, potato, and soybean were 51000 ₹/ha, 115200 ₹/ha, 74880 ₹/ha, 240000 ₹/ha, and 57600 ₹/ha, respectively, in Kohima. In Dimapur, the production value of the wetland paddy, maize, chili, potato, and soyabean were 71400 ₹/ha, 151488 ₹/ha, 496392 ₹/ha, 480000 ₹/ha, and 55000 ₹/ha. The highest gross profit for Kohima was shown in potato cultivation (218000 ₹/ha) with a benefit-cost ratio (BCR) of 9.9, whereas in Dimapur, the highest gross profit was shown in chili cultivation (475252 ₹/ha) with a BCR of 22.5. In contrast, the lowest gross profit was found in paddy production in both districts as 17000₹/ha and 374000₹/ha in Kohima and Dimapur, respectively.

Table 4.16 Cost of cultivation and mechanization index of the major crops

District	Major crops	Total production value, (₹/ha)	Productivity, (₹/kg)	Gross Profit, (₹/ha)	BCR	MI, %
Kohima	Jhum Paddy	51000	11.33	17000	0.5	1.8
	Maize	115200	50.73	81170	2.4	1.9
	Chilli	74880	55.98	53740	2.5	2.8
	Potato	240000	27.25	218000	9.9	2.8
	Soyabean	57600	29.58	35500	1.6	2.7

Dimapur	Wetland Paddy	71400	17.81	37400	1.1	2.7
	Maize	151488	53.83	117458	3.5	2.9
	Chilli	496392	74.68	475252	22.5	4.2
	Potato	480000	28.63	458000	20.8	4.2
	Soyabean	55000	27.42	32900	1.5	4.1

Source: Compiled by scholar

4.4.2 Assessment of mechanization index

The mechanization index was assessed using the mathematical interpretation explained in section 3.6.4. **Table 4.16** shows the cost of cultivation and mechanization index (MI) for the major crops. The results revealed the highest MI in chilli and potato in both the districts, Kohima (2.8%) and Dimapur (4.2%).

The primary determinants contributing to the lower mechanization index identified in the study area were a lack of understanding of farm machinery and implement usage, reduced annual income of farmers, and the presence of marginal farmers who cannot acquire costly machinery and implements.

4.4.3 Recommendation of agriculture implements

Given all the findings above, a list of tools and implements has been recommended to be used in water scarcity situations, as shown in **Tables 4.17 and 4.18**. The recommended agricultural implements would be feasible in hilly as well as plain regions, and when there is less water available. At the National level, research institutions, with the help of some manufacturing industries, are developing such tools, implements, and types of machinery are being developed. Topographically condition-wise, these implements and types of machinery are recommended for the state government and end users to be used as per their requirement.

Table 4.17 List of tools and implements recommended to be used in the hilly region

Field Operation	Existing tools and implements	Recommended tools and implements	Technical specification (L x B x H), mm	Field capacity, ha/hr

Tillage	Naga *Dao* (large knife), *Vekhuro* (sickle), Spade, Power tiller (10-15 hp), *Choktchu* (small spade), Hand fork	Power tiller (3hp)	600 x 80-150	0.11
		Melur plough	-	0.008
		Bose plough	-	0.016
		Adjustable row marker	-	0.1-0.2
Sowing and Planting	Manual sowing, Khurpi	Manually operated seed drill	2000 x 1040 x 700	0.50
		Seed treating drum	0.90 x 0.70 x 0.40	0.015
Weeding and Hoeing	*Ehe* (hand weeder), Hand hoe, Hand fork, *Kheya* (Bamboo and wooden)	Hand rake	350	0.005
		Wheel hand hoe	1400 x 450 x 800	0.03-0.05
		Cono-weeder	2140 x 500 x 1070	0.18
		Battery operated portable wetland weeder	1200 x 500 x 1000	0.2-0.3
Plant protection	*Ehe* (hand weeder), Hand fork, Manual hand sprayer	Battery operated low volume sprayer	380 x 250 x 725	1.5
		Knapsack sprayer	-	0.04
		Foot compression operated sprayer	-	0.2
	Kholo (wooden stick), *Vekhuro*	Pedal-operated paddy thresher	900 x 585 x 760 mm	0.07

Harvesting and Threshing	(sickle), Naga *dao-Lepok*	Self-propelled vertical conveyor reaper	2200 x 950 x 1100	0.125
		Pedal-operated tubular maize sheller	980 x 490 x 650	0.19

Table 4.18 List of tools and implements recommended to be used in the plain region

Operation	**Existing tools/implements**	**Recommended tools/implements**	**Technical specification (L x B x H), mm**	**Field capacity, ha/hr**
Tillage	Naga *Dao* (large knife), *Vekhuro* (sickle), Spade, Power tiller (10-15 hp), *Choktchu* (small spade), Hand fork	Power tiller operated slasher cum insitu shedder	-	0.033
		Improved iron plough	3500 x 250 x 900	0.021
		Drill plough	-	0.03-0.04
Sowing and Planting	Manual sowing, Khurpi, Spade, Hand fork	Bullock-drawn seed planter	2000 x 1040 x 700	0.50
		Broadcaster	0.90 x 0.70 x 0.40	0.015
		Birsa animal-drawn seed drill	850 x 440 x 170	0.002
		Gorru	1080 x 1180 x 925	0.04
Weeding and Hoeing	*Ehe* (hand weeder), Hand hoe, Hand fork,	Manual weeder	-	0.02
		Bullock drawn weeder	-	0.03-0.04

	Kheya (Bamboo and wooden)	TNAU improved dryland weeder	1100x650x1050	0.002
		Power rotary weeder	2400 x 1750 x 1100	0.04-0.05
Plant protection	Ehe (hand weeder), Hand fork, Manual hand sprayer	Areca sprayer	600 x 600 x 1500	-
		Footwear operated sprayer	-	0.2
Harvesting and Threshing	*Kholo* (wooden stick), *Vekhuro* (sickle), Naga *dao-Lepok*	Paddy reaper harvester	2200 x 850 x 1170	0.04
		Maize husk cum sheller	3000 x 710 x 1450	-
		Hand cum Pedal Operated Chaff Cutter	920 x 540 x 1225	0.19

SUMMARY AND CONCLUSIONS

The present research was undertaken to evaluate the Agricultural Water Availability Index (I_{AWA}) and its impact on climate change on a short and long-term basis in Kohima and Dimapur districts, Nagaland. The scarcity of water is a global issue affecting both developed and developing countries. With population growth, urbanization, and industrialization combined with climate change, water scarcity has become a significant concern. Conflicts over future water allocations have been reported in many countries. Climate change can impact water supply availability and short-term uncertainty, leading to increased droughts and floods. The per capita availability of water has decreased due to spatial variation in rainfall. The northeastern states face increasing water scarcity due to inadequate water management, with farmers relying on the southwest monsoon for agricultural activities. To address this issue, a water availability index was developed, including factors such as quantity, quality, and accessibility, to provide a comprehensive picture of water availability for agriculture.

The I_{AWA} deals with the factors influencing water availability, including rainfall, soil moisture, groundwater, and runoff, and provides a detailed methodological framework for assessing these parameters. The daily rainfall data for 18 years (2003 to 2020) was collected from the Department of Soil and Water Conservation, Government of Nagaland, Kohima, and used for the calculation of all rainfall-related parameters. The raw data was analyzed data utilizing ArcGIS, SDSM, and CROPWAT software, emphasizing the temporal and spatial variation of water resources under different climate change scenarios. The MODIS (Moderate Resolution Imagery Spectroradiometer) data products of LST (Land Surface Temperature) and NDVI (Normalized Difference Vegetation Index) were used to estimate the spatial and temporal changes in soil

moisture status. The groundwater depth (2004-2019) and quality data (2020) were collected from the India WRIS (Water Resource Information System). The SCS curve number method (U.S. Soil Conservation Service, 1986) was used in this study to estimate the surface runoff. Future projections of rainfall and temperature were made by statistical downscaling. Evaluation of the Mechanization Index was calculated based on a survey in the study area, and suitable agricultural implements were recommended for use in water crisis scenarios.

By integrating various parameters, the Agricultural Water Availability Index (I_{AWA}) was evaluated using data on rainfall, soil moisture, surface runoff, and groundwater depths. The index provides a holistic view of water availability, which is crucial for effective agricultural planning. The result revealed that in January and February, the average water availability was close to 10 mm, which was the lowest level compared to July, when the highest water availability was seen, peaking at about 380 mm. It illustrates a seasonal pattern of variation of rainfall in water availability, which increases sharply during monsoon and declines during the winter season. The rainfall interpolation showed that July received the highest rainfall (556.33 mm), on the contrary, December received the lowest rainfall (3.56 mm). Consequently, the soil moisture index indicated the depletion of over 50 percent moisture during the winter season. The study also revealed that the groundwater depth fluctuates, showing a clear trend of depletion during the dry season. The groundwater in the study area meets permissible quality standards for key parameters like pH, electrical conductivity, nitrate, and fluoride. While the surface runoff was assessed, the result showed the minimum surface runoff was in January (0.22 mm) and the maximum in July (385.18 mm).

Climate change showed an impact on temporal and spatial variation of water availability. Climate change is a major concern in Nagaland, where 70% of the population relies on climate-sensitive sectors like agriculture. The statistical downscaling model (SDSM) was used in this study. The

SDSM has a good simulation effect on rainfall with the coefficient of determination (R^2) of 0.92 and 0.85 for Kohima and Dimapur, respectively. The R^2 values for maximum and minimum temperature in Kohima station were determined to be 0.99 and 0.98, respectively. The R^2 for the maximum temperature at Dimapur was found to be 0.92, while for the minimum temperature, it was 0.93. The RCP4.5 scenario in Kohima station predicted higher rainfall than RCP8.5 in 2021-2038, except in May, September, and October, while the future period in the year 2100 showed more rainfall in all months except July (299 mm), showing a decreasing trend. The RCP8.5 scenario in Dimapur station projected higher rainfall than the RCP4.5 scenario in all future periods except in March, September, and May. However, in May and June, rainfall was lower than historical observations, with fluctuating conditions in November.

In Kohima station, the projected maximum and minimum temperatures were lower than the baseline period in January, February, March, and April under both RCP4.5 and RCP8.5 scenarios. In May, June, July, and August, the projected maximum temperatures were more or less equal to the baseline. The RCP8.5 scenario shows higher minimum temperatures compared to the RCP4.5. There is a consistent trend of temperature increase in all future periods, with temperatures expected to rise by around 2 to 3°C. In Dimapur station, the projected maximum temperatures under both scenarios are lower than the baseline period, except from July to September. In comparison, the projected minimum temperature under both RCP4.5 and RCP8.5 scenarios exceeded the baseline period. The year 2100 forecasts in Kohima and Dimapur stations, particularly under the RCP8.5 scenario, highlighted the highest warming potential.

The present water availability in May, June, and July was higher in comparison to the future periods, with a notable upward trend in the winter months due to increasing temperatures and shifting peak river runoff. This indicated enhanced water security in the study area. The projected monthly

water availability was greater under the RCP8.5 scenario, attributed to the very high greenhouse gas emission scenario. Due to climate change, insufficient monsoons are expected in the future, affecting crop production in the Northeastern region. The increasing temperatures and shifting rainfall patterns could lead to reduced crop production due to water scarcity caused by droughts, heat waves, and floods.

The reference crop evapotranspiration (Eto) in Kohima station showed the highest (3.4 mm/day) and lowest value (1.5 mm/day) in June and December, respectively, whereas in Dimapur station, the ETo was the highest (3.9 mm/day) in May and lowest value (1.5 mm/day) in December. From April to September, most of the crop water needs were comfortably met, whereas, in January, February, October, November, and December, the availability of water may not fully meet the demands of crops like sugarcane and soyabean. The water availability in the Dimapur and Kohima districts was adequately matched with the crop requirements during the monsoon period but posed challenges during the dry periods. The results of the Eto indicated that the farmers might experience difficulties in scheduling their planting and harvesting periods, which would negatively impact crop yields and food security. It emphasizes the need for integrated policies that consider the interconnectedness of the source of water and its sustainably managed use in light of climate change.

Recommendations included the adoption of rainwater harvesting systems to capture and store excess rainfall. A crucial need for the construction of reservoirs and check dams to ensure water availability in surplus and scarcity periods to provide a steady supply for agricultural and domestic purposes. Policymakers are motivated to encourage sustainable practices like conservation agriculture, efficient water use technologies, and community-led water management initiatives that can improve resilience against water scarcity. This will provide better coordination of stakeholders, from farmers to government agencies and NGOs, in promoting sustainable water usage.

The economic analysis revealed that among the six major crops studied, chilli and potato cultivation provided the highest gross profit and benefit-cost ratio, making it the most economically viable option for farmers. In contrast, maize cultivation was found to be the least profitable, primarily due to lower market prices and higher production costs. This result indicated that farmers should consider shifting towards more profitable crops like chili and potato, especially in the context of fluctuating water availability, to enhance their income and sustainability. The study also showed a significant reliance on power tillers among farmers, indicating a trend toward increased mechanization in agricultural practices. This mechanization is crucial for improving efficiency and productivity, especially in water-scarce conditions. To increase productivity and lower labor intensity, it promotes the implementation of region-specific mechanization solutions, such as lightweight machinery appropriate for hilly terrains.

Based on the results obtained, the following conclusions were chosen.

i. The present research revealed that the present Agricultural Water Availability Index (I_{AWA}) has significant seasonal variation, with the highest water levels found to occur in the monsoon months, especially peaking in July. In contrast, water availability decreases significantly throughout the winter months, with the lowest values observed in December. The Agricultural Water Availability Index (I_{AWA}) examined various water sources, including rainfall, soil moisture, surface runoff, and groundwater, in evaluating overall water availability for agricultural purposes.

ii. The overall amount of rainfall will be increased under both scenarios in the future, but at the same time, there will be more fluctuations in rainfall events as compared to the present-day scenario.

iii. As a consequence of climate change, the extremes of water

availability would become more severe. Thus, the vulnerability of the agriculture sector to climate change will increase in the future. This can be well explained by the highest and lowest values of the water availability index in August and January, respectively.

iv. The reliance on rainfall as the main source of water underlines the vulnerability of the agricultural sector to fluctuations in precipitation, which calls for improved management practices to ensure sufficient water allocation for crops, particularly for water-intensive crops like rice, which constitutes a significant portion of the cultivated area.

v. The study recommends adopting suitable climate change adaptation strategies and enhancing agricultural mechanization to manage water scarcity effectively.

vi. The research will support policymakers and stakeholders in addressing the challenges of water scarcity and climate change impacts in Nagaland.

Suggestions for future work:

i. Improving Water Utilization Techniques: Conceiving and implementing ways to improve water resources that equate the needs of the crops to the water that is accessible. This could involve implementing drip irrigation systems, harvesting rainwater, and better drainage techniques.

ii. Machine studies: Researching to come up with the best agricultural machines suited to address the needs of the region is in question. This considers the implementation of various agricultural tools and technologies to enhance productivity while reducing labor costs, particularly in water-scarce locations.

iii. Responsible farming: Foster farming methods that are ecologically friendly, conserve soil, consume minimal water, and enhance the

resilience of the crops to factors posing a threat to them. It may include training farmers on the best practices to follow in farming and the use of appropriate farming methods in the established farming systems.

iv. Crop Biochemical Engineering: Finding and advocating for plants that have higher resilience to droughts and environmental changes. This includes establishing a range of economically advantageous crops that adapt to different climates.

v. Collaborative Learning: Motivating farmers to actively engage in water management projects and enlightening them on how to use new forms of irrigation and technologies that minimize water. A bottom-up strategy can enhance the success of water management techniques.

vi. Policy Development: The creation of policies that integrate water resources with agricultural activities through the engagement of the farmers. This entails also lobbying for good infrastructure, such as water harvesting facilities for proper water resource utilization.

vii. Monitoring and Evaluation: Creating mechanisms to follow up on the availability of water and agricultural outputs for evaluating the effectiveness of the strategies employed and shifting them when required.

REFERENCES

Abbas, A., Minli, Y., Elahi, E., Yousaf, K., Ahmad, R., and Iqbal, T. (2017). Quantification of mechanization index and its impact on crop productivity and socioeconomic factors. *International Agricultural Engineering Journal*, **26**(3): 49–54.

Abraham, T., Woldemicheala, A., Muluneha, A., and Abateb, B. (2018). Hydrological responses of climate change on Lake Ziway catchment, Central Rift Valley of Ethiopia. *J. Earth Sci. Clim. Change*, **9**(6): 474.

Adhikary, P. P., and Dash, C. J. (2017). Comparison of deterministic and stochastic methods to predict spatial variation of groundwater depth. *Applied Water Science*, **7**(1): 339–348.

Aher, S., Shinde, and Gawali, P. (2019). Spatio-temporal analysis and estimation of rainfall variablity in and around upper Godavari River basin, India. *Arab J Geosci*, **12**.

Ahmad, W. (2011). Development of an agricultural water availability index and its application under climate change in Rechna Doab, Pakistan (Doctoral dissertation, Asian Institute of Technology).

Ahmadi-Sani, N., Jalili, S., and Daneshmand, A. (2022). Effect of land-use change on runoff in Hyrcania: An SCS-CN and GIS analysis. Land, **11**(2): 220.

Aivazidou E., Tsolakis N., Iakovou E., and Vlachos, D. (2016). The emerging role of water footprint in supply chain management: a critical literature synthesis and a hierarchical decision-making framework. *J. Clean. Prod*. **137**:1018–1037.

Akash K., Rejani R., D. Jawaharlal, N. H., and Pasha, L. (2023) Spatial estimation of runoff using SCS-CN Embedded in GIS environment: A case study of Nalgonda district of Telangana,

India. *International Journal of Environment and Climate Change*, **13**(9): 3109–3120.

Al-Ghafri, A., Gunawardhana, L., and Al-Rawas, G. (2014). An assessment of temperature and precipitation change projections in Muscat, Oman from recent global climate model simulations. *International Journal of Students' Research in Technology & Managemen*t, **2**: 109–112.

Allen, R. G. (2000). Crop evapotranspiration: guidelines for computing crop water requirements. F.A.O.

Allen, R. G., and Pereira, L. S. (1998). Crop evapotranspiration guidelines for computing crop requirements. FAO Irrig. Drain. Report modeling and application. *Journal of Hydrology*.

Allen, R. G., Pruitt, W. O., Wright, J. L., Howell, T. A., Ventura, F., Snyder, R., Itenfisu, D., Steduto, P., Berengena, J., Yrisarry, J. B., Smith, M., Pereira, L. S., Raes, D., Perrier, A., Alves, I., Walter, I., and Elliott, R. (2006). A recommendation on standardized surface resistance for hourly calculation of reference ETo by the FAO56 Penman-Monteith method. *Agricultural Water Management*, **81**(1–2): 1–22.

Allen, R. G., Wright, J. L., Pruitt, W. O., Pereira, L. S., and Jensen, M. E. (2007). Water requirements. American society of agricultural and biological engineers. In Design and Operation of Farm Irrigation Systems, 2nd Edition, 208–288.

Altieri, M. A. (2004). Linking ecologists and traditional farmers in the search for sustainable agriculture. *Frontiers in Ecology and the Environment*, **2**(1): 35–42.

Anand, B., Karunanidhi, D., Subramani, T., Srinivasamoorthy, K. and Suresh, M. (2020). Long-term trend detection and spatiotemporal analysis of groundwater levels using GIS techniques in Lower

Bhavani River basin, Tamil Nadu, India. *Environment, Development and Sustainability*, **22**(4): 2779–2800.

Anandhi, A., Srinivas, V., Nanjundiah, R.S., and Nagesh, K. D. (2008). Downscaling precipitation to river basin in India for IPCC SRES scenarios using support vector machine. *International Journal of Climatology: A journal of the Royal Meteorological Society*, **28**: 401–420.

Anandhi, A., Srinivas, V.V., Kumar, D.N., and Nanjundiah, R.S. (2009). Role of predictors in downscaling surface temperature to river basin in India for IPCC SRES scenarios using support vector machine. *International Journal of Climatology,* **29**(4): 583–603.

Anderson, R., Bayer, P. E., and Edwards, D. (2020). Climate change and the need for agricultural adaptation. *Current opinion in plant biology*, **56**: 197–202.

Anon1. (2016). District Irrigation Plan Dimapur. Retrieved from https://pmksy.gov.in/mis/Uploads/2016/20160517101451170-1.pdf4. on 24.11.2024.

Anon2. (2023). Statistical Handbook of Nagaland. Retrieved from https://statistics.nagaland.gov.in/statistics/category/181 on 18.08.2024.

Anon3. (2013). Master plan for artificial recharge to groundwater in India. Central Groundwater Board, Ministry of Water Resources, Government of India. Retrieved from https://cgwb.gov.in/cgwbpnm/publication-detail/324 on 03.05.2022.

Anon4. (2019). Nagaland Basic Facts 2023. Retrieved from https://ipr.nagaland.gov.in/node/13268 on 10.01.2024.

Ara, Z. and Zakwan, M. (2018). Estimating runoff using SCS curve number method. *International Journal of Emerging Technology and Advanced Engineering*, **8**(5): 195–200.

Armain, M. Z. S., Hassan, Z., and Harun, S. (2021). Climate change impact under CanESM2 on future rainfall in the state of Kelantan using Artificial Neural Network. *IOP Conference Series: Earth and Environmental Science*, **646**(1).

Aryal, S. (2013). Rainfall and water requirement of rice during growing period. *Journal of Agriculture and Environment*, **13**.

Asif, Z., Chen, Z., Sadiq, R., and Zhu, Y. (2023). Climate change impacts on water resources and sustainable water management strategies in North America. *Water Resources Management*, **37**(6): 2771–2786.

Azhoni, A., Holman, I., and Jude, S. (2017). Adapting water management to climate change: Institutional involvement, inter-institutional networks and barriers in India. *Global Environmental Change*, **44**: 144–157.

Bagoria, N., Vimal, V. K., Singh, Y.K., Kumari, R., Kumari, R., Kumar, R.K., Kumar, B., and Kumar, S. B. R. (2020). Spatial variability of soil pH, EC and organic carbon in different panchayats of Sabour block of Bhagalpur district, Bihar, India. *International Journal of Current Microbiology and Applied Sciences,* **9**: 756–763.

Bai, X., Zhang, L., He, C., and Zhu, Y. (2020). Estimating regional soil moisture distribution based on NDVI and land surface temperature time series data in the upstream of the Heihe River Watershed, Northwest China. *Remote Sensing*, **12**(15): 2414.

Banerjee, R., Acharyya, T., and Agarwal, P. (2021). Case Study on Exploring Suitability of Sustainable Agriculture in Western

Rajasthan. *In Resource Efficiency, Sustainability, and Globalization*, 81–98.

Banyopadhyay, A., Bhadra, A., Raghuwanshi, N. S., and Singh, R. (2009). Temporal trends in estimates of reference evapotranspiration over India. *Journal of Hydrologic Engineering*, **14**(5): 508–515.

Barman, S., Deka, N., and Deka, P. (2019). Factors affecting farm mechanization–A case study in Assam, India. *Asian J Agric Extension, Econ Sociol*, **32**(1): 1–7.

Bartlett, J. A., and Dedekorkut-Howes, A. (2023). Adaptation strategies for climate change impacts on water quality: a systematic review of the literature. *Journal of Water and Climate Change*, **14**(3): 651–675.

Bates, B. C., Kundzewicz, Z., Wu, S., and Palutikof, J. (2008). Intergovernmental Panel on Climate Change. Working Group II. *Climate change and water*.

Bawatharani, R., and Karunarachchi, K. A. (2017). Evaluation of mechanization index of vegetable crops in Bandarawela, Srilanka. *Scholars Journal of Agricultural and Veterinary Sciences*, **4**(6): 236–239.

Behera, B., Chowdhury, K., Mishra, T., and Rahut, D. B. (2024). Climate variability, rainwater-harvesting structures and groundwater levels in Odisha, India: an empirical analysis. *International Journal of Water Resources Development,* **40**(3): 487–505.

Belho. K., and Rawat, M. S. (2023). Response of Hydro-Meteorological Hazards to Environmental Degradation in Kohima District of Nagaland, North East India. *International Journal of Scientific Research in Science, Engineering and Technology*, 339–349.

Bhambure, T. V., Gharde, K. D., Mahale. D. M., Nandgude, S. B., Mane, M. S., and Bhattacharyya, T., (2017). Comparative study of different Vegetation indices for Savitri Basin using Remote sensing data. *Advanced Agricultural Research & Technology Journal*, **2**(1): 69–75.

Bhandari, R. (2018). Analyzing Streamflow Variability under CMIP5 Projections Using SWAT Model. Southern Illinois University at Carbondale.

BIS. (2012). IS 10500 – Drinking Water Specification (Second Revision). Bureau of Indian Standards, New Delhi.

Bora, S. L., Bhuyan, K., Hazarika, P. J., Gogoi, J., and Goswami, K. (2022). Analysis of rainfall trend using non-parametric methods and innovative trend analysis during 1901-2020 in seven states of North East India. *Current Science*, **122**(7): 801–811.

Brown, T. C., Mahat, V., and Ramirez, J. A. (2019). Adaptation to future water shortages in the United States caused by population growth and climate change. *Earth's Future*, **7**(3): 219–234.

Carlson, T. N. (2024). The Right Triangle Model: Overcoming the Sparse Data Problem in Thermal/Optical Remote Sensing of Soil Moisture. *Remote Sensing*, **16**(17).

Central Ground Water Board (CGWB). (2013). Ground Water Information Booklet: Dimapur and Kohima Districts, Nagaland. Ministry of Water Resources, Government of India.

Central Ground Water Board (CGWB). (2019). District Ground Water Information Booklet: Dimapur District, Nagaland. Ministry of Jal Shakti, Government of India.

Cerdà, A. (1997). The effect of patchy distribution of Stipa tenacissima L. on runoff and erosion. *Journal of Arid Environments*, **36**: 37–51.

Chai, Q., Gan, Y, Zhao, C., Xu, H.L., Waskom, R.M., Niu, Y., and Siddique, K.H. (2016). Regulated deficit irrigation for crop production under drought stress. *A review. Agron Sustain Dev,* **36**(1):1–21.

Chakma, B., Yurembam, G. S., Jhajharia, D., Patle, G. T., Salam, R., & Saha, S. (2025). Study of temporal behaviour of meteorological drought using innovative polygon trend and scaling hypothesis methods in Kolasib district, Mizoram, *India. Scientific Reports,* **15**(1): 19266.

Chakraborty, D., Roy, A., Singh, N. U., Saha, S., Das, S. K., Mridha, N., Yumnam, A., Paul, P., Gowda, C., Biam, K. P., Patra, S., Amrutha, T., Singh, B. P., and Mishra, V. K. (2025). Assessing Climate Change Impact on Rainfall Patterns in Northeastern India and Its Consequences on Water Resources and Rainfed Agriculture. *Earth (Switzerland)*, **6**(1).

Chandra, R., and Kumari, S. (2021). Estimation of crop water requirement for rice-wheat and rice-maize cropping system using CROPWAT model for Pusa, Samastipur district, Bihar. *Journal of AgriSearch*, **8**(2): 143–148.

Chaturvedi, R.K., Joshi, J., Jayaraman, M., Bala, G., and Ravindranath, N.H. (2012). Multi-model climate change projections for India under representative concentration pathways. *Current Science*, 791–802.

Chaudhari, A., Mehta, D., and Sharma, N. (2021). An assessment of groundwater quality in South-West zone of Surat city. *Water Supply*, **21**(6): 3000–3010.

Chen, F. W., and Liu, C. W. (2012). Estimation of the spatial rainfall distribution using inverse distance weighting (IDW) in the middle of Taiwan. *Paddy and Water Environment,* **10**: 209–222.

Chengcheng, X., Kaixuan, G., Jama, A. H., Chuiyu, L., Qingyan, S., Xu, L., and Lingjia, Y. (2024). Simulation and prediction of precipitation and temperature under RCP scenarios. *Water Supply*, **24**(5), 1676–1688.

Chien, F., Chau, K. Y., and Sadiq, M. (2023). Impact of climate mitigation technology and natural resource management on climate change in China. *Resources Policy*, **81**: 103367.

Chim, K., Tunnicliffe, J., Shamseldin, A., and Chan, K. (2021) Identifying Future Climate Change and Drought Detection Using CanESM2 in the Upper Siem Reap River, Cambodia. *Dyn. Atmos. Ocean*, **94**: 101182.

Chisango, F. F. T., and Dzama, T. (2013). An assessment of agricultural mechanization index and evaluation of agricultural productivity of some fast-track resettlement farms in Bindura district of Mashonaland Central Province, Zimbabwe.

Chu, J., Xia, J., Xu, C.Y., and Singh, V. (2009) Statistical downscaling of daily mean temperature, pan evaporation and precipitation for climate change scenarios in Haihe River, China. *Theor Appl Climatol*, **99**(1):149–161.

Dahal, P., Shrestha, M. L., Panthi, J., and Pradhananga, D. (2020). Modeling the future impacts of climate change on water availability in the Karnali River Basin of Nepal Himalaya. *Environmental Research*, **185**.

Das, A., Ghosh, P. K., Choudhury, B. U., Patel, D. P., Munda, G. C., Ngachan, S. V., and Chowdhury, P. (2009). ISPRS Archives XXXVIII-8/W3 Workshop Proceedings: Impact of Climate Change on Agriculture 32 Climate Change in Northeast India: Recent Facts and Events-Worry For Agricultural Management.

Das, M., Hazra, A., Sarkar, A., Bhattacharya, S., and Banik, P. (2017). Comparison of spatial interpolation methods for estimation of weekly rainfall in West Bengal, India. *MAUSAM,* **68**: 41–50.

Dash, J., Sarangi, A., and Singh, D. (2010). Spatial variability of groundwater depth and quality parameters in the National Capital Territory of Delhi. *Environmental Management*, **45**(3): 640–650.

Dash, S. K., Sharma, N., Pattnayak, K. C., Gao, X. J., and Shi, Y. (2012). Temperature and precipitation changes in the north-east India and their future projections. *Global and Planetary Change*, 98–99, 31–44.

de Fraiture, C., and Wichelns, D. (2010). Satisfying future water demands for agriculture. *Agricultural Water Management*, **97**(4): 502–511.

Debnath, J., Das, N., and Sahariah, D. (2022). Impacts of temperature–rainfall and land use/land cover changes on the hydrological regime in the Muhuri River basin, Northeast India. *Sustainable Water Resources Management*, **8**(5).

Dikshit, K. R., and Dikshit, J. K. (2014). Weather and Climate of North-East India. *Land, People and Economy,* 149–173.

Dirks, K., Hay, J., Stow, C., and Harris, D. (1998). High-resolution studies of rainfall on Norfolk Island part II: Interpolation of rainfall data. *Journal of Hydrology*, **208**: 187–193.

Down to Earth. (2021). *Climate crisis in North East India: What is behind water scarcity in the region.* Retrieved from https://www.downtoearth.org.in.

Drema, L., Gautam, S., and Rawat, S. (2024). Climatic trends and its impact on reference evapotranspiration and crop water requirement of rice crop in Aruncahal Pradesh, India. *Journal of Agrometeorology*, **26**(2): 220–224.

Dube, S., R. K. Mehta and Das, G., (1991). Development of curve number for prevalent land use in Himalayan watersheds. *J. of Agril. Engg*., Special issue, 176–179.

Ebrahimi, M., Kazemi, H., Ehtashemi, M., and Roc, T. (2016). Assessment of groundwater quantity and quality and saltwater intrusion in the Damghan basin, Iran. *Chemie Erde-Geochemistry*.

Elgendy, M., Hassini, S., and Coulibaly, P. (2024). Review of Climate Change Adaptation Strategies in Water Management. *Journal of Hydrologic Engineering*, **29**(1).

FAO. (2010). Natural Resources and Environmental Department. Retrieved 11 23, 2010, from Food and Agriculture organization of the UN.

FAO. (2017). Water for sustainable food and agriculture: A report produced for the G20 Presidency of Germany. Rome: Food and Agriculture Organization of the United Nations.

Felegari, S., Sharifi, A., Moravej, K., Golchin, A., and Tariq, A. (2022). Investigation of the relationship between ndvi index, soil moisture, and precipitation data using satellite images. *Sustainable Agriculture Systems and Technologies,* 314–325.

Feng, Z., Zhnag, Li-W., SHI, J. J., and Huang, J. F. (2014). Soil moisture monitoring based on land surface temperature vegetation index space derived from MODIS data. *Pedosphere,* **24**(4): 450–460.

Feng-Wen, C., and Chen-Wuing, L. (2012). Estimation of the spatial rainfall distribution using inverse distance weighting (IDW) in the middle of Taiwan. *Paddy Water Environ,* **10**:209–22.

Fowler, H. J., Blenkinsop, S., and Tebaldi, C. (2007). Linking climate change modelling to impacts studies: Recent advances in

downscaling techniques for hydrological modelling. *International Journal of Climatology*, **27**(12): 1547–1578.

Gabr, M. E. (2023). Impact of climatic changes on future irrigation water requirement in the Middle East and North Africa's region: a case study of upper Egypt. *Applied Water Science*, **13**(158).

Gade, S. A., and Khedkhar, D. D. (2023). Implication of climate change on crop water requirement in the semi-arid region of Western Maharashtra, India. *Environ Monit Assess*, **195**(829).

Gagnon, S., Singh, B., Rousselle, J., and Roy, L. (2005). An application of the statistical downscaling model (SDSM) to simulate climatic data for streamflow modelling in Québec. *Canadian Water Resources Journal*, **30**(4): 297-314.

Gandhi, F.R. and Patel, J.N. (2019). Estimation of surface runoff for sub-watershed of Rajkot district, Gujarat, India using SCS–Curve Number with integrated geospatial technique. *International Journal of Engineering and Advanced Technology*, **8**(5): 33–41.

Gao, Y., Liu, T., Huang, C., Zhao, J., and Liu, H. (2017). Modeling the contribution of shallow groundwater to evapotranspiration and yield of maize in an arid area. Scientific Reports, **7**: 43122.

Gautam, U., Nema. A. K., and Jaiswal, R. K. (2019). Estimation of crop water requirement (CWR) of major vegetable crops of selected Agro-climatic zones of Madhya Pradesh, India. *International Journal of Current Microbiology and Applied Sciences*, **8**(10): 895–904.

Gebrechorkos, S.H.; Hülsmann, S.; Bernhofer, C. (2019). Statistically Downscaled Climate Dataset for East Africa. Sci. *Data*, **6**(31).

Geological Society of India. (2022). Groundwater conservation and management in North India hills. *Journal of the Geological Society of India*, **93**(2): 250–260.

Ghoderao, S. B., Meshram, S. G., and Meshram, C. (2022). Development and evaluation of a water quality index for groundwater quality assessment in parts of Jabalpur district, Madhya Pradesh, India. *Water Supply*, **22**(6): 6003–6012.

Goyal, M. K., Shivam, G., and Sarma, A. K. (2019). Spatial homogeneity of extreme precipitation indices using fuzzy clustering over northeast India. *Natural Hazards,* **98**(2): 559–574.

Gulacha, Metekiya M., and Deogratias, MM Mulungu. (2017). Generation of climate change scenarios for precipitation and temperature at local scales using SDSM in Wami River Basin Tanzania. *Physics and Chemistry of the Earth,* Parts A/B/C **100**: 62–72.

Gupta, N., Patel, J., Gond, S., Tripathi, R. P., Omar, P. J., and Dikshit, P. K. S. (2022). Projecting future maximum temperature changes in river ganges basin using observations and statistical downscaling model (SDSM). *River dynamics and flood hazards: Studies on risk and mitigation*, 561–585.

Gupta, S. K., Rao, D. U. M., Nain, M. S., and Kumar, S. (2021). Exploring agro-ecological bases of contemporary water management innovations (CWMIs) and their outscaling. *Indian Journal of Agricultural Sciences*, **91**(2): 263-268.

Han, Y., Wang, Y., and Zhao, Y. (2010). Estimating soil moisture conditions of the greater ChangbaiM,mnoo (untains by land surface temperature and NDVI. *IEEE Transactions of Geoscience and Remote Sensing*, 2509–2515.

Hangshing, L., Vijayan, D. S., and Sivasuriyan, A. (2022). A study of rainwater harvesting for sustainable water resource management in Nagaland, Northeast India – a review. *Acta Sci. Pol. Architectura,* **21**(4): 53–61.

Hassan, Z., Shamsudin, S., and Harun, S. (2013). Application of SDSM and LARS-WG for GCM downscaling using atmosphere circulation indices. International journal of GCMs, statistical downscaling and hydrological models in the study of climate change impacts on runoff. *Journal of Hydrology,* **36**(45): 434–435.

Hassim, M., Yuzir, A., Razali, M. N., Ros, F. C., Chow, M. F., and Othman, F. (2020). Comparison of rainfall interpolation methods in Langat River Basin. *In IOP Conference Series: Earth and Environmental Science,* **79**(1): 012018.

He, C., Liu, Z., Wu, J., Pan, X., Fang, Z., Li, J., and Bryan, B. A. (2021). Future global urban water scarcity and potential solutions. *Nat Commun*, **12**: 4667.

Heggen, R. J. (2010). Continuing evolution of rainfall-runoff and the curve number precedent. University of Arizona, Tucson.

Hoang, H. A., Kha, C. T., Lê, T. T., and Huỳnh, T. Đ. (2020). Assessing the status of mechanization and proposing technical solutions for lime farming in the Mekong River Delta. *Tạp chí Nông nghiệp và Phát triển*, **19**(6): 39–52.

Hossain, A. K., Easson, G., and Boken,V. K. (2006). Mapping spatial variation in surface moisture using reflective and thermal aster imagery for southern Africa. *Journal of Remote Sensing*, **10**: 75–88.

Huang, J. F., fei, Z., L.I.U, xue, Z., X.U, and Z.H.A.O, F. (2008). Analysis of Future Climate Change in the Taihu Basin Using Statistical Downscaling. *Resources Science*, **30**(12): 1811–1817.

ICAR-CRIDA. (2021). Agriculture Contingency Plan for District: Kohima (Nagaland) and Dimapur (Nagaland). Hyderabad: Central Research Institute for Dryland Agriculture.

ICMR, 1975. Manual of Standards of Quality for Drinking Water Supplies. *Indian Council of Medical Research*, **44**(27).

Iglesias, A., and Garrote, L. (2015). Adaptation strategies for agricultural water management under climate change in Europe. *Agricultural water management,* **155**: 113–124.

India Meteorological Department (IMD). (2020). Climatological Tables of Observatories in India (1991–2020). Pune: IMD.

Indian Academy of Sciences (IASc). (2024). Spatial and temporal trend analysis of rainfall in Nagaland. *Journal of Earth System Science*, **133**(1).

IPCC Technical Summary Arias PA. (2022). Climate Change 2021: The Physical Science Basis. Contribution of Working Group I to the Sixth Assessment Report of the Intergovernmental Panel on Climate Change Cambridge University Press, Cambridge, United Kingdom and New York, NY, USA, 33−144.

Isselhorst, S., Berking, J. and Schütt, B. (2019). Water Harvesting in Drylands Water Knowledge from the Past for Our Present and Future.

Jain, S. K., Kumar, V., and Saharia, M. (2013). Analysis of rainfall and temperature trends in northeast India. *International Journal of Climatology*, **33**(4): 968–978.

Jain, S., Srivastava, A., Vishwakarma, D. K., Rajput, J., Rane, N. L., Salem, A., and Elbeltagi, A. (2024). Protecting ancient water harvesting technologies in India: strategies for climate adaptation and sustainable development with global lessons. *Frontiers in Water*, **6**: 1441365.

Jaiswal, Rahul Kumar., Tiwari, H.L. and Lohani, A.K. (2018b). Climate Change Assessment of Precipitation in Tandula Reservoir System.

Journal of the Institution of Engineers (India): Series A, **99**(1): 17–27.

Jaiswal, Rahul Kumar., Tiwari, H.L. and Narwariya, K.S. (2016). Study of Climate Change for Precipitation over Tighra Dam Catchment Gwalior, Madhya Pradesh, India. *International Journal of Engineering and Technical Research,* **5**(1): 2454–469.

Jaiswal, Rahul Kumar., Tiwari, H.L., Lohani, A.K. and Yadava, R.N. (2018a). Statistical Downscaling of Minimum Temperature of Raipur (CG) India. Climate Change Impacts. *Springer, Singapore,* 35–45.

Jalalzadeh, B., Borghei, A. M., and Almassi, M. (2016). Modeling the effect of mechanization level index on crop yield approaching system dynamics methodology.

Jamir, C., Kapoor, C., and Jagannath, P. (2023). Climate Change and Agroecosystems in the Hill and Mountain Regions of Northeast India. *Sustainable Food Value Chain Development*, 37–60.

Jamir, W. Z. (2023). Rainfall Trend Analysis of Nagaland by using Mann-Kendall Test. *International Journal of Science and Research (IJSR)*, **12**(3): 917–921.

Javaherian, M., Ebrahimi, H., and Aminnejad, B. (2021). Prediction of changes in climatic parameters using CanESM2 model based on Rcp scenarios (case study): Lar dam basin. *Ain Shams*

Jiang,Y., Wang, X.X., Meng, H., Xu, Y.W., Wang, S., and Wang, S.D. (2022) Photosynthetic physiology performance and expression of transcription factors in soybean of water use efficiency difference. *Russ J Plant Physiol*, **69**(1):1–10.

Jongkor, T., Krishnaiah, Y. V., and Longkumer, L. (2022). A comparative study of urban infrastructure facilities of Kohima, Dimapur, and Mokokchung towns, Nagaland, India.

Joshi, S.K., Gupta, S., Sinha, R., Densmore, A.L., Rai, S.P., Shekhar, S., Mason, P.J. and van Dijk, W.M. (2021). Strongly heterogeneous patterns of groundwater depletion in Northwestern India. *Journal of hydrology,* **598**: 126492.

Kale, S. S. (2022). Estimation of Runoff of Kudavale micro watershed using SCS Curve Number method and GIS Approach. *International Journal of Novel Research and Development,* **7**(5): 296–304.

Kalita, A. (2018). Factors affecting agricultural mechanization in Assam. *International Journal of Research in Engineering, IT and Social Sciences,* **8**(12): 111–117.

Keditsu, V., Rao, B. V., and Vero, A. (2022). Assessment of groundwater quality in and around Chiephobozou town, Kohima district, Nagaland. Journal of Applied Geochemistry, **24**(3).

Khaniya, B., Gunathilake, M. B., and Rathnayake, U. (2021). Ecosystem-Based Adaptation for the Impact of Climate Change and Variation in the Water Management Sector of Sri Lanka. *Mathematical problems in engineering*, **1**: 8821329.

Kılkış, Ş., Krajačić, G., Duić, N., and Rosen, M. A. (2022). Effective mitigation of climate change with sustainable development of energy, water and environment systems. *Energy conversion and management*, **269**: 116146.

Koley, S., and Jeganathan, C. (2020). Estimation and evaluation of high spatial resolution surface soil moisture using multi-sensor multi-resolution approach. *Geoderma,* **378**: 114618.

Kousar, S., and Shirazi, S. A. (2023). Spatio-Temporal Variations of Land-Use Land-Cover in Response to RUSLE Model in Swat Basin Using Remote Sensing and GIS Techniques. *Sarhad Journal of Agriculture*, **39**(3): 722–737.

Krishna Kumar, K., Rupa Kumar, K., Ashrit, R. G., Deshpande, N. R., and Hansen, J. W. (2004). Climate impacts on Indian agriculture. *International Journal of Climatology,* **24**(11): 1375–1393.

Krishnaiah, Y. V., Rongsenchiba., and Jongkor, T. (2017). Water availability and crop suitability in Nagaland. *Hill Geographer*, **33**(1): 87–94.

Krishnan, R. B., and Sankararajan, V. (2021). Hydrogeochemical and geospatial analysis of water quality for domestic and irrigation purposes in Padmanabhapuram, Kanyakumari District, India. *Arabian Journal of Geosciences,* **14**: 1–31.

Kroes, J. G., van Dam, J. C., and van Walsum, P. E. V. (2018). Impact of capillary rise and recirculation on simulated crop yields. *Hydrology and Earth System Sciences*, **22**(6): 2937–2952.

Kulshrestha, U. C., Granat, L., Engardt, M., and Rodhe, H. (2005). Review of precipitation monitoring studies in India - A search for regional patterns. *Atmospheric Environment*, **39**(38): 7403–7419.

Kumar, K., Singh, A. K., and Krishnan, S. (2024). Assessment of Mechanization Index of Sugarcane Cultivation in Mandya District, Karnataka, India. *Archives of Current Research International*, **24**: 251–256.

Kumar, N., Singh, S. K., Singh, V. G., and Dzwairo, B. (2018). Investigation of impacts of land use/land cover change on water availability of Tons River Basin, Madhya Pradesh, India. *Modeling Earth Systems and Environment,* **4**(1): 295–310.

Kumar, P.S., Babu, M. J. R. K., Praveen, T.V. and Kumar, V.V. (2010). Analysis of the runoff for watershed using SCS-CN method and Geographic Information Systems. *International Journal of Engineering Science and Technology,* **2**(8): 3947–3654.

Kumar, R., Singh, S., and Raghav, R. (2025). Ensuring sustainable water management for India. *Science of the Total Environment*, **913**: 168432.

Kumar, S., Kumar, R., Singh, M. K., Yadav, S., and Kumar, P. (2024). Crop water requirement of rice in different agroclimatic zones of Jharkhand. *Journal of Agrometeorology*, **26**(2): 233–237.

Kumar, S.S., Venkateswaran, S. and Kannan, R. (2017). Rainfall–runoff estimation using SCS–CN and GIS approach in the Pappiredipatti watershed of the Vaniyar sub basin, India. *Model Earth System Environment,* **3**(24): 1–8.

Kuorinka, I., Jonsson, B., Kilbom, A., Vinterberg, H., Biering-Sørensen, F., Andersson, G., and Jørgensen, K. (1987). Standardised Nordic questionnaires for the analysis of musculoskeletal symptoms. *Applied ergonomics,* **18**(3): 233–237.

Kusre, B. C., and Singh, K. S. (2012b). Study of spatial and temporal distribution of rainfall in Nagaland (India). *International Journal of Geomatics and Geosciences*, **2**(3): 712.

Kusre, B. C., and Singh, S. (2012a). Frequency analysis of different time series rainfall at Kohima, Nagaland, India. *J. Inst. Eng. India Ser. A*, **93**(2): 105–109.

Laishram, R. J., and Alam, W. (2024). Estimation of rainfall-runoff potential using SCS-CN and geospatial approach for Loktak Lake Watershed, India. *International Journal of Hydrology Science and Technology*, **18**(1): 77–105.

Lalmalsawmzauva, K. C., Chatterjee, U., Roy, A. D., Koley, B., Bhunia, G. S., and Shit, P. K. (2021). Rainwater harvesting potential in Nagaland, India. *In Modern cartography series*, **10**: 641–657.

Li, J., Ma, W., Botero-R, J. C., and Quoc Luu, P. (2023). Mechanization in land preparation and irrigation water productivity: Insights

from rice production. *International Journal of Water Resources Development*, **40**(3): 379–400.

Liu, J., Chen, S., Li, L., and Li, J. (2017). Statistical Downscaling and Projection of Future Air Temperature Changes in Yunnan Province, China. *Advances in Meteorology*.

Liu, Q., Yang, Z., Cui, B., and Sun, T. (2010). The temporal trends of reference evapotranspiration and its sensitivity to key meteorological variables in the Yellow River Basin, China. *Hydrological Processes*.

Liu, W., Zhang, Z. H. E., and Wan, S. (2009). Predominant role of water in regulating soil and microbial respiration and their responses to climate change in a semiarid grassland. *Global Change Biology*, **15**(1): 184–195.

Ma, S., Gao, X., Zhang, Y., and Li, Q. (2024). Deforestation-induced runoff changes dominated by forest-climate feedbacks. *Nature Communications,* **15**: 2345.

Mahalingam, B., Ramu, Bharath, and Jayshree. (2014). Rainfall variability in space and time, a case of Mysore district, Karnataka, India. *Current trends in technology and science,* **3**(3).

Mahdaoui, K., Chafiq, T., Asmlal, L., and Tahiri, M. (2024). Assessing hydrological response to future climate change in the Bouregreg watershed, Morocco. *Scientific African*, **23**.

Mahdaoui, K., Tahiri, M., and Asmlal, L. (2023). Downscaling future climate changes under RCP emission scenarios using CanESM2 climate model over the Bouregreg catchment, Morocco. *Modeling Earth Systems and Environment*, **9**(2): 2797–2807.

Mahmood, R., and Babel, M. S. (2012). Evaluation of SDSM developed by annual and monthly sub-models for downscaling temperature

and precipitation in the Jhelum basin, Pakistan and India. *Theoretical and Applied Climatology*, **113**(1–2): 27–44.

Mahmood, R., and Babel, M.S. (2013). Evaluation of SDSM developed by annual and monthly sub-models for downscaling temperature and precipitation in the Jhelum basin, Pakistan and India. *Theoretical and applied climatology,* **113**(2): 27–44.

Mallick, K., Bhattacharya, B. K., and Patel, N. K. (2009). Estimating volumetric surface moisture content for cropped soils using a soil wetness index based on surface temperature and NDVI. *Agricultural and Forest Meteorology,* **149**(8): 1327–1342.

Mammeri, A., Tiri, A., Belkhiri, L., Salhi, H., Brella, D., Lakouas, E., and Mouni, L. (2023). Assessment of surface water quality using water quality index and discriminant analysis method. *Water*, **15**(4): 680.

Medeo, M., and Jamir, A. (2023). Rainfall trend analysis of Nagaland using Mann–Kendall test (2004–2021). International Journal of Scientific Research, **12**(3): 1172–1176.

Meena, G. L., Sethy, B. K., Meena, H. R., Ali, S., Kumar, A., Singh, R. K., and Kumar, K. (2023). Quantification of impact of land use systems on runoff and soil loss from ravine ecosystem of western India. *Agriculture*, **13**(4): 773.

Mishra, B. K., Kumar, P., Saraswat, C., Chakraborty, S., and Gautam, A. (2021). Water security in a changing environment: Concept, challenges and solutions. *Water,* **13**(4): 490.

Mishra, S.K., Sansalone, J.J., and Singh, V.P. (2004). Partitioning analog for metal elements in urban rainfall-runoff overland flow using the soil conservation service curve number concept. *Journal of Environmental Engineering*, **130**(2): 145–154.

Mohapatra, S., Sahoo, D., Sahoo, A. K., Sharp, B., and Wen, L. (2023). Heterogeneous climate effect on crop yield and associated risks to water security in India. *International Journal of Water Resources Development*, **40**(3): 345–378.

Mongabay. (2023). Ruza, a traditional water harvesting system for the water-scarce mountains. Retrieved from https://india.mongabay.com

Monir, M. M., and Sarker, S. C. (2024). Analyzing post-2000 groundwater level and rainfall changes in Rajasthan, India, using well observations and GRACE data. *Heliyon*, **10**(2).

Moss, R. H., Edmonds, J. A., Hibbard, K. A., Manning, M. R., Rose, S. K., van Vuuren, D. P., Carter, T. R., Emori, S., Kainuma, M., Kram, T., Meehl, G. A., Mitchell, J. F. B., Nakicenovic, N., Riahi, K., Smith, S. J., Stouffer, R. J., Thomson, A. M., Weyant, J. P., and Wilbanks, T. J. (2010). The next generation of scenarios for climate change research and assessment. *In Nature*, **463**(7282): 747–756.

Mujeeb, M. (2023). Estimation of surface runoff using SCS-CN remote sensing and GIS in Sanjab Watershed.

Mukheibir, P. and Zievogal, G. (2007). Developing a Municipal Adaptation Plan (MAP) for Climate Change: the city of Cape Town. *Environment and Urbanization,* **19**: 143–157.

Mukherjee, M., Kumar, A., Rahman, A.H., Yangdhen, S., Sen, S., Adhikari, B. S., Nianthi, R., Sachdev, S., and Shaw, R. (2023). Extent and evaluation of critical infrastructure, the status of resilience and its future dimensions in South Asia. *Progress in Disaster Science*, **17**: 100275.

Muneer, A. S., Afan, H. A., Kamel, A. H., and Sayl, K. N. (2022). Runoff mapping using the SCS-CN method and artificial neural

network algorithm, Ratga Basin, Iraq. *Arabian Journal of Geosciences,* **15**(7): 1–10.

Muthu, A. L., and Santhi, M. H. (2015). Estimation of surface runoff potential using SCS-CN method integrated with GIS. *Indian Journal of Science and Technology*.

Naga, R., A., Abinaya, S., Purna Durga, G., and Lakshmi Kumar, T. V. (2023). Long-term relationships of MODIS NDVI with rainfall, land surface temperature, surface soil moisture and groundwater storage over monsoon core region of India. *Arid Land Research and Management,* **37**(1): 51–70.

Nagaland PSC Notes. (2022). Rainfall distribution in Nagaland. Retrieved from https://nagaland.pscnotes.com/nagaland-geography/rainfall-distribution-in-nagaland/.

Nagaland State Disaster Management Authority (NSDMA). (2019). Nagaland State Action Plan on Climate Change (SAPCC), 2012–2030. Kohima: Government of Nagaland.

Naleo, V., Khape, K., Nagaraju, D., Pramoda, G., and Nagesh, P. (2020). Hydrochemical study of Patkai Campus: Dimapur Nagaland, India. IOSR *Journal of Applied Geology and Geophysics*, **8**(4): 17–31.

Narasimha Murthy, K. V., Saravana, R., and Rajendra, P. (2018). Critical comparison of north east monsoon rainfall for different regions through analysis of means technique. *In MAUSAM:* **69**(3).

Neog, R. (2023). Monitoring land use dynamics, urban sprawl, and land surface temperature in Dimapur urban area, Nagaland, India. *International Journal of Environmental Science and Technology*, **20**(7): 7519–7532.

Ngullie, T. Z. and Deka, P. K. (2022). Food grains production in Nagaland: An evaluative study. *Economic Affairs*, **67**(5), 815–821.

Nienu, V. (2024). Antiquity of the Kachari Civilization. *Journal of History, Art and Archaeology*, **4**(1): 1–17.

Njaben, H.S. (2018). Comparison and evaluation of GIS-based spatial interpolation methods for estimation groundwater level in AL-Salman District— Southwest Iraq. *Journal of Geographic Information System,* **10**(4): 362.

Noor, I. M. M., Prasetyowati, S. S., and Sibaroni, Y. (2022). Prediction map of rainfall classification using random forest and inverse distance weighted (IDW). *Building of Informatics, Technology and Science (BITS),* **4**(2): 723–731.

Olaoye, J. O., and Rotimi, A. O. (2010). Measurement of agricultural mechanization index and analysis of agricultural productivity of farm settlements in Southwest Nigeria. *Agricultural Engineering International: CIGR Journal,* **12**(1).

Olmstead, S. M. (2014). Climate change adaptation and water resource management: A review of the literature. *Energy Economics,* **46**: 500–509.

Pamei, M., Hemso, B. E., and Puzari, A. (2022). Evaluation of the Physico-Chemical and the sustainability of ground and surface water quality using statistical correlation method and Water Quality Index in Dimapur District, Nagaland. *Environmental Nanotechnology, Monitoring & Management*, **18**: 100699.

Pandey, A., Dabral, P. P., Chowdary, V. M., and Mal, B. C. (2009). Estimation of runoff for agricultural watershed using SCS curve number and GIS. *In Map India Conference. Geospatial World.*

Pandey, N., Panwar, K., Sharma, M., and Punia, M. (2016). Analysis of spatial interpolation for rainfall data using various methods: A case study of Bisalpur catchment area. *International Journal of Engineering Research & Technology.*

Pandey, R.P., Jain, M.K., Mishra, S.K., and Singh, V.P., (2008). A rain duration and modified AMC-dependent SCS-CN procedure for long-duration rainfall-runoff events. *Water Resources Management,* **22**(7): 861–876.

Pandey, V. and Pandey, P. (2010). Spatial and temporal variability of soil moisture. *International Journal of Geosciences,* **1**: 87–98.

Panme, A. K., and Sethi, N. L. (2022). Estimation of crop water requirements and irrigation scheduling for major crops grown in India's North-Eastern Region. *Current Applied Science and Technology*, **23**(4).

Paradkar, V., and Mittal, H. K. (2024). Analysing Spatial and Temporal Rainfall Variability of Southern Rajasthan using GIS Approach. *Environment and Ecology*, **42**(2A): 598–605.

Parida, B. R., and Oinam, B. (2015). Unprecedented drought in North East India compared to western India. *Current Science*, 2121–2126.

Parikh, J., and Nair, J. (2019). Analysis of water shortage in India. *International Journal of Advance Research, Ideas and Innovations in Technology*, **5**(2): 1564–1569.

Pathak, H., Bhatia, A., and Jain, N. (2014). Greenhouse gas emission from Indian agriculture: trends, mitigation, and policy needs. *Indian Agricultural Research Institute*.

Pathak, S., Chielie, M., Satish, Y., and Kusre, B. C. (2024). Spatial and temporal trend analysis of rainfall in Nagaland (India) using

machine learning techniques. *Journal of Earth System Science,* **133**(2): 105.

Patle, G. T., and Panggeng, T. (2024). Assessment of crop water requirement and irrigation scheduling for selected crops in the Kohima district, Nagaland. *Water Practice and Technology*, **19**(3): 812–823.

Patle, G. T., Salam, R., Bisen, S., Misra, S., Chakraborty, B., Raju, P. L., and Saha, S. (2025). Study of temporal behaviour of meteorological drought using innovative polygon trend and scaling hypothesis methods in Kolasib district, Mizoram, India. *Scientific Reports, **15***: 19266.

Pawar, S. V., Vallabhbhai, S., Lal, P., Vallabhbhai, P. S., Mirajkar, A., Pawar, S. v, Patel, P. L., and Mirajkar, A. B. (2021). Estimation of Potential Evapotranspiration in command area of New Mutha Right Bank Canal, Pune, Maharashtra, India.

Peng, W., Wang, J., Zhang, J., and Zhang, Y. (2020). Soil moisture estimation in the transition zone from the Chengdu Plain region to the Longmen Mountains by field measurements and LANDSAT 8 OLI/TIRS-derived indices. *Arabian Journal of Geosciences,* **13**(4): 168.

Peseyie, R., and Rao, B. V. (2017). Assessment of groundwater quality for drinking purpose in and around Dimapur town, Nagaland. *Journal of Applied Geochemistry*, **19**(4): 464–470.

Phad, S., Sayyad, R., and Dakhore, K. K. (2024). Estimation of crop water requirement of soyabean and cotton crops for Marathwada region, India. *International Journal of Current Microbiology and Applied Sciences*, **13**(3): 133–138.

Potithep, S., Ishii, R., and Suzuki, R. (2009). The potential of Normalized Difference Soil Index (NDSI) for soil water content

estimation in Mongolia. *Asian association on remote sensing. Japan Agency for Marine-Earth Science and Technology Research Institute for Global Change*, 3713–25.

Prabhu, Shravan and Vishwas Chitale. (2024). Decoding India's Changing Monsoon Patterns: A Tehsil-level Assessment. *New Delhi: Council on Energy, Environment and Water*.

Pradhan, A., Jayasuriya, H. P., and Mbohwa, C. (2016). Status and potentials of agricultural mechanization in Sunsari District, Nepal. *Applied Engineering in Agriculture,* **32**(6): 759–768.

Puzari, A., Khan, P., Thakur, D., Kumar, M., Shanu, and K., Chutia, P. (2015). Quality assessment of drinking water from Dimapur district of Nagaland and Karbi-Anglong district of Assam for possible related health hazards. *Current World Environment,* **10**(2): 634–650.

Qazi, N. Q., Pokharel, B., and Dutta, D. (2017). Impact of forest degradation on streamflow regime in the Garhwal Himalaya, Northern India. *Hydrological Sciences Journal*, **62**(5): 759–768.

Raghavan, R., Rao, K. V., Shirahatti, M. S., Srinivas, D. K., Reddy, K. S., Chary, G. R., Gopinath, K. A., Osman, M., Prabhakar, M., and Singh, V. K. (2022). Assessment of Spatial and Temporal Variations in Runoff Potential under Changing Climatic Scenarios in Northern Part of Karnataka in India Using Geospatial Techniques. *Sustainability (Switzerland)*, **14**(7).

Rahmat, S. N., Tarmizi, A. H. A., and Tukimat, N. N. A. (2021). Impacts of Climate Change on Rainfall Trends Under RCP Scenarios in Johor, Malaysia. *International Journal of Integrated Engineering*, **5**: 272–280.

Raina, A., Thakur, R., and Kumar, S. (2021). Extent and impact of farm mechanisation in hilly state of Himachal Pradesh. *Indian Journal of Extension Education,* **57**(1): 61–66.

Ramakrishnaiah C. R., Sadashivaiah, C., and Ranganna, C. (2009). Assessment of Water Quality Index for the Groundwater in Tumkur Taluk, Karnataka State, India. *E-Journal of Chemistry,* **6**(2): 523–530.

Rana, M. M., Adhikary, S. K., Nath, H., Rana, M. M., Adhikary, S. K., Nath, H., and El-Shafie, A. (2023). Assessment of Annual and Seasonal Climate Change Impact in Rajshahi District of Bangladesh using SDSM. *In Architecture and Civil Engineering*.

Rao, K. T. V. S., Venkatesh, D. V., and Ahmed, S. F. (2018). Assessment and comparison of groundwater quality in Guntur District, Andhra Pradesh by using ArcGIS. *International Journal of Innovative Science and Research Technology,* **3**(4): 201–213.

Rasooli. S. V., and Ranjbar, I. (2008). Determination of the degree, level and capacity indices for agricultural mechanization in Sarab Region. *Journal of Agricultural Science and Technology,* **10**(3): 215–223.

Ray, S. R., Saha, S., Chatterjee, D., and Deka, B. (2015). A guide for soil nutrient management with special reference to Wokha.

Rodriguez, D., de Fraiture, C., and Bharati, L. (2017). Assessing India's drip irrigation boom. *Water International*, **42**(3): 278–294.

Roja, M., Deepthi, C., and Reddy, M. D. (2020). Estimation of crop water requirement of maize crop using FAO CROPWAT 8.0 model. *Ind. J. Pure App. Biosci.*, **8**(6): 222–228.

Roy, N., Debnath, A., and Nautiyal, S. (2020). Livelihood Strategies and Agricultural Practices in Khonoma Village of Nagaland, India: Observation from a Field Visit. *Springer, Cham*, 425–434.

Ryu, S., Song, J. J., Kim, Y., Jung, S. H., Do, Y., and Lee, G. (2021). Spatial interpolation of gauge measured rainfall using compressed sensing. *Asia-Pacific Journal of Atmospheric Sciences,* **57**: 331–345.

Sabah, A., and Afsar, S. (2020). Assessing spatio-temporal changes of soil moisture: a case study at Karachi, Pakistan. *Arabian Journal of Geosciences,* **13**: 1–13.

Sadat-Noori, S. M., Ebrahimi, K., and Liaghat, A. M. (2014). Groundwater quality assessment using the Water Quality Index and GIS in Saveh-Nobaran aquifer, Iran. *Environmental Earth Sciences,* **71**: 3827-3843.

Saha, M., Sauda, S. S., Real, H. R. K., and Mahmud, M. (2022). Estimation of annual rate and spatial distribution of soil erosion in the Jamuna basin using RUSLE model: A geospatial approach. *Environmental Challenges*, **8**.

Salman, S. A., Shahid, S., Afan, H. A., Shiru, M. S., Al-Ansari, N., and Yaseen, Z. M. (2020). Changes in climatic water availability and crop water demand for Iraq region. *Sustainability (Switzerland),* **12**(8).

Sami, S.S., Ali, A.A., and Jalal, A.D. (2024). An Application of the Statistical Downscaling Model (SDSM) to Simulate Precipitation Data in the Iraqi Western Desert. *In Proceedings of the 2nd International Conference for Engineering Sciences and Information Technology (ESIT 2022): ESIT2022 Conference Proceedings, Al Anbar, Iraq*, 030113.

Saraf, V.R. and Regulwar, D.G. (2016). Assessment of Climate Change for Precipitation and Temperature Using Statistical Downscaling Methods in Upper Godavari River Basin, India. *Journal of Water Resource and Protection,* 31–45.

Sarath. P. S. V., Magesh, N. S., Jitheshlal, K. V., Chandrasekar, N., and Gangadhar, K. (2012). Evaluation of groundwater quality and its suitability for drinking and agricultural use in the coastal stretch of Alappuzha District, Kerala, India. *Applied Water Science*, **2**(3): 165–175.

Sarkar, S. S. (2017). Rainwater harvesting in North-East India. CAB International, 145–168.

Sarkar, S., and Maity, R. (2020). Increase in probable maximum precipitation in a changing climate over India. *Journal of Hydrology,* **585**: 124806.

Sati, V. P. (2013). Towards sustainable livelihood and ecosystem security in the hill agro-ecosystems of Northeast India. Environment, Development and Sustainability, **15**(3): 1–16.

Sema, H. V., Guru, B., and Veerappan, R. (2017). Fuzzy gamma operator model for preparing landslide susceptibility zonation mapping in parts of Kohima Town, Nagaland, India. *In Modeling Earth Systems and Environment*, **3**(2): 499–514.

Seng, C.K., Weng, T.K., and Nakayama, A. (2021). Development of Statistically Downscaled Regional Climate Model Based on Representative Concentration Pathways for Ipoh, Subang and KLIA Sepang in Peninsular Malaysia. *IOP Conf. Ser. Earth Environ. Sci.*, 012022.

Shadeed, S., Jagyousi, A., Khader, A., Chawla, C., and Kunstmann, H. (2022). Comparative aalysis of interpolation methods for rainfall mapping in the Faria catchment, Palestine. *J. Res(N.Sc)*, **36**.

Shah, S. H., and Narain, V. (2019). Re-framing India's "water crisis": An institutions and entitlements perspective. *Geoforum,* **101**: 76–79.

Shankar, S., Ojha, C. S. P., and Prasad, K. S. H. (2012). Irrigation scheduling for maize and Indian-mustard based on daily crop water requirement in a semi-arid region. *International Journal of Civil and Environmental Engineering*, **6**: 300–309.

Sharkh, M.S.A. (2009). Estimation of runoff for small watershed using watershed modelling system (WMS) and GIS. *Thirteenth International Water Technology Conference, IWTC 13, Hurghada, Egypt,* 1199–1200.

Sharma, A., and Kanga, S. (2020). Surface Runoff Estimation of Sind River Basin Using SCS-CN Method and GIS Technology. *Geographic information system*.

Sharma, M., Bangotra, P., Gautam, A. S., and Gautam, S. (2022). Sensitivity of normalized difference vegetation index (NDVI) to land surface temperature, soil moisture and precipitation over district Gautam Buddh Nagar, UP, India. *Stochastic Environmental Research and Risk Assessment,* 1–11.

Sharma, S., Khadkha, N., Nepal, B., Ghimire, S. K., Luitnel, N., and Hamal, K. (2021). Elevation dependency of precipitation over southern slope of Central Himalaya. *Jalawaayu*, **1**: 1–14.

Shinde, P., Shinde, T. P., Shinde, P. S., and Pawar, G. A. (2025). Morphometric Assessment of the Banganga River Basin in Satara District, Maharashtra. *Mukt Shabd Journal*, **15**.

Shrestha, D., Sharma, S., Bhandari, S., and Deshar, R. (2021). Statistical downscaling and projection of future temperature and precipitation change in Gandaki Basin. *Journal of Institute of Science and Technology*, **26**(1): 16–27.

Shrestha, D., Sharma, S., Hamal, K., Jadoon, U. K., and Dawadi, B. (2021). Spatial distribution of extreme precipitation events and its trend in Nepal. *Environment Sciences*, **9**, 58–66.

Singh, A., Panda, S., Kumar, K., and Sharma, C. (2013). Artificial groundwater recharge zones mapping using remote sensing and GIS: A case study in Indian Punjab. *Environmental Management,* **52**(1): 61–71.

Singh, A., Thakur, S., and Adhikary, N. C. (2021). Analysis of spatial and temporal rainfall characteristics of the North East region of India. *Arabian Journal of Geosciences*, **885**: 1–16.

Singh, D., Jain, S.K., and Gupta, R.D. (2015). Statistical downscaling and projection of future temperature and precipitation change in middle catchment of Sutlej River Basin, India. J. *Earth Syst. Sci.* **124**: 843–860.

Singh, G. (2006). Estimation of a mechanisation index and its impact on production and economic factors—A case study in India. *Biosystems engineering,* **93**(1): 99–106.

Singh, L. S., Uchoi, A., and Das, G. (2023). Impact of farm mechanization training on knowledge development of farmers: A study in Kamrup district of Assam. *Indian Res. J. Ext. Edu,* **23**(2): 81–85.

Singh, O., Arya, P., and Chaudhary, B. S. (2013). On rising temperature trends at Dehradun in Doon valley of Uttarakhand, India. *Journal of Earth System Science*, **122**(3).

Singh, R. S., and Kumar, M. (2017). Economic evaluation and mechanization index of selected cropping pattern in Madhya Pradesh. *Economic Affairs,* **62**(3): 439–446.

Sinha, A., Ray, S., Majumder, S., Dash, B., Barik, B. R., and Reddy, M. D. (2024). Assessment of Wheat Crop Water Requirement for South Bihar by FAO CROPWAT 8.0. *Agricultural Science Digest - A Research Journal.*

Sinha, R. K., Jain, S. K., and Prabhakar, D. (2020). Assessing the impacts of land cover and climate change on runoff and sediment yield of a river basin in India. International Journal of River Basin Management.

Soil & Land Use Survey of India (SLUSI). (2020). Inventory of Soil Resources of Kohima District, Nagaland (SRM-76) and Dimapur District (SRM-82). Govt. of India.

Solomon, S. (Atmospheric chemist), Intergovernmental Panel on Climate Change., & Intergovernmental Panel on Climate Change. Working Group I. (2007). Climate change 2007: the physical science basis: contribution of Working Group I to the Fourth Assessment Report of the Intergovernmental Panel on Climate Change. *Cambridge University Press.*

Souvignet, M., Gaese, H., Ribbe, L., Kretschmer, N. and Oyarzún, R. (2010). Statistical downscaling of precipitation and temperature in north-central Chile: an assessment of possible climate change impacts in an arid Andean watershed. *Hydrol. Sci. J,* **55**(1): 41–57.

Srinidhi, A., Werners, S. E., Dadas, D., D'Souza, M., Ludwig, F., and Meuwissen, M. P. M. (2023). Retrospective climate resilience assessment of semi-arid farming systems in India. International Journal of Water Resources Development, **40**(3): 506–531.

Srinivas, P., Kumar, G., and Hemalatha, T. (2011). Generation of groundwater quality index map: A case study. *Civil and Environmental Research,* **1**(2): 9–20.

Statistical Handbook of Nagaland. (2021). District-wise Rainfall Data. Directorate of Economics & Statistics, Government of Nagaland.

Suo, M. Q., Zhang, J., Zhou, Q., and Li, Y. P. (2019). Applicability Analysis of SDSM Technology to Climate Simulation in Xingtai

City, China. *IOP Conference Series: Earth and Environmental Science*, **223**(1).

Tailor, D., and Shrimali, N.J. (2016). Surface runoff estimation by SCS curve number method using GIS for Rupen-Khan watershed, Mehsana district, Gujarat. *Indian Water Resources Society,* **36**(4): 1–5.

Tao, T., Chocat, B., Liu, S., and Xin, K. (2009). Uncertainty analysis of Interpolation methods in rainfall spatial distribution- A case of small catchment in Lyon. *Journal of Water Resources and Protection,* **1**: 136–144.

Thakor, F., Bhoi, D., Dabhi, H., Pandya, S., and Nikitarai, B. (2011). Water quality index of Pariyej lake, Kheda, Gujarat. *Current World Environment,* **6**(2): 225–231.

Thebe, T. A., and Koza, T. (2012). Agricultural mechanization interventions to increase the productivity of smallholder irrigation schemes in Zimbabwe.

Tidwell, V. C., Moreland, B. D., Shaneyfelt, C. R., and Kobos, P. (2018). Mapping water availability, cost and projected consumptive use in the eastern United States with comparisons to the west. *Environmental Research Letters,* **13**(1).

U.S. Soil Conservation Service. (1986). Urban Hydrology for Small Watersheds, Technical Release 55. USDA (U.S. Department of Agriculture).

Uddin, M. T., and Dhar, A. R. (2020). Assessing the impact of water-saving technologies on Boro rice farming in Bangladesh: economic and environmental perspective. *Irrigation Science*, **38**(2): 199-212.

Van, V., Edmonds, D. P., Kainuma, J. J., Riahi, M., Thomson, K., Hibbard, A., Hurtt, K., Kram, G. C., Krey, T., Lamarque, V.,

Masui, J. F., Meinhausen, T., Nakicenovic, M., Smith, N., S. J., and Rose, S. K. (2011). The representative concentration pathways: An overview. *Climatic Change*, **109**(1): 5–31.

Vasanthavigar, M., Srinivasamoorthy, K., Vijayaragavan, K., Rajiv Ganthi, R., Chidambaram, S., Anandhan, P., and Vasudevan, S. (2010). Application of water quality index for groundwater quality assessment: Thirumanimuttar sub-basin, Tamil Nadu, India. Environmental monitoring and assessment, **171**(1): 595–609.

Verma, A., Francois, L., Lanssens, B., Hambuckers, A., Jacquemin, I., and Tölle, M. (2022). Modelling mortality drivers of tree species under changing climatic conditions RCP 2.6 and RCP 8.5 at a regional scale using the CARAIB dynamic vegetation model. *International Symposium "Global Changes and Transition Management: Singular or Plural?"*.

Vero, A., Rao, B., Haokip, P., Medo, T., and Keditsu, V. (2023). Assessment of Groundwater Quality in Kohima. *Journal of Applied Geochemistry*, **25**(1): 40–52.

Vijayakumar, S., Nayak, A. K., Ramaraj, A. P., and Swain, C. K. (2021). Rainfall and temperature projections and their impact assessment using CMIP5 models under different RCP scenarios for the eastern coastal region of India. *Current Science*, **121**(2): 222–232.

Vohra, K., and Franklin, M. L. (2021). Water Resources Management—An Indian Perspective. *Springer, Singapore*, 237–252.

Walanus, A., and Prokop, P. P. (2003). Trends and periodicity in the longest instrumental rainfall series for the area of most extreme rainfall in the world Northeast India. *ResearchGate*, **76**(2): 22–31.

Walega, A., Amatya, D. M., Caldwell, P., Marion, D., and Panda, S. (2020). Assessment of storm direct runoff and peak flow rates

using improved SCS-CN models for selected forested watersheds in the Southeastern United States. *Journal of Hydrology: Regional Studies,* **27**.

Wan, Z., Wang, P., and Li, X. (2004). Using MODIS land surface temperature and normalized difference vegetation index products for monitoring drought in the southern Great Plains, USA. *International journal of remote sensing,* **25**(1): 61–72.

Wang, J., Rich, P. M., and Price, K. P. (2003). Temporal responses of NDVI to precipitation and temperature in the central Great Plains, USA. *International Journal of Remote Sensing*, **24**(11): 2345–2364.

Wang, L., Qu, J. J., Zhang, S., Hao, X., and Dasgupta, S. (2007). Soil moisture estimation using MODIS and ground measurements in eastern China. *International Journal of Remote Sensing,* **28**(6): 1413–1418.

Wang, W., Chen, Y., Wang, W., Zhu, C., Chen, Y., Liu, X., and Zhang, T. (2023). Water quality and interaction between groundwater and surface water impacted by agricultural activities in an oasis-desert region. *Journal of Hydrology,* **617**: 128937.

Wilby, R. L., and Harris, I. (2006). A framework for assessing uncertainties in climate change impacts: Low-flow scenarios for the River Thames, UK. *Water Resources Research*, **42**.

Wilby, R. L., Dawson, C. W., and Barrow, E. M. (2002). SDSM-a decision support tool for the assessment of regional climate change impacts. *In Environmental Modelling & Software*, **17**.

Wilby, R.L. and Dawson, C.W. (2013). The Statistical DownScaling Model (SDSM): Insights from one decade of application. *International Journal of Climatology*, **33**: 1707–1719.

Workneh, H. T., Chen, X., Ma, Y., Bayable, E., and Dash, A. (2024). Comparison of IDW, Kriging and orographic based linear interpolations of rainfall in six rainfall regimes of Ethiopia. *Journal of Hydrology: Regional Studies,* **52**: 101696.

Yadav, K., Gupta, N., Kumar, V., Arya, S., and Singh, D. (2012). Physico-chemical analysis of selected groundwater samples of Agra city, India. *Recent research in science and technology,* **4**(11): 51-54.

Yang, L., Soyam, P. S., Patil, R. P., Ray, A., Waghmare, V. V., Haswani, D., and Pandithurai, G. (2023). Impact of nylon and teflon filter media on the sampling of inorganic aerosols over a high altitude site. *Environmental Advances*, **12**: 100373.

Yang, X., Xie, X., Liu, D., Ji, F., and Wang, L. (2015). Spatial interpolation of daily rainfall data for local climate impact assessment over Greater Sydney Region. *Advances in Meteorology,* 1–12.

Yang. X.., J.J. Wu, P.J. Shi, and F. Yan. (2013). Modified triangle method to estimate soil moisture status with moderate resolution imaging spectroradiometer (MODIS) products. *The international archives of the photogrammetry, remote sensing and spatial information sciences,* **37**: 555–559.

Yu, B. (1998). Theoretical justification of method for runoff estimation. *J. Irrig. Drain. Engrg.,* **124**: 306–310.

Yunfei, S., Lin, L., and Lingling, Z. (2007). Application and comparing of IDW and Kriging interpolation in spatial rainfall information. *SPIE,* **6753**: 1.

Zavareh, M. M., Mahjouri, N., Rahimzadegan, M., and Rahimpour, M. (2023). A drought index based on groundwater quantity and

quality: Application of multivariate copula analysis. *Journal of Cleaner Production,* **417**: 137959.

Zhan, Z., Qin, Q., and X. Wang, 2004. The Application of LST/NDVI Index for Monitoring Land Surface Moisture in Semiarid Area. Geoscience and Remote Sensing, IGARSS '04. *Proceedings 2004 IEEE International,* **3**: 1551– 1555.

Zhang, Y., Zhao, Z., and Zheng, J. (2020). CatBoost: A new approach for estimating daily reference crop evapotranspiration in arid and semi-arid regions of Northern China. *Journal of Hydrology*, **588**.

Zhu, Q., Ma, Y., He, H., Li, Z., and Liu, S. (2018). Estimating the contribution of groundwater to the root zone under different groundwater depths and soil textures. *Vadose Zone Journal*, **17**(1): 1–12.

APPENDIX – I

Table 1: List of the 26 NCEP predictors

Sl. No.	Predictors	Description of predictors
1.	Mslpgl	Mean sea level pressure
2.	p1_fgl	1000 hPa Wind speed
3.	p1_ugl	1000 hPa Zonal velocity
4.	p1_vgl	1000 hPa Meridional velocity
5.	p1_zgl	1000 hPa Vorticity
6.	p1thgl	1000 hPa Divergence
7.	p1zhgl	500 hPa Wind speed
8.	p5_fgl	500 hPa Zonal velocity
9.	p5_ugl	500 hPa Meridional velocity
10.	p5_vgl	500 hPa Vorticity
11.	p5_zgl	500 hPa Geopotential height
12.	p500gl	500 hPa Wind direction
13.	p5thgl	500 hPa Divergence
14.	p5zhgl	850 hPa Wind speed
15.	p8_fgl	850 hPa Wind speed
16.	p8_ugl	850 hPa Zonal velocity
17.	p8_vgl	850 hPa Meridional velocity
18.	p8_zgl	850 hPa Vorticity
19.	p850gl	850 hPa Geopotential height
20.	p8thgl	850 hPa Wind direction
21.	p8zhgl	850 hPa Divergence
22.	Prcpgl	Precipitation
23.	s500gl	500 hPa Specific humidity
24.	s850gl	850 hPa Specific humidity
25.	shumgl	1000 hPa Specific humidity
26.	Tempgl	Screen (2 m) air temperature

APPENDIX – II

Table I: Questionnaire for data collection to assess the mechanization

Sl. No.	
1.	Name of the farmer/owner
2.	Nature of appointment
3.	Gender
4.	Age
5.	Stature (cm)
6.	Weight (kg)
7.	Ethnic group
8.	Education qualification
9.	Annual income
10.	Working experience
11.	Hours of working per day and per week
12.	Working habit (right-handed or left-handed)
13.	Type of crops grown
14.	Type of implements and tool used
15.	Number of implements and tools owned/hired
16.	Owned/hired implements/machinery
17.	Price of the implements/tools

APPENDIX – III

Table I: The FAO classification of wet, average wet and dry years (FAO, 2010)

Probability of Exceedance (Percent)	Type
20	Wet year
50	Normal or average wet year
80	Dry year

Table II: Selection of the average wet year (50 percent probability of exceedance)

Year	Mean annual rainfall	Rank	Probability of exceedance
2003	1222.39	1	5.26
2007	974.35	2	10.53
2017	887.44	3	15.79
2010	885.94	4	21.05
2016	869.35	5	26.32
2004	859.43	6	31.58
2008	836.06	7	36.84
2015	834.53	8	42.11
2018	830.99	9	47.37
2011	824.48	10	52.63
2019	780.82	11	57.89
2013	780.37	12	63.16
2020	769.64	13	68.42
2005	736.54	14	73.68
2006	728.41	15	78.95
2014	684.91	16	84.21
2012	675.60	17	89.47

2009	610.01	18	94.74

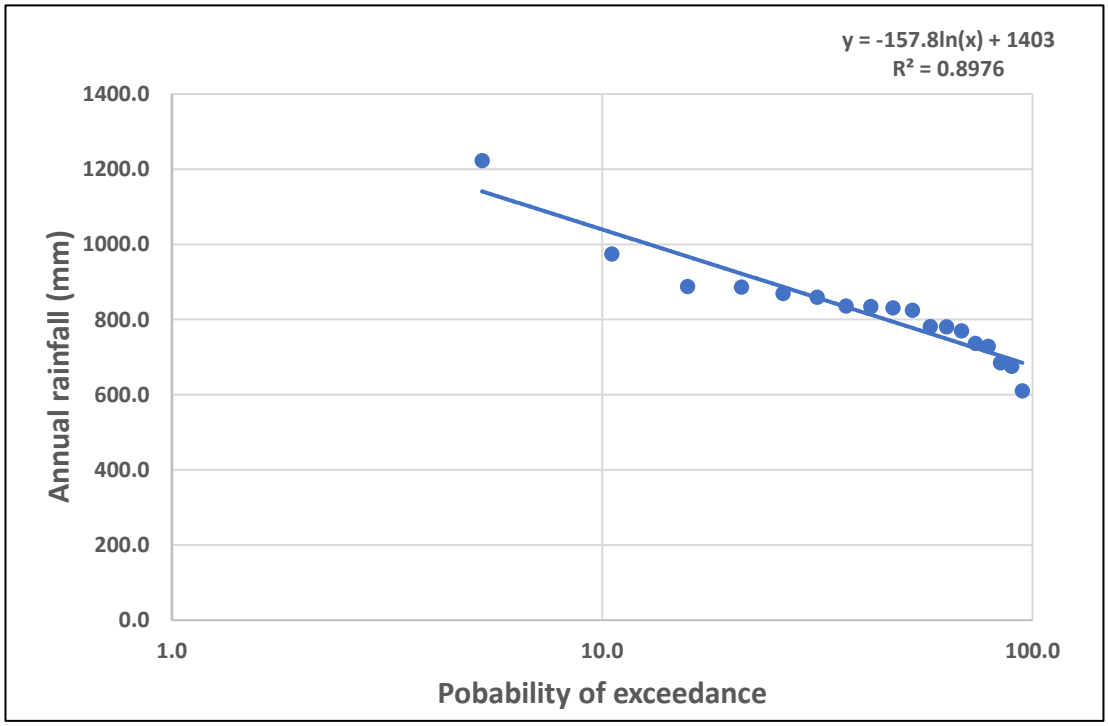

Fig I: The graphical representation of wet, average, and dry years

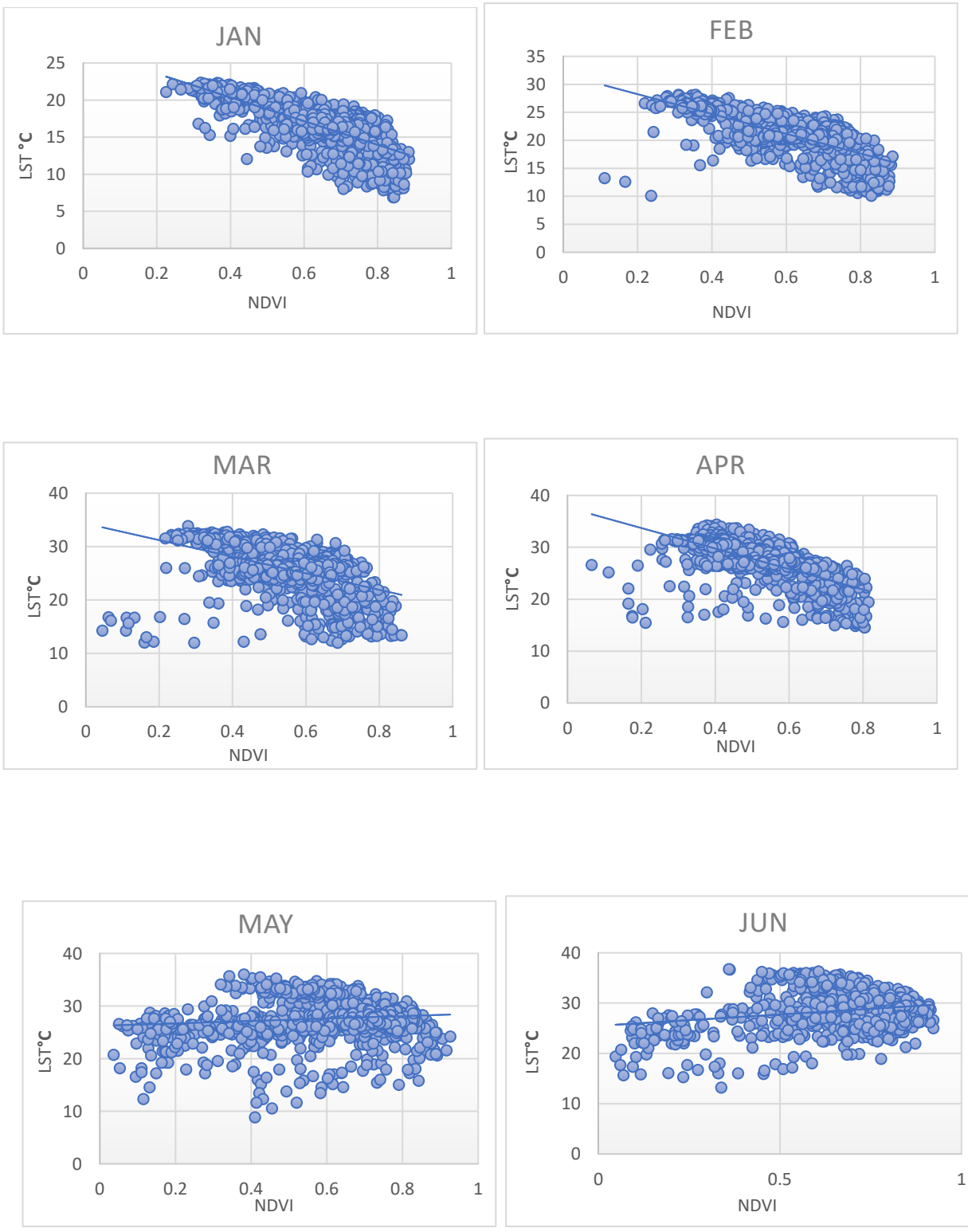

Fig II: NDVI vs LST scatter plot

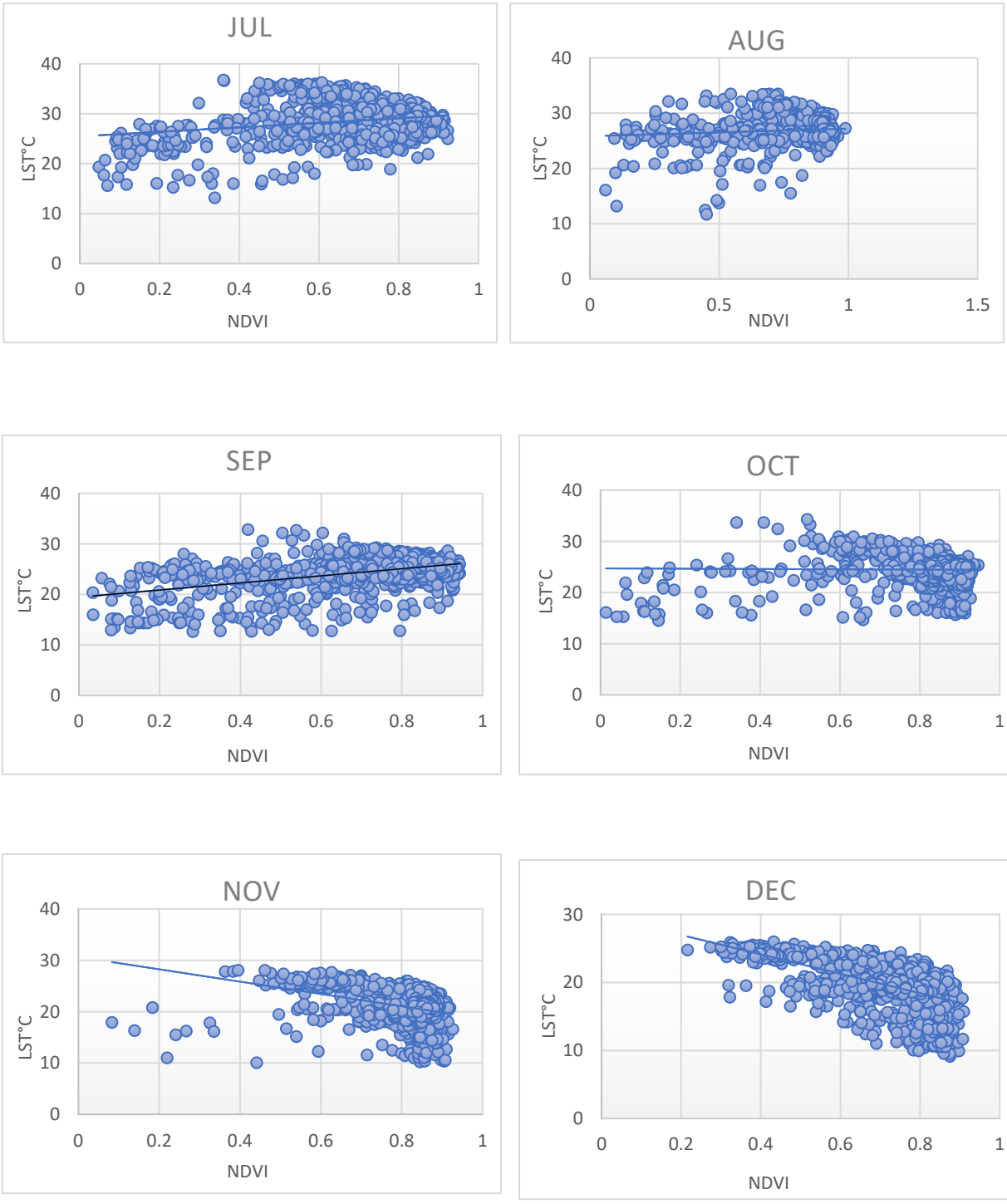

Fig III: NDVI vs LST scatter plot

APPENDIX – IV

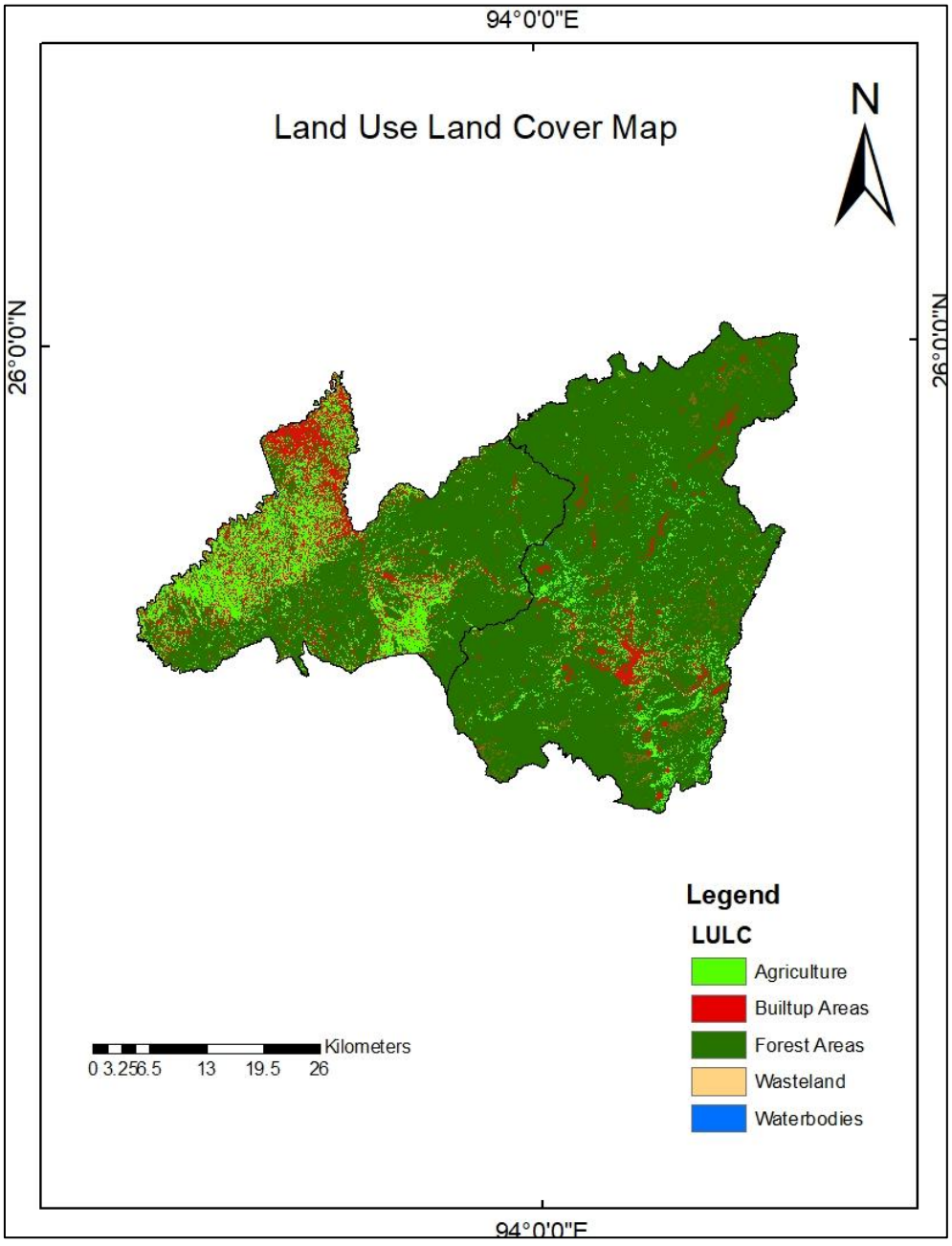

Fig I: Land use land cover map of the study area

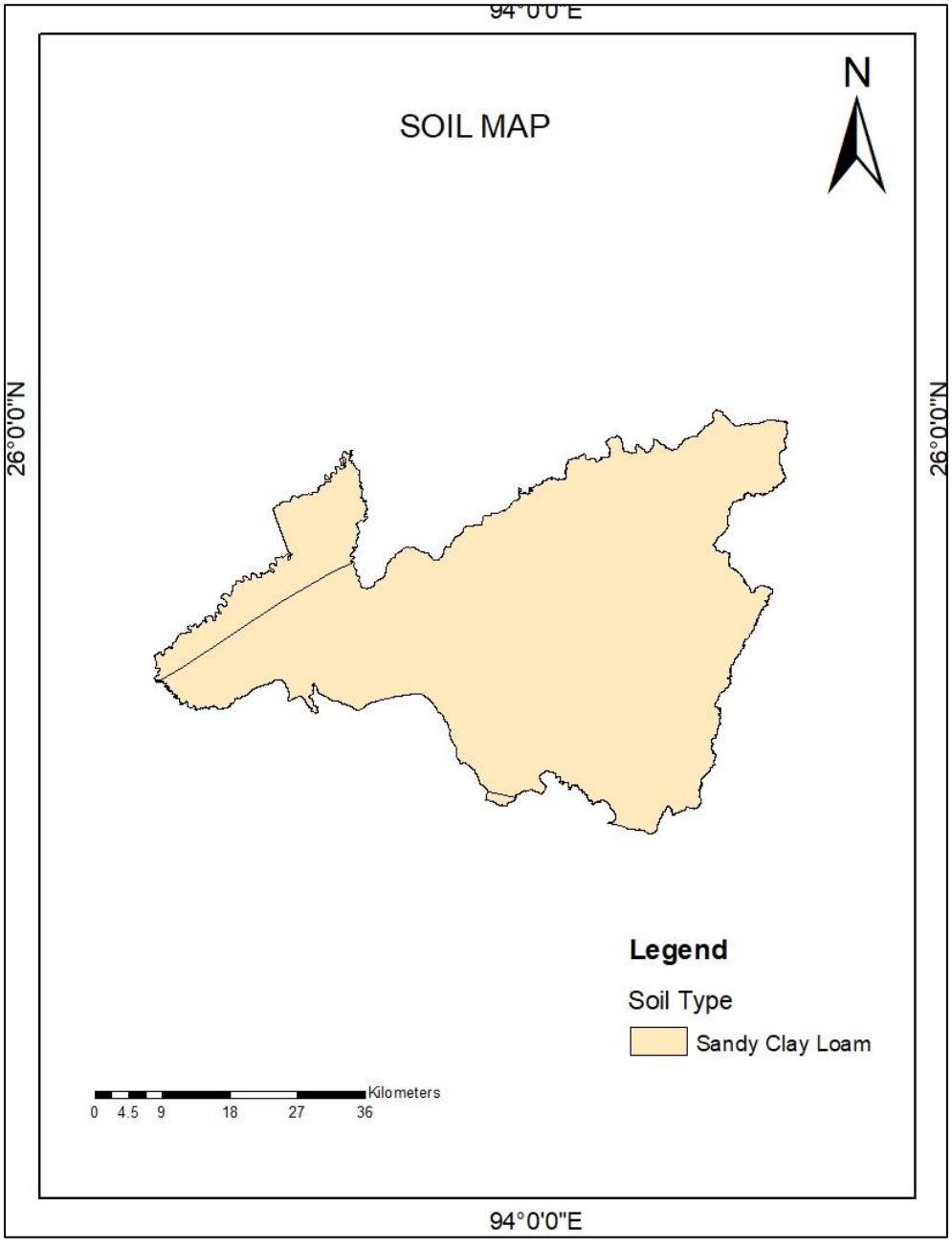

Fig II: Soil cover map of the study area

Calculation for AMC-I and AMC-II:

To get the Curve Number (CN) values for AMC-I and AMC-III, the correction factors were applied. The CN for AMC-I and AMC-III had been obtained by conversion of AMC-II (weighted CN) using the following formulae (Handbook of Hydrology, 1972):

For AMC-1:

$$CN_I = \frac{CN_{II}}{2.281 - 0.01281 CN_{II}}$$

For AMC-III:

$$CN_{III} = \frac{CN_{II}}{0.427 + 0.00573 CN_{II}}$$

Where,

CN_I is the Curve Number for dry condition

CN_{II} is the Curve Number for average or normal condition

CN_{III} is the Curve Number for wet condition

APPENDIX – V

Table 1: Rainfall data for Kohima station from 2003 to 2020

Year/Month	January	February	March	April	May	June	July	August	September	October	November	December
2003	14.0	14.5	54.9	107.8	117.5	218.6	291.0	358.4	347.4	154.6	5.2	52.2
2004	4.4	3.5	10.6	217.0	183.2	235.4	505.8	243.5	296.7	157.6	13.8	0.3
2005	3.5	18.9	80.0	62.0	160.3	307.4	191.8	322.9	263.6	177	9.0	2.7
2006	0.0	39.2	8.6	80.7	170.9	298.7	206.4	139.5	283.5	83.7	26.2	1
2007	s0.0	70.3	16.1	146.5	343.5	241.5	314.5	416.5	182.2	191.4	79.4	1.8
2008	43.8	5.0	54.1	35.0	170.7	398.4	453.1	393.3	320.0	125.7	0.0	0.0
2009	0.0	10.6	24.6	32.1	138.4	205.7	277.2	388.2	316.8	129.4	13.4	0.0
2010	1.4	8.2	56.9	60.8	119.5	347.1	530.6	464.3	226.5	162	2.1	21.2
2011	9.8	5.2	56.8	34.9	265.6	308.2	437.7	239.9	336.3	31.7	9.7	0.0
2012	10.0	27.1	93.7	101.2	158.5	128.1	226.1	262.4	198.4	5.6	1.5	29.6
2013	19.6	20.2	118.8	152.3	167.0	143.4	239.0	289.1	14.2	35.4	57.4	0.8
2014	5.2	0.5	22.4	6.8	181.7	273.6	268.5	403.8	368.8	233.1	9.1	4.5
2015	30.1	11.0	65.0	76.1	1800	218.3	424.9	547.2	204.8	199.3	1.5	0.0
2016	6.6	104.0	11.1	78.5	180.2	360.0	336.7	148.5	328.2	133.4	43.4	0.0
2017	2.2	0.8	93.0	163.7	234.6	326.9	482.1	250.4	340.6	204	5.4	31.9
2018	13.2	3.6	45.0	127.6	279.2	338.1	568.4	359.4	139.6	85.2	1.2	65.4
2019	80.6	15.4	58.2	83.0	175.0	208.1	286.4	355.9	266.6	216.6	37.2	0.0
2020	35.8	9.4	21.0	130.2	181.6	319.6	328.0	215.6	154	237.6	0.0	0.0

Table II: Rainfall data for Dimapur station from 2003 to 2020

Year/Month	January	February	March	April	May	June	July	August	September	October	November	December
2003	0.0	0.0	0.0	0.0	0.0	128.8	105.3	440.0	245.3	137.7	8.2	19.3
2004	7.9	0.0	15.2	229.4	18.8	186.0	368.0	91.0	224.4	158.2	6.6	0.0
2005	15.2	12.4	69.2	59.8	79.2	113.4	169.4	288.1	89.6	143.0	0.0	2.6
2006	0.0	0.0	26.4	58.4	345.9	176.2	185.8	104.2	142.2	79.2	35.4	6.6
2007	0.0	113.8	3.4	121.6	186.7	176.9	128.7	346.0	188.0	154.4	46.7	10.2
2008	8.9	0.3	49.7	32.6	95.4	321.7	186.6	78.5	283.9	81.2	0.0	0.0
2009	0.0	0.0	7.3	15.1	66.1	167.9	167.6	93.0	79.8	26.8	0.0	0.0
2010	0.0	0.2	29.6	103.6	124.8	205.4	153.6	111.4	80.0	54.8	0.0	0.0
2011	12.0	0.8	10.2	49.8	120.2	411.9	117.3	207.6	43.3	8.2	0.0	0.0
2012	0.2	0.8	0.0	49.8	5.6	174.8	132.2	103.2	102.8	108.7	0.0	0.0
2013	0.0	12.0	62.8	23.4	139.2	129.5	232.4	48.7	116.9	31.4	0.0	0.0
2014	0.0	7.0	12.9	5.7	80.2	90.1	165.8	185.9	59.3	61.2	0.0	0.0
2015	5.0	8.0	0.0	99.9	51.9	110.8	92.7	139.7	78.3	96.6	6.6	0.0
2016	21.0	5.6	2.2	92.9	98.2	180.4	114.6	141.7	202.4	35.6	93.6	0.0
2017	0.2	0.2	33.1	126.6	53.2	101.6	242.2	178.8	99.2	156.9	5.2	5.4
2018	5.5	0.5	8.0	17.6	52.9	127.2	113.8	310.6	78.2	11.5	0.2	20.0
2019	0.0	7.1	30.2	76.5	195.1	133.4	129.6	43.9	64.3	292.5	18.8	0.0
2020	0.4	0.4	8.4	33.4	80.6	168.0	192.5	53.9	140.1	233.5	0.0	0.0